UNIVERSITÄT BAYREUTH

Investigation of Uptake and Detoxification Mechanisms of Thioarsenates in Different Species

Evolution of Mechanisms Providing Arsenic Tolerance

Dissertation

zur Erlangung des akademischen Grades eines Doktors der Naturwissenschaften (Dr. rer. nat.) in der Bayreuther Graduiertenschule für Mathematik und Naturwissenschaften (BayNat) der Universität Bayreuth

vorgelegt von

Sebastian Haider

geboren in Lauf a.d. Pegnitz

Bayreuth, 2025

Die vorliegende Arbeit wurde in der Zeit von Juni 2020 bis einschließlich Dezember 2024 in Bayreuth am Lehrstuhl für Pflanzenphysiologie unter der Betreuung von Prof. Dr. rer. nat. Stephan Clemens angefertigt.

Vollständiger Abdruck der von der Bayreuther Graduiertenschule für Mathematik und Naturwissenschaften (BayNAT) der Universität Bayreuth genehmigten Dissertation zur Erlangung des akademischen Grades eines Doktors der Naturwissenschaften (Dr. rer. nat.).

Form der Dissertation: Monographie

Dissertation eingereicht am: 20.08.2025

Zulassung durch das Leitungsgremium: 07.10.2025

Wissenschaftliches Kolloquium: 22.01.2026

Amtierender Dekan: Prof. Dr. Jürgen Senker (Direktor)

Prüfungsausschuss:

Prof. Dr. Stephan Clemens (Gutachter)

Prof. Dr. Angelika Mustroph (Gutachterin)

Prof. Dr. Klaus Ersfeld (Vorsitzender)

Prof. Dr. Andreas Möglich

Teile der Arbeit wurden in Plan, Cell & Environment am 28.01.2026 publiziert (https://doi.org/10.1111/pce.70400).

Phosphate Transporters Mediate the Uptake of Monothioarsenate.

Sebastian Haider[1], Sylvia Hafner[2], Britta Planer-Friedrich[2], Stephan Clemens[1]

[1] Plant Physiology, Bayreuth Center for Ecology and Environmental Research (BayCEER), University of Bayreuth, D-95440 Bayreuth, Germany

[2] Environmental Geochemistry, Bayreuth Center for Ecology and Environmental Research (BayCEER), University of Bayreuth, D-95440 Bayreuth, Germany

https://doi.org/10.1111/pce.70400

Table of Contents

I. Abbreviations

A. thaliana; At	*Arabidopsis thaliana*
As	Arsenic
As^{III}	Arsenite
As^{V}	Arsenate
ΣAs	Total-Arsenic
AQP	Aquaglyceroporin
BART	Bile/Arsenite/Riboflavin Transporter
bp	Base Pairs
BYA	Billion Years Ago
Cd	Cadmium
CDS	Coding Sequence
CPB	Citrate Phosphate Buffer
CPE	Cretaceous-Paleogene Extinction
DMA^{III}	Dimethylated Arsenite
DMA^{V}	Dimethylated Arsenate
DMMTA	Dimethylated Monothioarsenate
DTT	Dithiothreitol
γ-EC	γ-Glutamylcysteine
γ-GT	γ-Glutamly Transpeptidase
E. coli; Ec	*Escherichia coli*
EFSA	European Food Safety Authority

EMM	Edinburgh Minimal Medium
ER	Endoplasmic Reticulum
FDA	Food and Drug Administration
FW	Fresh Weight
gDNA	Genomic DNA
GOE	Great Oxidation Event
Grx	Glutaredoxin
GSH	Glutathione (reduced)
GSSG	Glutathione Disulfide (oxidized)
HGT	Horizontal Gene Transfer
iAs	Inorganic Arsenic Species
IARC	International Agency for Research on Cancer
ICP-MS	Inductively Coupled Plasma - Mass Spectrometry
IC-ICP-MS	Ion Chromatography coupled with Inductively Coupled Plasma - Mass Spectrometry
MFS	Major Facilitator Superfamily
MIP	Major Intrinsic Proteins
MMA^{III}	Monomethylated Arsenite
MMA^{V}	Monomethylated Arsenate
MTA	Monothioarsenate
MTs	Metallothioneins

oAs	Organic Arsenic Species
PCs	Phytochelatins
PM	Plasma Membrane
PSR	Phosphate Starvation Response
PTP	Protein Tyrosine Phosphatases
RT	Room Temperature
S. cerevisiae; Sc	*Saccharomyces cerevisiae*
S. pombe; Sp	*Schizosaccharomyces pombe*
thioAs	Thioarsenates
Trx	Thioredoxin
WB	Westernblot
WHO	World Health Organization
WT	Wild-Type
YNB	Yeast Nitrogen Base

Nomenclatures

The following text applies the current nomenclatures for the names of genes and gene products of the respective organisms mentioned. *S. pombe* gene names are written in lowercase italics (e.g. *ggt1*), while protein names are non-italicized with the first letter capitalized (e.g. Ggt1). Mutant names are written in italics with lowercase letters[1]. *S. cerevisiae* gene names are italicized in uppercase letters (e.g. *ECM38*), and protein names are non-italicized with the first letter capitalized (e.g. Ecm38). Mutant names are italicized in lowercase letters[2]. For plant mutant lines, gene names are written in italicized uppercase letters (e.g. *HAC1*), while protein names are non-italicized, also with capital letters (e.g. HAC1)[3]. Gene names of *E. coli* are also italicized, consisting of three lowercase letters, with an uppercase letter added to distinguish between genes with the same mnemonic." (e.g. *glpF*). Protein names are non-italicized with the first letter capitalized (e.g. GlpF). Mutant names are italicized in lowercase letters[4]. For vertebrates, gene names are italicized with capitalized letters (e.g., *AQP7*), while protein names are not italicized, but are also written in capital letters (e.g., AQP7)[5].

II. Summary

Research on the uptake and metabolism of various arsenic compounds, including the organic compounds MMA and DMA as well as the inorganic forms As^{III} and As^{V}, has significantly deepened our understanding of these processes over the past two decades. Concurrently, strategies to minimize arsenic exposure have been developed. A previously overlooked group of compounds, the thioarsenates (particularly monothioarsenate (MTA) and dimethylthioarsenate (DMMTA)), has gained attention due to advances in analytical and sample extraction methods[6,7]. Toxicological studies have shown these compounds to be more toxic than MMA and DMA, and in case of DMMTA, even more toxic than As^{III} and As^{V}. They have been detected in rice and rice products worldwide[8,9], highlighting their importance in food safety.

Against this background, it was necessary to investigate the uptake and metabolism of this new group of arsenic compounds in greater detail. By utilizing multiple model organisms, this work offers new insights into the uptake and detoxification of MTA and DMMTA, as well as broader mechanisms of As^{III} tolerance in the absence of phytochelatins.

For the first time, it was demonstrated that MTA is taken up via P_i transporters in *A. thaliana* and *S. cerevisiae* similarly to As^{V}. Both, the loss of a P_i transporter (*pht1;1* in *A. thaliana*, *pho84Δ* in *S. cerevisiae*) or an impaired P_i starvation response (*phr1-1phl1* in *A. thaliana*) led to reduced MTA uptake and translocation. These differences were also reflected in vital parameters such as anthocyanin concentrations, fresh weight, root length, and chlorophyll content, which indicated delayed MTA uptake in the mutants compared to the wild type. Furthermore, thiol profiles after exposure to MTA and As^{V} showed comparable levels of PC formation across all genotypes, indicating that differences in uptake and translocation were not due to variations in sequestration rates.

Although the question remains as to whether As^{V} reductases contribute to the conversion of MTA to As^{III}, a non-enzymatic conversion of this compound was demonstrated in protein extracts from *E. coli* and *S. pombe*. Elemental analyses of root and shoot samples from *A. thaliana* exposed to MTA and As^{V} under P_i-deficient conditions revealed differences in translocation, suggesting further divergences between these two P_i analogs.

A key starting point for identifying relevant candidate genes in providing As^{III} tolerance was an As^{III} evolution project, which isolated four mutants with a *pcsΔ* background exhibiting significantly increased tolerance to As^{III}. Genome resequencing of these mutants (M1-M4) identified five single-nucleotide polymorphisms (SNPs) in coding sequences, including two in the E3 ligase *pof1* (M1, M3) and three in genes involved in GSH metabolism, specifically the γ-glutamyl transpeptidases *ggt1* (M2) and *ggt2* (M4). Only one SNP in the phospholipase-1 sequence (*plb1*) in the M2 mutant deviated from this pattern.

The increased tolerance of all mutants to As^{III} was also associated with improved tolerance to Cd and As^{V}. Knockout analyses of the γ-glutamyl transpeptidases and thiol profiling supported the hypothesis that elevated GSH concentrations played a significant role in the enhancement of tolerance levels.

In the investigation of the methylated sulfur-arsenic compound DMMTA, factors influencing its stability, toxicity, and uptake were identified. The resulting data suggest that DMMTA toxicity in *S. pombe* and *S. cerevisiae* is likely influenced by the carbon source. The reduced DMMTA toxicity in the presence of fructose instead of glucose appears to be of metabolic origin rather than uptake related. Furthermore, as part of the investigation of the mutants and the corresponding knockouts from the As^{III} evolutionary project, it was shown that the vacuole-localized γ-glutamyl transpeptidase 2 (Ggt2) in *S. pombe* may contribute to tolerance against DMMTA and DMDTA. In contrast, the loss of the endoplasmic reticulum-localized γ-glutamyl transpeptidase 1 (Ggt1) in the *pcsΔ*-background did not lead to increased sensitivity to DMMTA.

III. Zusammenfassung

Forschungen über die Aufnahme und Metabolisierung verschiedener Arsenverbindungen, darunter die organischen Verbindungen MMA und DMA sowie die anorganischen As^{III} und As^{V}, haben in den letzten zwei Jahrzehnten das Verständnis dieser Prozesse erheblich vertieft. Gleichzeitig wurden Strategien zur Minimierung der Arsenexposition entwickelt. Eine bisher wenig beachtete Gruppe von Verbindungen, die Thioarsenate (insbesondere Monothioarsenat (MTA) und Dimethylthioarsenat (DMMTA), geriet durch neue Analyse- und Probenextraktionsmethoden zunehmend in den Fokus[6,7]. Diese Verbindungen erwiesen sich in toxikologischen Studien als toxischer im Vergleich zu MMA und DMA und teilweise sogar als As^{III} und As^{V}. Sie konnten weltweit in Reis und Reisprodukten nachgewiesen werden[8,9], weshalb sie auch aus Gründen der Lebensmittelsicherheit von Bedeutung sind.

Vor diesem Hintergrund war es notwendig, die Aufnahme und Metabolisierung dieser neuen Gruppe von Arsenverbindungen genauer zu untersuchen. Durch den Einsatz verschiedener Modellorganismen konnten in dieser Arbeit neue Erkenntnisse über die Aufnahme und Detoxifikation von MTA und DMMTA, sowie über allgemeine Mechanismen der Toleranz gegenüber As^{III}, in Abwesenheit von Phytochelatinen gewonnen werden.

Erstmals wurde gezeigt, dass MTA über P_i-Transporter in *A. thaliana* und *S. cerevisiae* ähnlich wie As^{V} aufgenommen wird. Sowohl der Verlust eines P_i-Transporters (*pht1;1* in *A. thaliana*, *pho84Δ* in *S. cerevisiae*), als auch eine beeinträchtigte P_i-Mangelantwort (*phr1-1phl1* in *A. thaliana*) führten zu einer reduzierten MTA-Aufnahme und einer geringeren Translokation in den Spross. Diese Unterschiede spiegelten sich auch in Vitalparametern wie Anthocyan-Konzentrationen, Frischgewicht, Wurzellänge und Chlorophyllgehalt wider, die bei den Mutanten im Vergleich zum Wildtyp auf eine verzögerte MTA-Aufnahme hinwiesen. Darüber hinaus zeigten die Thiolprofile nach der Exposition gegenüber MTA und As^{V} vergleichbare PC-Bildungsniveaus in allen Genotypen, was darauf hinweist, dass Unterschiede in Aufnahme und Translokation nicht auf unterschiedliche Sequestrationsraten zurückzuführen sind.

Obwohl die Frage offenbleibt, inwieweit As^{V}-Reduktasen MTA in As^{III} umwandeln können, wurde eine nicht-enzymatische Umwandlung dieser Verbindung in Proteinextrakten von *E. coli* und *S.*

pombe nachgewiesen. Elementanalysen von Wurzel- und Sprossproben von *A. thaliana* nach Exposition gegenüber MTA und As^{V} unter P_i-Mangelbedingungen zeigten Unterschiede in der Translokation, was auf weitere Divergenzen zwischen diesen beiden P_i-Analoga hindeutet.

Ein Ausgangspunkt für die Identifikation relevanter Kandidatengene war das As^{III}-Evolutionsprojekt, bei dem vier Mutanten mit *pcsΔ*-Hintergrund isoliert wurden, welche eine deutlich erhöhte Toleranz gegenüber As^{III} aufwiesen. Die Resequenzierung der Genome dieser Mutanten (M1-M4) ergab fünf Single-Nucleotide-Polymorphisms (SNPs) in kodierenden Sequenzen, darunter zwei in der E3-Ligase *pof1* (M1, M3) und drei in Genen des GSH-Metabolismus, nämlich den γ-glutamyl-Transpeptidasen *ggt1* (M2) und *ggt2* (M4). Nur ein SNP in der Phospholipase-1-Sequenz (*plb1*) der M2-Mutante fiel aus diesem Muster.

Die erhöhte Toleranz aller Mutanten gegenüber As^{III} war mit einer verbesserten Cd- und As^{V}-Toleranz verbunden. „Knockout"-Analysen der γ-glutamyl-Transpeptidasen und die Bestimmung der Thiolprofile stützen die Hypothese, dass höhere GSH-Konzentrationen zu den erhöhten Toleranzniveaus beitrugen.

Bei der Untersuchung der methylierten Schwefelarsenverbindung DMMTA konnten Einflussfaktoren auf deren Stabilität, Toxizität und Aufnahme identifiziert werden. Die daraus resultierenden Daten deuten auf eine Abhängigkeit der DMMTA-Toxizität von der jeweilig verwendeten Kohlenhydratquelle in *S. pombe* und *S. cerevisiae* hin. Dabei scheint die verringerte DMMTA-Toxizität in Anwesenheit von Fruktose anstelle von Glukose nicht auf eine veränderte Aufnahme, sondern auf metabolische Prozesse zurückzuführen zu sein. Darüber hinaus konnte im Zuge der Untersuchung der Mutanten und der dazugehörigen „Knockouts" des As^{III}-Evolutionsprojektes gezeigt werden, dass die vakuolär lokalisierte γ-glutamyl-transferase 2 (Ggt2) in *S. pombe* eventuell zur Toleranzvermittlung gegenüber DMMTA respektive DMDTA beiträgt. Im Gegensatz dazu führte der Verlust der im endoplasmatischen Retikulum lokalisierten γ-glutamyl-transferase 1 (Ggt1) im *pcsΔ*-Hintergrund nicht zu einer erhöhten Sensitivität gegenüber DMMTA.

1. Introduction

1.1 An Invisible Threat: Toxic Metalloids and Heavy Metals and the Need for Preventive Strategies

While significant attention is given to developing clinical treatments for chronic diseases such as type II diabetes, cardiovascular disorders, and cancer[10–12], preventive strategies often receive less focus. Yet, millions of new cases could potentially be avoided by reducing exposure to environmental risk factors - particularly toxic xenobiotics. These foreign compounds, including toxic metalloids like arsenic (As) and heavy metals like cadmium (Cd), have been strongly linked to increased incidence of various pathologies, including cancer[12,13].

Avoiding or minimizing these toxic non-essential elements is a key preventive measure. However, due to widespread environmental pollution and the natural occurrence of these elements, unintentional exposure remains a major challenge. Unlike essential elements such as iron (Fe) or copper (Cu), which are required for physiological functions, non-essential elements like arsenic can exert harmful effects even in trace amounts[14].

Importantly, because these elements are not required by organisms, there has been no evolutionary pressure to develop specific uptake or metabolization mechanisms. This raises critical questions: Why are toxic non-essential elements taken up at all? And how do they interfere with cellular metabolism once inside the body?

Understanding the pathways of uptake, transformation, and detoxification of toxic non-essential elements is necessary for developing effective prevention strategies. This work aims to explore these questions for different arsenic species, a globally prevalent and highly toxic metalloid.

1.2 The Hidden Dangers of Arsenic: A Call for Revised Food Safety Guidelines

Known since ancient times, arsenic has been infamous as a poison and has been involved in numerous documented cases. One of the most prominent legends suggests that the Borgia family, particularly Pope Alexander VI and his daughter Lucrezia Borgia, used arsenic-befouled wine to eliminate their enemies through acute arsenic poisoning[15]. Though frightening, the symptoms of

acute arsenic toxicity include fever, abdominal pain, bloody diarrhea, hypertension, vomiting, coma, heart failure, and ultimately death.

In contrast to chronic arsenic poisoning, the number of acute toxicity incidents per year is almost negligible. Although the toxicity of As has been known since ancient times, the mechanisms affecting human health are not completely understood even today. Severe short- and long-term effects related to an ongoing exposure to this toxic metalloid are known. In populations exposed to high levels of As, an increase in various diseases can be observed. In the long-term, exposure to As increases the risk for diabetes type II[10,16], cardiovascular diseases[17,18], peripheral neuropathy[19,20] and in the case of pregnant women, a higher probability of miscarriages and developmental disorders[21,22]. Based on the relationship between As uptake and bodyweight especially women and infants[23] are the most vulnerable groups. Approximately 230 million people are exposed to elevated levels of this toxic metalloid day by day, in consequence of polluted groundwater and food[24]. Counterintuitively, the reasons for contaminated groundwater and food are not only related to anthropogenic sources, but also to the natural occurrence of As minerals[25]. However anthropogenic sources[26] like mining, industrial effluents or the use of arsenic containing pesticides in the past, were also shown to be responsible for the local occurrence of arsenic pollution. The predominant source of arsenic exposure to humans is contaminated groundwater followed by dietary sources like rice and seafood[27].

Countries like Cambodia[28,29], Vietnam[28], China[30], India[31], Pakistan[32], and Bangladesh[33] are just a few examples of regions where local rice cultivation is affected by the natural occurrence of arsenic in soil and groundwater. As mentioned above, rice - an important dietary component in many populations - contributes significantly to As uptake by humans in comparison to other cereals[34], accounting for up to 60% of dietary intake in China[35]. Although not directly linked, bioavailability, toxicity, and uptake are significantly influenced by the predominant species[36]. Due to the cultivation of rice in flooded soils, the trivalent arsenite (As^{III}) is the predominant inorganic form under the reducing conditions of paddy fields, whereas under aerobic, oxidizing conditions, the pentavalent arsenate (As^{V}) prevails. Methylated organic species such as monomethylated arsenate (MMA) and demethylated arsenate (DMA) likely result from microbial methylation

processes in the soil. For food safety concerns, many countries differentiate between organic (oAs) and inorganic arsenic species (iAs), as iAs are generally more toxic[7].

Currently, no specific recommendations or thresholds for oAs in rice and rice-based products have been set by the World Health Organization (WHO), the European Food Safety Authority (EFSA) or the Food and Drug Administration (FDA). Only a few countries worldwide include oAs species in their limits by setting threshold for total arsenic, due to their lower toxicity and a lack of evidence regarding long-term adverse health effects. In contrast, the inorganic ones are classified as Group I carcinogens by the International Agency for Research on Cancer (IARC)[13,37], meaning that there is sufficient evidence for the association of exposure to these species and the risk of cancer[38–41].

The latest update from the European Food Safety Authority (EFSA) also confirms a relatively low value for the so-called Margin of Exposure (MOE)[42], indicating a significantly increased risk for consumers, even on a continent where rice consumption is among the lowest globally. Values between 2.0 and 0.4 for average consumers and 0.9 and 0.2 for those with higher exposure are considered critical and point to an elevated risk of health damage even at low levels of exposure. Considering that this update only addresses the long-known inorganic arsenic compounds, it becomes evident that the actual health risk would likely be even greater if additional toxicologically concerning arsenic species were taken into account.

In recent years, a new debate arose about a possible blind spot in the detection of a certain group of As-species, overlooked by the standard acidic extraction-based analysis methods[7]. Thioarsenates are primarily formed under sulfur-reducing and often alkaline conditions, where As^{III} reacts with reduced sulfur species such as sulfide or elemental sulfur[9,43,44]. These conditions are commonly found in a wide range of natural environments, including geothermal waters, flooded soils, and paddy fields. Their presence in paddy fields has raised concerns about potential uptake by rice plants, similar to other arsenic species, or whether they remain confined to soil and water compartments. Importantly, thioarsenates are suspected to be as toxic as iAs species - or potentially even more harmful - posing a significant risk to food safety[7].

Usually, when As-totals (ΣAs) are not exceeded, sample speciation does not occur. However, when ΣAs are exceeded, thioarsenates (thioAs), such as monothioarsenate (MTA) and

dimethylthioarsenate (DMMTA), cannot be detected using the default methods employed in most laboratories. The most common sample preparation technique prior to speciation is based on acidic extraction at high temperatures using a microwave system. In the case of MTA, a conversion to the iAs-species As^{III} can be observed, while DMMTA converts to the oAs-species DMA[8]. This is particularly concerning because DMMTA is about four to seven times more cytotoxic than As^{III} [45,46]. Contrary, MTA, which is mistakenly identified as As^{III} with the standard analytical approach, is less problematic in respect to its lower toxicity in relation to As^{III}. Given the focus on iAs-species in most food safety guidelines, it becomes apparent why DMMTA, misidentified as DMA, may represent a potential blind spot[7]. With this in mind, the question arose, whether DMMTA can be found in substantial amounts in rice and rice-based products[8]. Previously published data provided evidence for the abundance of DMMTA and MTA, among other thioAs, in rice and rice-based products. Furthermore, a screening of 140 market-basket rice samples originating from six continents and 16 countries revealed an ubiquitous abundance of this highly toxic thioAs[9]. In fact, only two of the 140 samples tested were free of DMMTA, while concentrations in the remaining samples ranged from > 0.2 µg/kg to 30.4 µg/kg, accounting for 1.4 to 16 % of ΣAs.

Consequently, the requirement to rethink the actual guidelines and recommendations regarding the differentiation between oAs and iAs becomes apparent. Nonetheless, the recently published EFSA report "Update of the risk assessment of inorganic arsenic in food,"[42] recommends lowering the thresholds for iAs. However, a revised risk assessment for oAs, taking into account new findings regarding their potential origin from species with higher toxicity, is still missing.

1.3 Arsenic Uptake and Translocation: Current Knowledge and Challenges

To develop strategies for reducing adverse health effects caused by an ongoing exposure to arsenic, it is essential to understand the mechanisms underlying its uptake and detoxification. As is the case for other non-essential and toxic elements, such as Cd, arsenic uptake occurs inadvertently - that is, unintentionally and without a biological need, often as a byproduct of absorbing other essential nutrients. The uptake and toxicity of arsenic varies strongly depending on the predominant species present. Over the last two decades, substantial progress has been made in understanding the mechanisms involved in detoxification of the inorganic As-species (As^{III}

and As^{V}) and the organic As-species (MMA and DMA). Furthermore, several transporters and transporter families have been identified that are involved in the unidirectional- or bidirectional transport of those species.

In contrast, the transporters and detoxification mechanisms for most thioAs are much less understood due to a lack of analysis and sample preparation methods capable of capturing those species in the past[7]. Nevertheless, the knowledge derived from the investigation of the inorganic and organic As-species can be used as a point of departure to address the current issues of understanding uptake and toxicity of thioAs like MTA and DMMTA.

Preventing adverse health effects caused by arsenic ingestion highlights the importance of identifying transporters involved in the uptake and translocation of different As-species. This knowledge is crucial for developing strategies to lower As-content in our diet. Based on their relative toxicity, iAs species As^{III} (As^{III}: IC_{50} ≈ 72 -74 µM)[46,47] and As^{V} (As^{V}: IC_{50}: 1400/3914 µM)[46,47] have been the primary focus of most previous studies, as they are significantly more toxic compared to the oAs MMA (MMA: IC_{50}: 28000 µM)[46] and DMA (DMA: IC_{50}: 6030 µM)[46].

As a guide throughout this work, Figure 1 depicts the uptake and intracellular fate of the As-species mentioned above[48,49]. The schematic illustrates arsenic uptake and detoxification in *O. sativa* as a representative of higher plants and one of the most important food crops, as well as in *S. cerevisiae* and *S. pombe*, which are key eukaryotic model organisms for investigating these processes.

1.3.1 Uptake and Translocation of the Inorganic Arsenic Species

As a result of sharing physiochemical properties with inorganic phosphate (P_i)[50], the uptake and toxicity of As^{V} appear to be influenced by the ion promiscuity of enzymes and transporters toward both substrates. There is compelling evidence for As^{V} uptake via PHT1 transporters of the PHT1 family in plants, exemplified by the increased tolerance of *A. thaliana pht1;1* and *pht1;4* knockout lines upon As^{V} exposure, and by the involvement of the rice transporter OsPT8 in As^{V} uptake[51–55]. Heterologous expression of the *PvPHT1;3*[56] transporter of the As^{V} hyperaccumulating plant *Pteris vittata* revealed comparable affinities for P_i and As^{V}. Further evidence for P_i-transporter-mediated As^{V} transport has also been found for *E. coli*[57,58] and *S. cerevisiae*[59].

In addition to As^V also the inorganic thioarsenate MTA is suspected to be taken up via P_i-transporters[6,60]. Physiochemical similarities between MTA, As^V and P_i comprise their tetrahedral structure, comparable dissociation constants of MTA and P_i [$pK_{a2}(HAsSO_4^{2-}) = 7.3$; $pK_{a2}(HPO_4^{2-}) = 7.2$] and similar molecular weights of MTA and As^V [$MW(HAsSO_4^{2-}) = 155.99$ g/mol; $(HAsO_4^{2-}) = 139.93$ g/mol]. Experiments with the *A. thaliana* mutants *cad2*, *cad1-3*, *abcc1abcc2*[60] (see below for more details) and the observation of correlating uptake kinetics and toxic effects with the amount of P_i available[6], suggest that MTA and As^V may share similar uptake and detoxification mechanisms. However, direct evidence for their common uptake and detoxification is still lacking. These findings underscore the need for further investigation into shared and distinct mechanisms involved.

For As^{III} several transporters have been identified as being responsible for its uptake and translocation. They belong to the Major Intrinsic Protein Family (MIP) (Fig. 1). In the budding yeast *Saccharomyces cerevisiae,* two routes for As^{III} uptake are known, contributing to approximately 90 % of the overall uptake.[61] Under hexose-limited growth conditions, about 20-25% of the observed AsIII uptake is mediated by the aquaglyceroporin (AQP) Fps.[62]. In both cases As^{III} can be transported bidirectionally. Overexpression of *FPS1* leads to enhanced As^{III} tolerance due to higher efflux levels, whereas loss of function mutations result in higher tolerance by reducing uptake. Due to the high redundancy of hexose transporters[63], knockout of a single transporter does not significantly affect the capability of glucose rather than As^{III} uptake. By creating the *S. cerevisiae* strains EBY.VW367$^+$ (and EBY.VW4000)[64] using the Cre/loxP-system, mutants were generated that lack all high-affinity hexose transporters, rendering them unable to grow in presence of glucose. Interestingly, additional knockout of the *FPS1* gene in a mutant lacking all hexose transporters and the As^{III} efflux transporter Acr3 revealed the major role of hexose transporter in As^{III} uptake under hexose-depleted conditions. This ultimately provided evidence that hexose transporters account for up to 70-80% of total As^{III} uptake in the absence of glucose *in S. cerevisiae*. Additionally, based on quantitative proteomic approaches[65], a subset of glucose transporters was identified as being proteasomally degraded upon As^{III} treatment. In the case of the glucose transporters ScHxt2 and ScHxt7, arsenic-dependent ubiquitination sites were identified, enabling the targeted downregulation of these transporters, resulting in reduced As^{III}

uptake. Further evidence for the involvement of glucose permeases in uptake and translocation of As^{III} was provided by experiments showing the GLUT1[66] and GLUT3[67] mediated transport of As^{III} in mammalian cells. Recently, evidence was found that the expression levels of *GLUT3* in human

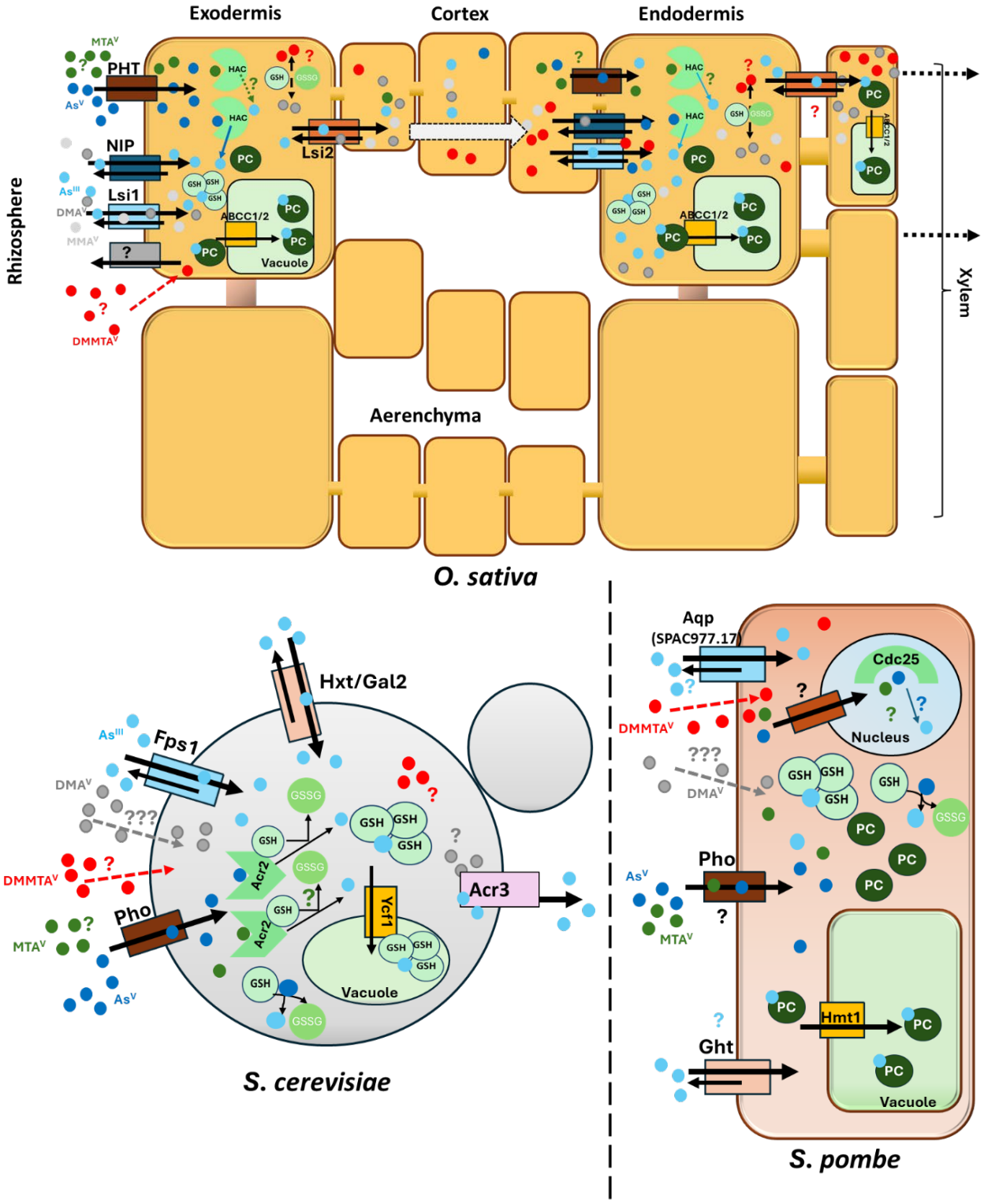

Fig.1: Overview of arsenic uptake and metabolism in *O. sativa* (top), *S. cerevisiae* (bottom left) and *S. pombe* (bottom right). The schematic illustrates the uptake and metabolism of different arsenic species. DMMTA (red), DMA (grey), As^{III} (pale blue), As^{V} (dark blue), MTA (green). Arrows indicate the direction of transport. PC (Phytochelatins), GSH (Glutathione, reduced), GSSG (Glutathione disulfide, oxidized). Question marks indicate mechanisms of uptake or metabolism that are not well characterized. Members of the MIP family, including NIPs are shaded pale blue and aquaglyceroporins are NIPs (Lsi1; Fps1; SPAC977.17) are shaded dark blue. P_i transporters (PHT; Pho) are shown in brown, hexose permeases (Hxt; Gal2; Ght) in pale red, As^{III}-efflux transporters in lilac, Arsenite-Antimonite (ArsB) transporter family member (Lsi2) in orange and vacuolar membrane transporters of the ATP-Binding Cassette (ABC) (ABCC1/2 in rice there is only ABCC1; Ycf1; Hmt1) in yellow. As^{V} reductases (HAC; Acr2) and protein tyrosine phosphatases (Cdc25), which catalyze or are proposed to catalyze the reduction of As^{V} (and potentially MTA) to As^{III}, are shown in green. The figures illustrating arsenic uptake and detoxification in *O. sativa* and *S. cerevisiae* are inspired by and adapted from Fang-Jie Zhao et al., (2021)[49] for *O. sativa* and Ewa Maciaszczyk-Dziubinska et al., (2012)[48] for *S. cerevisiae*.

cells also change upon As^{III} exposure, whereas transporter downregulation in *S. cerevisiae*[65] was shown to be the consequence of a post-transcriptional response.

Another subgroup of the major facilitator family (MST) has also been reported for its capacity to mediate As^{III} transport. In *A. thaliana*, knockout of the inositol symporter-encoding genes *AtINT2* and *AtINT4* significantly reduced the accumulation of As^{III} in shoots, siliques, and seeds[68]. By contributing to As^{III} seed accumulation, these transporters present promising candidates for strategies aimed at reducing As^{III} grain accumulation.

As one of the main sources of arsenic intake by humans, many studies have focused on understanding the uptake and detoxification processes of different As-species, particularly As^{III}, in rice. Due to the anaerobic conditions in paddy fields, rice accumulates higher amounts of As^{III}, compared to other crops, as well as ΣAs, owing to the higher bioavailability[69] of this As-species. Similar to *S. cerevisiae* Fps1[62], mammalian AQPs[70] and *E. coli* GlpF[71], aquaglyceroporins in *O. sativa* also contribute to As^{III} uptake. All three NIP-family subgroups have shown the capacity to transport As^{III}. Ma et al. (2008)[72,73] identified the silicon transporter *OsLsi1* as the most promising candidate due to its high expression levels among the *NIP* genes tested. Indeed, exposing the mutant line *lsi1* to As^{III} in absence of silicon resulted in a 53% reduction in As^{III} root levels and a 71% reduction in shoots levels. OsLsi2 which is not related to OsLsi1 and is not a member of the NIP-family, has been shown to act as silicon-efflux transporter, responsible for transporting Si from the exo- and endodermis to the stele[74]. Field experiments comparing As^{III} uptake in an *lsi1*

mutant together with two different *lsi2* mutants showed that only in the shoots and grains of the *lsi2* mutants, the As concentration was significantly reduced[73].

1.3.2 Uptake and Translocation of Organic Arsenic Species and Thioarsenates

Methylated oxyarsenates can be formed by microorganisms[75] from the iAs-species As^{V} and As^{III} under anaerobic conditions such as those found on rice paddy fields[76]. Like As^{III}, also the methylated As-species MMA^{V} and DMA^{V} have been shown to be transported through members of the aquaglyceroporin family[77,78]. In rice, OsLsi1 appears to be one route for MMA^{V} and DMA^{V} uptake, whereas the translocation of these species remains largely unclear. Knockout of the peptide transporter OsPTR7 in rice [79] led to reduced As accumulation in shoots and grains, when the plants were exposed to DMA^{V}. Interestingly, DMA^{V} is known to be much less toxic than the iAs-species in humans[11]. However, there are conflicting data in respect to the toxicity of this As-species towards plants[80–82].

Nevertheless, it is widely accepted that DMA^{V} is taken up by plants at a much slower rate compared to other As-species, such as the iAs species and thioarsenates[80,83]. Once inside the plant, DMA^{V} exhibits considerably higher mobility, resulting in faster translocation to shoots and grains[81].

One hypothesis that may explain the opposing toxic effects caused by DMA^{V} towards plants, is its conversion to DMMTA through thiolation processes within the plant. The methylated thioarsenate DMMTA has already been shown to be highly toxic in *A. thaliana*, causing a significant reduction in photosynthetic pigments, accumulation of anthocyanins and strong ROS formation[81]. These effects were less pronounced when plants were treated with As^{III} or absent when treated with DMA^{V}. Moreover, a recently published article provides evidence for the conversion of DMA into DMMTA by thiolation processes[84]. In both *O. sativa* and *A. thaliana,* plants exposed to DMA or DMMTA exhibited significant conversion of the species via thiolation and dethiolation processes, respectively. GSH-deficient mutants of *A. thaliana*, lacking the γ-glutamylcysteine synthetase (*cad2-1*) or the glutamate-cysteine ligase (*pad2-1*), showed significantly reduced thiolation, when exposed to DMA^{V}, demonstrating that DMA thiolation depends on sulfur-containing metabolites of the GSH cycle. These findings align with the

understanding that the formation of methylated thioarsenates involves a nucleophilic attack of sulfide on MMA or DMA[85].

The observed differences in uptake and translocation kinetics, stability and contributions to ΣAs of methylated thioarsenates and MTA in rice plants[83] suggest variability in uptake and/or detoxification mechanisms within the group of thioarsenates. Unlike MTA, there is currently no evidence pointing to specific transporter candidates for DMMTA. Additionally, the physiochemical properties of DMMTA such as the pK_a and its impact on uptake and toxicity, remain unanswered to date.

1.4 As-Detoxification Mechanisms in the Context of Evolution

First, the term "detoxification-mechanism" can be misleading, although it is commonly used in the literature. In the context of evolution, several questions arise. What is the reason for the widespread occurrence of mechanisms that lead to the transformation of less toxic to more toxic As-species, such as the enzymatically driven transformation of As^{V} to As^{III} by As^{V}-reductases[86,87]? How did these mechanisms spread across the different kingdoms of life? Why did they persist in descendants living in environments with minimal arsenic exposure? The following section clarifies the traditional use of the term "detoxification mechanisms," explains why it can sometimes be misleading, and highlights that, in some cases, the detoxification function is secondary or coincidental.

To understand the evolution of mechanisms providing arsenic tolerance, a retrospective into Earth's history is necessary. Bioavailability, and consequently toxicity, of arsenic has changed dynamically, influenced by factors such as global climate changes, the redox state, and disruptions like volcanic eruptions[88,89]. From the outset, the first organisms had to cope with high levels of the toxic inorganic arsenic species As^{III}. In this anaerobic atmosphere - resulting from the absence of oxygen-producing photosynthetic organisms - the abundance and bioavailability of arsenic were clearly enhanced, and As^{III} was the predominant form of bioavailable arsenic[90], while As^{V} was only present in low quantities. Approximately 2.4 billion years ago, the "Great Oxidation Event" (GOE) led to an enrichment of Earth's atmosphere with oxygen[91], causing a tremendous shift in the global composition of As-species over a relatively short period from an evolutionary

perspective. In response to changes in atmospheric oxygen levels, arsenic speciation has shifted multiple times throughout Earth's history, contributing as an evolutionary driver (Fig.2)[47,87,90–105].

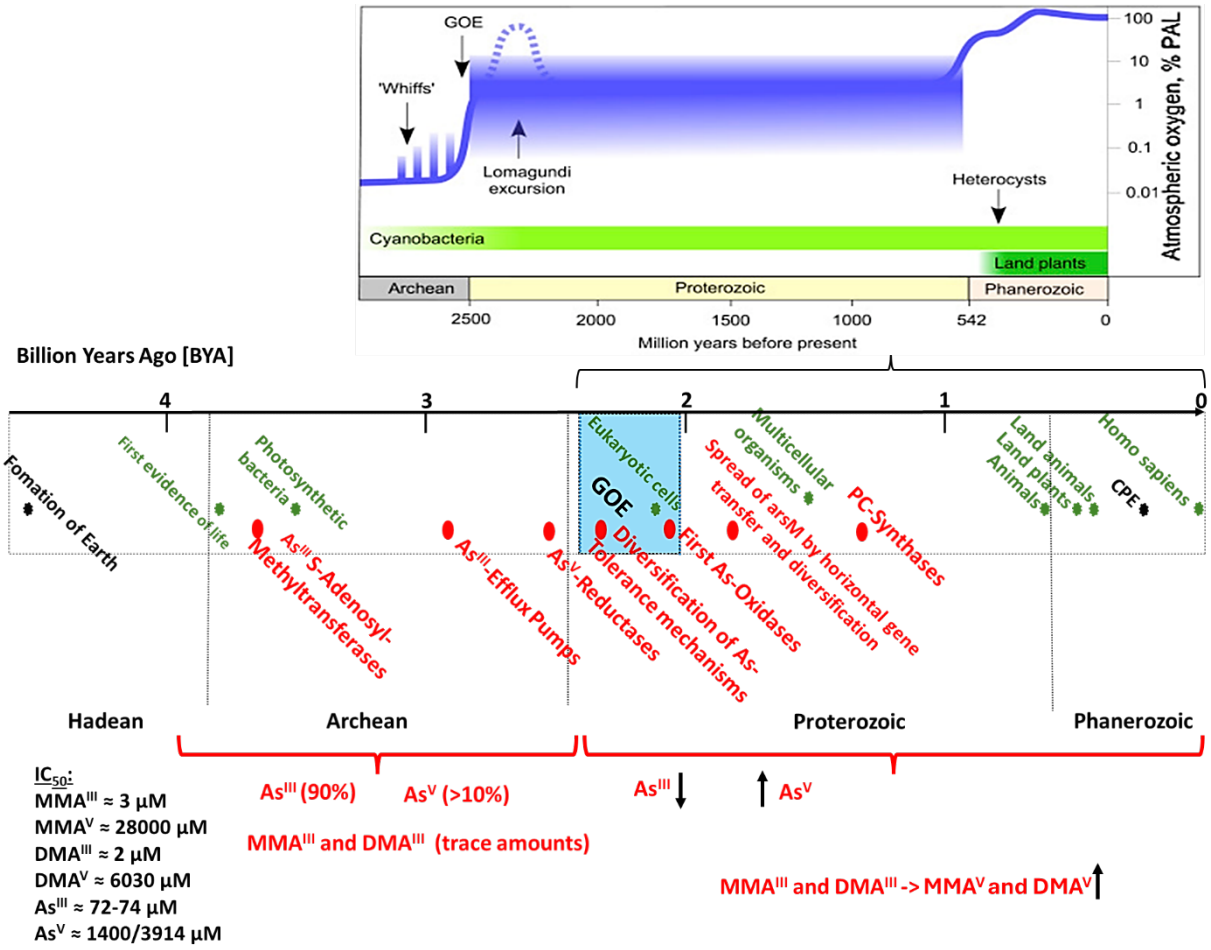

Fig.2: Timeline of Earth's history. This figure highlights key evolutionary milestones (green) on a geological timescale. The gradual oxygenation of Earth's atmosphere following the "Great Oxidation Event" (GOE) is emphasized (blue), with oxygen levels depicted in the section above based on John F. Allen et al. (2019)[90]. Red dots indicate the approximate emergence of various arsenic tolerance mechanisms. The most relevant arsenic species are shown below the timeline, with their approximate distribution before the GOE indicated in brackets, and arrows depicting changes in their percentage share after the GOE. The IC_{50} values of various organic and inorganic arsenic species are presented in a table (bottom left). "Cretaceous-Paleogene Extinction" (CPE).

1.4.1 Methylation of Arsenic: Emergence for Detoxification or Toxification?

As^{III} S-adenosylmethionine methyltransferases (SAM) originated more than 3.5-3.7 billion years ago and spread across distinct kingdoms of life through horizontal gene transfer (HGT)[92,106]. Phylogenetic analyses have revealed a common ancestral origin of methyltransferase (ArsM), which can be found in bacteria, archaea, animals and fungi[106]. There is evidence supporting six events of HGT, leading to the widespread distribution of *arsM* orthologs, such as *AS3MT* in mammals.

It is noteworthy that, even though methylated As-species can be found partially in high quantities in plants[107], plants lack the ability to convert iAs into oAs. Therefore, the methylated As-species, and indirectly also the methylated thioAs, found in plants are derived from microbial processes in the soil[75,83]. Under aerobic conditions, the methylation of As^{III} to the trivalent species MMA^{III}/DMA^{III}, followed by subsequent non-enzymatical oxidation to the pentavalent forms MMA^{V}/DMA^{V}, is a key mechanism in detoxifying iAs and is widespread across different phyla.

Counterintuitively, these enzymes, which are known to contribute to higher arsenic tolerance, evolved in an anaerobic atmosphere, catalyzing the transformation of less toxic As^{III} into the extremely toxic methylated trivalent species MMA^{III} ($IC_{50} \approx 3$ µM)[46] and DMA^{III} ($IC_{50} \approx 2$ µM)[46]. One hypothesis regarding the evolution of As^{III} SAMs before the GOE suggests that these enzymes evolved to produce MMA^{III} as an antibiotic against competitors[108]. In light of the ability of some soil microbes to reduce MMA^{V} to MMA^{III} [109], and in the absence of the capacity for demethylation, this hypothesis becomes even more plausible.

Meanwhile, the investigation of arsenic methylation has gained attention in studies of arsenic toxicity in plants. A recent article shows a correlation between soil redox state, DMA concentration, *arsM* abundance and the occurrence and severity of rice straighthead disease[110]. Based on their findings, A-X. Gao et al. (2024), emphasized that in depending on the soil's redox state and microbial composition, the formation of highly toxic trivalent methylated As-species (MMA^{III}, DMA^{III}) might be supported, thereby increasing the frequency and severity of straighthead disease. However, as an alternative explanation, the formation of the thioarsenate DMMTA cannot be excluded[84].

1.4.2 Energy-Driven Efflux and Oxidation of Trivalent Species

In addition to SAMs, another mechanism providing arsenic tolerance evolved prior to the GOE and is not found in higher plants. While efflux of As^{III} has already been shown to occur from plant roots to the rhizosphere[111], this efflux is mediated by aquaglyceroporins such as OsLsi1 being known to transport As^{III} and DMA bidirectionally[112]. But unlike As^{III} efflux pumps such as ScAcr3[101] in *S. cerevisiae* and arsB[71] in *E. coli*, this transport is passive and gradient-dependent. Therefore, it is not surprising that the aforementioned *lsi1* mutant did not show appreciable differences in arsenic accumulation in grains and shoots[73]. Conversely, heterologous expression of ScAcr3 was shown to be a promising approach to reduce ∑As in rice grains[113].

The first evidence for an ancestor of *ACR3*, a member of the bile/arsenite/riboflavin superfamily (BART)[114], emerged approximately 3 billion years ago[92], while the arsB family (subfamily of MFS) probably originated 2 billion years ago. Another group of efflux pumps, the so-called methylarsenite efflux permeases such as arsP, primarily found in anaerobes and frequently in co-existence with arsM[106], enable their host to detoxify the even more toxic trivalent As-species MMA^{III} and DMA^{III}. Again, the frequent co-existence of arsM and arsP, especially in anaerobes, supports the hypothesis that these mechanisms evolved for antibiotic defense rather than for detoxification in an anaerobic environment[115].

Even though the evolution of arsenic oxidases (arsH) might have enabled the oxidation of pentavalent methylated species prior to efflux by arsP, phylogenetic and functional analysis are inconsistent with this hypothesis. On the one hand, arsH activity is O_2 dependent[116] and inoperable under anaerobic conditions. On the other hand, phylogenetic clustering apart from arsM[106], along with an estimated emergence 1.7 billion years after arsM (Fig.2 and Tab.1), makes it unlikely that both enzymes share a common trajectory.

Evolutionary imprints related to changes in the bioavailability and distribution of As-species are especially concentrated around the GOE[92]. In general, the constitutive oxygenation of Earth's atmosphere was a key driver in the evolution of mechanisms providing arsenic tolerance. Particularly in environments with changing arsenic abundance and the composition of As-species, there was pressure for rapid adaptations to these altered conditions. An increase in pentavalent oxyarsenates and a decrease in trivalent oxyarsenites could have led to a loss of importance of

already evolved mechanisms providing arsenic tolerance. However, neither a reduced functional relevance nor a complete loss of these early evolved detoxification mechanisms is necessarily the outcome, as will be discussed further below.

1.4.3 As^{V} Reductases: Revival of Established Detoxification Mechanisms?

An evolutionary showcase for a family of enzymes that arose at least three times independently by convergent evolution in response to this altered redox conditions are As^{V} reductases[86]. The reduction of the less harmful iAs As^{V} to the highly toxic As^{III} appears counterintuitive. However, it enabled the rehabilitation of the earlier evolved detoxification mechanisms in an anaerobic environment. These group of enzymes can be clustered into three different families of independent origin[117]. One family of reductases, comprising the As^{V} reductase R773 of *E. coli*, uses glutathione (GSH) and glutaredoxin (Grx) as reductants, while another family, including *S. aureus pI258 arsC*, uses thioredoxin (Trx) as electron donor. A third family, found only in eukaryotes also uses GSH and Grx for catalyzing the reduction of As^{V} to As^{III} [118]. The *S. cerevisiae* ScAcr2[119], *A. thaliana* AtHAC1[120] and *O. sativa* OsHAC4[121] are members of this family, which is also known as Protein Tyrosine Phosphatase (PTP) family.

Although the fate of As^{III} derived from the reduction of As^{V} differs depending on the organism, the predominant function is the detoxification of intracellular arsenic. While in *S. cerevisiae* and *E. coli*, As^{III} is mainly detoxified via extrusion through efflux pumps[122] in higher plants complexation via thiol compounds followed by vacuolar sequestration is the predominant fate[123,124]. Complexation via thiol compounds followed by vacuolar sequestration and/or efflux via specific transporters, as well as methylation of As^{III} are all part of strategies contributing to convey tolerance.

However, detoxification is not always the purpose when it comes to the enzymatic reduction of As^{V}. Unlike the As^{V} reductases of the three cytoplasmically localized enzyme families, there is a special case of so-called respiratory As^{V} reductases that are localized in the periplasmic space of Gram-negative bacteria[103]. These enzymes are coupled to the respiratory chain to provide energy under anaerobic conditions, using As^{V} as a terminal electron acceptor[117]. Nonetheless, this type

of reductase is only expressed at subtoxic As^{V} levels and is replaced by the expression of the *ars*-operon, when toxic concentrations are exceeded.

For the sake of completeness, not all detoxification mechanisms derived from the changes during and after the period of the GOE operate through the revival of the formerly evolved mechanisms by reduction of the pentavalent oxyarsenates. Detoxification in heterotrophic bacteria[116,125] via oxidation of highly toxic trivalent species to the pentavalent ones, as well as energy generation in chemolithoautotrophic[126] and chemoheterotrophic bacteria[127], has been shown by this class of enzymes.

1.4.4 Low Molecular Weight (LMW) Thiols: A Broad Group of Complexing Agents

Even essential elements can cause toxicity when present in excess[98], making it indispensable to tightly regulate the homeostasis of micronutrients. Across all kingdoms, thiol rich compounds, in particular, play a crucial role in minimizing the amount of unbound micronutrients. In addition to this, low-molecular-weight thiols (LMW), including GSH, metallothioneins (MTs), Phytochelatins (PCs) and others, contribute to the detoxification of non-essential elements like Cd and As[128–130]. In the case of arsenic detoxification, complexation prior to efflux and/or vacuolar sequestration is facilitated by the binding of As^{III} to the sulfhydryl-group of this cysteine-rich peptide compounds[128]. In addition to their role in direct detoxification through complexation of these toxic species, they also contribute to arsenic tolerance by mitigating secondary impacts e.g. through their action as ROS-scavengers[131,132].

The tripeptide GSH (L-γ-glutamyl-L-cysteinyl-glycine) can be found in plants, mammals, fungi and several prokaryotic organisms[133–136]. Besides its role as ROS-scavenger and participation in ROS-signaling, GSH is pivotal for maintaining the cell's redox state[137]. The ratio of the oxidized form glutathione disulfide (GSSG), to its reduced form glutathione (GSH), is controlled by the GSH-reductases (GR)[138,139]. Being a major source of reduced sulfur, it is no surprise that GSSG:GSH ratio in healthy tissue is maintained around 0.05, or even lower depending on the cellular compartment[140].

Enzymatically catalyzed in a two-step ATP-dependent reaction, the process starts with the conjugation of glutamate and cysteine to γ-glutamylcysteine (γ-EC) via GSH1 (in plants), followed

by the subsequent addition of glycine via GSH2 (in plants), resulting in L-γ-glutamyl-L-cysteinyl-glycine (GSH). The atypical ω-peptide bond between the γ-carboxy (instead of the α-carboxy group) of glutamate and the amide group of cysteine protects GSH from hydrolysis by peptidases[141]. Nevertheless, the breakdown of GSH has been reported for other enzymes, including γ-glutamyl-transpeptidases (GGTs)[142,143].

In plants, mammals and yeasts such as *S. pombe* and *S. cerevisiae*, intracellular GSH concentrations are in the range between 1-10 mM[144,145] and are divided into three main intracellular pools[146]. The vast majority of GSH can be found in the cytosol (80-85 %), while the remaining GSH is primarily located in mitochondria and – in the case of plants - chloroplasts (10-15%)[147], with a smaller fraction allocated to the endoplasmic reticulum (ER). Although the cytosol serves as the main GSH reservoir, the highest concentrations are typically found in other compartments. In *A. thaliana*, the highest GSH-concentrations have been shown to occur in mitochondria (15 mM) and nuclei (6.4 mM), followed by the cytosol (4.5 mM), peroxisomes (4.4 mM), chloroplasts (1.2 mM) and the vacuole (0.08 mM)[148]. In *Arabidopsis thaliana*, GSH biosynthesis involves both an incomplete cytosolic pathway, which alone cannot fully synthesize GSH[149], and a plastidic pathway that is capable of complete GSH synthesis[150]. In mammals and *A. thaliana*, mutations resulting in a loss of GSH biosynthesis have been shown to be lethal[151–153]. Considering the abundance of a second highly concentrated antioxidant in plants (ascorbate), it becomes apparent that the role of GSH extends beyond ROS-scavenging.

However, contrary to eukaryotes, GSH is less far distributed within prokaryotes, and other LMW thiols emerged acting as GSH analogs[135]. Many of them had already evolved prior to Earth´s oxygenation and consequently did not develop to protect against the hazards of aerobic metabolism. Nonetheless, increasing oxygen levels brought a higher risk of autoxidation, to which free cysteine is prone[154]. The presence of heavy metals and especially some metalloids like arsenic (particularly As^{III}), accelerates the process of autooxidation by binding to the sulfhydryl-group, thereby promoting the formation of oxygen radicals up to twofold faster than GSH. This illustrates the advantages of GSH as reservoir of reduced sulfur[155,156]. Additionally, GSH provides protection for proteins from oxidation, e.g. caused by Cd or As^{III}, through thiol-disulfide exchange and the formation of mixed disulfides before ROS can develop[157]. Complexation prior to efflux from the

cell and/or sequestration into the vacuole has been shown to play a major role in several organisms in preventing ROS formation[158].

1.4.5 Phytochelatins: Combining Metal Homeostasis and Detoxification

Phytochelatins (PCs), another group of LMW thiols, are found in higher plants[98], nematodes like the nematode *C. elegans*[159], some fungi such as *S. pombe*[160], and certain bacteria and algae[161]. PCs are non-translationally synthesized small peptides, formed by transferring a γ-Glu-Cys moiety from one GSH molecule to another GSH (PC2)[162] or onto already produced PCs for chain elongation (PC_n). This process results in the general structure of $(\gamma\text{-Glu-Cys-Gly})_n$-Gly (n=2-11)[163]. Evidence for the induction of PC biosynthesis[164,165], as well as the formation of complexes with toxic elements such as As^{III}, Cd^{2+} or essential elements Cu^{2+}, Zn^{2+} has been shown more than two decades ago[166]. Although PCs play a crucial role in the detoxification of As^{III} and Cd through chelation and subsequent vacuolar sequestration, they also contribute to the accumulation and distribution of these elements within the plant tissue[123,163,167].

Notably, whether the induction of PC formation is directly driven by the interaction of these metals/metalloids with the PCS, or indirectly stimulated through an unknown mechanism, remains an open question. Induction of PC synthesis at transcriptional or translational level plays a minor role, given the constitutive expression of PCS and the proven capability of crude protein extract from plants grown under control conditions to generate PCs upon the addition of Cd^{2+} [162,168,169].

Moreover, differences in the affinity of rice OsPCS1 and OsPCS2 for activation by As^{III} and Cd^{2+} have been reported, suggesting two distinct pathways for detoxifying these toxic elements[170,171]. Currently, there is limited understanding of how the presumed discrimination between these elements manifests in the differential activation of OsPCS1 and OsPCS2.

Phylogenetic analysis supports the hypothesis of a prokaryotic origin for early PCS-like genes, which spread to eukaryotic organisms through multiple events of horizontal gene transfer[172]. The evolutionary manifestation of phytochelatin synthases includes numerous duplications, losses, and insertions of full-length PCS genes in green algae and vascular plants. Evidence suggests that the acquisition of PCS genes via HGT under environmental stress is more plausible for

extremophilic algae[173] than for vascular plants, where the spread of PCS genes appears to follow a different origin[174].

Still, the question remains whether these enzymes initially evolved for the detoxification of toxic elements or for metal homeostasis. It is also plausible that, once evolved for one purpose, environmental changes led to functional adaptations, resulting in the acquisition of ambiguous roles.

1.4.6 Enhancing Arsenic Tolerance: Improving Transport Specificity and Expanding the Detoxification Machinery

The habitats of most organisms generally do not exhibit significant contamination with As or Cd. Therefore, the lack of selective pressure to gain further tolerance raises questions about whether most tolerance mechanisms evolved specifically in response to these toxic elements, and how these mechanisms have been maintained over time. Apart from primitive prokaryotes that were exposed to high concentration of highly toxic trivalent As-species, most prokaryotic and all eukaryotic organisms emerged during periods in Earth's history when As-bioavailability and toxicity were strongly reduced after the GOE[175]. Various hypotheses, including pleiotropy of genes involved in arsenic tolerance[176], evolutionary legacy[177] and cross protection[178,179], are discussed and supported by several findings. For instance, *Xanthomonas oryzae* (IXO1088) exhibits cross-protection through an *ars*-cassette, providing reduced susceptibility towards As^{III} and As^{V} exposure, while also enhancing its pathogenicity in rice. Similar associations of As-tolerance genes with ROS tolerance have been observed in various organisms.

In eukaryotes, a comparative study showed an interesting pattern of vertically inherited core arsenic tolerance genes, combined with an expansion through horizontal gene transfer[180]. Functional phylogenomic analysis has revealed a connection between the degree of arsenic susceptibility and the expansion of detoxification mechanisms through HGT events, for eukaryotes found in arsenic-contaminated environments. Thus, in arsenic-tolerant eukaryotic lineages, vertically inherited core arsenic tolerance genes are frequently complemented by a high prevalence of HGT-derived arsenic tolerance genes.

Organisms that are constitutively exposed to high arsenic levels and/or known for hyperaccumulation serve as important models for studying arsenic uptake and susceptibility. The fern *Pteris vittata* has been identified as As^{V} hyperaccumulating plant[56]. In contrast to other known members of the PHT1 family, PvPHT1;3 exhibits similar affinities for P_i and As^{V}, which is unique among the P_i-transporters that typically prioritize P_i uptake[181]. *P. vittata* unlike most plant species, can tolerate highly elevated arsenic concentrations of up to 100,000 mg/kg dry soil[182] (e.g. *O. sativa* ~70-100 mg/kg dry soil)[183], likely due to synergistic enhancements of its detoxification machinery. Despite extensive research aimed at elucidating the mechanisms underlying *P. vittate* As-tolerance[184–188], much remains to be understood about the orchestra of mechanisms involved. Elevated GSH-levels, increased upregulation of ROS scavenging mechanisms, As^{III}-efflux and efficient cellular compartmentalization of arsenic have been identified to contribute to *P. vittata*'s superior As-tolerance. Nonetheless, further investigations are needed to explore how this fern copes with different As-species beside As^{III} and As^{V}, conduct comparative metabolome analyses to gain insights into the mechanisms underlying tolerance, and perform structural analyses of PvPHT1;3 to better understand its lack of substrate selectivity.

An alternative strategy for coping with arsenic involves transporters with enhanced substrate specificity, which reduced arsenic uptake by minimizing the likelihood of being hijacked by arsenic. For example, the Atlantic killifish (*Fundulus heterolitus*), a model organisms for toxicological studies, is known for its reduced sensitivity to arsenic exposure[189]. A splicing variant of the AQP *kfAQP3a* in the Atlantic killifish has been shown to exhibit almost no capacity for As^{III} uptake, in contrast to the putative alternative splicing variants *kfAQP3b* and *kfAQP3c*, when heterologously expressed in HEK293 cells[190,191]. Another example of gaining arsenic tolerance through reduced uptake is the proteolytic degradation of hexose transporters in *S. cerevisiae*[65]. Upon As^{III} exposure, high-affinity hexose transporters are ubiquitinylated to be primed for proteasomal degradation, thereby decreasing As^{III} uptake rates.

1.4.7 Filling the Gap: Raising Synergies and Preventing Antagonisms?

Prominent models, such as bacterial *ars*-operons, suggest a constitutive acquisition of additional arsenic tolerance features. However, numerous puzzling observations persist regarding the distribution and evolutionary development of arsenic tolerance. While evidence unequivocally

supports the hypothesis of a constitutive increase of synergistically acting detoxification mechanisms across all domains of life[88,89,92,106,180], many questions concerning the remarkable distribution and combination of detoxification mechanisms remain unanswered. A closer examination of the occurrence and combination of different detoxification machineries reveals conspicuous distributions.

Albeit the initial step of As^{V} reduction is ubiquitous, subsequent steps of detoxification diverge into mainly two branches. Both As^{III} efflux and As^{III} complexation followed by sequestration are potent pathways of arsenic detoxification. Nevertheless, aside from some prokaryotes expressing PCS-like genes, the combined occurrence of efflux and complexation via PCs is restricted to some ferns, such as *P. vittata*, where PC formation plays only a minor role in detoxification.

The oma PSI-BLAST analysis[192] presented here as a Venn diagramm[193] (Fig. 3) illustrates the co-occurrence of the four main arsenic detoxification mechanisms: As^{V} reduction, As^{III} methylation, As^{III} efflux, and sequestration via phytochelatins. The analysis reveals a lower frequency of co-occurrence between phytochelatin synthases, such as AtPCS1 in higher plants, with As^{III} efflux transporters found in many prokaryotes (*ArsB*-family; *ACR3*-family) and eukaryotes (*ACR3*-family), compared to the co-occurrence of other mechanisms like As^{III} efflux and As^{V} reduction. This observation aligns with findings reported over 20 years ago and has been experimentally addressed.

Wysocki et al. (2003) have shown by heterologous expression of *TaPCS* and *SpPCS* in *S. cerevisiae*, that this leads to increased As^{III} but decreased As^{V} tolerance[194]. Furthermore, heterologous expression of the *S. cerevisiae* As^{III} efflux pump *ScACR3* in the *S. pombe* mutant *pcsΔ,* which lacks the ability to synthesize PCs, conferred superior arsenic tolerance compared to WT cells expressing *ScACR3*. Hence, the presence of both PC-Synthases and As^{III} efflux pumps seems to exhibit partially antagonistic effects.

One plausible explanation is that PC synthesis causes a strong depletion of the GSH pool, consequently affecting the GSH-dependent catalytic activity of the As^{V} reductase, reducing the amount of As^{III} available for extrusion. Additional evidence for this hypothesis, is provided by the

observation that *AtPCS1* overexpression in *A. thaliana* leads to hypersensitivity – rather than enhanced tolerance - toward Cd, an effect that is reversed upon GSH supplementation[195].

Alternatively, PC-As^{III} complexes may hinder the highly efficient detoxification by As efflux, which is normally mediated in form of unbound As^{III} [101,196]. However, contrary to the findings of Wysocki et al. (2003)[194], the co-occurrence of PC-synthases and potential As^{III}-efflux pumps appears to be more widespread than originally thought (Fig. 3), encompassing several prokaryotes as well as higher plants such as *Taxus chinensis*, *Triticum aestivum*, *Oryza punctata*, and *Ginkgo biloba*.

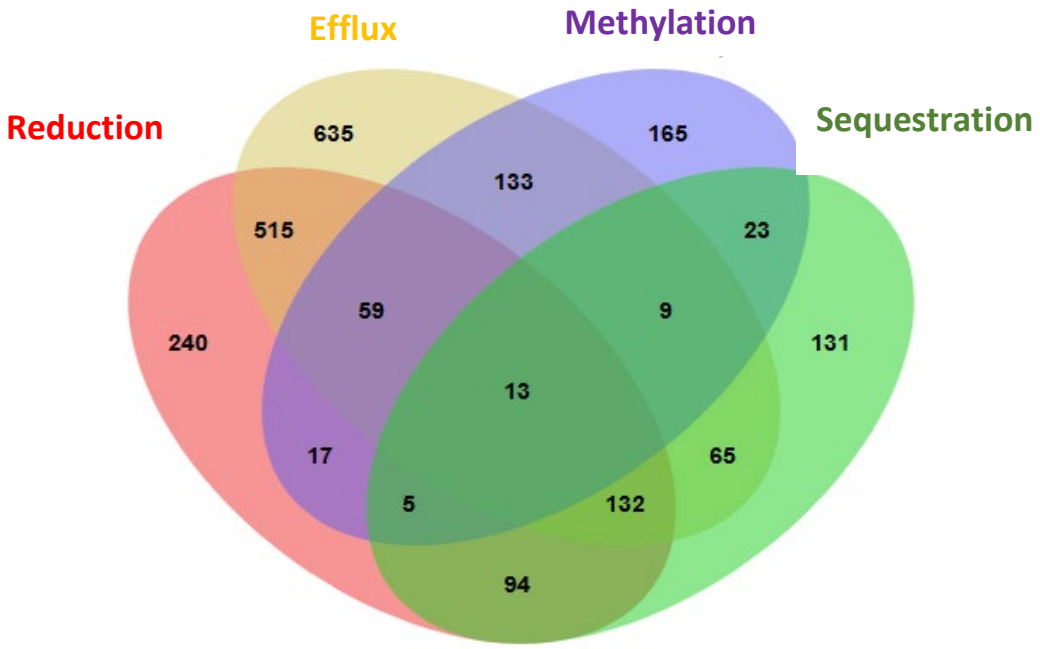

Fig. 3: Co-occurrence of detoxification mechanisms. The Venn[186] diagram illustrates the co-occurrence of mechanisms which provide arsenic tolerance, including As^{V} reductases (Reduction), As^{III} efflux pumps (Efflux), As^{III}-S-adenosyl-methyltransferases (Methylation), and phytochelatin synthases (Sequestration). These results are derived from an oma[185] PSI-BLAST search for orthologs.

Another case of mutually exclusive detoxification mechanisms might be the absence of arsenic methylation in higher plants. Surprisingly, heterologous expression of the S-Adenosyl-methyltransferase *CrArsM* from *C. reinhardtii* in *A. thaliana* resulted in heightened sensitivity to As^{III} [197]. It is questionable whether the observed toxicity is directly related to elevated levels of DMA^{V} considering its lower toxicity[81], or to the formation of undetected, more toxic species such as DMA^{III} and/or DMMTA. For the latter, thiolation of DMA^{V} to DMMTA has been shown previously[84], but not to an extent that could explain the described toxic effects.

The absence of arsenic methylation in higher plants, coupled with the ubiquitous presence of PC synthases, raises the question of whether these mechanisms create antagonistic effects rather than cooperating in detoxification. Considering the distribution of S-adenosyl-methyltransferases by horizontal gene transfer (Fig. 2), the lack of occurrence in PC synthesizing organisms appears conspicuous.

1.5. Choosing the Right Model

The following experiments were conducted with three different model organisms - *A. thaliana*, *S. pombe* and *S. cerevisiae* - each offering distinct advantages for the issues addressed. These widely used model organisms are valued for their short generation times, availability of mutant strains for almost all non-essential genes, relatively small genome sizes, ease of handling, and availability of established assays and gene editing methods. Additionally, each exhibits specific properties that make them ideal for the investigation of arsenic uptake and detoxification. Both processes have been investigated in all three models, with numerous articles published revealing transporters and detoxification pathways, as mentioned above.

In respect to the high concordance of transporter families responsible for the uptake of the different As-species in higher plants and the models *S. cerevisiae* and *S. pombe* (Fig. 1A-C), preliminary investigations in these unicellular organisms enable rapid screening for transporter candidates. Notably, *S. cerevisiae* has been one of the most important models for elucidating arsenic toxicity in eukaryotes for decades[198,199]. It is not surprising, therefore, that experiments with *S. cerevisiae* have contributed significantly to our understanding of arsenic uptake and detoxification.

Neither *S. pombe* nor *S. cerevisiae* are closely related to each other or to higher plants such as *A. thaliana*[200]. However, beside common uptake mechanisms they are also valuable models for the investigation of arsenic detoxification for various reasons. *S. pombe* is widely recognized as a model organism for studying eukaryotic cell cycle control and genetics. Beyond these applications, its ability to produce phytochelatins positions it as a useful model for preliminary studies on the role of these LMWs in detoxifying different arsenic species[201]. By contrast, *S. cerevisiae* is unable to synthesize PCs but known for its high capacity regarding As^{V} reduction and

As^{III} efflux, provides a robust platform for investigating the relevance of these mechanisms in providing arsenic tolerance[101].

Based on these advantageous traits, the aforementioned model organisms were used in this work to acquire further knowledge regarding the transporters responsible for the uptake of the thioarsenates MTA and DMMTA, and to investigate mechanisms providing tolerance against them. Moreover, the emergence of reduced As^{III} susceptibility within a so-called As^{III} evolutionary project using *S. pombe* as a model, was performed to gain insights into the mechanisms related to As^{III} detoxification.

1.6 Aim of this work

Over the past two decades, significant progress has been made in understanding arsenic uptake and toxicity. The identification of transporters exploited by arsenic, as well as the pathways it disrupts, has provided a substantial foundation for developing strategies to reduce the uptake of both inorganic and organic arsenic species that were known to be toxicologically relevant at the time. However, with advancements in sample preparation and speciation techniques, a new group of arsenic species, known as thioarsenates, has emerged as a focal point of toxicological interest.

This work aims to address the knowledge gap concerning the uptake and metabolism of this relatively unexplored group of arsenic species. Specifically, this work focuses on identifying transporters involved in the uptake and uncovering mechanisms that confer tolerance to the two most relevant thioarsenates, MTA and DMMTA. By combining the strengths of the model organisms *A. thaliana*, *S. pombe*, and *S. cerevisiae*, and building on existing knowledge of inorganic and organic arsenic species, similarities and differences in their uptake and metabolism were aimed to be identified. Especially, by leveraging the *S. cerevisiae* knockout collection and existing knowledge of several genes involved in the uptake and detoxification of inorganic arsenic species, it was investigated whether these candidates might also play roles in the uptake and detoxification of the thioarsenates MTA and DMMTA.

This research also involved establishing protocols for studying the uptake and detoxification of thioarsenates, as well as identifying candidate genes involved in their transport or metabolism.

These efforts are intended to provide a solid foundation for future research projects. Furthermore, one of the objectives was to provide evidence supporting the hypothesis of P_i transporter-mediated uptake of MTA, which has been suggested for several years and is already known for the structural analogue As^V.

In addition to the focus on thioarsenates, this work also included the "As^{III}-evolutionary project," which aimed to investigate mechanisms that develop in a phytochelatin synthase-deficient mutant strain exposed to sublethal doses of As^{III}. This part of the work sought to identify mechanism providing As^{III} tolerance and to determine whether the acquired adaptations resulted from stable genetic mutations or epigenetic adaptations. Such insights could enhance our understanding of how reduced susceptibility to As^{III} arises and may also shed light on mechanisms relevant to other As-species of toxicological relevance.

2. Material and Methods

2.1 Technical Devices

Tab. 1 List of Technical Devices.

Devices	Designation	Manufacturer
Centrifuge	5415R	Eppendorf (Hamburg, Germany)
	5424	Eppendorf (Hamburg, Germany)
	5810R	Eppendorf (Hamburg, Germany)
ELISA-Reader	PowerWave$_x$ 340	BioTek Instruments, Inc. (Vermont, USA)
IC	Dionex™ ICS-3000	Thermo Fisher (Karlsruhe, Germany)
ICP-MS	XSeries 2 ICP-MS	Thermo Fisher (Karlsruhe, Germany)
HPLC system	X-LC™ 3059 AS (autosampler)	JASCO (Pfungstadt, Germany)
	PU-2085 PLUS (pumps)	JASCO (Pfungstadt, Germany)
	DG-2080-54 (4-line degasser)	JASCO (Pfungstadt, Germany)
	MD2010 PLUS (detector)	JASCO (Pfungstadt, Germany)
	ReproSil 100 C18 (column) 250 x 4 mm; pore size 5 µm	Dr. Maisch HPLC GmbH (Mainz, Germany)
Nanophotometer	NanoPhotometer P300	Implen GmbH (Munich, Germany)
PCR-Cycler	SensoQuest Labcycler48	SensoQuest GmbH (Göttingen, Germany)
	MJ Mini™	Bio-Rad Laboratories, Inc. (Feldkirchen, Germany)
Photometer	Ultrospec 4051, LKB Biochrom	Pharmacia Biosystems (Freiburg, Germany)
Shaking cabinet	Infors HT Ecotron (CH-4103)	INFORS HT (Bottmingen, Switzerland)
	New Brunswick Innova® 44	Eppendorf (Hamburg, Germany)

2.2 Organisms and Strains

Tab. 2 Strains. List of *A. thaliana*, *E. coli*, *S. cerevisiae* and *S. pombe* strains used within the course of this work.

Organism	Strain	Resistences/Auxotrophies	Source
A. thaliana	Col-0		NASC, European Arabidopsis Stock Center
	pht1;1 (SALK_088586)	Kanamycin	NASC, European Arabidopsis Stock Center
	phr1-1phl1		R. Bustos et al. (2010)[202]
E. coli	DH10β	*Δ*(*lacZYA-argF*)U169, ϕ80d*lacZ*ΔM15Δ*lac*X74, *galU*, *galK* - *rpsLnupG endA1*, *recA1*, *deoR*, *araD139D (ara, leu)*7697,	S. Grant et al. (1990)[203]
	W3110		A. Carlin et al. (1995)[204]
	ΔarsC	W3110	A. Carlin et al. (1995)[204]
	ΔarsC+AtHAC1 (*AtARQ1*$^{Col-0}$)	W3110 Ampicillin	E. Sánchez-Bermejo et al. (2014)[120]
S. cerevisiae	WT (BY4741) *	*MATa, his3-1, leu2-0, met15-0, ura3-0*	Brachmann CB, et al. (1998)[205]
	ecm38 *	BY4741 *ecm38::KanMX4*	E. Winzeler et al. (1999)[206] G. Giaever et al. (2002)[207]
	WT (BY4742) *	*Matα, his3-1, leu2-0, lys2-0, ura3-0*	Brachmann CB, et al. (1998)[205]
	fps1 *	BY4742 *fps1::KanMX4*	E. Winzeler et al., (1999)[206] G. Giaever et al. (2002)[207]
	pho84 *	BY4742 *pho84::KanMX4*	E. Winzeler et al. (1999)[206] G. Giaever et al. (2002)[207]

ptr2 *	BY4742 *ptr2::KanMX4*	E. Winzeler et al. (1999)[206] G. Giaever et al. (2002)[207]
gal2 *	BY4742 *gal2*::KanMX4	E. Winzeler et al. (1999)[206] G. Giaever et al. (2002)[207]
WT (Cen.PK2-1c)	*MATa leu2-3,112 ura3-52 trp1-289 his3-1 MAL-8c SUC2*	K. Entian and P. Kötter, (2007)[208] (provided by E. Boles; Goethe University of Frankfurt)
hxt0 (EBY.VW4000)	Cen.PK2-1c *hxt13::loxP hxt15::loxP hxt16::loxP hxt14::loxP hxt12::loxP hxt9::loxP hxt11::loxP hxt10::loxP hxt8::loxP hxt4-1-5::loxP hxt2::loxP hxt3-6-7loxP gal2:(ura3/FOA) stl1::loxP agt1::loxP mph2(ydl247w)::loxP Mph3(yjr160c)::loxPm can1::RMD6-KanMX*	R. Wieczorke et al. (1999)[64] (provided by E. Boles; University of Frankfurt)
HD9	*MATα, ura3-52 his6 leu2-3,112 his3-200 trp1-901 lys2-801 suc[unknown]Δycf1::hisG acr3::URA3 fps1::leu2*	Z. Liu et al. (2002)[209]
HD100	CEN.PK2-1C *fps1::leu2 acr3::his3*	Z. Liu et al. (2004)[61]
HD200	EBY.VW367^{+} *fps1::leu2 acr3::his3*	Z. Liu et al. (2004)[61]

S. pombe	WT (FY261)	*h⁺ ade6-M216 leu1-32 ura4-Δ18 can1-1*	S. Forsburg Salk Institute, La Jolla, CA
	ggt2Δ	FY261 *ggt2Δ::KanMX4*	This work
	pcsΔ	FY261	S. Clemens et al. (1999)[160]
	pcsΔggt1Δ#1	FY261	This work
	pcsΔggt1Δ#2	FY261	This work
	pcsΔggt2Δ#1	FY261	This work
	pcsΔggt2Δ#2	FY261	This work
	M1	*pcsΔ*[160]	This work
	M2	*pcsΔ*[160]	This work
	M3	*pcsΔ*[160]	This work
	M4	*pcsΔ*[160]	This work
	M4_*ggt2Δ*	*pcsΔ*[160]*; ggt2Δ::KanMX4*	This work

*****Strains were provided by Benedikt Westermann and Till Klecker from the chair of cell biology of the University of Bayreuth

2.3 Plasmids, Constructs and Primers

Tab. 3 List of Plasmids and Constructs. Plasmids and constructs used within the course of this work.

Plasmid/Construct	Characteristics/Purpose	Source
pSGP72	amp^R, LEU2, nmt1 promoter, triple HA-Tag (C-term)	S. Forsburg Salk Institute, La Jolla, CA
pSGP72-eGFP	amp^R, LEU2, nmt1 promoter, eGFP-Tag (C-term)	S. Forsburg Salk Institute, La Jolla, CA
pSGP72-*ggt1*	Expression of *ggt1* in *S. pombe*	This work
pSGP72-*ggt1-eGFP*	Expression of *ggt1* in *S. pombe*	This work
pSGP72-*ggt2*	Expression of *ggt2* in *S. pombe*	This work
pSGP72-*ggt2-eGFP*	Expression of *ggt2* in *S. pombe*	This work
pSGP72-*plb1*	Expression of *plb1* in *S. pombe*	This work
pSGP72-*plb1-eGFP*	Expression of *plb1* in *S. pombe*	This work
pSGP72-*pof1*	Expression of *pof1* in *S. pombe*	This work
pSGP72-*pof1-GFP*	Expression of *pof1* in *S. pombe*	This work
pSGP72-*AtHAC1*	Heterologous expression of *AtHAC1* in *S. pombe*	Sebastian Haider (Master Thesis)
pSGP72-*AtHAC1-GFP*	Heterologous expression of *AtHAC1* in *S. pombe*	Sebastian Haider (Master Thesis)
pLSB-Nat	amp^R,natMX^R, adh1 promoter, Cas9, sgRNA cassette, tRNA promoter, SV40-NLS, GFP-placeholder	S. Torres-Garcia et al. (2020)[210]
pLSB-Nat-sgRNA*ggt1*	Knockout of *ggt1*	This work
pLSB-Nat-sgRNA*ggt2*	Knockout of *ggt2*	This work
pLSB-Nat-sgRNA*plb1*	Knockout of *plb1*	This work
pLSB-Nat-sgRNA*pof1*	Attempting to knockout *pof1*	This work

pCloneKan1	amp^R, KanMX^R, SP6 promoter	M. Spirek et al. (2011)[211]
pCloneHYG	amp^R, HYG^R, SP6 promoter	M. Spirek et al. (2011)[211]

Tab. 4 List of Primers. Sequences and their applications.

Primer	Sequence (5´ -> 3´)	Application
delcheck_ggt1_fw	TGTAGAAGTTGCGGTTGGCT	Deletion check
delcheck_ggt1_rev	CTCTCATCCCAGCCACAAGC	Deletion check
delcheck_ggt2_fw	TCAAAGTCAACAACCAGGCT	Deletion check
delcheck_ggt2_rev	GCGTCTGAAAGAAGCTAGCTC	Deletion check
ggt2_delcheck_seq	GCCTCTACGAGGCTTGGAAG	Sequencing
delcheck_plb1_fw	ATGCTTTTCCGCGGATTAAG	Deletion check
delcheck_plb1_rev	CAGTACCAACGAGATAGTCA	Deletion check
delcheck_pof1_fw	CATTTTGGCAACCCGAGCAA	Deletion check
delcheck_pof1_rev	CTACCCGCATCATCCGTGAT	Deletion check
ggt1_pSGP72_fw	AAAACTCGAGATGGGTATCAATACGTCT	Cloning
ggt1_pSGP72_rev	AGAAGATCTGCTTAATAGGCAGCAGCAAC	Cloning
ggt2_pSGP72_fw	AAAACTCGAGATGAGCCCTACAGACACT	Cloning
ggt2_pSGP72_rev	AGAAGATCTGCTTAATAAGCGGCAGCCTG	Cloning
pof1_pSGP72_fw	AAAACTCGAGATGACTACAGGTTATGAA	Cloning
pof1_pSGP72_rev	AGAAGATCTGCCTACGATTGAATCGACAC	Cloning
plb1_pSGP72_fw	AAAACTCGAGATGCTTTTCCGCGGATTA	Cloning
plb1_pSGP72_rev	AGAAGATCTGCTTAAATGCCTTCACCAAG	Cloning
ggt2_smut_72_1fw	GTTAATTTCTTCTCTAGTGGAATTGGTGGAGGT	Mutagenesis PCR
ggt2_smut_72_1rev	TCCACCAATTCCACTAGAGAAGAAATTAAC	Mutagenesis PCR
ggt2_smut_72_2fw	TTTCCTGTGACTCGGGCAATGGAAAGAGTTTTG	Mutagenesis PCR
ggt2_smut_72_2rev	TTTCAAAACTCTTTCCATTGCCCGAGTCACAGG	Mutagenesis PCR
sgRNA_ggt1_fw	GACTGGTCTTTCCGTTGCCGTCCC	Gene editing
sgRNA_ggt1_rev	AAACGGGACGGCAACGGAAAGACC	Gene editing
sgRNA_ggt2_fw	GACTATTAAAGCAGGTCCACTCGT	Gene editing

sgRNA_ggt2_rev	AAACACGAGTGGACCTGCTTTAAT	Gene editing
sgRNA_pof1_fw	GACTATTATCAGAGGGTTCGGAAG	Gene editing
sgRNA_pof1_rv	AAACCTTCCGAACCCTCTGATAAT	Gene editing
sgRNA_plb1_fw	GACTTTTTCCGCGGATTAAGCCTG	Gene editing
sgRNA_plb1_rv	AAACCAGGCTTAATCCGCGGAAAA	Gene editing
pGEMT-fw	GCAAGGCGATTAAGTTGGGTAAGC	Construct check
ggt2_prom	TCTTTACCATTTTGAGAGG	Insertion check
ggt2_term	GGCATTGACATCTGTTAAAGT	Insertion check
ggt2_up_XbaI_fw	AAAATCTAGACATGGTCATCCAAAATCAATCCGTTACACA	Gene Insertion/Deletion
ggt2_up_XhoI_rv	AAAACTCGAGGGGTAACGAGAACAGTTGAATAACTC	Gene Insertion/Deletion
ggt2_down_BglII_fw	AAAAAGATCTGGTACATTTAAAGCGTATGAGAAATCGTCAA	Gene Insertion/Deletion
ggt2_down_XbaI_rv	AAAATCTAGACATCTAGGTTCCCATATTCGTGGT	Gene Insertion/Deletion
pof1_prom	TATGAGTGGCAGATTGCGC	Insertion check
pof1_term	AGTATTGTTACAAAGCCGGTGATTCC	Insertion check
pof1_up_XbaI_fw	AAAATCTAGACATTATCTTCGGATTCGTAATTTTGAGA	Gene Insertion/Deletion
pof1_up_XhoI_rv	AAAACTCGAGCAGAAATGATTTGGATAAGATG	Gene Insertion/Deletion
pof1_down_BglII_fw	AAAAAGATCTGGCATCCCGGCATACAGTTTA	Gene Insertion/Deletion
pof1_down_XbaI_rv	AAAATCTAGAGATAGTGAGTGTTGATATAATTTGCT	Gene Insertion/Deletion
kanMX4_full_fw	CCGCGATTAAATTCCAACAT	Insertion check
kanMX4_full_rev	TTAGAAAAACTCATCGAGCATC	Insertion check
kanMX4_1	AATCGATAGATTGTCGCACC	Insertion check
kanMX4_2	GCCTCGGTGAGTTTTCTCCT	Insertion check
prom_pcs_fw	CATGGGGGAATGGGACAATC	Genotyping
SpPCS_fw	CGAGCAGTCCCAGAATTACTGAG	Genotyping
SpPCS_rev	CAGCAGCTTGAACTACAACACC	Genotyping
URA4_rev	CCGTTAATGTGGCAGCAACCTTTACG	Genotyping

2.4 Chemicals

For all media listed, along with the washing steps for sample preparation, were prepared using deionized water (dH_2O) purified through the Advantage A10® Milli-Q® system (Millipore, Billerica, USA). Unless otherwise indicated, the chemicals used were obtained from Duchefa (Haarlem, Netherlands), Merck (Darmstadt, Germany), VWR Chemicals (Darmstadt, Germany), Sigma-Aldrich (Steinheim, Germany), Biozym (Oldendorf, Germany), Macherey-Nagel (Düren, Germany), and Carl Roth (Karlsruhe, Germany). All oligonucleotides were ordered from Eurofins Genomics (Ebersberg, Germany).

2.5 Medium and Supplement Preparation

If necessary, the medium was autoclaved at 120°C and 1 bar for 20 min. Antibiotics and thiamine were added to the autoclaved medium after it cooled to below 45°C. Similarly, sterile-filtered sugar solutions were added as needed to prevent the loss of available sugars due to the Maillard reaction.

Tab. 5 List of Media. Ingredients and their concentrations used in this study.

Medium	**Chemicals**	**Final concentration**
EMM	$C_8H_5KO_4$	14.7 mM
(Edinburgh Minimal Media)	Na_2HPO_4	15.5 mM
	NH_4Cl	93.5 mM
	Glucose x1 H_2O	111 mM
	Adenine	225 mg/l
	$MgCl_2$ x6 H_2O	5.2 mM
	$CaCl_2$ x2 H_2O	99.8 µM
	KCl	1.34 mM
	Na_2SO_4	0.282 mM
	Pantothenic acid	4.2 µM
	Nicotinic acid	81.2 µM
	Inositol	55.5 µM

	Biotin	40.8 nM
	H_3BO_3	8.9 µM
	$MnSO_4$ x1 H_2O	2.37 µM
	$ZnSO_4$ x7 H_2O	1.39 µM
	$FeCl_3$ *6 H_2O	0.74 µM
	Na_2MoO_4 x2 H_2O	0.247 µM
	KI	0.602 µM
	$CuSO_4$ x5 H_2O	0.16 µM
	Citrat x1 H_2O	4.76 µM
YE5S	Yeast extract	5 g/l
	Glucose	3 % (w/v)
	Adenine	100 mg/l
	Cysteine	100 mg/l
	Histidine	100 mg/l
	Leucine	100 mg/l
	Uracil	100 mg/l
LB (Luria broth medium)	LB salt	25 g/l
YNB (Yeast Nitrogen Base)	Yeast Nitrogen Base without Amino acids and without $(NH_4)_2SO_4$	1.7 g/l
		5 g/l
	Drop out mix -Ura, -Trp	0.8 g/l
	Glucose*	20 g/l
	Amino Acids**	30 mg

2x YNB (SD-AS 0.1 CPB)[212]	pH-values were adjusted with the respective amounts of 1 M Citrate and 1 M Phosphate Buffer based on R. Prins and S. Billerbeck, 2021, Supplementary Fig. 1 and 4	
YPD (Yeast Extract Pepton Dextrose)	Yeast Extract	10 g/l
	Bacto Peptone	20 g/l
	Glucose*	20 g/l
1/10 Hoagland (solid)	$Ca(NO_3)_2$ x4H_2O	0.28 mM
	KNO_3	0.6 mM
	$MgSO_4$ x7H_2O	0.2 mM
	$(NH_4)H_2PO_4$	0.1 mM
	Fe-HBED	5 µM
	Sucrose***	1 % (w/v)
	MES	5 mM
	Type E Agar	1 % (w/v)
	KOH	To pH = 5.7
1/10 Hoagland (liquid)[X]	$Ca(NO_3)_2$ x4H_2O	0.28 mM
	KNO_3	0.6 mM
	$MgSO_4$ x7H_2O	0.2 mM
	$(NH_4)H_2PO_4$	0.1 mM
	Fe-HBED	5 µM
	H_3BO_3	4.63 µM
	$CuSO_4$ x4H_2O	32 nM

	$MnCl_2$ x4H_2O	0.915 µM
	$ZnSO_4$ x7H_2O	77 nM
	MO_3	11 nM
	KOH	To pH = 5.7
P_i differing medium (solid)[213]	KNO_3	2.5 mM
	$MgSO_4$	1 mM
	$Ca(NO_3)_2$	1 mM
	Fe-HBED	25 µM/ 10 µM
	KH_2PO_4	(see experimental setup)
	H_3BO_3	35 µM
	$MnCl_2$	7 µM
	$CuSO_4$	0.25 µM
	$ZnSO_4$	0.5 µM
	$NaMoO_4$	0.1 µM
	NaCl	5 µM
	$CoCl_2$	5 nM
	Sucrose	0.5 % (w/v)
	MES (pH = 6.0)	20 mM
	Agar (Duchefa, Plant Agar)	0.8 % (w/v)
P_i differing medium (liquid)[213]	KNO_3	0.25 mM
	$MgSO_4$	0.1 mM
	$Ca(NO_3)_2$	0.1 mM
	Fe-HEBED	1.75 µM
	KH_2PO_4	0.25 mM
	H_3BO_3	3.5 µM
	$MnCl_2$	0.7 µM
	$CuSO_4$	25 nM

	$ZnSO_4$	50 nM
	$NaMoO_4$	10 nM
	NaCl	0.5 µM
	$CoCl_2$	0.5 nM
	MES (pH = 6.0)	2 mM
Uptake solution[214]	Hepes/Tris	10 mM
	$MgCl_2$	100 µM
	Carbon source of choice	2 % (w/v)

* If indicated maltose was used as carbon source

**YNB was supplemented with amino acids required for growth of the respective *S. cerevisiae* strains

***If indicated other sugars were added to equimolar amounts

[x] 250 µM of the respective sugars were added to the medium within the time period of the 24 hours DMMTA treatment if indicated

2.6 Cultivation of Plants

To generate seeds, plants were cultivated in a soil mixture comprising pricking-out soil (Ökohum, Herbertingen), type GS90L soil (Einheitserde Werkverband, Sinntal-Altengronau), and vermiculite (Deutsche Vermiculite Dämmstoff GmbH, Sprockhövel) in a 3:3:1 ratio. After three weeks of growth under short-day conditions (8 h light/16 h dark, 22°C,~100 µE), the plants were transferred to long-day conditions (16 h light/8 h dark, 22°C, ~100 µE) to induce flowering and seed maturation.

2.6.1 Sterilization of Seeds

Seeds were placed in 2 ml Eppendorf reaction tubes and, with the lids open, put into a desiccator. Sterilization was initiated by adding 5 ml of HCl to 10 ml of sodium hypochlorite. The seeds were

sterilized for 45 min. After removing the remaining chlorine gas, the seeds were transferred to the respective plates or tip boxes (hydroponic system).

2.6.2 DMMTA Uptake Experiment Using the Hydroponic System

PCR tubes were placed in tip boxes and autoclaved. After filling the PCR tubes with 350 µl of 1/10 Hoagland with type E agar, the tips of the PCR tubes were cut off. Sterilized Col-0 seeds were placed on the PCR tubes, and the tip box was filled with 1/10 Hoagland medium. Boxes were placed at 4 °C in the dark, for 48 hours to stratify the seeds. For germination and growth, the boxes were incubated at 21 °C for 10 h (short day) in a Percival climate chamber.

For germination and growth, the boxes were incubated at 21 °C for 10 h under short-day conditions in a Percival climate chamber. Three weeks after germination, young seedlings grown in the tip boxes were transferred to 50 ml tubes containing 1/10 Hoagland medium. Plants were maintained for four weeks under short-day conditions (8 h of light per day) before the treatment began.

For the 24 hours of DMMTA exposure, plants were transferred to 1/10 Hoagland medium supplemented with 300 µM of the respective sugar and 15 µM DMMTA.

2.6.3 MTA and As^V Uptake Experiments in the Hydroponic System

Seeds were sterilized and placed on PCR tubes in tip boxes containing phosphate P_i-differing medium with 250 µM KH_2PO_4. After stratification for 2 days at 4 °C, the tip boxes were transferred to a climate chamber. Seedlings were grown for 3-4 weeks under short-day conditions at 23 °C and then transferred to 50 ml tubes, where they were cultivated under the same conditions. Before the uptake experiment, plants were transferred to P_i-differing medium with 2 µM three days prior, and to P_i-free medium 1 day before the treatment. For the treatment, plants were transferred to P_i-free medium with or without 10 µM MTA or As^V. After 24 hours, plants were harvested and separated into root and shoot, followed by four wash steps. Roots and shoots were either dried at 60 °C for 7 days (determination of ∑As) or flash-frozen in liquid nitrogen (As-speciation).

2.6.4 Seedling Assay

Five sterilized seeds of each genotype and treatment were placed into individual wells of a 6-well plate, each filled with 5 ml of P_i Differ medium. After stratification, the plates were incubated for 7 days under long-day conditions (16 h light/8 h dark, 22°C,~100 µE) with gentle shaking. Fresh weights of all seedlings in each well were measured and normalized to the total number of seedlings.

2.6.5 Root Length and Fresh Weight Assays on MTA- and As^V- Containing Plates

For each genotype, 5 sterilized seeds were placed on plates with P_i differing medium supplemented with 55 µM KH_2PO_4 and 0.8 % (w/v) plant agar. Plants were cultivated for 14 days under long-day conditions, either with or without 50 µM MTA or 12.5 µM As^V. The root lengths and fresh weights of each seedling were measured.

2.6.6 Cultivation for the Analysis of Chlorophyll and Cyanidin Contents upon MTA and As^V Exposure

Plants were grown as described above, but for a prolonged period of time of 18 days to generate more plant material. For each treatment, 5-10 shoots of each genotype were harvested, and the fresh weight was determined. Plant material was flash-frozen in liquid nitrogen and stored at -80 °C. Chlorophyll contents was measured as described Ticconi et al. (2001)[215] based on D.J. Champman et al. (1988)[216], and cyanidin content was measured as described in H. Li et al. (2023)[217].

2.6.7 Cultivation for the Analysis of PC-Induction upon MTA and As^V Exposure

For each genotype, 18 sterilized seeds were placed on plates with P_i differing medium supplemented with 30 µM KH_2PO_4 and 0.8 % (w/v) type E agar. Plants were cultivated for 14 days under long-day conditions. For each treatment and genotype, seedlings were transferred to P_i-free plates containing P_i differing medium with or without 130 µM MTA or As^V and, cultivation under long-day conditions was prolonged for 24 hours and 72 hours. After the respective exposure periods, seedlings were harvested and divided into roots and shoots. Fresh weight of the shoots and roots was determined, and the plant material was flash-frozen in liquid nitrogen and stored at -80°C for later extraction.

2.7 Cultivation of Microorganisms

E. coli was cultured in LB medium supplemented with the respective antibiotic selection marker at 37°C. *S. pombe* was cultivated at 30°C, and *S. cerevisiae* at 32°C, in both liquid and solid media. Liquid cultures were incubated at the respective temperatures shaking at 220 rpm. Complete media used for cultivation included YE5S for *S. pombe* and YPD or YPM for *S. cerevisiae*. Selective media included EMM for *S. pombe* and YNB or 2xYNB 0.1 CPB for *S. cerevisiae*, supplemented with the respective amino acids, as required. To regulate ectopic gene expression, S. pombe cells harboring constructs with a pSGP72 backbone were supplemented with thiamine to reduce expression levels.

2.7.1 Uptake Experiments with *S. cerevisiae* and *S. pombe*

Logarithmically growing cells were harvested by centrifugation (3000 rpm, 2 min). Cells from the pre-cultures were washed twice with 10 ml of sterile water and then transferred to the respective medium or uptake solution. At each time point, 30 to 50 ml of cultures from each genotype and treatment (depending on the experimental setup) were harvested by centrifugation and washed (see 2.10.1.3.). Samples were dried at 60 °C for 30 to 42 h prior to acidic digestion in the microwave.

2.7.2 DMMTA Uptake Experiments with *S. pombe*

Wild-type (WT) *S. pombe* cells were cultivated (30 °C, 220 rpm) in EMM medium, supplemented with the respective amino acids. Logarithmically growing cells were harvested (3000 rpm, 2 min) and washed twice with sterile water and transferred into the uptake solution (Tab. 5), which contained 2% (w/v) glucose, or sorbitol. The treatment was initiated by adding 7.5 µM DMMTA or As^{III}. Samples of 35 ml were taken after 5, 15, 30, and 60 min (3000 rpm, 2 min) of cells treated at 30 °C or after 15 and 60 min of cells treated at 4°C and the OD_{600} value was determined for subsequent data normalization. Experiments at 4 °C were conducted in parallel and cells were derived from the same pre-cultures as used for the experiments at 30°C. The samples were centrifuged for 2 min at 3000 rpm, and the cells were washed three times (see 2.10.1.3.).

2.7.3 Efflux Experiments with *S. cerevisiae* exposed to DMMTA and As^{III}

A 50 ml overnight culture was prepared for each strain. For the pre-culture, 300 ml of fresh YNB medium were inoculated to an OD_{600} = 0.4, followed by a 3-h incubation at 30°C with shaking at 220 rpm. Then, the pre-culture was divided into two equal portions, with 150 ml transferred into each of two flasks containing 150 ml of YNB medium (OD_{600} ≈ 0.4). The OD_{600} of each flask was measured to ensure consistency, and either As^{III} or DMMTA was added to the cultures at a final concentration of 10 µM. The cultures were then incubated for an additional 2 h at 30°C.

Following this incubation, the cells were collected at 3000 rpm for 2 min. The harvested cells were washed prior to being transferred into fresh medium (see 2.10.1.3.).

The washed cells were subsequently transferred into fresh flasks containing 100 ml of YNB medium and incubated further. At time points of 15, 45, 60, 180, and 240 min, 10 ml of culture medium was sampled from each flask. The OD_{600} was measured at each time point, and the samples were centrifuged at 3200 g for 5 min. Finally, 5 ml of the supernatant was transferred into a fresh tube for subsequent analysis via ICP-MS.

2.7.4 MTA and As^{V} Uptake Experiments with *S. cerevisiae* WT and *pho84*

S. cerevisiae (BY4742) WT and *pho84* strains were grown at 30°C and 220 rpm in complete medium (YPD) to ensure maximum P_i supply. Logarithmically growing cells were harvested (3000 rpm, 2 min) and washed twice in sterile water (3000 rpm, 2 min) before being resuspended in the respective uptake solution. A 40 ml sample of each genotype was taken from the resuspended cells before splitting them into three different treatment groups. Exposure was initiated by adding 50 µM MTA, As^{V}, or As^{III}. For cultures exposed at 30°C, 45 ml samples were harvested after 15, 30, 45, and 60 min. For experiments conducted at 4°C, 45 ml samples were harvested after 15 and 60 min. All samples were centrifuged (3000 rpm, 2 min) and washed to ensure the removal of residual surface-bound arsenic (see 2.10.1.3). The OD_{600} value of each culture was determined at each time point for later data normalization.

2.7.5 Growth Curve Analysis with *S. pombe* and *S. cerevisiae*

For each genotype, an overnight culture of 3.0 ml of the respective SD medium with the required supplements was inoculated. Strains were grown at 30°C and 220 rpm for approximately 16 h,

then washed twice with 3 ml of sterile water. Pre-cultures for each treatment were inoculated (OD_{600} = 0.025) with the respective strain in 3.0 ml of SD medium with the necessary supplements. Each well of a 96-well plate was filled with 100 µl of the pre-culture or SD medium alone as a blank. The treatment was initiated after 4 h of pre-cultivation at 30°C and 220 rpm by adding the stressor of interest. The lid of the 96-well plate was sealed with Leucopore tape to maintain sterility under aerobic conditions. In the ELISA reader, the 96-well plates were incubated at 30°C for 32-36 h (depending on the specific experiment), while shaking, and OD_{600} values were recorded every 30 or 60 min.

2.7.6 Serial Dilution Assays

Strains were cultivated at 30 °C / 220 rpm overnight in 3.0 ml SD medium with the required supplements. Overnight cultures were washed twice with 3 ml sterile water. Based on the OD_{600} values, a serial dilution was prepared to obtain OD_{600} values of 1.0, 0.5, 0.1, 0.66, 0.33 and 0.1. For each dilution, 5 µl were dropped onto a plate of the respective SD medium with or without the stressor of interest. Plates were incubated at 30 °C, and photos were taken at intervals between 24 hours to 72 hours, depending on the experiment conducted.

2.7.7 Setup of the As^{III} Tolerance Evolutionary Project

Several cultures of the As^{III} sensitive *pcsΔ* knockout were cultivated in 3.5 ml YE5S medium for 12 weeks at 21 °C in presence of 10 or 50 µM As^{III}. Tolerance of those cultures was monitored by measuring the OD_{600} every 7 days before they were freshly inoculated to an OD_{600} of 0.05. The Glycerin stocks were taken from cultures with enhanced growth on 10 or 50 µM As^{III}. After two weeks of enhanced growth the As^{III} concentration was risen. Single colonies were picked after streaking samples of the taken stocks on YE5S plates by the “four-way streak method”. Several of those isolated colonies were then tested in a liquid assay to identify potential mutants responsible for the higher As^{III} tolerance observed in the culture. For the liquid assays 3.5 ml of YE5S medium with or without 150 µM As^{III} were inoculated with an overnight culture of the respective candidate to an OD_{600} value of 0.05 and incubated at 30 °C, 220 rpm for 20 h. After 20 h the As^{III} sensitivity was determined by measuring the OD_{600} values. Genomic DNA was extracted from four of the five isolated mutants and sent for resequencing (Macrogen Europe). Results were analyzed via

"mapping by sequencing" to identify alterations in coding sequences in comparison to the related *pcsΔ* mutant.

2.8 Molecular Biological Methods

2.8.1 Isolation of DNA from Plants

Plant material was harvested and placed in a 2 ml reaction tube containing two steel balls. The frozen tissue was ground in a ball mill for 1 min. For gDNA extraction, 500 µl of an extraction buffer (200 mM Tris-HCl, pH 8.5; 25 mM EDTA, pH 8.0; 250 mM NaCl; 0.5% (w/v) SDS) were added. After spinning down the cell debris (14,000 rpm, 5 min), 300 µl of the supernatant were transferred to a new reaction tube, followed by the addition of 300 µl isopropanol. The mixture was mixed by inverting. Centrifugation was performed, and the supernatant was discarded. The pellet was washed twice with 70% ethanol. Finally, the air-dried pellet was dissolved in 40 µl dH2O and stored at 4 °C.

2.8.2 Isolation of DNA from Yeasts

For genotyping purposes, gDNA of *S. pombe* or *S. cerevisiae* was isolated by taking a small amount of cell material from plates with freshly grown cells and digesting it in 25 µl of 25 mM NaOH at 98°C for 12 min. For resequencing or cloning, 10 ml of logarithmically growing cells (OD_{600} ≈ 0.8 – 1.0) were harvested (3000 rpm, 2 min), and the pellets were washed with 1 ml of sterile water. After centrifugation (3000 rpm, 2 min) and removal of the supernatant, the pellets were resuspended in 500 µl of a zymolyase solution (1 M sorbitol, 0.1 M EDTA, pH 8.0, 123 units zymolyase (Nacalai Tesque Inc., Japan)) and incubated at 37 °C for 1 h to digest the cell walls. After centrifugation (3000 rpm, 2 min) and discarding the supernatant, the pellet was resuspended in 450 µl of 5xTE buffer (50 mM Tris-HCl, 5 mM EDTA, pH 8.0). After adding 50 µl of 10% (w/v) SDS and incubating for 5 min at room temperature, 150 µl of 5 M potassium acetate were added, and the incubation was extended for 10 min on ice. After centrifugation (17,000 rpm, 10 min), 550 µl of the supernatant were transferred to a new reaction tube and mixed with 550 µl of isopropanol. The precipitated gDNA was spun down (17,000 rpm, 10 min) and washed twice with 70% ethanol. The air-dried pellet was resuspended in 40 µl TE buffer for target gene amplification for cloning or Sanger sequencing.

For gDNA resequencing, the washed pellet was resuspended in 5x TE buffer, and 5 µl of RNase A (10 mg/ml) (Fisher Scientific, Germany) were added. After a 15-min incubation at 37 °C, 20 µl of proteinase K (400 Units) (recombinant Proteinase K, Invitrogen™, Fisher Scientific, Germany) and 4 µl of 10% (w/v) SDS were added and the incubation was extended at 55 °C. Subsequently, 500 µl of a phenol-chloroform-isoamyl alcohol mixture (50:49:1) were added and mixed by inverting, followed by centrifugation (17,000 rpm, 5 min). The upper aqueous layer was transferred to a new reaction tube, and the purification step was repeated. The aqueous layer was again transferred and mixed with 500 µl of isopropanol and 25 µl of 3 M sodium acetate. After a 10-min incubation on ice and centrifugation (17,000 g, 10 min), the supernatant was discarded. The ethanol washing steps were repeated, and the air-dried pellet was resuspended in 60 µl TE buffer and incubated for 20-30 min at 60 °C.

2.8.3 Polymerase Chain Reaction for Cloning and Genotyping Purposes

Target sequences for cloning were amplified using the Phusion™ High-Fidelity Polymerase (Thermo Scientific, Germany) with a PCR protocol based on the manufacturer's specifications. For genotyping, the same procedure was followed using Taq polymerase (Thermo Scientific, Germany), diluted 1:30 in glycerol. Annealing temperatures were calculated with the Thermo Fisher T_M Calculator web tool, using settings specific to Phusion or Taq polymerase, respectively. The oligonucleotides used in this work are listed in table 4. As templates, 20 ng of genomic DNA (gDNA), 10 ng of cDNA, or 1–5 ng of PCR product was added. Schematic layouts of the PCR programs used are shown in table 5.

Tab. 5. Scheme of PCR Programs. Polymerase specific settings for target sequence amplification.

Polymerase	Step	Cycles (x)	Temperature (°C)	Duration (s)
Taq	Initial Denaturation	1	95	30
	Denaturation	30-35	95	30
	Primer Annealing	30-35	Primer pair T_M	40-60
	Extension	30-35	72	60 s/kb
	Final Extension	1	72	300
	Hold	1	10	∞
Phusion™ High Fidelity	Initial Denaturation	1	98	30
	Denaturation	28-35	98	30
	Primer Annealing	28-35	Primer pair T_M	40-60
	Extension	28-35	72	30 s/kb
	Final Extension	1	72	300
	Hold	1	10	∞

2.8.4 Cloning of Constructs for the Complementation Analysis

To complement the mutants derived from the As^{III} evolutionary project and the knockouts generated using the CRISPR-Cas9-based "SpEDIT" system, the vector pSGP72, with or without a C-terminal GFP tag, was digested using the restriction enzymes XhoI and BglII. Coding sequences of the genes of interest were amplified with additional restriction enzyme recognition sites at the 5' and 3' ends. The purified PCR products were digested with the same restriction enzymes. Digested vectors and PCR products were ligated using T4 DNA ligase (Fisher Scientific, Karlsruhe), following the manufacturer's instructions.

2.8.5 Transformation of Competent *E. coli* Cells

Aliquots of 50 µl (OD_{600} ≈ 0.4–0.6) of competent *E. coli* cells (DH10B) for restriction enzyme-based cloning or DB3.1 for the Gateway system) were stored at -80°C. For transformation, the cells were mixed with 5 µl of the ligation mixture on ice. After 30 min on ice, the cells were heat-shocked at 42°C for 60 s and then returned to ice for 1 - 3 min. Following this, 1 ml of LB medium was added,

and the cells were incubated at 37°C while shaking at 220 rpm. The cells were then centrifuged at 5000 × g for 5 min. After removing the supernatant, the pellet was resuspended in 80 µl of LB and spread on plates containing the appropriate antibiotic for selection. Plates were incubated overnight at 37°C, and colonies were picked and re-streaked onto fresh LB plates containing the antibiotic.

Isolated clones were used to inoculate an overnight culture in 3.5 ml of LB medium with the respective antibiotic. Clones were grown overnight at 37°C (220 rpm) and subsequently harvested to isolate plasmids using the GeneJET Plasmid Miniprep Kit (Fisher Scientific, Germany) or the NucleoSpin Plasmid Mini Kit (Macherey-Nagel, Germany). Constructs were confirmed by Sanger sequencing (Macrogen Europe).

2.8.6 Transformation of *S. cerevisiae* and *S. pombe*

Cells were freshly streaked on complete medium plates or SD medium plates, respectively, the day before transformation. For yeast transformation, denatured ssDNA from herring sperm (Promega, USA) was prepared by heating at 95°C for 5 min, followed by cooling on ice before use. Two scoops of freshly grown yeast cells were transferred with a loop to 200 µl of one-step buffer solution (Tab. 6). Approximately 1000 ng of purified plasmid DNA was added to the resuspended cells along with 4 µl of herring sperm ssDNA (approximately 40 µg). After 4 h of incubation at 42°C, cells were spread on plates with or without the appropriate selection marker. For knockouts generated using the gap repair protocol, the transformed cells were first grown on complete medium without a selection marker (16 h, 30°C) before being transferred by stamping onto plates containing the respective selection markers. Yeast cells transformed with constructs for complementation analysis or for the heterologous expression of foreign genes were directly plated on medium lacking the appropriate amino acids.

Tab. 7 One-Step Buffer. Ingredients and volumes.

Buffer	Composition	Volume for 10 reactions
One-Step-Buffer	PEG3350 60% (w/v)	1333 µl
	dH_2O	266 µl
	Li-Acetate (1M)	200 µl
	10xTris Buffer (100 mM Tris-HCl pH = 7.5, 10 mM EDTA)	200 µl

2.8.7 Creating Knockouts via the CRSIPR-Cas9 System "*SpEdit*"

Using the CRISPR-Cas9 system "SpEdit"[210] two knockout strains of *GGT1* and *GGT2* were generated in a *pcsΔ* background. The pLSB-Nat plasmid used in this work was friendly provided by S. Torres-Garcia from the Allshire lab in Edinburgh.

Using the sgRNA search tool CRISP4P (bählerlab.info) sgRNA for the respective target genes were selected and modified for the cloning procedure into the pLSB-Nat vector. Attachment of the sequence "GACT" at the 5´-end of the sgRNA forward Primer and "AAAC" at the 5´-end of the sgRNA reverse Primer provided the compatible overhangs for the ligation into the pLSB-NAT vector after digestion via BsaI. One µl of 100 µM Forward and reverse Primer of the sgRNA were added to 2 µl of Annealing Buffer and 16 µl of dH_2O. The forward and reverse Primers of the respective gRNA were annealed by incubation at 95 °C for 5 min and stepwise reduction of the temperature (5 °C steps for 30 s) down to 20 °C before they were stored at 4 °C. Using the protocol for small fragments Golden Gate assembly the annealed oligos were cloned into the pLSB-Nat vector. Competent *E. coli* cells (DH10B) were transformed with the construct by adding 5 µl of the Golden Gate reaction. Cells were spread on plates with 50 µg/ml Carbenicillin and incubated for 16 h at 37 °C. Four *E. coli* colonies were picked, and liquid cultures were set up with 3.5 ml of LB (+ 75 µg/ml Ampicillin). After isolation of the constructs via the GeneJet Plasmid-Kit (Fisher Scientific, Germany), a 500 ng sample of the minipreparation was sent for Saenger sequencing (EZ-macrogen, Europe) using the pGEMT-fw primer to confirm the sgRNA insertion into the backbone.

S. pombe cells were freshly grown on YE5S plates the day before the transformation. One scoop of cells was transferred to 200 µl of "one step buffer" (Tab. 7) and carefully resuspended. After addition of 100 ng construct, cells were vortexed for 10 s and incubated for 4 h at 42 °C, before they were spread on YE5S plates containing 100 µg/ml Nourseothricin. Plates were incubated at 30 °C for two to seven days and monitored for the occurrence of resistant colonies. Clones were picked and streaked on YE5S plates without Nourseothricin. To test the loss of the plasmid, picked colonies were re-streaked on YE5S + Nou. to check their lack of resistance.

Next, clones were checked via colony PCR using the respective delcheck forward and reverse primers to amplify the gene of interest. PCR products were purified by gel extraction and a sample containing approximately 500 ng of PCR product was sent for Saenger sequencing (Macrogen Europe) using the respective delseq and/or delcheck primer(s) to check the coding sequence for mutations at the target site. Knockout strains were stocked at -80 °C in 40 % glycerol.

2.8.8 Chromosomal Gene Replacement

To generate knockout mutants via homologous recombination[218,219], 200–500 bp of the 5´UTR and 3´UTR flanking the gene of interest were amplified, introducing specific target sites for subsequent cloning into the target vector and ligating both PCR products. After cloning into the target vector, the constructs were linearized by cutting at the ligation site between the 5´ and 3´UTR using XbaI (FD XbaI, Fisher Scientific, Germany), thereby creating homologous arms to the gene of interest, which was to be replaced. The purified constructs were transformed into *S. pombe* (see Transformation of *S. cerevisiae* and *S. pombe*). Transformed cells were plated on YE5S and incubated for 16 h at 30 °C before being stamped onto plates containing 100 mg/ml G418. After 2-5 days, the appearing clones were restreaked onto new plates and checked via colony PCR for successful target gene disruption.

2.9 Biochemical Methods

2.9.1 SDS-PAGE and Western Blot Analysis

2.9.1.1 Protein extraction

S. pombe cells logarithmically grown in SD medium for 6 h without thiamine, and 10 ml of culture (OD_{600} ≈ 0.8) were harvested by centrifugation (2 min at 3000 rpm). The cell pellet was washed twice with 10 ml of dH_2O. For cell wall removal, 300 µl of dH_2O and 300 µl of 0.6 M NaOH were added to the cells, and the mixture was incubated for 10 min at room temperature (RT). After discarding the supernatant, 70 µl of modified sample buffer (60 mM Tris-HCl, pH 6.0, 4% (v/v) β-mercaptoethanol, 4% (w/v) SDS, 5% (v/v) glycerol, 0.01% (w/v) bromophenol blue) were added, and the cells were boiled for 3 min in a water bath. Following this, cell debris were pelleted by centrifugation, and the supernatant was transferred to a new reaction tube.

2.9.1.2 SDS PAGE

For size-dependent protein separation, 30 µl of denatured protein extract was loaded onto an SDS-PAGE gel (see Table 8 for details). As a molecular weight standard, the PageRuler™ Prestained Protein Ladder (Fisher Scientific, Germany) was diluted 1:2 in modified sample buffer, and 30 µl was loaded onto the gel. A vertical double gel system (PEQLab Biotechnology, Germany) was used, filled with SDS running buffer (25.01 mM Tris, 192.4 mM glycine, 3.47 mM SDS). The electrophoresis was conducted in two phases: an initial phase at 10 mA/gel for 40 min, followed by a second phase at 20 mA/gel for 70 min.

2.9.1.3 Blotting

Whatman filter papers and the nitrocellulose (NC) membrane (GE Healthcare, Germany) were incubated for 2 min in transfer buffer (190 mM glycine, 28.9 mM Tris, 20% (v/v) methanol). For blotting the membranes from the SDS-gel onto the NC membrane, a semi-dry transfer system was used (PEQLab, Germany), placing two Whatman filter papers on the apparatus base, followed by the NC membrane, the gel, and two additional Whatman filter papers on top. Blotting was conducted by applying 45 mA/gel (≈0.8 mA/cm²) for 70 min. The membrane was then washed three times for 5 min each in TBS-T (10 mM Tris, 150 mM NaCl, 0.1% (v/v) Tween20). After

washing, the NC membrane was transferred to a blocking solution (10% (v/v) skim milk powder in TBS-T) and incubated overnight at 4°C.

The next day, the blocking solution was removed, and the NC membrane was washed again three times with TBS-T. Following removal of the blocking solution, the primary antibody anti-GFP (11814460001, Hoffmann-La Roche, Switzerland) was added at a 1:1000 dilution in blocking solution. The NC membrane was incubated for 1 h at room temperature (RT), after which the primary antibody was removed, and the membrane was washed three times with TBS-T. The secondary anti-mouse antibody (A9044, Sigma-Aldrich, USA) was then added at a 1:10000 dilution in blocking solution, and the NC membrane was incubated for another 1 h at RT, followed by removal of the antibody and repetition of the three washing steps with TBS-T.

For detection, 300 µl of a 1:4.25 diluted chemiluminescent substrate mixture (substrate A + substrate B, diluted in 150 mM Tris, pH 8.8) was applied to the NC membrane, and the signal was detected after a 3 min exposure time using a chemiluminescent detector (Intas Science Imaging Instruments GmbH, Germany).

Subsequently, the NC membrane was stained to visualize the loaded protein. After a brief rinse with dH_2O, the membrane was incubated for 10 seconds in amido black solution (0.1% (w/v) amido black, 40% (v/v) methanol, 10% (v/v) acetic acid). Following removal of the amido black solution, the membrane was washed three times for 5 min in dH_2O, and a photo of the protein bands was taken.

Tab. 8 SDS-PAGE. Ingredients and volumes.

Gel	Chemicals	Volume (per gel)
Stacking gel	dH_2O	2.8 ml
	Acrylamid 30% (v/v)	660 µl
	0.5 M Tris-HCl (pH = 6.8)	500 µl
	SDS 10% (w/v)	40 µl
	Ammonium persulfate 10% (w/v)	40 µl
	TEMED	4 µl
Separating gel	dH_2O	6.6 ml
	Acrylamid 30% (v/v)	8 ml
	1.5 M Tris-HCl (pH = 8.8)	5 ml
	SDS 10% (w/v)	200 µl
	Ammonium persulfate 10% (w/v)	200 µl
	TEMED	12 µl

2.9.2 γ-glutamyl Transpeptidase Assay

The following protocol is based on the description by Adamis et al. (2008)[220].

For each strain, 50 ml of logarithmically growing *S. pombe* cells (OD_{600} ≈ 0.4–0.6) were harvested and washed twice with sterile dH_2O (3000 rpm, 2 min). Pellets were resuspended on ice in 5 ml of 0.1 M Tris-HCl (pH 9.0). Cells were lysed by sonication on ice (2 min at 40% power, followed by 3 min at 60% power). The protein concentration of each extract was determined via BCA assay.

Several dilutions of protein extract were prepared (1:2, 1:5, and 1:10), and additional samples of denatured protein extract were prepared by boiling in a water bath to verify the enzymatic nature of the reaction. For the measurement, 50 µl of protein extract was mixed with 50 µl of the donor/acceptor mixture (2 mM L-7-glutamyl-p-nitroanilide, 200 mM glycylglycine). The increase in absorbance was measured at 412 nm and 37°C over one hour while shaking at intensity 3 on the ELISA reader. The γ-GT activity was calculated based on the linear slope of absorbance

increase and normalized to a blank consisting of 50 µl Tris-HCl and 50 µl of the donor/acceptor mixture.

2.10 Analytical Methods and Bioinformatics

2.10.1 Sample Preparation For Elemental Analysis and Arsenic Speciation

2.10.1.1 Preparation of *A. thaliana* and *O. sativa* Protein Extracts for the As^V Reductase Assay

Plants of the *A. thaliana hac1* mutant and WT Col-0 were grown in the hydroponic system for 5 to 6 weeks using 1/10 Hoagland medium (detailed description see 2.6.2). *O. sativa* (Kitaake) was grown as described in Kerl et al. (2019)[83]. Roots were harvested and stored at -80 °C. Roots of three or four plants were crushed with a mortar and 250 mg of crushed plant material was diluted in 13.5 ml extraction buffer (Kerl et al., 2019)[83]. Protein concentrations were measured using the Pierce™ BCA-Assay Kit (Fisher Scientific, Germany)[221].

Protein extract of *A. thaliana* Col-0 and *hac1* or *O. sativa* (Kitaake) was diluted to equimolar concentrations and MTA was added to a final concentration of 330 ppb. After incubation of 1, 2, 3, 5 and 10 min at 37 °C the samples were measured after transferring the protein extract containing MTA into a veil using 20 µm CA filters (Machery-Nagel, Germany). Samples were immediately speciated using an ion chromatograph coupled to an inductively coupled mass spectrometer (IC-ICP-MS) (see 2.10.3). As a negative control MTA of the same amount was added to boiled protein extract.

2.10.1.2 Preparation of *A. thaliana* Protein Extracts for the As^V Reductase Assay

S. pombe cells of the WT strain harboring either pSGP72-*AtHAC1-GFP* or pSGP72-GFP were grown overnight at 30°C while shaking at 220 rpm in 50 ml EMM supplemented only with adenine (Tab. 5) and 20 µM thiamine. Cells were washed twice with sterile water (3000 rpm, 2 min), and 200 ml of EMM without thiamine was inoculated to an OD_{600} of 0.2. After 6 h of incubation (30°C, 220 rpm), the logarithmically growing cells were harvested and washed twice in sterile water (3000 rpm, 2 min). The cell pellets were flash-frozen in liquid nitrogen and stored at -80°C.

Proteins were extracted by grinding the pellets over dry ice using quartz sand (Honeywell Fluka™, Fisher Scientific, Germany). The ground material was resuspended in 2 ml of extraction buffer on ice (see 2.10.1) and centrifuged at 1500 rpm for 10 min at 4°C. A total of 1.5 ml of the supernatant was transferred to a desalting spin column equilibrated with 2.5 ml of extraction buffer (PD-10 columns with Sephadex G-25 resin, Cytiva, USA). After adding 1 ml of extraction buffer to the supernatant, the protein extract was desalted as described in the PD Spin protocol. Protein concentrations of the desalted extracts were measured using the Pierce™ BCA Assay Kit (Fisher Scientific, Germany)[221].

2.10.1.3 Sample Preparation for ∑As Measurements and Speciation Analysis

Yeast pellets and root material were washed in 1 mM KH_2PO_4, followed by 0.5 mM $Ca(NO_3)_2$ and 5 mM MES (10 min, 4°C). Samples for speciation analysis were flash-frozen in liquid nitrogen, while samples for ∑As determination were dried at 60°C for 32 hours (yeast pellets) or 7 days (plant material).

For ∑As determination, whole yeast pellets or 5–20 mg of plant material were microwave-digested (START 1500, MLS GmbH, Germany) with 2 ml of 65% HNO_3 and 1 ml of H_2O_2.

For speciation analysis, 10–80 mg of frozen plant material was ground. The ground material was transferred to 2 ml reaction tubes, and 400 mg of glass beads were added before 1.5 ml of PBS buffer (2 mM NaH_2PO_4, 0.2 mM Na_2-EDTA, pH 6.0). The samples were then boiled for 5 min in a water bath and cooled on ice for 2 min. After cooling, the samples were vortexed for 53 min under a nitrogen/hydrogen (N_2/H_2 95/5% v/v) atmosphere in a glove box (COY). The extracts were subsequently filtered using 0.2 µm cellulose-acetate filters (Macherey-Nagel, Germany) and directly analyzed via ion chromatography coupled with inductively coupled plasma mass spectrometry (IC-ICP-MS).

2.10.1.4 Preparation of Medium Samples for Speciation Analysis

For speciation analysis, 1 ml of medium from each treatment was taken and centrifuged for 5 min at 3000 g and 4°C. Subsequently, 500 µl of the supernatant was filtered using a 20 µm cellulose acetate filter (Macherey Nagel) and flash-frozen in liquid nitrogen. The samples were stored until speciation at -80°C.

2.10.2 Determination of ∑As

The digested *S. pombe*, *S. cerevisiae*, and *A. thaliana* samples were analyzed using an inductively coupled plasma mass spectrometer (ICP-MS, XSeries 2, Thermo Scientific) to measure AsO^+ at m/z 91, with rhodium (Rh^+, m/z 103) as the internal standard.

2.10.3 Generating Yeast Material for Thiol Analysis

For thiol analysis upon MTA and As^V exposure in WT and *pcsΔ* strains heterologously expressing *AtHAC1*, cultures of logarithmically growing cells were exposed for 18 h to 8 µM MTA or 0.5 µM As^V. Cells were cultivated in EMM supplemented with adenine and 15 nM thiamine.

To generate cell material for thiol analysis of mutant strains derived from the As^{III}-evolutionary project and the respective double knockout mutants, logarithmically growing cells were exposed to 10 mM As^{III} for 18 h in YE5S medium.

Cells were harvested at 3,000 x g for 3 min and washed twice with 5 ml of sterile dH_2O, then lyophilized for 48 hours (using an ALPHA 2-4 with LDC-1M control, Martin Christ Gefriertrocknungsanlagen GmbH, Osterode am Harz, Germany).

2.10.4 Speciation Analysis

Arsenic species in the protein extracts of *S. pombe*, *E. coli*, and *A. thaliana* (see As^V Reductase Assays), as well as in root and shoot material of plants, as well as medium samples (see Uptake experiments) were analyzed using an ion chromatography (IC) system (Dionex ICS-3000) coupled to an ICP-MS system (XSeries 2, Thermo Scientific) with oxygen as the reaction cell gas (AsO^+, m/z 91). An AS16 column (Dionex AG/AS16 IonPac) with a flow rate of 1.2 ml/min and a NaOH gradient of 2.5–100 mM was used to separate the As-species[222].

2.10.5 Thiol Extraction and Profiling

To extract thiol compounds, 3 volumes of extraction buffer (0.1% (v/v) trifluoroacetic acid, 6.3 mM diethylenetriamine pentaacetic acid (DTPA), and 0.04 mM N-acetylcysteine as an internal standard) were added per mg of plant material fresh weight. When extracting thiols from lyophilized *S. pombe* cells, 83.33 µl of extraction buffer was added to a sample with an OD_{600} value corresponding to 1.0. Samples were vortexed for 1 min and then chilled on ice for 15 min. Cell

debris were removed by centrifugation (14,000 rpm, 15 min, 4°C), and the supernatant was transferred to a new 1.5 ml reaction tube.

32.25 µl of each extract was transferred to amber-colored 1.5 ml reaction tubes to protect the sample from light after the labeling procedure. For derivatization, 77 µl of 200 mM EPPS containing 6.3 mM DTPA (pH 8.2, adjusted with NaOH) and 3.13 µl of tris(2-carboxyethyl)phosphine, dissolved in 200 mM EPPS (pH 8.2), were added, and the mixture was incubated for 10 min at 45°C. The labeling reaction was initiated by adding 2.5 µl of 50 mM monobromobimane (dissolved in acetonitrile). After a 30 min incubation at 45°C, the reaction was stopped by adding 12.5 µl of 1 M methanesulfonic acid. Samples were stored at -20°C until HPLC analysis.

Thiol profiles were determined as described in Fischer et al. (2014) [223].

2.10.6 Bioinformatics

The results from the gDNA resequencing of *S. pombe* mutants derived from the As^{III} evolutionary project were analyzed using Geneious Prime 2021/2022. The "Find Variation/SNPs" function was applied to identify non-synonymous polymorphisms in coding sequences (CDS). The sequenced genomes were aligned to the *pcsΔ* reference genome, and the analysis was performed using the default settings.

To identify orthologous genes, the OMA browser[192] was used to analyze the distribution of As^{V} reductases, As^{III} efflux transporters, phytochelatin synthases, and S-adenosyl-methyltransferases across different kingdoms of life (default settings, PSI-BLAST). As query inputs, *A. thaliana PCS1*, *C. elegans PCS1*, *S. pombe pcs2*, *T. turgidum PCS1*, *E. coli arsC* and *arsB*, *A. thaliana HAC1*, *S. cerevisiae ACR2* and *ACR3*, *H. sapiens AS3M* and *Clostridium sp. arsM* were used. After removing redundancies, the co-occurrence of these detoxification mechanisms were visualized using a Venn diagram generated with the jVenn tool[193].

Protein structure predictions were generated using the alpha-fold version (22-11-01)[224,225].

3. Results

3.1 Monothioarsenate (MTA)

3.1.1 Uptake of MTA via P_i Transporters

Aside from the presumption that As^V and MTA share common detoxification mechanisms, it is also assumed that MTA, like As^V, is taken up via transporters of the PHT family[52,60]. Experiments in rice, showing a correlation between MTA uptake and available P_i concentrations, further support this hypothesis[6]. This work aimed to bridge the gap between the presumed role of P_i transporters in MTA uptake and direct experimental evidence supporting this hypothesis.

To investigate whether MTA uptake is indeed mediated by P_i transporters, first uptake experiments using the *S. cerevisiae pho84* mutant were conducted, providing initial evidence for P_i transporter-mediated MTA uptake. Exposure to As^V (Fig. 4A), as well as MTA (Fig. 4B), resulted in significantly reduced arsenic accumulation in the *pho84* mutant compared to the WT. The determined ∑As in cells exposed to MTA was about 25 times lower than in cells treated with the same concentration of As^V. As a control, As^{III} treatments confirmed the species-specific transport of As^V and MTA by Pho84, as indicated by the lack of differences in ∑As between WT and *pho84* (Fig. 4C). Arsenic uptake of cells exposed to any of the tested species at 4°C was nearly completely abolished (Fig. 4D-F), demonstrating that the arsenic accumulation observed at 30°C was the result of active transport through the plasma membrane rather than passive diffusion. Speciation analysis from one of these uptake experiments (Fig. S1) reveals that only trace amounts of MTA and As^V were converted to As^{III} (As^V: 0.162%/0.096%; MTA: 0.049%/0.079%).

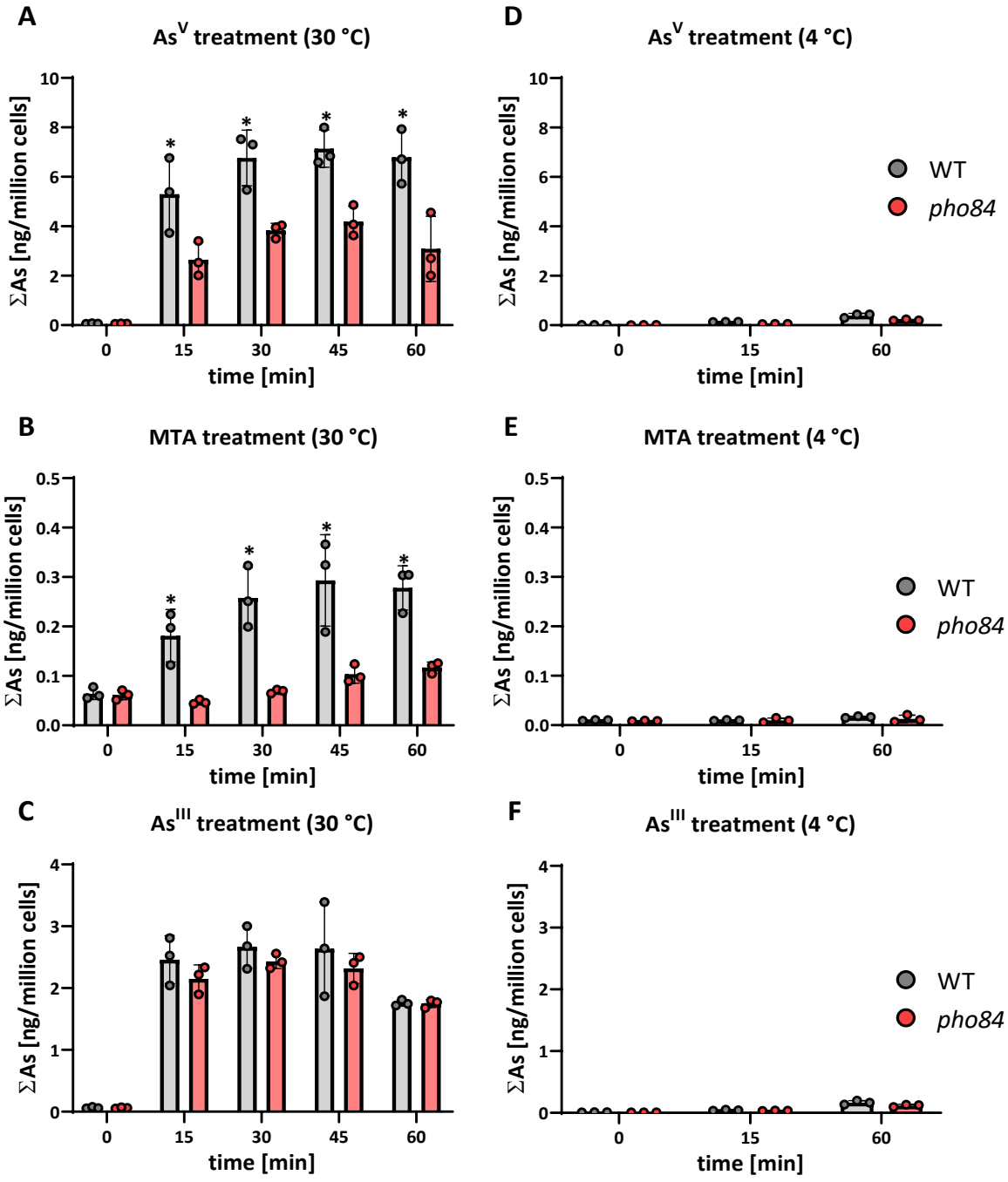
A
As^V treatment (30 °C)
ΣAs [ng/million cells]
time [min]
B
MTA treatment (30 °C)
C
As^III treatment (30 °C)
D
As^V treatment (4 °C)
E
MTA treatment (4 °C)
F
As^III treatment (4 °C)
WT
pho84

Fig. 4: Arsenic accumulation in *S. cerevisiae* BY4742 WT and the *pho84* mutant exposed to 50 µM MTA, As^{V} or As^{III} under P_i-depleted conditions. Logarithmically growing cells were transferred to an uptake solution containing 50 µM MTA, As^{V} or As^{III}, and cells from each genotype were harvested at 0, 15, 30, 45 and 60 min for treatments conducted at 30°C (A-C), or at 0, 15 and 60 min for treatments at 4°C (D-F). ∑As in *S. cerevisiae* cells was quantified using an ICP-MS and normalized to the OD_{600} value measured at each time point. Statistical analysis was performed using the two-sample t-test for pooled variance to assess significant differences in ∑As among the genotypes for each treatment and time point separately ($p < 0.05$). Statistically significant differences are indicated by an asterisk (*). Data represent the mean ± standard deviation of three biological replicates (n = 3).

Based on these results, experiments with the *A. thaliana pht1;1* T-DNA insertion line (SALK_088586) were conducted, to evaluate whether these findings align with the uptake of MTA in plants. Due to the high redundancy of PHT transporters in plants, under P_i-sufficient conditions, the effects of a single transporter knockout can be obscured by its paralogs. Consequently, deciphering the roles of individual transporters within the PHT1 cluster, primarily responsible for P_i uptake (e.g., PHT1;1, PHT1;2, and PHT1;3 in *A. thaliana*) [226], can be challenging. Therefore, it is essential to determine an optimal P_i supply that balances between excessively high and low concentrations. The effect of losing a single transporter can also be masked either by the presence of excess P_i or by the upregulation of other members of the cluster when P_i availability is limited[227]. Under P_i-starvation conditions, the upregulation of P_i transporters is primarily mediated by the transcription factors PHR1 and PHL1[228]. Hence, the following experiments were conducted using the *pht1;1* mutant and the *phr1-1 phl1* double mutant[202] to investigate how the loss of a key P_i transporter[51] and an impaired P_i starvation response (PSR)[228] affect MTA uptake and toxicity under P_i-sufficient and P_i-deficient conditions.

Assuming that reduced MTA uptake might enhance the tolerance, toxicity assays were conducted (Fig. 5A-C). To test whether the loss of a key P_i transporter (*pht1;1*) or the impairment of the PSR (*phr1-1 phl1*) manifests in higher tolerance to MTA, root lengths and fresh weights of seedlings grown for 14 days on plates containing 50 µM MTA or 12.5 µM As^{V} were determined (Fig. 5D-F). Significantly longer primary roots and higher fresh weights of *pht1;1* and *phr1-1 phl1* mutants compared to Col-0 provided initial evidence for a P_i transporter-mediated uptake of MTA, similar to what is already known for As^{V} in *A. thaliana*[52]. Fresh weights and root lengths of *pht1;1* and *phr1-1 phl1* seedlings grown under control conditions were comparable to WT growth, indicating that the mutants were not affected by the diminished P_i concentrations (55 µM). Repeating this

experiment with elevated P_i levels (2.5 mM) eliminated the growth-inhibitory effects of MTA and As^V, highlighting the correlation between P_i availability and the toxicity of MTA and As^V (Fig. 6A-D). Furthermore, the superior growth observed in both mutants was lost under elevated P_i levels, coinciding with the marked reduction in toxicity. Notably, the *ph1-1phl1* double mutant performed even worse under these conditions than when exposed to the same dosage of As^V.

Measurements of chlorophyll and cyanidin content provided further evidence that the mutants were less affected by As^V and MTA treatments (Fig. 5F-I). Col-0 seedlings treated with As^V or MTA accumulated more cyanidin (Fig. 5I) and exhibited reduced chlorophyll levels compared to *pht1;1* and *phr1-1 phl1* (Fig. 5F-H), reinforcing the idea of reduced MTA uptake in the mutants. Moreover, the mutants displayed comparable or even lower chlorophyll and similar anthocyanin levels under P_i-sufficient conditions, confirming that the observed chlorophyll depletion and anthocyanin increase were not due to P_i deficiency but rather to reduced arsenic stress.

These observations were also corroborated by a liquid seedling assay, where *pht1;1* and *phr1-1 phl1* mutants exhibited significantly higher fresh weights compared to Col-0 upon exposure to MTA or As^V (Fig. 7A-D), aligning with the hypothesis of P_i transporter mediated MTA uptake.

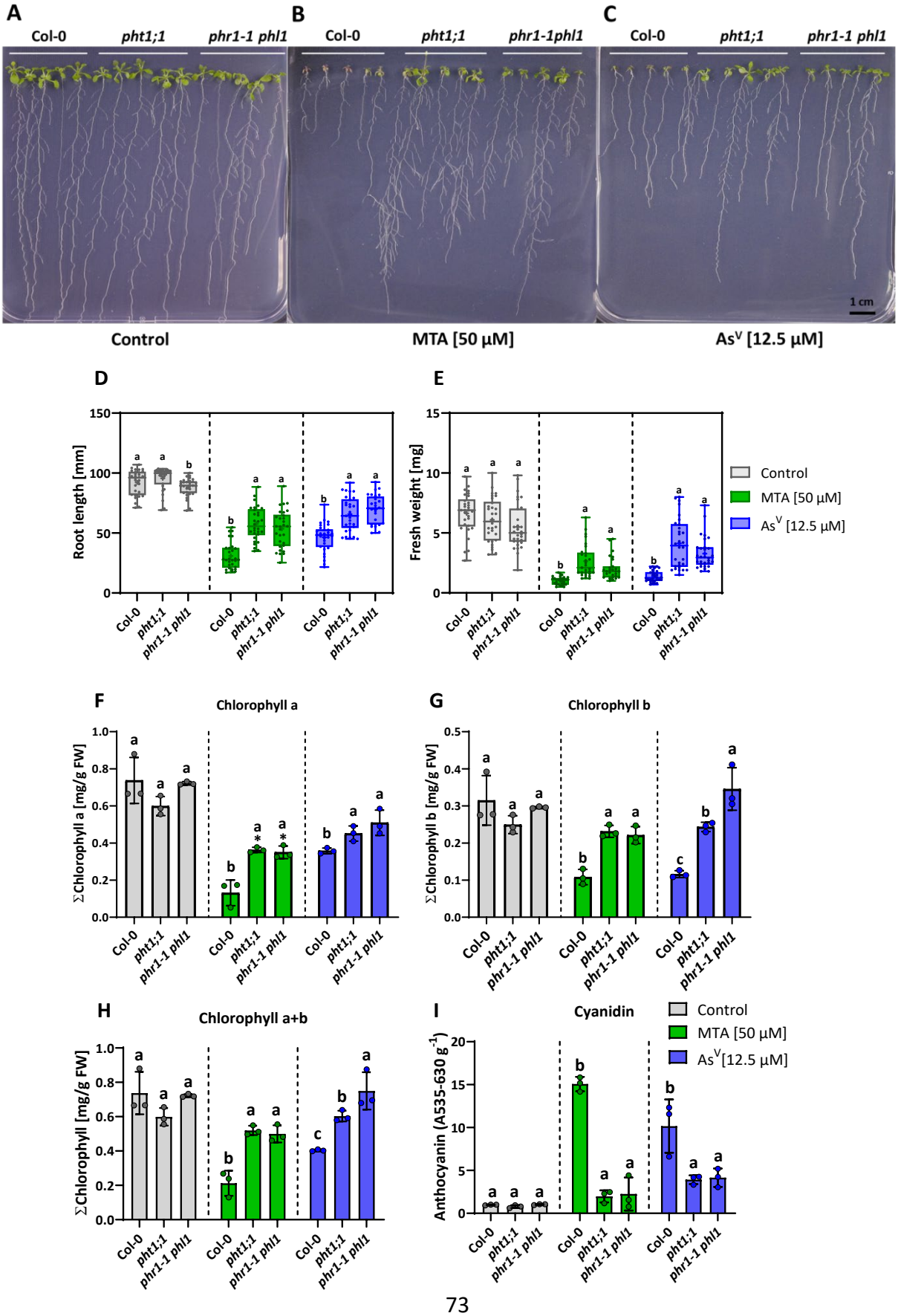
A
B
C
Col-0
pht1;1
phr1-1 phl1
phr1-1phl1
1 cm
Control
MTA [50 µM]
As^V [12.5 µM]
D
Root length [mm]
E
Fresh weight [mg]
Control
MTA [50 µM]
As^V [12.5 µM]
F
Chlorophyll a
ΣChlorophyll a [mg/g FW]
G
Chlorophyll b
ΣChlorophyll b [mg/g FW]
H
Chlorophyll a+b
ΣChlorophyll [mg/g FW]
I
Cyanidin
Anthocyanin (A535-630 g^-1)

Fig. 5: Loss of PHT1;1 and an impaired P_i starvation response enhance tolerance to MTA, reflected in reduced growth inhibition, maintained chlorophyll levels, and lower cyanidin accumulation. Seedlings of WT (Col-0), the *pht1;1* mutant and the *phr1-1 phl1* mutant grown for 14 days under control conditions (A), on plates with 50 µM MTA (B) or 12.5 µM As^V (C) each supplemented with 55 µM P_i. Comparison of root lengths (D) and fresh weights (E) of Col-0, the *pht1;1* mutant, and the double mutant *phr1-1 phl1* grown for 14 days on plates with or without MTA [50 µM] or As^V [12.5 µM] and 55 µM P_i. Statistical analysis was performed using the Kruskal-Wallis test to assess significant differences in ∑As among genotypes for each treatment separately, followed by a post hoc test for pairwise comparisons ($p < 0.05$). Statistically significant differences are indicated by different letters. Mean values are marked with a cross symbol. Data represent three biological replicates; n = 28-30 per condition and genotype.

Comparison of chlorophyll and cyanidin concentrations in seedlings of WT (Col-0), the *pht1;1* mutant, and the double mutant *phr1-1 phl1* grown for 14 days on plates with or without (grey), MTA [50 µM] (green) or As^V [12.5 µM] (blue). Chlorophyll a (F), chlorophyll b (G), and ∑chlorophyll concentrations (H) for each treatment are shown as bar plots with individual data points for each replicate. Cyanidin levels for each genotype are presented similarly (I). Statistical analysis was performed using a two-sample t-test with pooled variance to assess significant differences in chlorophyll and anthocyanin contents among genotypes through pairwise comparisons for each treatment ($p < 0.05$). Statistically significant differences are marked with an asterisk (*). Data represent the mean ± standard deviation of three biological replicates (n = 3); +/- the standard deviation (F-I) or max to min (D+E).

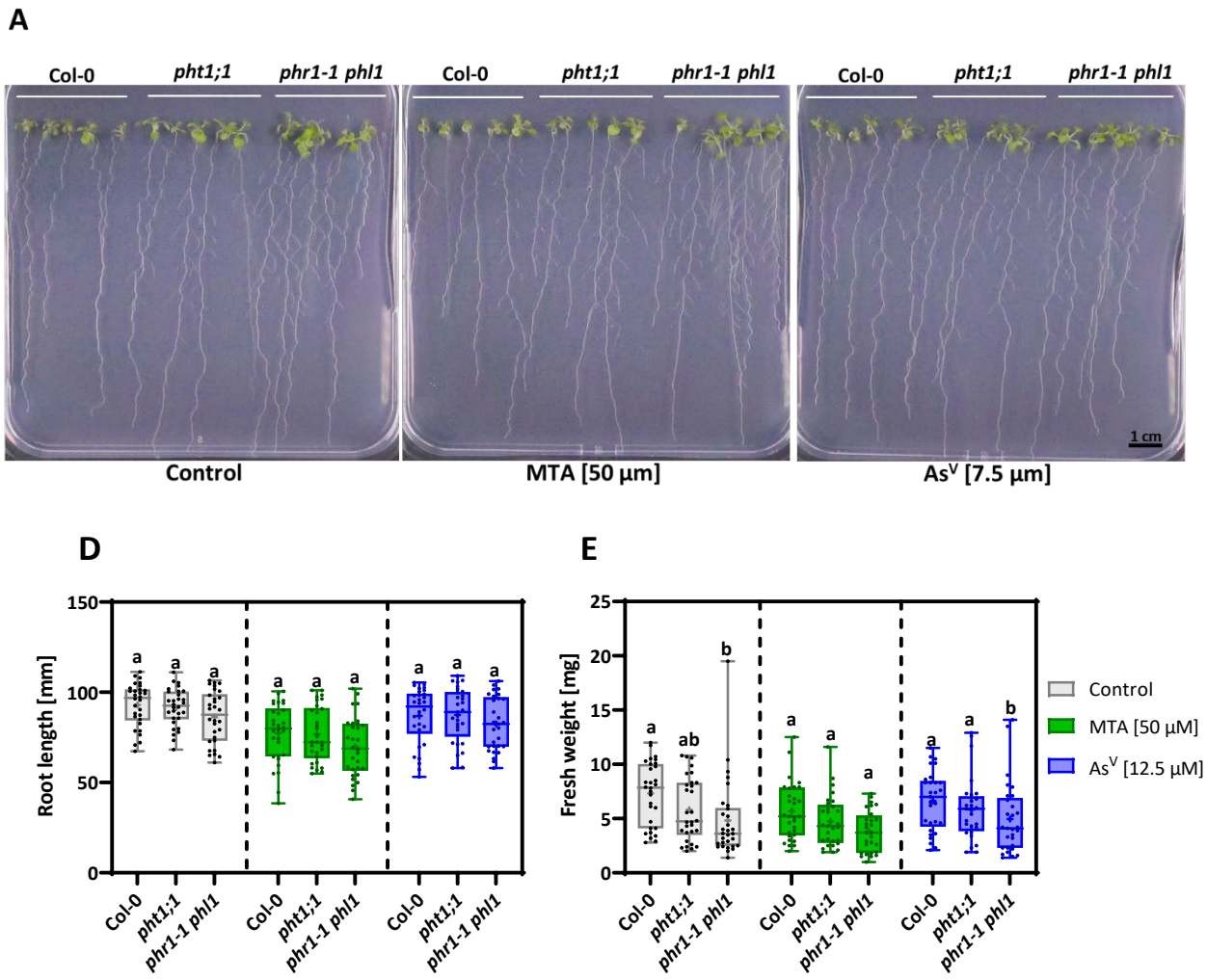

Fig. 6: Effect of P_i availability on MTA and As^V toxicity. Seedlings of WT (Col-0), the *pht1;1* mutant and the *phr1-1 phl1* mutant grown for 14 days under control conditions (A), on plates with 50 µM MTA (B) or 12.5 µM As^V (C) each supplemented with 2.5 mM P_i. Comparison of root lengths (D) and fresh weights (E) of Col-0, the *pht1;1* mutant, and the double mutant *phr1-1 phl1* grown for 14 days on plates with or without MTA [50 µM] or As^V [12.5 µM] and 2.5 mM P_i. Statistical analysis was performed using the Kruskal-Wallis test to assess significant differences in ∑As among genotypes for each treatment separately, followed by a post hoc test for pairwise comparisons ($p < 0.05$). Statistically significant differences are indicated by different letters. The medians are marked with a horizontal line.

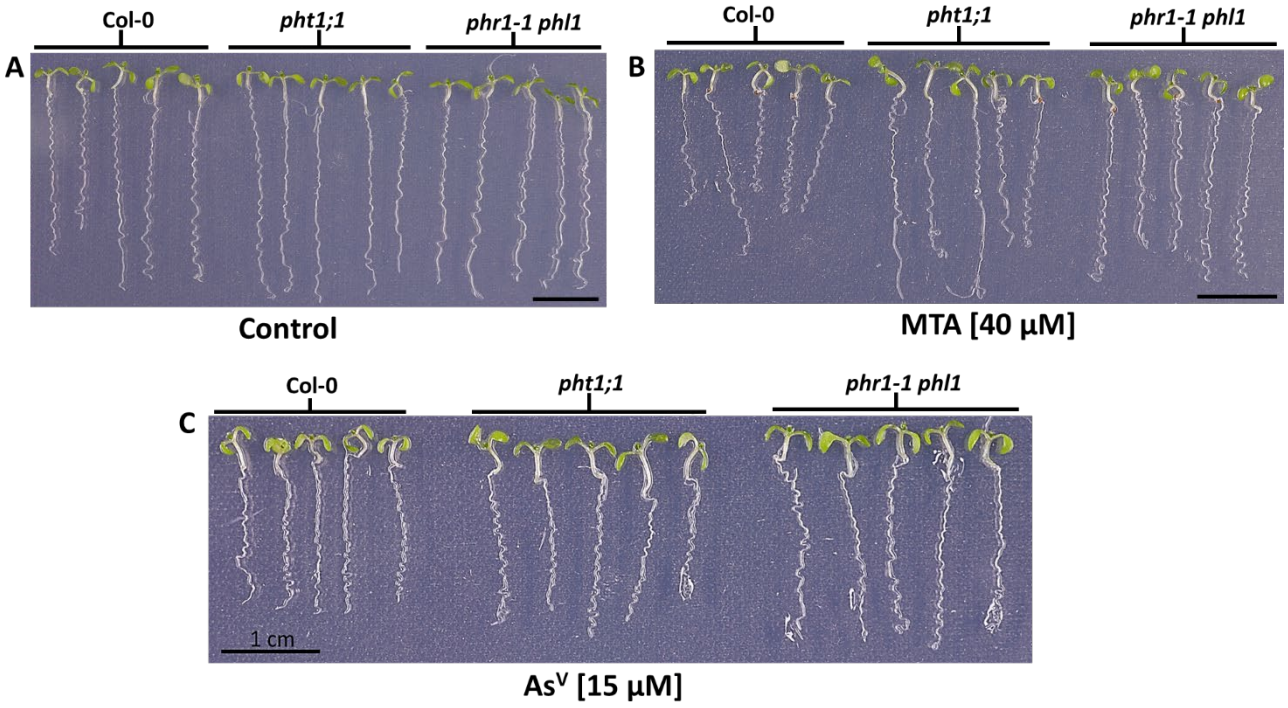
A
Col-0
pht1;1
phr1-1 phl1
Control
B
Col-0
pht1;1
phr1-1 phl1
MTA [40 µM]
C
Col-0
pht1;1
phr1-1 phl1
1 cm
AsV [15 µM]

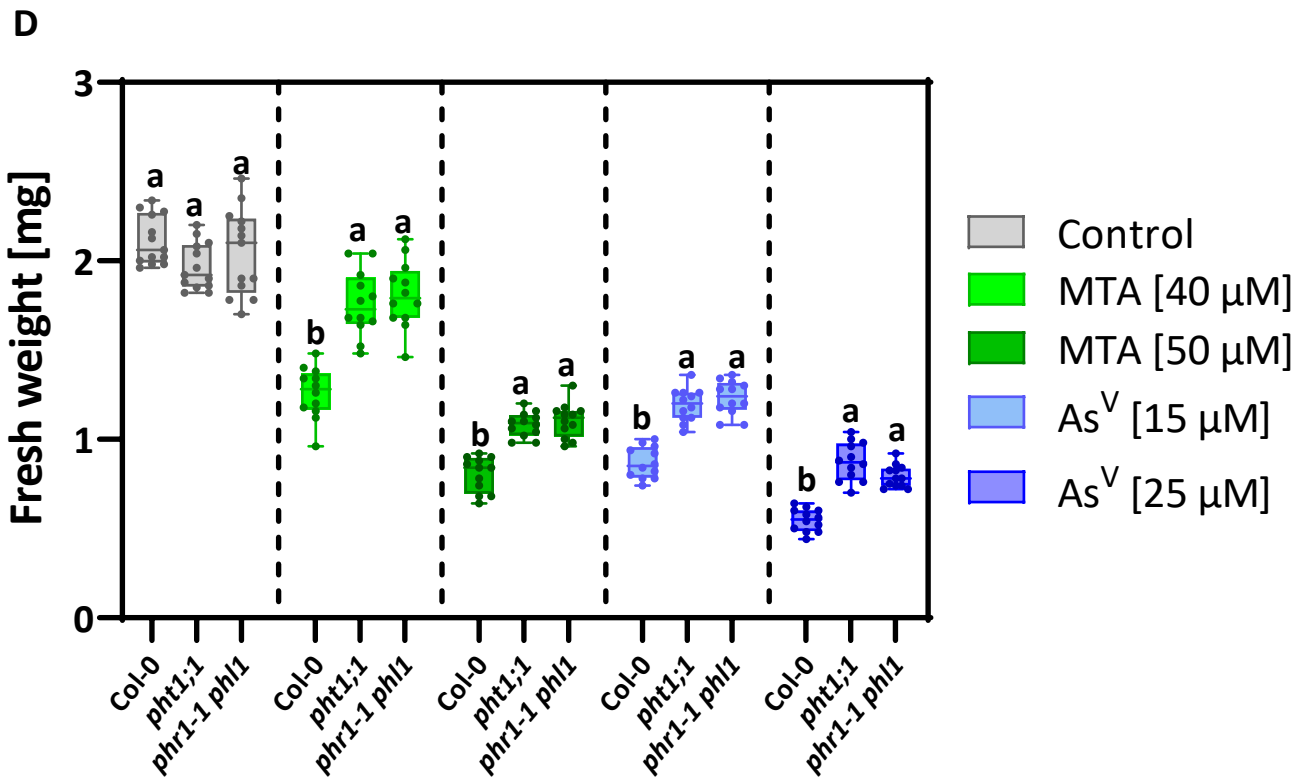
D
Fresh weight [mg]
0
1
2
3
a
b
Col-0
pht1;1
phr1-1 phl1
Control
MTA [40 µM]
MTA [50 µM]
AsV [15 µM]
AsV [25 µM]

Fig. 7: MTA tolerance is elevated in plants lacking PHT1;1 or with an impaired P_i starvation response. Representative photos of seedlings of WT (Col-0), the *pht1;1* mutant and the *phr1-1phl1* mutant grown for 7 days under control conditions (A), in liquid medium containing 40 µM MTA (B) or 15 µM As^V (C). Comparison of growth inhibition under MTA and As^V exposure among Col-0, the *pht1;1* mutant, and the *phr1-1 phl1* double mutant. Fresh weights of seedlings from each genotype were measured after cultivation for 7 days with or without MTA (40 or 50 µM) or As^V (15 or 25 µM). FWs were normalized to the number of seedlings in each well. Statistical analysis was performed using the Kruskal-Wallis Test ($p < 0.05$) to assess significant differences in FWs among genotypes for each treatment separately, followed by a post hoc test for pairwise comparisons ($p < 0.05$). Statistically significant differences are indicated by different letters. The medians are marked with a horizontal line. Data represent three biological replicates with 18-20 plants each genotype and treatment.

To test whether the observed phenotypes were related to reduced uptake kinetics of As^V and MTA due to the loss of PHT1;1 (*pht1;1*) respectively an impaired P_i starvation response (*phr1-1 phl1*), uptake experiments were performed. Plants hydroponically grown under P_i-sufficient conditions were transferred to low P_i medium (2 µM) 3 days prior and to P_i-free medium 24 hours before exposure to As^V or MTA. Roots and shoots from plants exposed to As^V or MTA for 24 hours were harvested for As-speciation or ∑As determination. Significantly reduced shoot ∑As of *pht1;1* and *phr1-1 phl1* plants exposed to 10 µM As^V for 24 hours suggested reduced uptake in comparison to Col-0. However, while ∑As of roots was significantly reduced in *phr1-1 phl1*, there was no significant difference between Col-0 and the *pht1;1* mutant. In comparison to plants exposed to 10 µM MTA ∑As of roots were over 100 times (roots) respectively 60 times (shoots) higher, when plants were treated with equimolar concentrations of As^V under P_i starvation conditions.

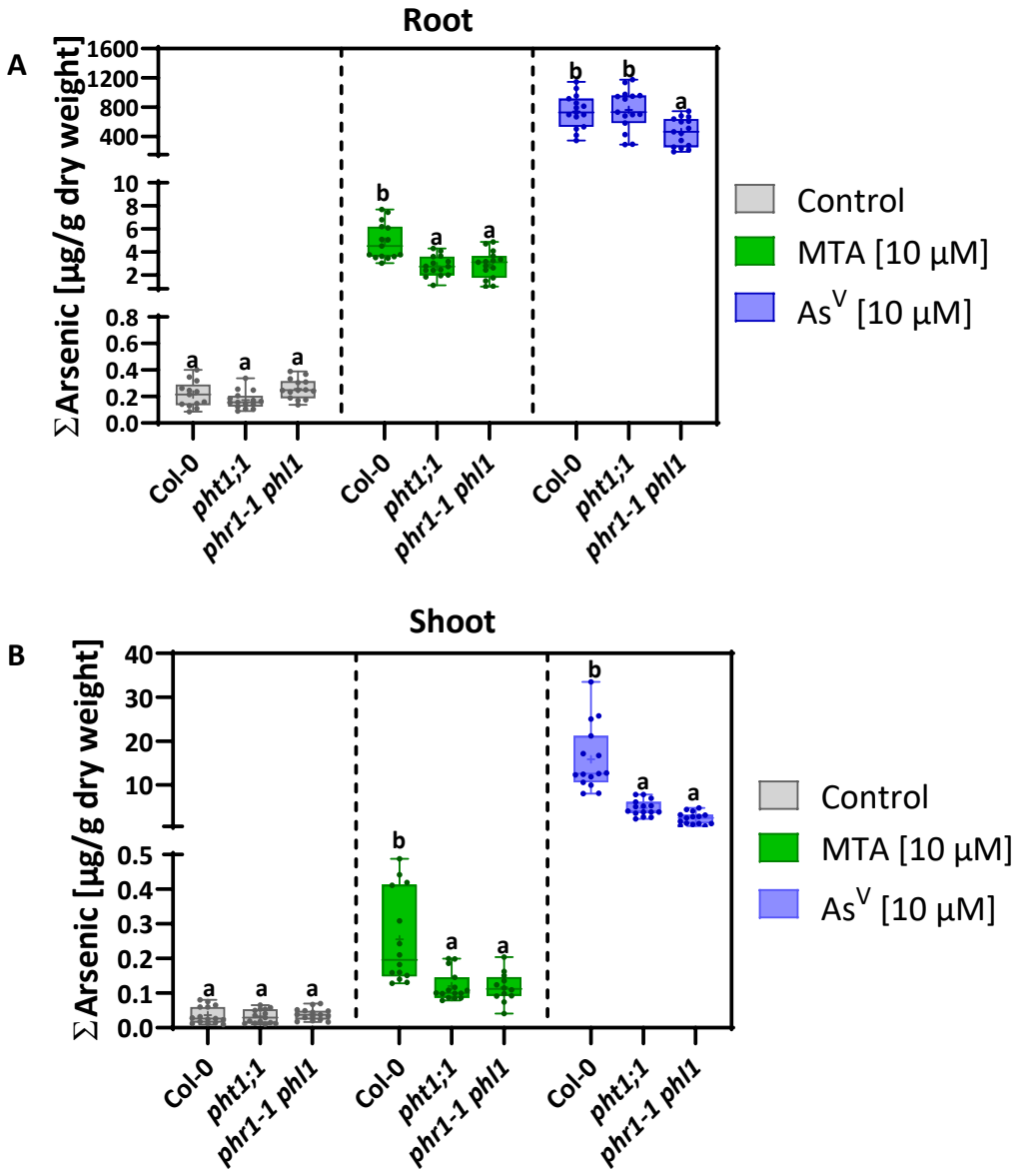

Fig. 8: Arsenic accumulation in *A. thaliana* roots and shoots of WT (Col-0), the *pht1;1* mutant, and the double mutant *phr1-1 phl1* exposed MTA or As^V under P_i-depleted conditions. Five- to six-week-old hydroponically grown plants were transferred to medium containing 2 µM P_i for three days and then to P_i-free medium one day prior to the exposure, to induce P_i- starvation conditions. Plants were treated with 10 µM MTA or As^V for 24 hours in P_i-free medium. The ∑As of 13-15 roots (A) and shoots (B) per treatment and genotype was quantified by ICP-MS. Statistical analysis was performed using the Kruskal-Wallis Test ($p < 0.05$) to assess significant differences in ∑As among genotypes for each treatment separately, followed by a post hoc test for pairwise comparisons ($p < 0.05$). Statistically significant differences are indicated by different letters. Mean values are marked with a cross symbol. Data represent three biological replicates; n = 13-15 per condition and genotype.

Speciation analysis of roots and shoots of Col-0 and *pht1;1* revealed that the majority of MTA and As^{V} taken up was reduced to As^{III}, accounting for over 80% of ∑As. No significant differences in the percentage distribution of As^{III}, and As^{V} were observed between the roots and shoots of Col-0 and *pht1;1*. Only in MTA-treated Col-0 shoots, the proportion of MTA was higher than in shoots of *pht1;1*. Interestingly, the shoots of As^{V}-exposed plants contained small quantities of MTA, accounting for approximately 2.4% to 7.9% of ∑As. Therefore, differences in ∑As of roots and shoots, as well as in the induction of PC synthesis (see below), did not appear to result from variations in the reduction kinetics between Col-0 and *pht1;1* plants. Above, the ∑As calculated from the speciation analysis (Fig. 9E+F) aligned with the ∑As analysis values and the differences between Col-0 and *pht1;1* (Fig. 8), considering an approximate dry-to-fresh weight ratio of 1:8 to 1:10. The only deviation was the absence of a difference in ∑As between Col-0 and *pht1;1* in MTA-treated shoots.

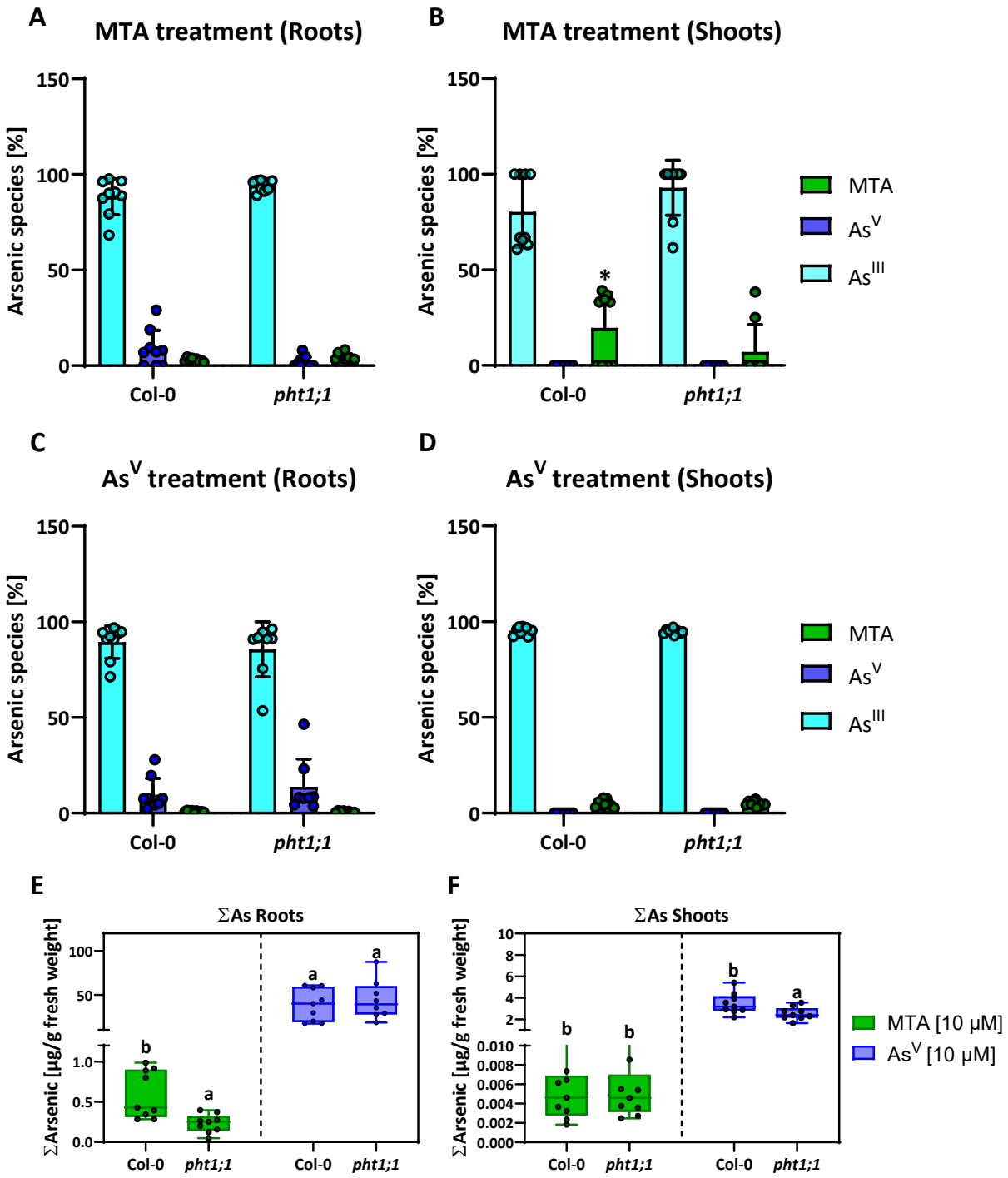
A
MTA treatment (Roots)
B
MTA treatment (Shoots)
Arsenic species [%]
150
100
50
0
Col-0
pht1;1
*
MTA
AsV
AsIII
C
AsV treatment (Roots)
D
AsV treatment (Shoots)
E
ΣAs Roots
ΣArsenic [µg/g fresh weight]
100
50
1.0
0.5
0.0
a
b
F
ΣAs Shoots
10
8
6
4
2
0.010
0.008
0.006
0.004
0.002
0.000
MTA [10 µM]
AsV [10 µM]

Fig. 9: Arsenic speciation of roots and shoots of WT (Col-0) and the *pht1;1* mutant exposed to MTA or As^V under P_i-depleted conditions. Five- to six-week-old hydroponically grown plants were transferred to medium containing 2 µM P_i for three days and then to P_i-free medium one day prior to the exposure, to induce P_i- starvation responses. Plants were treated with 10 µM MTA or As^V for 24 h in P_i-free medium. The speciation of nine roots (A+C) and shoots (B+D) per treatment and genotype was quantified by IC-ICP-MS. The percentage share of the different As-species in roots and shoots of each genotype and treatment are illustrated as bar plots (A-D), and the respective ∑As are depicted as box-plots (E+F). Statistical analysis was performed using the Kruskal-Wallis test to assess significant differences in ∑As among genotypes for each treatment separately, followed by a post hoc test for pairwise comparisons ($p < 0.05$). Statistically significant differences are indicated by letters (∑As) or as an asterix (*) (speciation analysis). Mean values are marked with a cross symbol (E+F). Data represent three biological replicates; $n = 9$ per condition and genotype; +/- standard deviation (A-D) or max to min (E+F).

Consistent with previous findings showing that the uptake of As^V and MTA stimulates PC synthesis[60,83], thiol profiles of seedlings exposed to 130 µM MTA or As^V were analyzed (Fig. 10). In contrast to the previous experiments using plant agar, these assays were conducted on type E agar plates, where preliminary tests showed only minor PC induction and less pronounced toxic effects for MTA and As^V concentrations below 80 respectively 130 µM. Consequently, higher MTA concentrations than those used in the earlier experiments were applied in this experiment. Seedlings were initially grown for 12 days on plates with diminished P_i-concentrations (30 µM P_i), before being transferred to P_i-free plates with the respective As-species, to avoid reduced uptake due to P_i saturation. Next, GSH and PC contents were measured in the roots and shoots of seedlings exposed to As^V or MTA for 24 or 72 hours (Fig. 10 A+B).

PC induction in the roots of *pht1;1* and *phr1-1 phl1* mutants was significantly lower for As^V and visibly lower for MTA treatments. PCs with longer chain length were less abundant in MTA- than in As^V-exposed seedlings for roots and shoots. Upon As^V exposure, PC formation was noticeably higher in both roots and shoots across all genotypes compared to MTA. This increase in PCs was accompanied by a decline in GSH levels, which partially recovered after 72 hours of exposure (Fig. 10 B). Over time, *pht1;1* and *phr1-1 phl1* roots accumulated PC amounts like WT after 72 hours of As^V exposure. The overall PC accumulation after three days of MTA treatment remained lower than in As^V-exposed seedlings. Although the difference in root PC concentrations between MTA- and As^V-treated seedlings decreased over time, PC formation in roots of Col-0 appeared to be more strongly enhanced than in *pht1,1* and *phr1-1 phl1*.

In shoots, PC levels were similar across all tested genotypes for both arsenic species but tended to be somewhat higher in the roots of both mutants. Thus, unlike the results observed in roots, shoot PC formation did not correlate with the reduced ∑As content in the shoots of *pht1;1* and *phr1-1 phl1* compared to Col-0. Moreover, although PC formation following MTA exposure was generally lower in seedlings treated with As^V compared to MTA, the reduction was not proportional to higher ∑As in roots and shoots. Additionally, PC concentrations in shoots of MTA-exposed seedlings were higher than expected, given that the ∑As in shoots after MTA exposure were much lower than in roots.

Unlike the root length and fresh weight assays conducted at a later time point of this experimental series (Fig. 5 and 6), type E agar was used for these early experiments, as reported in previous studies[60]. At the time, it was not known that this type of agar reduces the availability of MTA and, especially, As^V. Consequently, higher concentrations of MTA and As^V were used for the short-term treatment compared to those applied in the subsequent growth inhibition experiments described above.

A

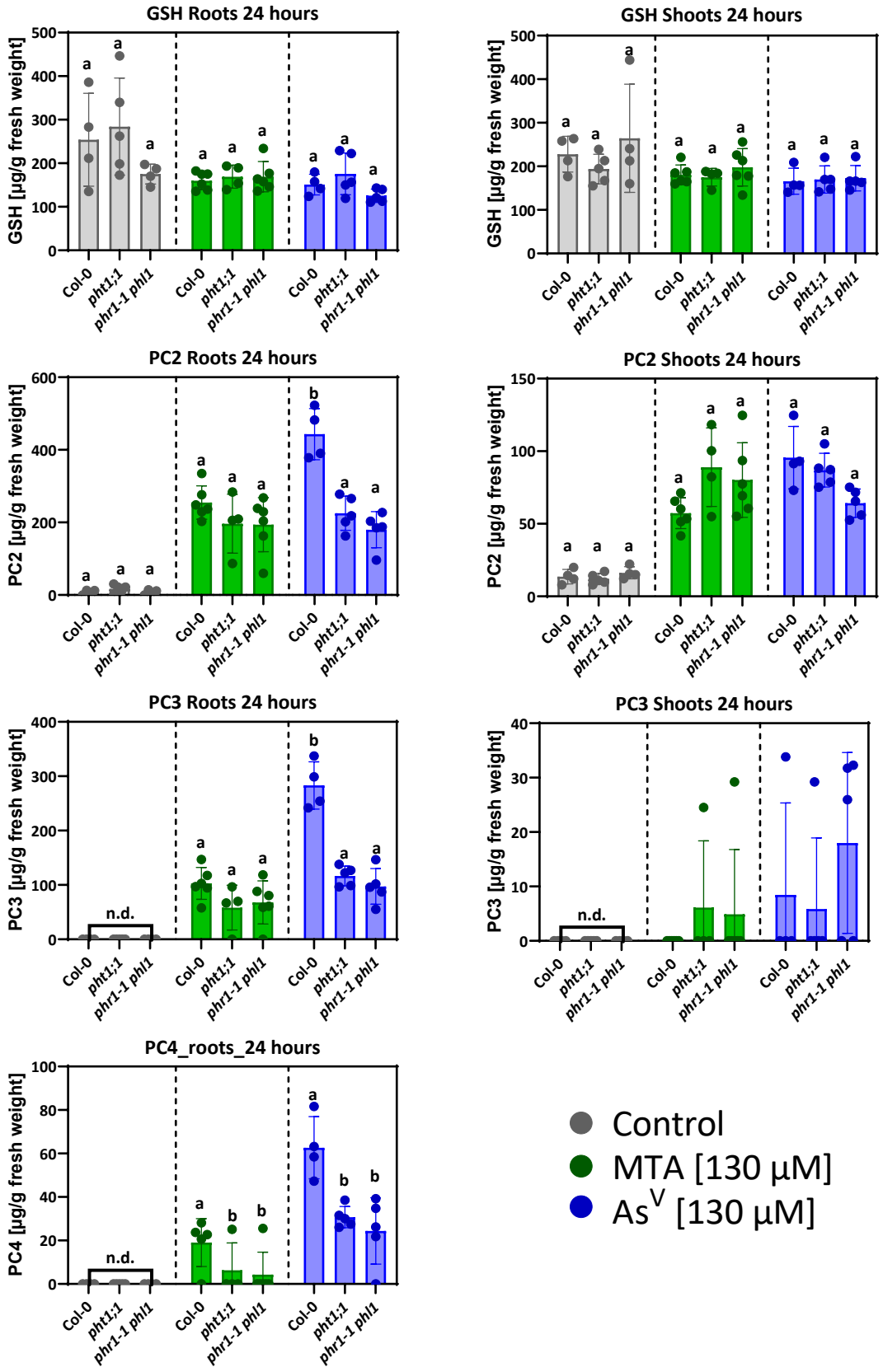
GSH Roots 24 hours
GSH [µg/g fresh weight]
GSH Shoots 24 hours
PC2 Roots 24 hours
PC2 [µg/g fresh weight]
PC2 Shoots 24 hours
PC3 Roots 24 hours
PC3 [µg/g fresh weight]
n.d.
PC3 Shoots 24 hours
PC4_roots_24 hours
PC4 [µg/g fresh weight]
Col-0
pht1;1
phr1-1 phl1
Control
MTA [130 µM]
As^{V} [130 µM]

B

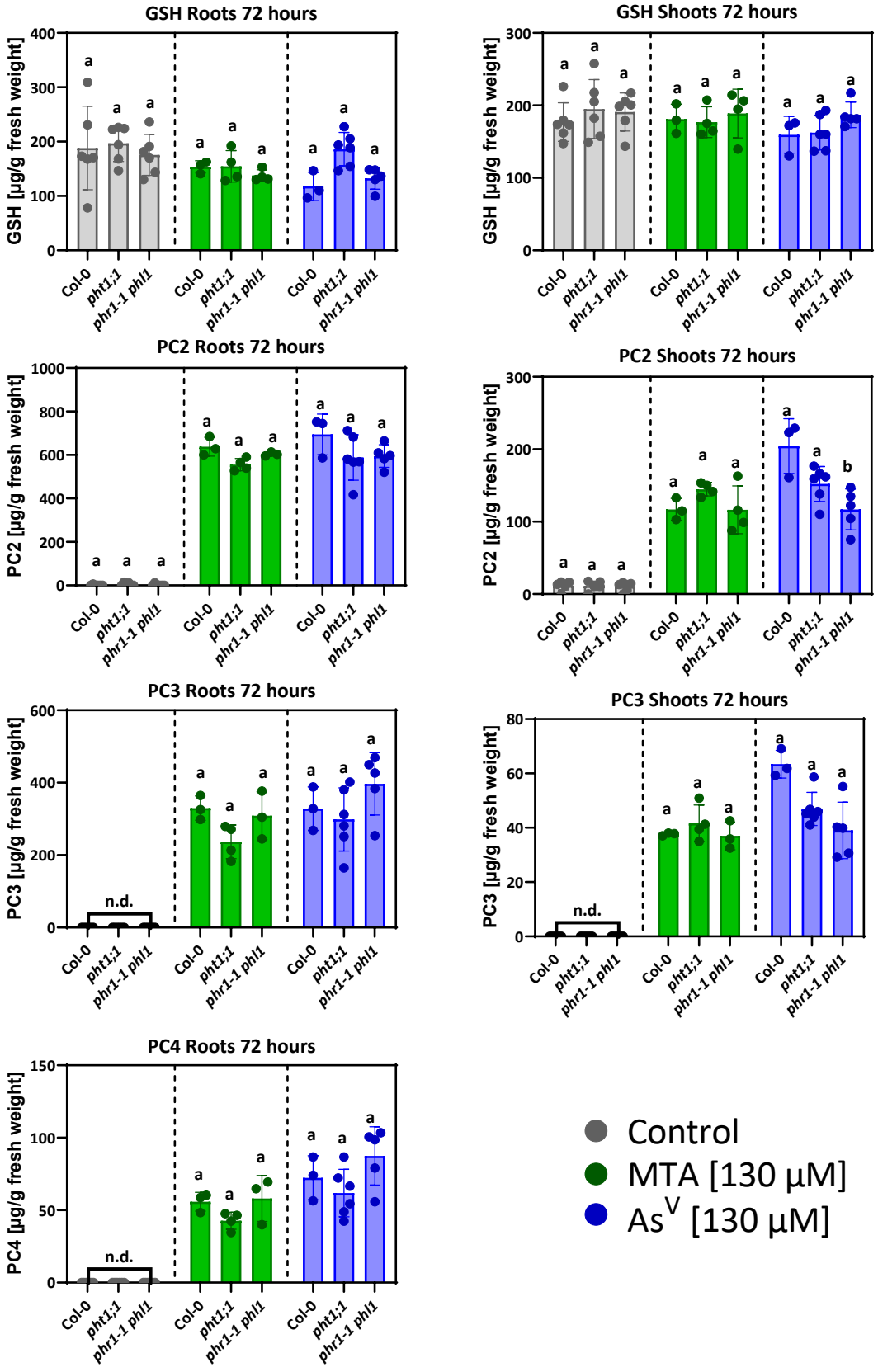
GSH Roots 72 hours
GSH [µg/g fresh weight]
GSH Shoots 72 hours
PC2 Roots 72 hours
PC2 [µg/g fresh weight]
PC2 Shoots 72 hours
PC3 Roots 72 hours
PC3 [µg/g fresh weight]
PC3 Shoots 72 hours
PC4 Roots 72 hours
PC4 [µg/g fresh weight]
n.d.
Col-0
pht1;1
phr1-1 phl1
Control
MTA [130 µM]
As^{V} [130 µM]

Fig. 10: Evaluation of thiol profiles in *A. thaliana* Col-0, *pht1;1* and *phr1-1phl1* seedlings upon MTA and As^V exposure. Seedlings grown for 14 days on plates containing 30 µM P_i were transferred to plates without P_i, supplemented with 130 µM MTA or As^V, or left untreated. Thiol profiles of roots (left) and shoots (right) of Col-0, *pht1;1* and *phr1-1phl1* seedlings were assessed after 24 hours (A) and 72 hours (B) of exposure to MTA (green) or As^V blue (A). For the thiol profile determination, statistical analysis was performed using the Kruskal Wallis Test to assess significant differences in GSH, PC2 and PC3 contents between *A. thaliana* Col-0 (WT), *pht1;1* and *phr1-1phl1* roots and shoots. No statistical analysis was performed for PC3 shoot contents after 24 hours due to values being near the quantification limit and influenced by outliers. PC4 was not detectable in shoots at either 24 or 72 hours and is therefore not shown. Significant differences are marked by lower case letters. Data represent three biological replicates with *n* = 1-2 samples each containing 34-36 roots or shoots (per condition/genotype); +/- the standard deviation.

3.1.2 Addressing the Role of AtHAC1 in the Detoxification of MTA

Despite some studies suggesting that MTA might be reduced by As^V reductases and sequestered by PCs, as is known for As^V, the mechanisms governing its intracellular fate remain poorly understood. Experiments demonstrating a higher sensitivity of PC-deficient mutants[60] to MTA, along with the observation of MTA's conversion to As^{III} in native protein extract[6], suggests that MTA might be detoxified like As^V. Additional support for this hypothesis comes from experiments in which enhanced tolerance to both As^V and MTA was observed in *S. pombe* WT expressing the *A. thaliana* As^V reductase *AtHAC1* heterologously, but not in *pcsΔ* cells (Master Thesis Sebastian Haider).

Following experiments showing the enzymatic MTA reduction in crude protein extract from various rice cultivars[6], further experiments were done. To evaluate the assay protocol of the experiments conducted by Kerl et al. (2019)[83], the assay protocol was reproduced, using crude protein extract of *O. sativa* (Kitaake), which resulted in a nearly complete reduction of MTA within 10 min, as previously described (Fig. 11A). This outcome was also observed in extracts from *A. thaliana* Col-0 and the *hac1* mutant at equal protein concentrations (Fig. 11A).

To provide evidence for the enzymatic reduction of MTA to As^{III} via AtHAC1, samples from crude protein extracts from the *A. thaliana* mutant *hac1* and Col-0 WT were speciated over time after MTA addition to assess differences in the kinetics of MTA reduction. In both WT and the *hac1* mutant extracts, a rapid and almost complete reduction of MTA to As^{III} was observed within 10 min (Fig. 11C). Neither the addition of MTA to buffer alone nor to samples of denatured protein

extract resulted in a rapid conversion of MTA to As^{III}, as observed in native protein extracts (Fig. 11A-C). However, in denatured protein extracts, MTA stability was lower than in buffer-only samples, though it remained stable throughout the measured time course.

Overall, the kinetics of MTA reduction were comparable between the WT and the *hac1* mutant. Reducing the temperature (20 °C instead of 37°C) and lowering the protein extract concentration (500 ng/µl instead of ~1.5 µg/µl) did not resolve the issue (data not shown), as these adjustments failed to enhance the resolution or reveal differences by slowing down the reduction kinetics.

Subsequently, MTA reduction was attempted in crude protein extracts of *S. pombe* heterologously expressing the *A. thaliana* As^{V} reductase AtHAC1. Initial findings (Master Thesis Sebastian Haider) indicated that *S. pombe* WT and the *pcsΔ* mutant exhibited comparable survival rate when exposed to As^{V} or MTA, respectively, suggesting a lack of As^{V} reductases in *S. pombe*. This observation was reinforced by the enhanced As^{V} and MTA tolerance of *S. pombe* WT expressing *AtHAC1-GFP*, prompting us to use this model due to its presumed lack of an As^{V} reduction capacity.

Unfortunately, in contrast to *A. thaliana* and *O. sativa*, MTA was unstable in samples containing denatured protein extracts from *S. pombe* (Fig. 12A). A similar instability was observed when MTA was added to denatured protein extracts from *E. coli* (Fig. S2A), despite MTA being highly stable in the buffer used. Again, no reduction of As^{V} to As^{III} occurred in crude or denatured protein extracts (data not shown). The absence of As^{V} reduction in crude protein extract of rice had already been reported by Kerl et al. (2019)[83].

Comparison of GSH and PC profiles in WT and *pcsΔ* cells heterologously expressing *AtHAC1-GFP* showed that MTA induced GSH-formation in *pcsΔ* and led to GSH depletion in WT cells as a result of PC2 and PC3 formation (Fig. 12B-D). However, GSH and PC concentrations of both WT and *pcsΔ* expressing *AtHAC1* resembled those of their respective controls. Interestingly, the induction of GSH formation in *pcsΔ* was observed only for MTA-treated cultures, but not for those treated with As^{V}. By contrast, GSH depletion and induction of PC-synthesis was detected in WT cells for both As^{V}- and MTA-treated cultures.

Finally, to investigate non-enzymatic MTA reduction, potential reducing agents of low-molecular-weight were removed, such as GSH, by desalting crude protein extracts from WT+*AtHAC1-GFP* and WT+*GFP*. For the first time, MTA reduction in denatured protein extract was impeded (Fig. 12 E).

The reduction of MTA after the addition of reduced glutathione to buffer-only samples was negligible within the tested time course, as was also the case for As^{V} (Fig. 12E+F). Furthermore, MTA remained stable in desalted crude protein extract until GSH was added. A comparison of MTA reduction between protein extracts from WT+*AtHAC1-GFP* and WT+ *GFP* revealed faster MTA reduction in extracts from cells expressing the As^{V} reductase (Fig. 11H). This finding suggests the presence of an endogenous As^{V} reductase in *S. pombe*, as MTA reduction was observed in both extracts. Although the kinetics of MTA reduction were higher in crude extracts from WT+*AtHAC1-GFP*, the difference to the control was less pronounced than expected, given that WB analysis confirmed *AtHAC1-GFP* overexpression (Fig. 2B). Again, no evidence for enzymatic As^{V} reduction was found. Given that these findings are from an initial test, additional replicates with more time points will be needed for future evaluations.

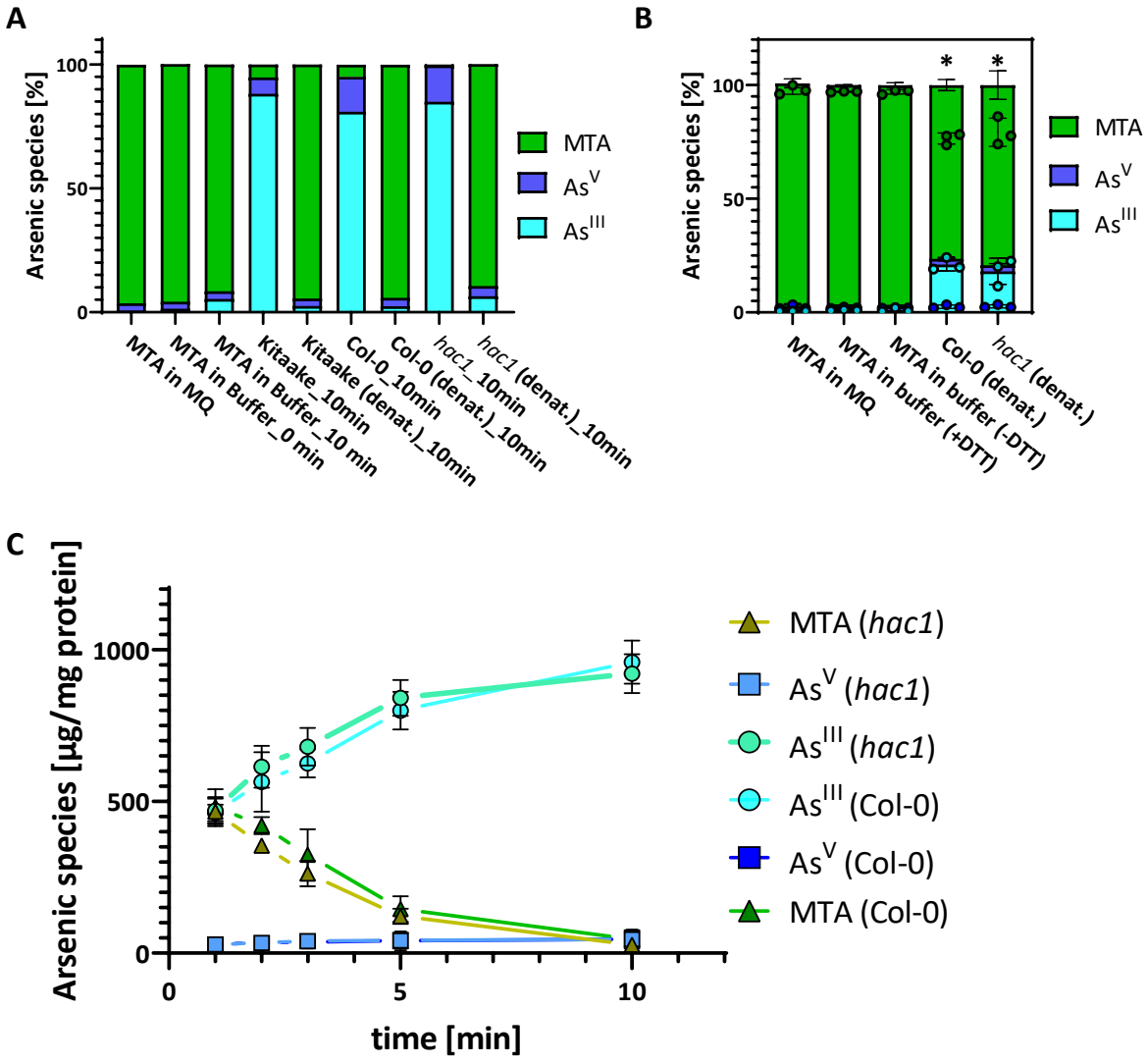

Fig. 11: Comparison of the MTA reduction kinetics in crude protein extracts from *A. thaliana* WT (Col-0) and the *hac1* mutant. (A) Evaluation of the assay protocol from Kerl et al. (2019)[79], involved root material from hydroponically grown *O. sativa* (Kitaake) and *A. thaliana* Col-0 and *hac1* mutant plants. (B) Evaluation of MTA stability was conducted in deionized water (MQ), buffer with 1 mM DTT (+DTT) or without (-DTT), and denatured protein extracts from Col-0 and *hac1* roots after 10 min of incubation at 37°C. (C) Protein extracts derived from root material of five- to six-week-old hydroponically grown Col-0 and *hac1* were inoculated with MTA. Samples were taken after 1, 2, 3, 5 and 10 min of incubation at 37°C with MTA. In these experiments, 6.66 µM MTA was added to protein extracts of equal concentrations, along with the respective controls (A-C). Denatured protein extracts were generated by boiling (5 min) before the addition of MTA. Speciation analysis was performed using an IC coupled with ICP-MS (A-C). Statistical analysis used the Permutation Test to assess significant differences in As^{III} formation between genotypes and control treatments. Pairwise comparisons were conducted using a post hoc test ($p < 0.05$). Statistically significant differences are indicated by letters or an asterisk (*). Data represent one (A) or three biological replicates (B+C) with $n = 1$ (per condition/genotype); +/- the standard deviation.

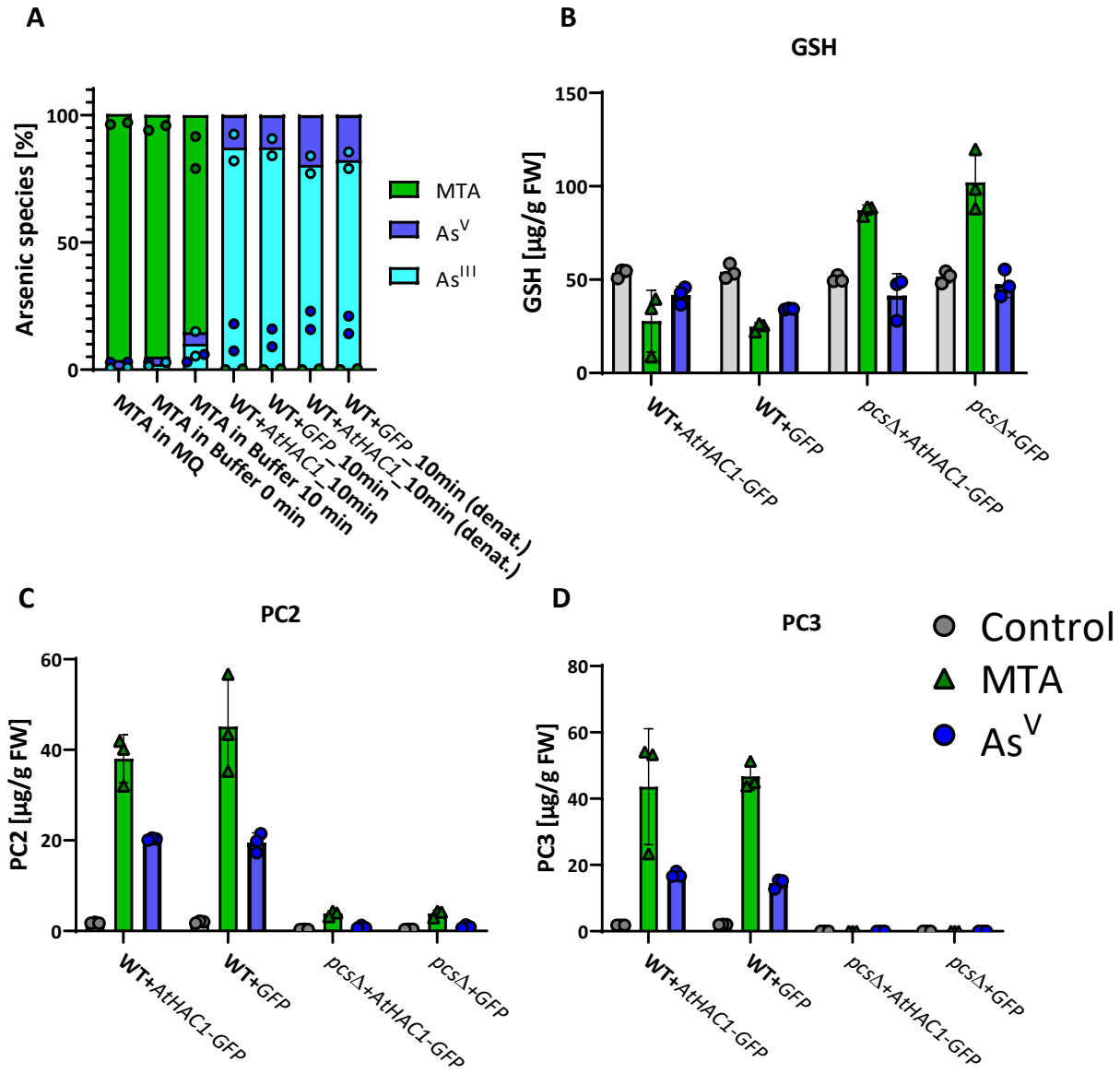
A
Arsenic species [%]
100
50
0
MTA
As^V
As^III
MTA in MQ
MTA in Buffer 0 min
MTA in Buffer 10 min
WT+AtHAC1_10min
WT+GFP_10min
WT+AtHAC1_10min (denat.)
WT+GFP_10min (denat.)
B
GSH
GSH [µg/g FW]
150
100
50
0
WT+AtHAC1-GFP
WT+GFP
pcsΔ+AtHAC1-GFP
pcsΔ+GFP
C
PC2
PC2 [µg/g FW]
60
40
20
0
WT+AtHAC1-GFP
WT+GFP
pcsΔ+AtHAC1-GFP
pcsΔ+GFP
D
PC3
PC3 [µg/g FW]
80
60
40
20
0
WT+AtHAC1-GFP
WT+GFP
pcsΔ+AtHAC1-GFP
pcsΔ+GFP
Control
MTA
As^V

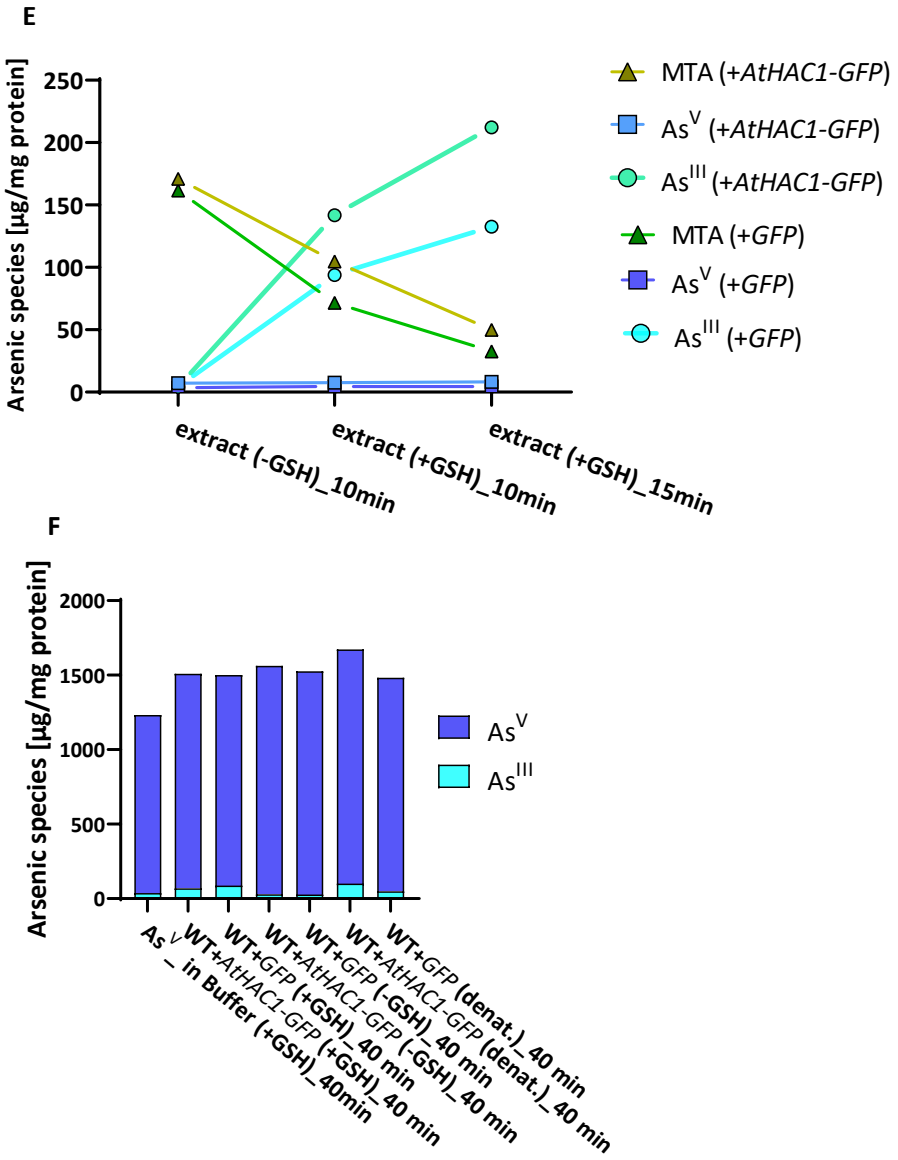

Fig. 12: Evaluation of MTA reduction kinetics in *S. pombe* WT+*AtHAC1-GFP* and WT+*GFP* protein extracts. Instability of MTA (4.5 µmol) in denatured crude protein extract of *S. pombe* (A). Thiol profiles of *S. pombe* WT+*AtHAC1-GFP*, WT+*GFP*, *pcsΔ+AtHAC1-GFP* and *pcsΔ+GFP* cells treated with or without (grey circles) 0.5 µM As^V (blue squares) or 8 µM MTA (green triangles) (B-D). Desalted protein extracts from *S. pombe* WT+*AtHAC1-GFP* and WT+*GFP* were incubated with or without 5 mM GSH and 4.5 µmol. Samples were taken after 10 min of incubation at 30°C (E). Evaluation of As^V reduction after 40 min incubation under the same conditions as described in (E), with or without the addition of 5 mM GSH (F). Samples were inoculated with 7.04 µM As^V. For the thiol profile determination (B-D), statistical analysis was performed using the Permutation Test to assess significant differences in GSH, PC2 and PC3 contents between *S. pombe* WT+*AtHAC1-GFP* and WT+*GFP* or *pcsΔ+AtHAC1-GFP* and *pcsΔ+GFP* cells under each treatment. No significant differences were observed. Data represent one (E+F), two (A) or three biological replicates (B-D) with $n = 1$ (per condition/genotype); +/- the standard deviation.

3.2 Dimethylmonothioarsenate (DMMTA): Uptake and Toxicity

Given the increasing experimental evidence pointing to the hidden risk of underestimated DMMTA exposure[7], the following section addresses the questions related to DMMTA uptake and detoxification. To develop strategies for lowering the risk associated with long-term exposure to this highly toxic As-species, acquiring better knowledge of how it enters our food chain is crucial. While the uptake and detoxification of MTA are still not fully understood - despite some transporters having been postulated - these processes are even less characterized for DMMTA. Aggravatingly, data regarding the physicochemical properties of DMMTA are contradictory[229,230], and experimental evidence in respect to its uptake, translocation and detoxification suggests divergence from other known As-species[83]. Unlike MMA and DMA, DMMTA is taken up at higher rates. While its mobility and translocation to the grain exceeds that of MMA and the iAs, it is still lower than that of DMA. Nevertheless, DMMTA exhibits greater mobility and toxicity compared to both inorganic and other organic arsenic species. By exploiting knowledge of the uptake and detoxification mechanisms of other known As-species (Fig. 1) the model organism *S. pombe* and *S. cerevisiae* were used to identify candidate genes related to DMMTA transport. In the following, various knockout strains were tested that have shown altered tolerance and/ or uptake kinetics of known iAs- and oAs-species. Furthermore, experiments to address issues related to the physicochemical properties of DMMTA were conducted, focusing on the until now unknown pK_a of this thioAs.

3.2.1 Investigation of DMMTA Uptake Using the Model Organism *S. cerevisiae*

First, a subset of *S. cerevisiae* knockout strains was compiled which were known from previous studies to be involved in the uptake of As^{III}, As^{V} and/or DMA or that were suspected to be involved based on evidence derived from experiments with orthologs of model organisms like *O. sativa* and *A. thaliana*. Access to the yeast knockout collection was gained[206,207] (see also Fig. 1), generously provided by the Chair of Cell Biology at the University of Bayreuth (Benedikt Westermann and Till Klecker). The selection of knockout strains comprised the *fps1* mutant, known for its enhanced As^{III} tolerance due to reduced uptake[62,231], and the *itr1* mutant, which lacks *ITR1,* an ortholog of *AtINT2* and *AtINT4*, both of which have been shown to contribute to As^{III} phloem loading[68]. Additionally, the *pho84*, which was found to take up less MTA and As^{V} than

the WT, and the *ptr2* mutant were tested for altered DMMTA tolerance in a growth assay. The latter has been chosen in respect to its homology to OsPTR7/OsNPF8.1 (23/42% identity/similarity; e-value: 6e-35)[232], shown to contribute to the translocation of DMA in rice[79,233].

Considering the unknown pK_a-value of DMMTA, a buffered SD-medium was used, specifically 2xYNB 0.1 CPB[212]. This citrate-phosphate buffered SD-medium enables the cultivation of *S. cerevisiae* for up to 48 hours without noteworthy pH-value fluctuations or adverse effects on growth, as can occur with standard SD medium. Given the estimated pK_a-value of DMMTA, between 4.24[230] and 5.39 (Marvin Sketch Version 23.14), the pH was adjusted to 5.6 to prevent effects caused by a transition in the protonation state of DMMTA during the exposure time. Logarithmically growing strains were tested with various concentrations of DMMTA, and growth was monitored for 32 hours to identify differences in their susceptibility to DMMTA (Fig. 13B+C). As a reference, these strains were also tested with As^{III} and As^{V} (Fig. 13D-F).

Increasing concentrations of As^{III} and As^{V} led to a concentration-dependent shift in the logarithmic growth phase, accompanied by an overall reduction in the maximum OD_{600} value. In contrast, DMMTA was already highly toxic at micromolar concentrations, whereas As^{III} and especially As^{V} required much higher concentrations to impair growth. In the case of As^{V}, a concentration of 2.5 mM was still too low to cause adverse growth effects, and even threefold higher concentrations did not induce toxicity comparable to that caused by 2 mM of DMMTA (Fig. 13D+F). DMMTA treatments were characterized by a narrow window of toxicity (Fig. 13B+C; Fig. 14), along with a relatively high standard deviation.

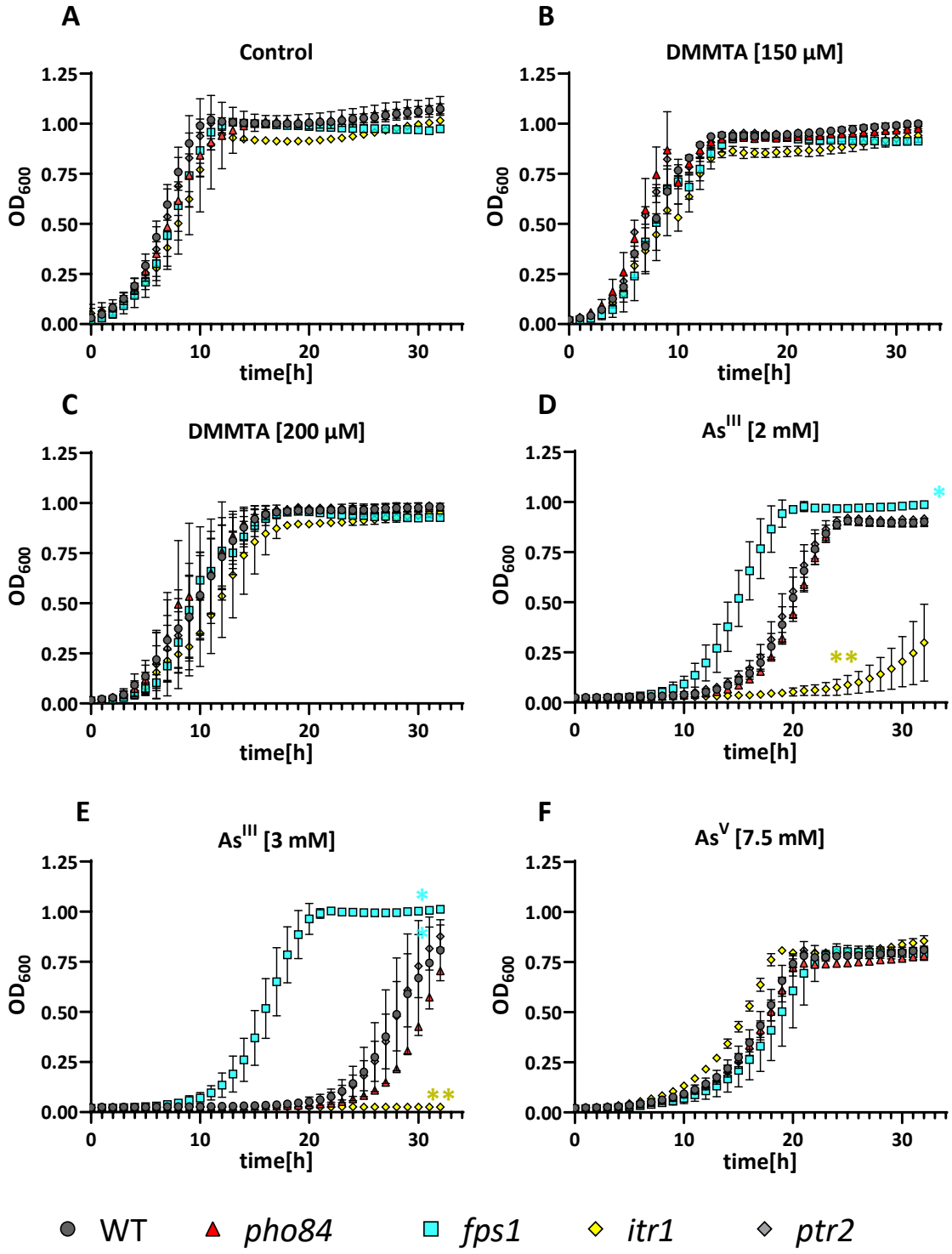
A
Control
B
DMMTA [150 µM]
C
DMMTA [200 µM]
D
As^III [2 mM]
E
As^III [3 mM]
F
As^V [7.5 mM]
OD600
time[h]
0.00
0.25
0.50
0.75
1.00
1.25
0
10
20
30
*
**
WT
pho84
fps1
itr1
ptr2

Fig. 13: Growth curves of *S. cerevisiae* knockout collection strains with transporter candidate knockouts assumed to effect arsenic tolerance. The growth curve progression of WT (BY4742) and the knockout strains *pho84* (red triangle), *fps1* (blue square), *itr1* (yellow hash) and *ptr2* (grey hash), was measured every hour for 32 hours under different conditions. Logarithmically growing cells were treated with no arsenic (A), 150 µM DMMTA (B), 200 µM DMMTA (C), 2 mM As^{III} (D), 3 mM As^{III} (E), or 7.5 mM As^{V} (F). To assess differences in growth between the WT and knockout strains, the cumulative OD_{600} values for each strain under each condition was compared to that of the WT grown under the same conditions. Statistical analysis was performed using the Wilcoxon Rank-Sum Test, with significant differences in growth curve profiles are indicated by asterisks: $p < 0.05$ (*), $p < 0.01$ (**), $p < 0.001$ (***). Data represent three biological replicates ($n = 1$ per condition/genotype) and are shown as mean ± standard deviation.

None of the tested candidates showed reduced sensitivity towards DMMTA than the WT, implying that DMMTA uptake differs from that of other As-species. The previously reported higher As^{III} tolerance of the *fps1* mutant was reproducible[62], whereas no growth advantage was observed for the *pho84* mutant in the growth assays when As^{V} was used as the stressor (Fig. 13 D; Fig. 14).

The generally high As^{V} tolerance of *S. cerevisiae* (BY4742), likely masks phenotypic differences in presence of P_i, as previously described[234]. Several unsuccessful attempts to conduct toxicity assays at low P_i concentrations or in the complete absence of a P_i source have been made, potentially explaining why As^{V} tolerance assays remain scarce in the literature despite *pho84* being a widely used knockout strain for heterologous P_i transporter expression[52,56,234] or the investigation of As^{V} uptake in general[59]. However, the strongly reduced As^{V} uptake of *pho84* in comparison to the WT, as demonstrated above (Fig. 4), confirms the known association of Pho84 with As^{V} uptake.

The *itr1* mutant, assumed of being capable to transport As^{III}, exhibited enhanced sensitivity towards As^{III}, but not As^{V}, in the growth assays (Fig. 13D+E). While the loss of Itr1 led to heightened sensitivity to As^{III}, it had no clear impact on DMMTA tolerance. For the sake of completeness, *ptr2* did not differ from the wild type in growth for any of the tested As-species.

Further evidence for the lack of altered DMMTA tolerance comes from the serial dilution assays performed to validate these findings in liquid medium (Fig. 14). Again, the knockouts strains

showed no difference in their DMMTA tolerance from the WT. Except for the *itr1* knockout, which appeared slightly more sensitive.

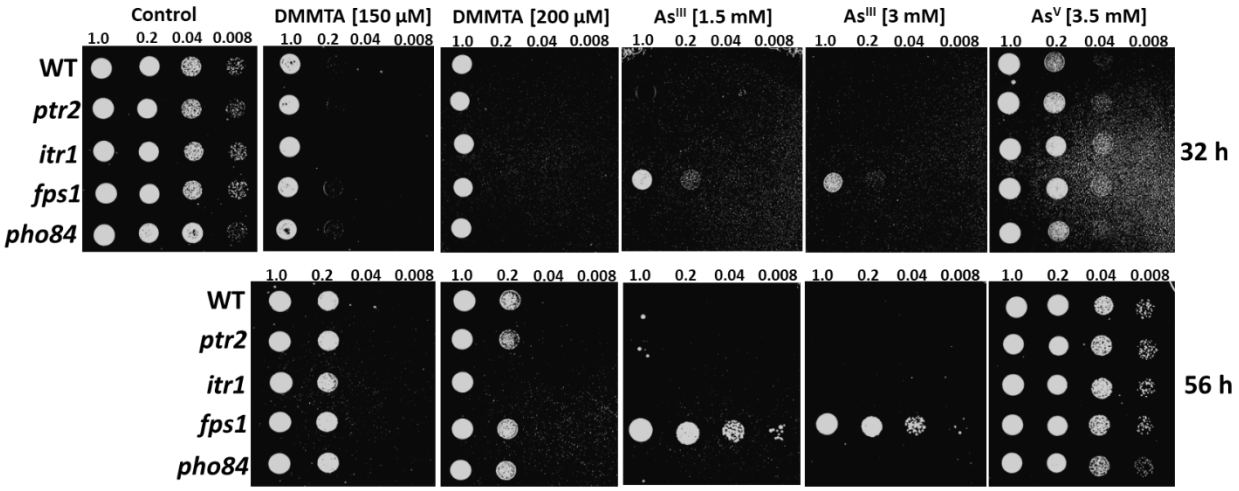

Fig. 14: Arsenic tolerance of *S. cerevisiae* knockout collection strains on plates with different arsenic species. WT (BY4742) and knockout strains (*pho84, fps1, itr1,* and *ptr2*) were serially diluted and spotted onto YPD plates with or without DMMTA [150 or 200 µM], As^{III} [1.5 or 3 mM], or As^{V} [3.5 mM]. Growth progression was documented at 32 hours (top panel) and 56 hours (bottom panel). The numbers above each spot indicate the OD_{600} value of the corresponding dilution step.

Consequently, after no promising candidate was identified, the focus was shifted to the *hxt0* mutant (EBY.VW4000), which was kindly provided by Eckhard Boles (Goethe University, Frankfurt). Hexose transporters, responsible for up to 80 % of As^{III} uptake in absence of any sugar[61], were assumed to be potential candidates for the entry of DMMTA, especially considering its high toxicity, which may be caused by rapid uptake.

Due to the knockout of 20 hexose transporters[64], *hxt0* is unable to grow on any other carbon source other than maltose. With hexose uptake abolished, As^{III} tolerance is strongly enhanced in this mutant. To investigate the potential involvement of hexose transporters in DMMTA uptake, growth assays were conducted while varying the concentration of maltose (for *hxt0* and WT) and/or glucose (for WT only) to examine hexose transporter-related differences in DMMTA toxicity. Growth curves of the WT and the *hxt0* mutant perfectly aligned when maltose of the same concentration was applied. Likewise, WT growth in SD-medium containing either glucose or maltose at equal concentrations, was identical. As observed previously, increasing concentrations of As^{III} led to a delayed entry into the logarithmic growth phase (Fig. 15), accompanied by a continuous decrease in the maximum OD_{600} value. Both the growth curve assays, and serial

dilution assays reproduced the known phenotype of reduced As^{III} sensitivity of the *hxt0* mutant, with only minor deviations between replicates. When As^{V} was added as the stressor (Fig. 15F), the *hxt0* mutant under low maltose conditions (0.5% w/v) and the WT in medium with high (4% w/v) or low glucose concentrations (0.5% w/v) showed increased sensitivity to As^{V}. Again, DMMTA toxicity was characterized by a narrow range of concentrations causing toxicity, followed by a sudden transition to lethality (Fig. 14B+C and Fig. 15).

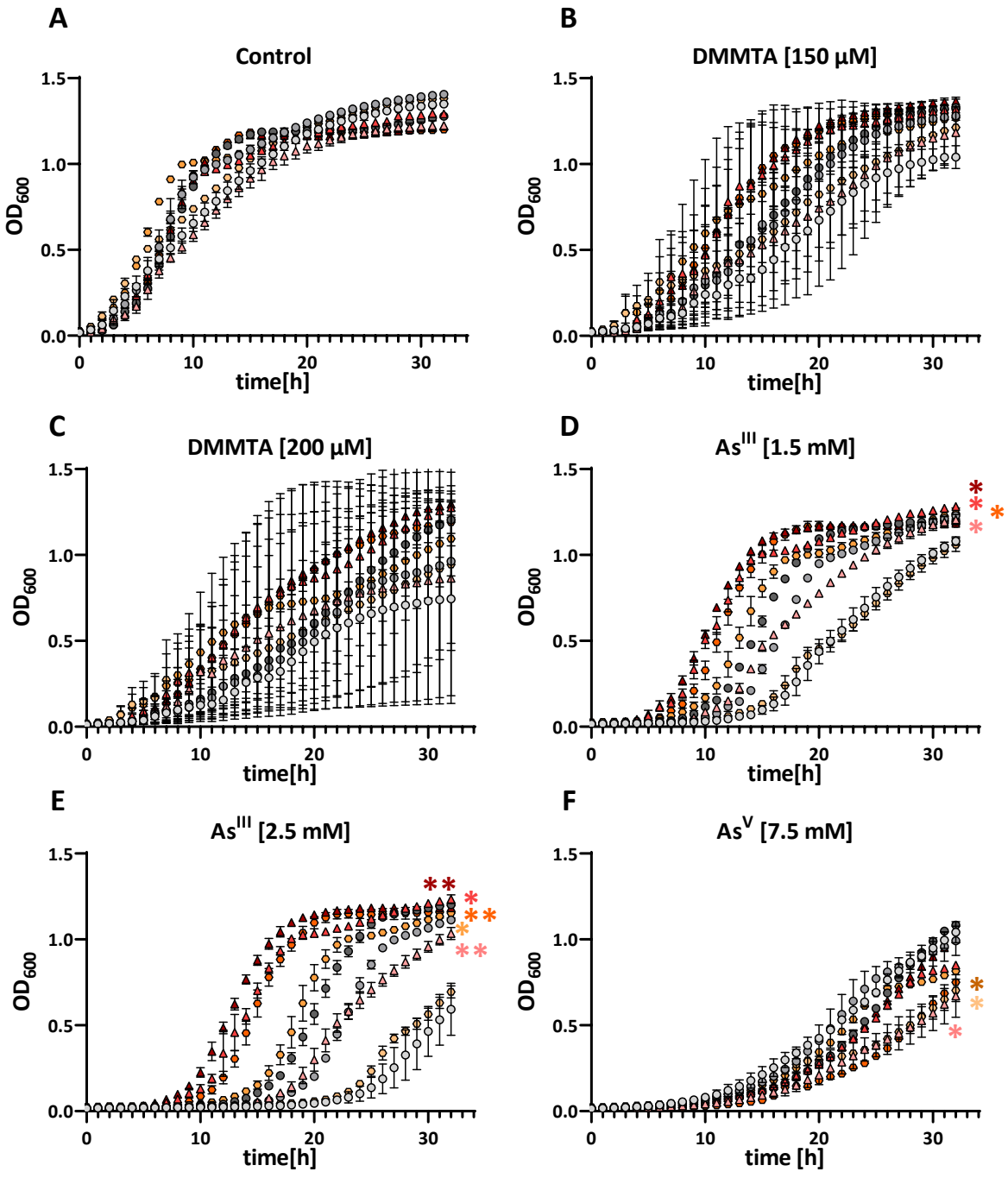
A
Control
B
DMMTA [150 µM]
C
DMMTA [200 µM]
D
As^III [1.5 mM]
E
As^III [2.5 mM]
F
As^V [7.5 mM]
OD600
time[h]
time [h]
0.0
0.5
1.0
1.5
0
10
20
30
WT maltose [0.5 % w/v]
WT glucose [0.5 % w/v]
WT maltose [2 % w/v]
WT glucose [2 % w/v]
WT maltose [4 % w/v]
WT glucose [4 % w/v]
hxt0 maltose [0.5 % w/v]
hxt0 maltose [2 % w/v]
hxt0 maltose [4% w/v]

Fig. 15: Arsenic tolerance of *S. cerevisiae* WT and the *hxt0* mutant under different maltose and glucose concentrations. The growth curve progression of WT (Cen.PK2-1c) and the knockout strain *hxt0* (EBY.VW4000) was measured every hour for 32 hours under various conditions. Logarithmically growing cells were treated with no arsenic (A), 150 µM DMMTA (B), 200 µM DMMTA (C), 1.5 mM As^{III} (D), 2.5 mM As^{III} (E), or 7.5 mM As^{V} (F). WT cultures were grown in medium with 0.5% w/v (pale grey circles), 2% w/v (grey circles), 4% w/v maltose (dark grey circles) and compared to WT cultures grown with 0.5% w/v (pale orange hexagons), 2% w/v (orange hexagons), 4% w/v glucose (dark orange hexagons) to assess their arsenic tolerance. Similarly, *hxt0* cultures were grown in maltose-containing medium of 0.5% w/v (pale red triangle), 2% w/v (red triangle) and 4% w/v (dark red triangle). To evaluate growth differences between WT and *hxt0*, as well as WT grown in glucose- versus maltose-containing medium, the sum of OD_{600} values for each strain was compared to WT growth in maltose-containing medium at the respective carbon-source concentrations. Statistical analysis was performed using the Wilcoxon Rank-Sum Test, with significant differences in growth curve profiles are indicated by asterisks in the respective treatment colors: $p < 0.05$ (*), $p < 0.01$ (**), $p < 0.001$ (***). Data represent three biological replicates ($n = 1$ per condition/genotype) and are shown as mean ± standard deviation.

Tab. 9: Growth inhibitory effects of different arsenic species on WT and *hxt0*. This table displays the average time (in hours) required for each strain to enter the logarithmic growth phase.

Growth conditions	Time to entry into the logarithmic growth phase [h] (± standard deviation of the corresponding OD_{600})			
	Control	DMMTA [75 µM]	DMMTA [150 µM]	DMMTA [200 µM]
WT glucose [0.5% w/v]	2 (+/- 0.021)	3 (+/- 0.084)	3 (+/- 0.009)	4 (+/- 0.081)
WT glucose [2% w/v]	2 (+/- 0.007)	3 (+/- 0.058)	3 (+/- 0.079)	4 (+/- 0.064)
WT glucose [4% w/v]	4 (+/- 0.019)	5 (+/- 0.039)	5 (+/- 0.062)	7 (+/- 0.09)
WT maltose [0.5% w/v]	3 (+/- 0.016)	5 (+/- 0.063)	6 (+/- 0.054)	9 (+/- 0.074)
WT maltose [2% w/v]	3 (+/- 0.021)	6 (+/- 0.055)	6 (+/- 0.064)	9 (+/- 0.061)
WT maltose [4% w/v]	4 (+/- 0.013)	5 (+/- 0.019)	5 (+/- 0.059)	9 (+/- 0.079)
hxt0 maltose [0.5% w/v]	4 (+/- 0.018)	6 (+/- 0.041)	6 (+/- 0.052)	7 (+/- 0.075)
hxt0 maltose [2% w/v]	3 (+/- 0.006)	5 (+/- 0.019)	5 (+/- 0.071)	6 (+/- 0.063)
hxt0 maltose [4% w/v]	4 (+/- 0.016)	4 (+/- 0.032)	4 (+/- 0.051)	6 (+/- 0.061)

Time to entry into the logarithmic growth phase [h] (± standard deviation of the corresponding OD_{600})				
As^{III}[500 µM]	As^{III}[1.5 mM]	As^{III}[2.5 mM]	As^{V}[2.5 mM]	As^{V}[7.5 mM]
6 (+/- 0.011)	14 (+/- 0.017)	23 (+/- 0.016)	4 (+/- 0.056)	13 (+/- 0.0004)
4 (+/- 0.016)	9 (+/- 0.021)	14 (+/- 0.013)	4 (+/- 0.006)	13 (+/- 0.012)
5 (+/- 0.023)	8 (+/- 0.02)	11 (+/- 0.065)	6 (+/- 0.085)	17 (+/- 0.002)
7 (+/- 0.037)	16 (+/- 0.039)	24 (+/- 0.027)	4 (+/- 0.047)	11 (+/- 0.018)
6 (+/- 0.01)	12 (+/- 0.061)	18 (+/- 0.069)	6 (+/- 0.063)	13 (+/- 0.018)
5 (+/- 0.012)	10 (+/- 0.044)	15 (+/- 0.063)	5 (+/- 0.005)	15 (+/- 0.008)
6 (+/- 0.007)	11 (+/- 0.006)	17 (+/- 0.011)	5 (+/- 0.036)	16 (+/- 0.034)
4 (+/- 0.008)	6 (+/- 0.014)	9 (+/- 0.023)	6 (+/- 0.085)	14 (+/- 0.022)
4 (+/- 0.013)	6 (+/- 0.024)	9 (+/- 0.014)	5 (+/- 0.058)	14 (+/- 0.008)

Unfortunately, within the tested concentration range, high standard deviations prevented a clear demonstration of the *hxt0* mutant's slightly enhanced growth in the presence of DMMTA. Therefore, the average entry into the logarithmic growth phase was calculated to highlight the slight growth advantage of the *hxt0* mutant compared to the WT, particularly pronounced at high concentrations of DMMTA (Tab. 9). The average hours were rounded to full hours since the OD_{600}

values were only determined every 60 minutes. Interestingly, both the WT strain grown in SD medium with elevated glucose and the *hxt0* mutant grown in SD medium supplemented with high maltose concentrations exhibited higher tolerance than the WT comparison group grown in maltose-containing medium, as evidenced by their growth curves and average entry times into the logarithmic growth phase (Fig. 15B+C; Tab. 9).

On plates, *hxt0* exhibited better growth within the first 24 hours of incubation (Fig. 16A), but its growth declined with prolonged incubation time (Fig. 16B+C). After 48 hours, WT growth had visibly surpassed that of the *hxt0* mutant on DMMTA-containing plates. While the *hxt0* mutant exhibited early sensitivity to As^{V} and superior growth on plates with elevated As^{III} concentrations, a shift in growth inhibitory effects was observed only during DMMTA exposure.

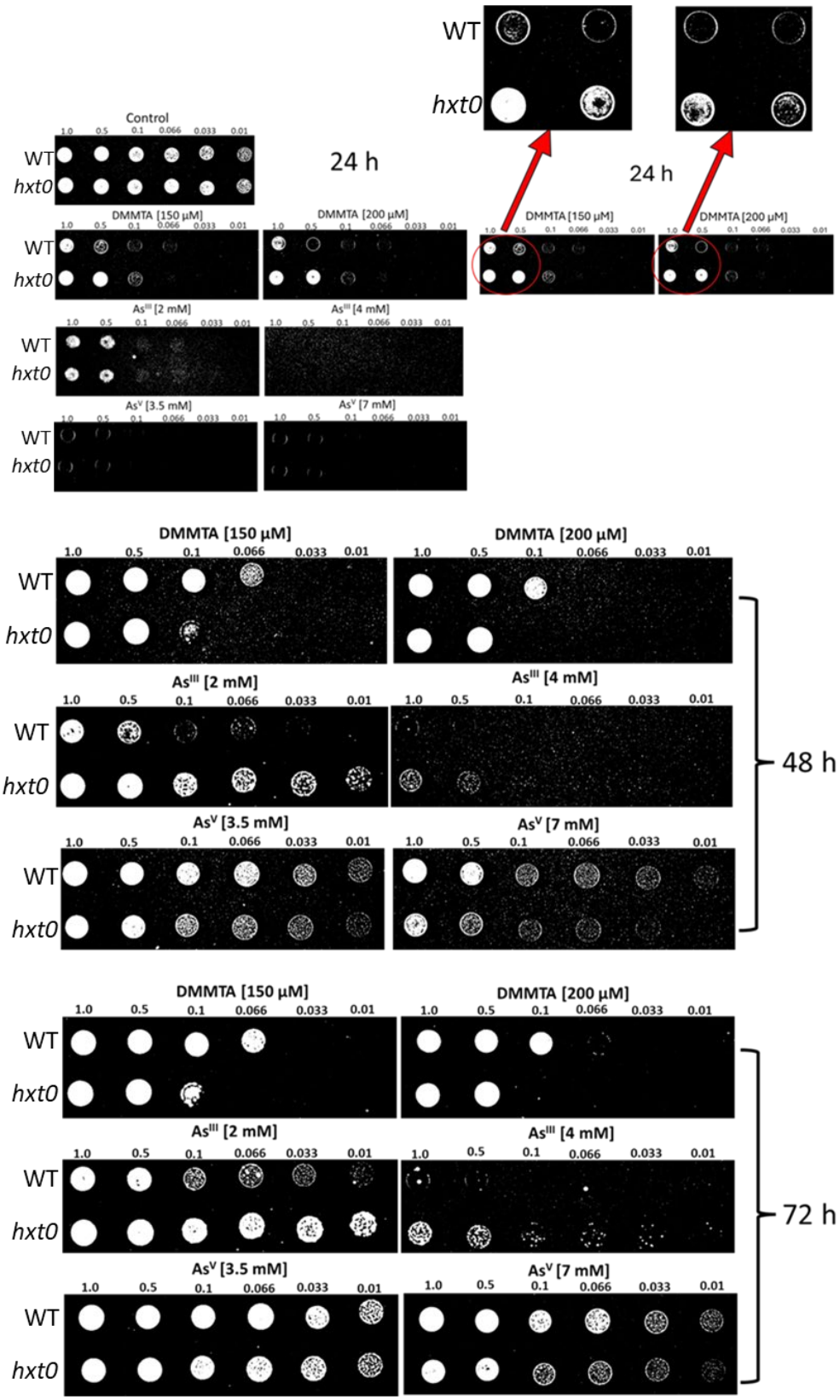
WT
hxt0
Control
24 h
DMMTA [150 µM]
DMMTA [200 µM]
24 h
DMMTA [150 µM]
DMMTA [200 µM]
As^III [2 mM]
As^III [4 mM]
As^V [3.5 mM]
As^V [7 mM]
1.0 0.5 0.1 0.066 0.033 0.01
48 h
72 h

Fig. 16: Tolerance of the *hxt0* mutant to different arsenic species. *S. cerevisiae* WT (Cen.PK2-1c) and the *hxt0* knockout strain (EBY.VW4000) were serially diluted and spotted onto YPM plates with or without DMMTA [150 or 200 µM], As^{III} [2 or 4 mM], or As^{V} [3.5 mM or 7 mM]. Growth progression was documented at 24 hours (top panel), 48 hours (middle panel), and 72 hours (bottom panel). The numbers above each spot indicate the OD_{600} value of the corresponding dilution step. Additionally, the top panel includes a zoomed-in view of the DMMTA-containing plates at 24 hours, shown on the right side. An additional representative replicate can be found in the appendix.

Next, uptake experiments with WT and *hxt0* were conducted to elucidate whether the observed phenotypic differences were related to uptake. The short-term DMMTA uptake experiments conducted (Fig. 17A), did not reveal any differences in DMMTA uptake between WT and the *hxt0* mutant.

In As^{III} treated cultures, ∑As was significantly lower in *hxt0* compared to WT exposed to As^{III} (Fig. 17A). Notably, ∑As in DMMTA-treated cells rapidly peaked after 90 min of exposure, being more than fourteen times higher than WT cells treated with As^{III}. Experiments done at 4 °C (Fig. 17B) showed that the majority of ∑As results from active transport. Nevertheless, As-levels in cells exposed to DMMTA at 4 °C were approximately 10 times higher than those in WT exposed to As^{III} at 30 °C. Despite the relatively high amounts of arsenic detected in DMMTA-treated cells at 4°C, these values remained three to six times lower than those measured at 30°C. Also, no visible increase was observed within 60 min at 4°C, indicating that equilibrium had been reached.

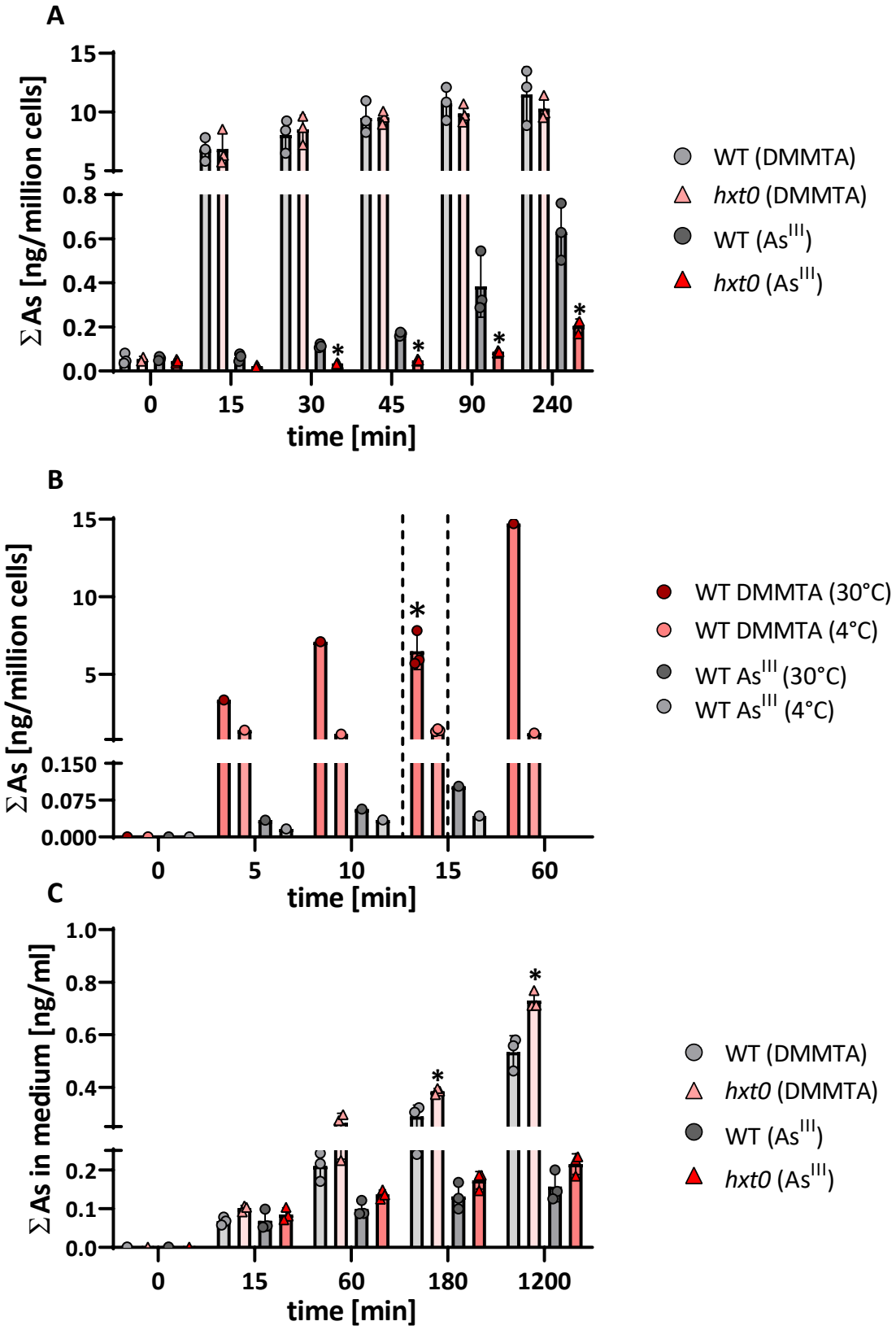
A
15
10
5
0.8
0.6
0.4
0.2
0.0
∑As [ng/million cells]
0
15
30
45
90
240
time [min]
WT (DMMTA)
hxt0 (DMMTA)
WT (As^III)
hxt0 (As^III)
B
15
10
5
0.150
0.075
0.000
∑As [ng/million cells]
0
5
10
15
60
time [min]
WT DMMTA (30°C)
WT DMMTA (4°C)
WT As^III (30°C)
WT As^III (4°C)
C
1.0
0.8
0.6
0.4
0.2
0.1
0.0
∑As in medium [ng/ml]
0
15
60
180
1200
time [min]
WT (DMMTA)
hxt0 (DMMTA)
WT (As^III)
hxt0 (As^III)

Fig. 17: DMMTA uptake and efflux in WT and *hxt0* cells. *S. cerevisiae* WT (Cen.PK2-1c) and the *hxt0* knockout strain (EBY.VW4000) were exposed to DMMTA [10 µM] or As^{III} [10 µM] at 30°C (A) or 4°C (B). ∑As in cells was measured after 0, 15, 30, 45, 90 and 240 min (A) or 0, 5, 10, 15 and 60 min. To assess arsenic efflux, WT and *hxt0* cells were exposed to DMMTA [10 µM] or As^{III} [10 µM] for 2 h at 30°C, then transferred to fresh, arsenic-free medium. ∑As was measured of medium samples after 0, 15, 60, 180 and 1200 min. ∑As were measured using ICP-MS. To evaluate differences in ∑As between WT and *hxt0* cells (A; B at 15 min) and in medium samples (C), values for each strain and time point were compared for statistical significance. Statistical analysis was performed using the Permutation Test, with significant differences in ∑As indicated by asterisks: $p < 0.05$ (*), $p < 0.01$ (**), $p < 0.001$ (***). Data represent three biological replicates ($n = 1$ per condition/genotype) (A+C) and 1-3 biological replicates for (B). Results are shown as mean ± standard deviation.

Attempts to remove potentially surface-bound DMMTA using different wash protocols were unsuccessful (data not shown). Thus, it remains unclear whether the relatively high values and rapid equilibrium of ∑As detected at 4°C were due to surface-bound DMMTA or the result of diffusion-based uptake.

In addition, efflux experiments were conducted (Fig. 17C) with cultures exposed for two hours to the subtoxic dose of 10 µM DMMTA or As^{III} as respective control. Within the first three hours after inoculation to fresh, arsenic-free medium, *hxt0* cultures released higher concentrations of arsenic into the medium than the WT for both, DMMTA and As^{III}. Twenty hours after inoculation, ∑As in the medium inoculated with cells exposed to DMMTA were approximately four times higher than those in the medium with As^{III}-treated cells. Furthermore, *hxt0* cells exposed to DMMTA and As^{III} enriched the medium with more arsenic than WT cells exposed to either of these species.

Considering that DMMTA uptake was about 24 times higher than that of As^{III}, the average arsenic efflux from DMMTA-treated cells was relatively low compared to cells treated with As^{III}. Based on the stability test of DMMTA and As^{III} in the uptake solution with and without cells, suggests that no conversion of the applied As-species occurred within the exposure time (Fig. 24A).

To determine whether bidirectional transport, particularly the efflux capacity of As^{III} and DMMTA, affects DMMTA tolerance, initial experiments were conducted using the HD9, HD100, and HD200 strains (Fig. 18). These strains are partially (HD9 and HD100) or almost completely (HD200) impaired in their bidirectional arsenic flux (see Tab. 2)[61]. The HD200 strain, which carries knockouts in the genes encoding the high-affinity hexose permeases Hxt3, Hxt6, and Hxt7, the

galactose transporter Gal2, the aquaglyceroporin Fps1, and the efflux pump Acr3, exhibited slightly enhanced DMMTA tolerance, similar to HD100, which is still capable of hexose uptake. However, the loss of nearly all transporters associated with As^{III} uptake and/or efflux did not strongly affect DMMTA tolerance.

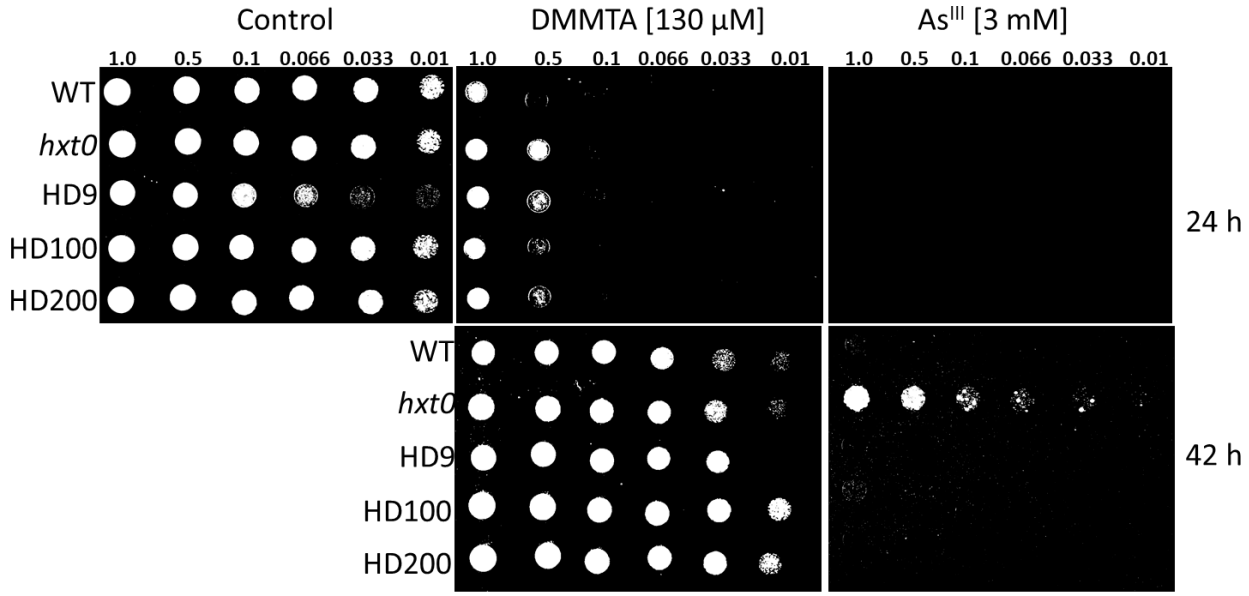

Fig. 18: The impact of the serial loss of bidirectional As^{III} transport capacity on DMMTA tolerance. *S. cerevisiae* WT (Cen.PK2-1c) and the knockout strains *hxt0* (EBY.VW4000), HD9, HD100, and HD200 were serially diluted and spotted onto YNB plates with or without DMMTA [130 µM], As^{III} [3 mM]. Growth progression was documented at 24 hours and 42 hours. The numbers above each spot indicate the OD_{600} value of the corresponding dilution step. An additional representative replicate can be found in the appendix.

3.2.2 DMMTA Uptake and Toxicity in the Presence of Different Carbon-Sources

3.2.2.1 Fructose Reduces DMMTA Toxicity Compared to Glucose in *S. pombe* and *S. cerevisiae*

Based on these initial observations, further assays were conducted to evaluate the effect of different sugars on DMMTA uptake and toxicity. Due to high fluctuations in *S. cerevisiae* growth when treated with DMMTA, a toxicity assay protocol was developed using *S. pombe* as a model. A protocol for toxicity assays with *S. pombe* was successfully established, enabling the investigation of DMMTA toxicity with less background noise caused by a high standard deviation between replicates (Fig. 19). For unknown reasons, using ½ EMM and adding glucose after

autoclaving affected the reproducibility of DMMTA toxicity compared to assays with 1xEMM and glucose added before autoclaving (see Fig. 33).

Unlike *S. cerevisiae*, testing different carbon sources was limited to glucose and fructose because of the lack or inefficient uptake and metabolism of other sugars in *S. pombe*. Although a slight delay in entry into the logarithmic growth phase was observed for cells cultivated with fructose (Fig. 19A), the maximum OD_{600} value and growth curve progression was similar. Growth of cultures exposed to As^{V} or As^{III} did not differ significantly depending on the sugar used for cultivation, considering the delayed entry into the logarithmic growth phase (Fig. 19D-G). By contrast, cells cultivated in fructose-containing medium exhibited sensitivity to DMMTA in a concentration-dependent manner (Fig. 19B+C). Astonishingly, higher concentrations of glucose were associated with enhanced DMMTA sensitivity, in contrast to the reduced toxicity observed with increasing concentrations of fructose.

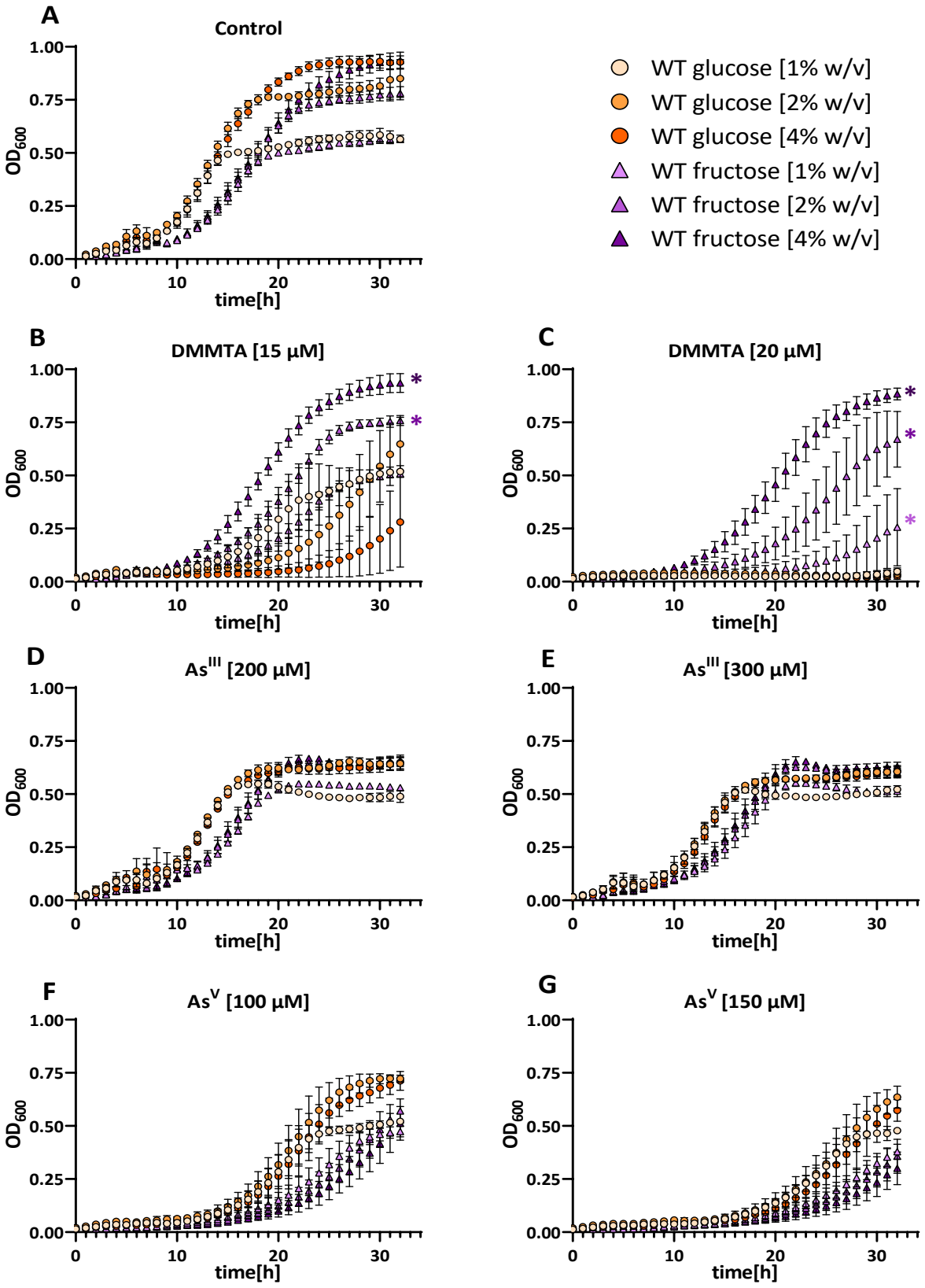
A
Control
B
DMMTA [15 µM]
C
DMMTA [20 µM]
D
As^III [200 µM]
E
As^III [300 µM]
F
As^V [100 µM]
G
As^V [150 µM]
OD600
time[h]
WT glucose [1% w/v]
WT glucose [2% w/v]
WT glucose [4% w/v]
WT fructose [1% w/v]
WT fructose [2% w/v]
WT fructose [4% w/v]

Fig. 19: Arsenic tolerance of *S. pombe* WT under different glucose and fructose concentrations grown in ½ EMM. The growth curve progression of WT (FY261) was measured every hour for 32 hours under various conditions. Logarithmically growing cells were treated with no arsenic (A), 15 µM DMMTA (B), 20 µM DMMTA (C), 200 µM As^{III} (D), 300 µM As^{III} (E), 100 µM As^{V} (F) and 150 µM As^{V} (G). WT cultures were grown in medium with 0.5% w/v (pale orange circles), 2% w/v (orange circles), 4% w/v glucose (dark orange circles) and compared to WT cultures grown with 0.5% w/v (pale purple triangles), 2% w/v (purple triangles), 4% w/v glucose (dark purple triangles) to assess their susceptibility to arsenic. To evaluate growth differences between WT grown in fructose- and WT grown in glucose-containing medium, the sum of OD_{600} values decline (in comparison to the control) for each condition was compared to the growth at the respective carbon-source concentrations. Statistical analysis was performed using the Wilcoxon Rank-Sum Test, with significant differences in growth curve profiles are indicated by asterisks in the respective treatment colors: $p < 0.05$ (*), $p < 0.01$ (**), $p < 0.001$ (***). Data represent three biological replicates ($n = 1$ per condition/genotype) and are shown as mean ± standard deviation.

Further evidence was obtained from experiments with *S. cerevisiae* WT and the *gal2* mutant exposed to DMMTA in presence of glucose or fructose (Fig. 20). Both strains showed lower sensitivity towards DMMTA when grown in fructose-containing medium compared to glucose. Based on the similar growth of WT and the *gal2,* the possibility that the observed effects are due to inhibition of *GAL2* transporter expression in the presence of glucose can be excluded. For As^{V} and lower As^{III} concentrations, neither WT nor *gal2* exhibited a carbon source-dependent tolerance. Only at very high As^{III} concentration (Fig. 20E) did WT and *gal2* show sugar-dependent differences in the growth curve progression. Similar to DMMTA, cells cultivated with fructose were more sensitive to As^{III}.

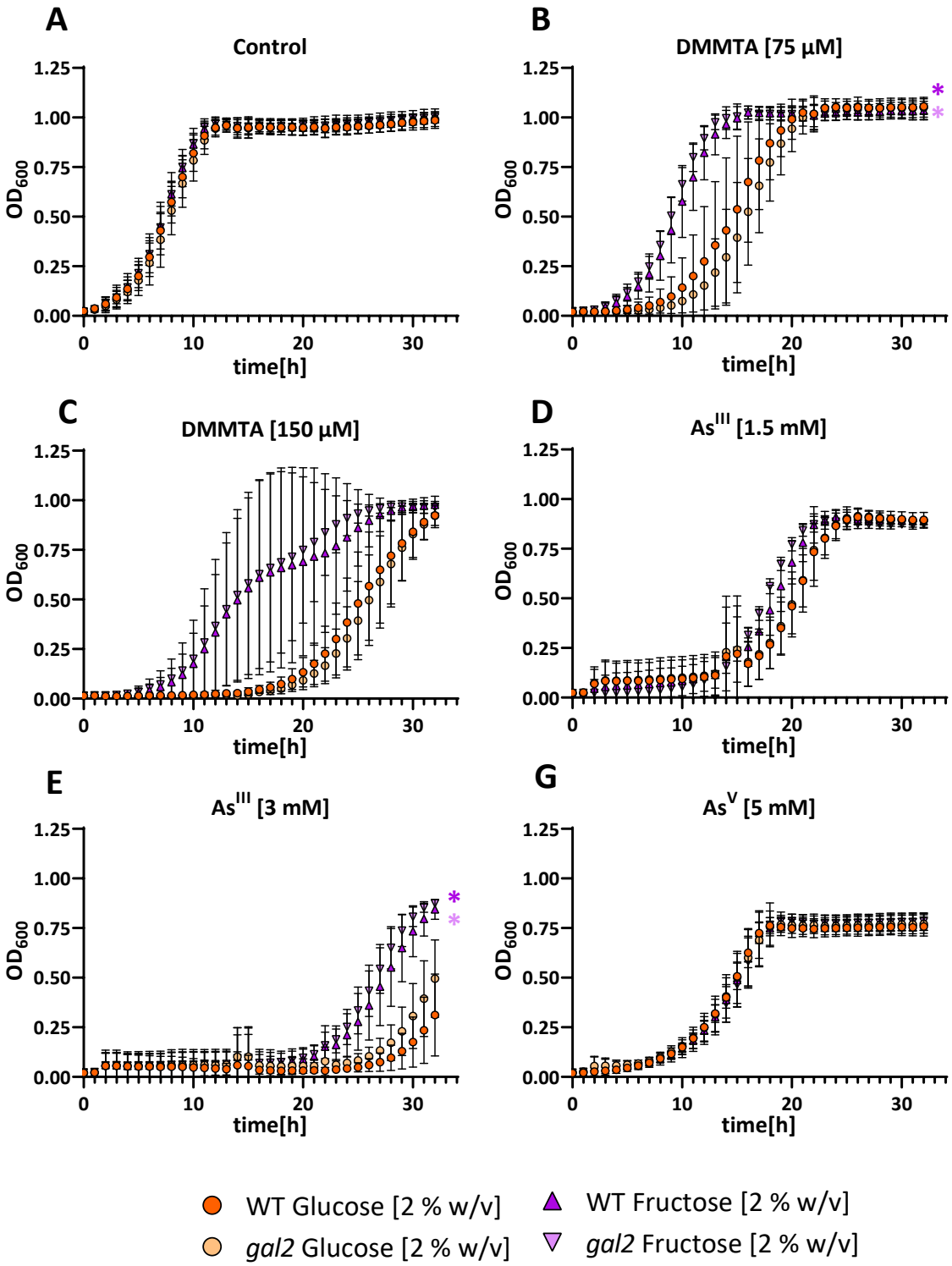
A
Control
B
DMMTA [75 µM]
C
DMMTA [150 µM]
D
As^III [1.5 mM]
E
As^III [3 mM]
G
As^V [5 mM]
OD600
time[h]
0.00
0.25
0.50
0.75
1.00
1.25
0
10
20
30
*
*
WT Glucose [2 % w/v]
gal2 Glucose [2 % w/v]
WT Fructose [2 % w/v]
gal2 Fructose [2 % w/v]

Fig. 20: Arsenic tolerance of *S. cerevisiae* WT and the *gal2* mutant under different glucose and fructose concentrations. The growth curve progression of WT (BY4742) and the knockout strain *gal2* was measured every hour for 32 hours under various conditions. Logarithmically growing cells were treated with no arsenic (A), 75 µM DMMTA (B), 150 µM DMMTA (C), 1.5 mM As^{III} (D), 3 mM As^{III} (E), or 5 mM As^{V} (F). WT and *gal2* cultures were grown in medium with 2 w/v glucose (WT: orange circles; *gal2* pale orange circles) or 2% w/v fructose (WT: purple triangles; *gal2* pale purple reversed triangles). To evaluate growth differences between WT and *gal2*, as well as WT and *gal2* grown in glucose- versus fructose-containing medium, the sum of OD_{600} values for each condition/strain was compared to WT growth at the respective carbon-source concentrations. Statistical analysis was performed using the Wilcoxon Rank-Sum Test, with significant differences in growth curve profiles indicated by asterisks in the respective treatment colors: $p < 0.05$ (*), $p < 0.01$ (**), $p < 0.001$ (***). Data represent three biological replicates ($n = 1$ per condition/genotype) and are shown as mean ± standard deviation. No significant differences were found between WT and *gal2* regardless of the carbon source and arsenic species.

3.2.3 The Impact of Sugars on the Uptake and Toxicity of DMMTA in *A. thaliana*

Seedlings grown on fructose instead of glucose or sucrose exhibited slightly reduced DMMTA toxicity, as indicated by a tendency of reduced root growth inhibition and higher fresh weights (Fig. 21A+B). The seedlings fell into two distinct groups (Fig. 21D+E), one experiencing early-stage DMMTA toxicity and another reaching a more advanced developmental stage with root lengths and fresh weights comparable to control conditions.

The scatter dot plots (Fig. 21A+B) illustrate this clear separation, showing small seedlings with severe DMMTA toxicity symptoms and others appearing unaffected. The strongest toxicity effects were observed in seedlings grown on glucose (median: 8.0 mg / 23.25 mm) and sucrose (median: 8.3 mg / 22.12 mm), while those on fructose-containing plates showed slightly, though not significantly, better growth (median: 9.15 mg / 24.29 mm). Under control conditions, glucose, fructose-, and sucrose-grown seedlings exhibited nearly identical median weights and root lengths (Glucose: 7.4 mg / 93.1 mm; Fructose: 7.4 mg / 91.2 mm; Sucrose: 7.3 mg / 93.4 mm).

Additionally, an initial uptake experiment with Col-0 plants treated with DMMTA for 24 hours - either alone or with 300 µM of glucose, galactose, fructose, maltose, or sucrose - revealed a sugar-dependent reduction in ∑As levels (Fig. 21C). Across all sugars tested, arsenic accumulation decreased by 20–30% in roots and by up to 500% in shoots. However, no clear trend emerged among the different mono- and disaccharides.

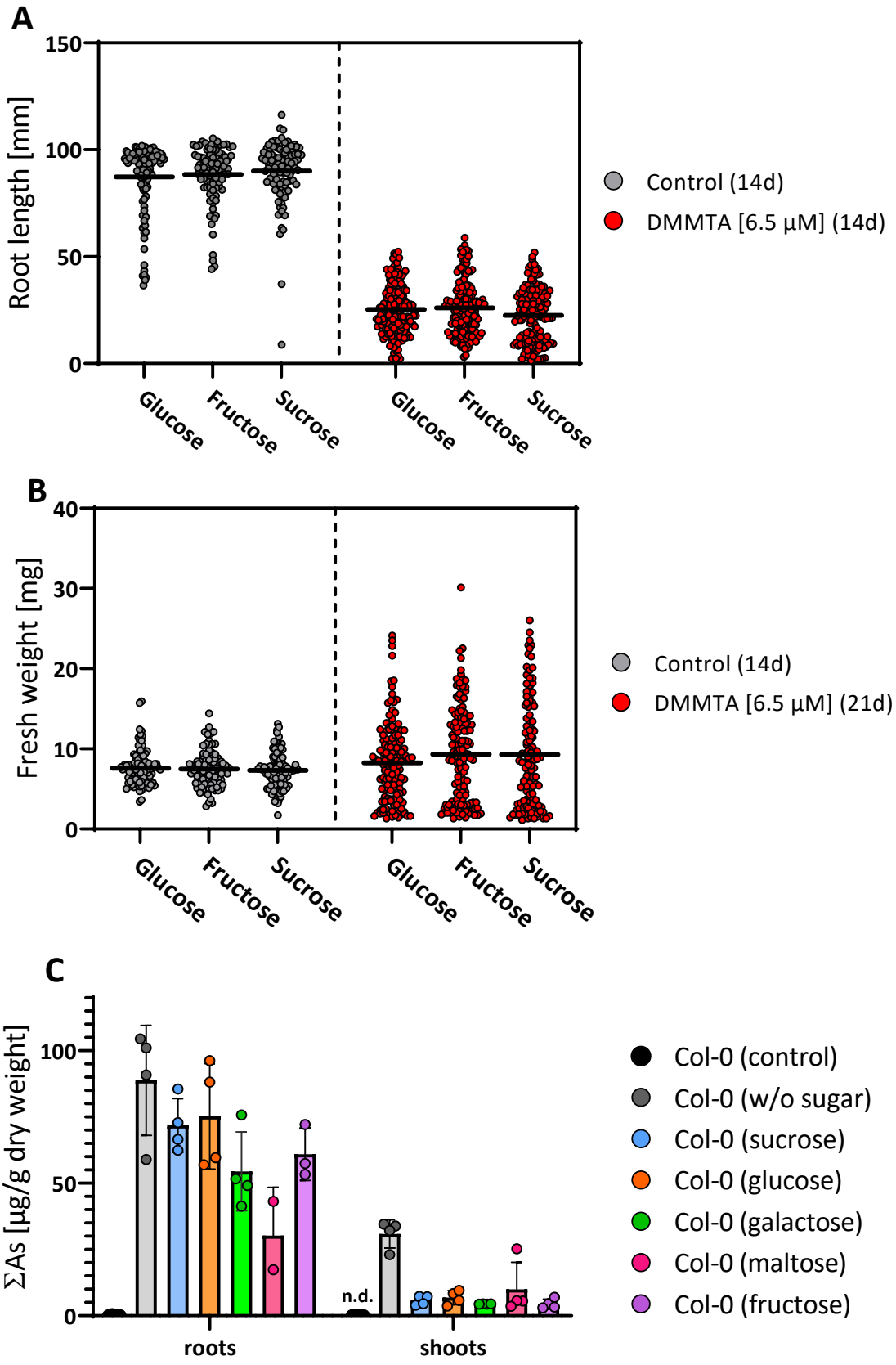
A
Root length [mm]
150
100
50
0
Glucose
Fructose
Sucrose
Glucose
Fructose
Sucrose
Control (14d)
DMMTA [6.5 µM] (14d)
B
Fresh weight [mg]
40
30
20
10
0
Glucose
Fructose
Sucrose
Glucose
Fructose
Sucrose
Control (14d)
DMMTA [6.5 µM] (21d)
C
ΣAs [µg/g dry weight]
100
50
0
n.d.
roots
shoots
Col-0 (control)
Col-0 (w/o sugar)
Col-0 (sucrose)
Col-0 (glucose)
Col-0 (galactose)
Col-0 (maltose)
Col-0 (fructose)

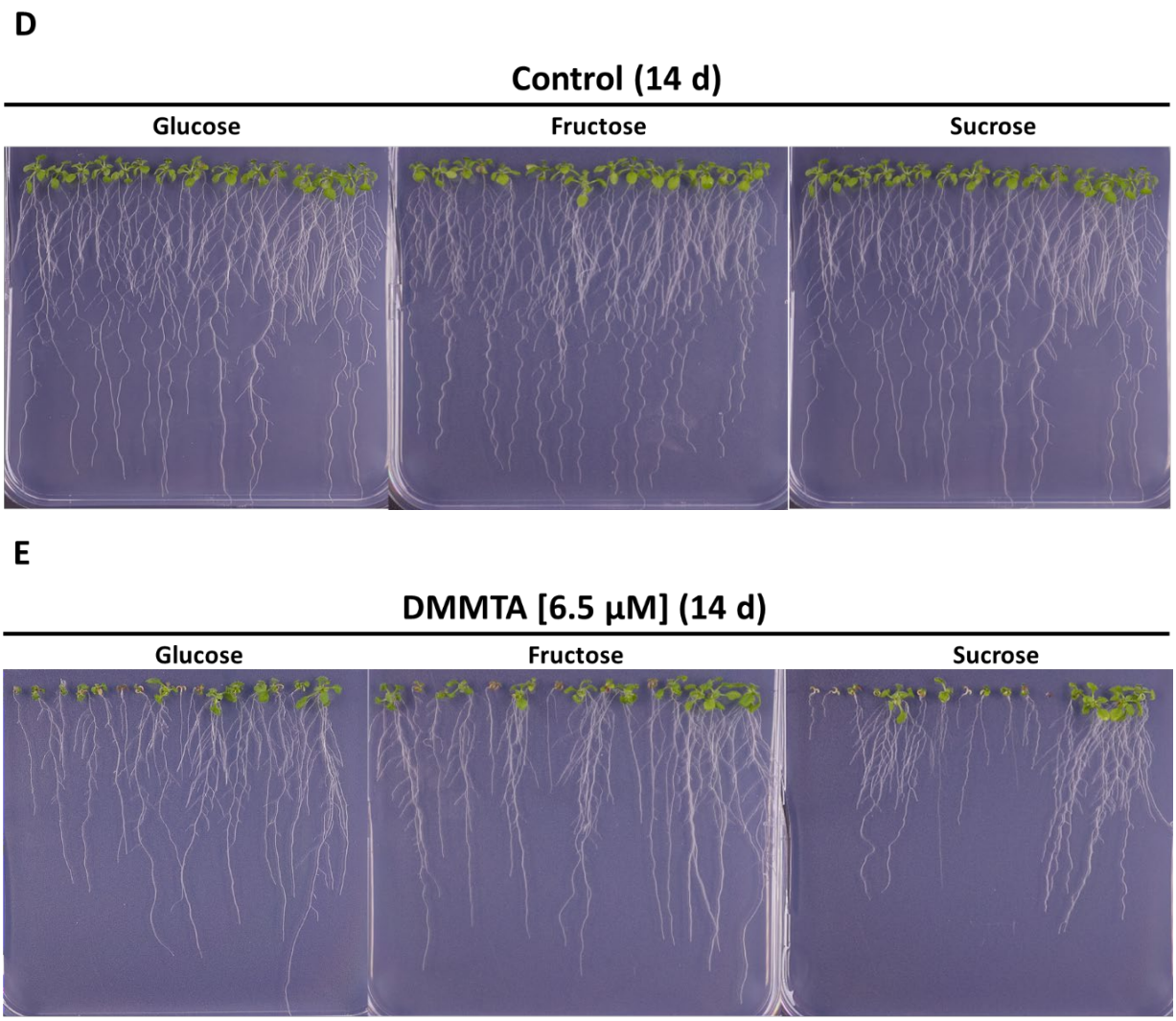

Fig. 21: DMMTA tolerance and uptake in presence of different carbon sources. Root length (A) and fresh weight (B) of *A. thaliana* Col-0 seedlings grown on plates containing 1% (w/v) glucose, fructose, or sucrose, with or without 6.5 µM DMMTA. Root length was measured after 14 days of growth under long-day conditions, while fresh weight was recorded after 14 days (control) or 21 days (DMMTA). ∑As content in roots and shoots (C) of six-week-old Col-0 plants treated with or without 15 µM DMMTA for 24 hours in the presence of 300 µM sucrose (blue), glucose (orange), galactose (green), maltose (red), fructose (purple), or without a carbon source (grey). Measurements were performed using ICP-MS. Images of Col-0 seedlings grown under control conditions for 14 days (D) or on 6.5 µM DMMTA-containing plates for 21 days (E). Statistical analysis was performed using the Kruskal-Wallis Test ($p < 0.05$) to assess significant differences in fresh weight and root length among sugars treatments. No significant differences were found. Medians are shown in red. Data represent one (C) or three biological replicates (A+B) with 26-32 plants per control condition or with 32-48 plants per treatment condition; +/- standard deviation.

3.2.3 Investigation of the Physicochemical Properties of DMMTA

As mentioned above, unlike MTA, the pK_a value of DMMTA remains unknown, and the existing literature presents a contradictory picture[229,230]. According to previous studies, the shift from the protonated to the deprotonated state of DMMTA is assumed to occur within a pH range of 4.2 to 7. Determining the exact range of this transition is crucial for understanding its uptake and toxicity.

Raml et al. (2006) [229] detected a remarkable decrease in retention time determining DMMTA with reversed-phase HPLC coupled with IC-MS, as the buffer pH was increased from 6.0 to 7.0. Based on these findings, they proposed a pK_a for DMMTA between 6.0 and 7.0, similar to that known for the structurally related DMA (pK_a = 6.2). To investigate this further, uptake experiments were conducted using *S. cerevisiae* WT (CEN.PK2-1c), treated with DMMTA and DMA at pH 5 and pH 7, to evaluate whether the pK_a value of DMMTA lies within this range (Fig. 22). Distinct from DMA, the uptake of DMMTA did not notably differ between cells treated at pH 5 and pH 7 with 10 µM DMMTA.

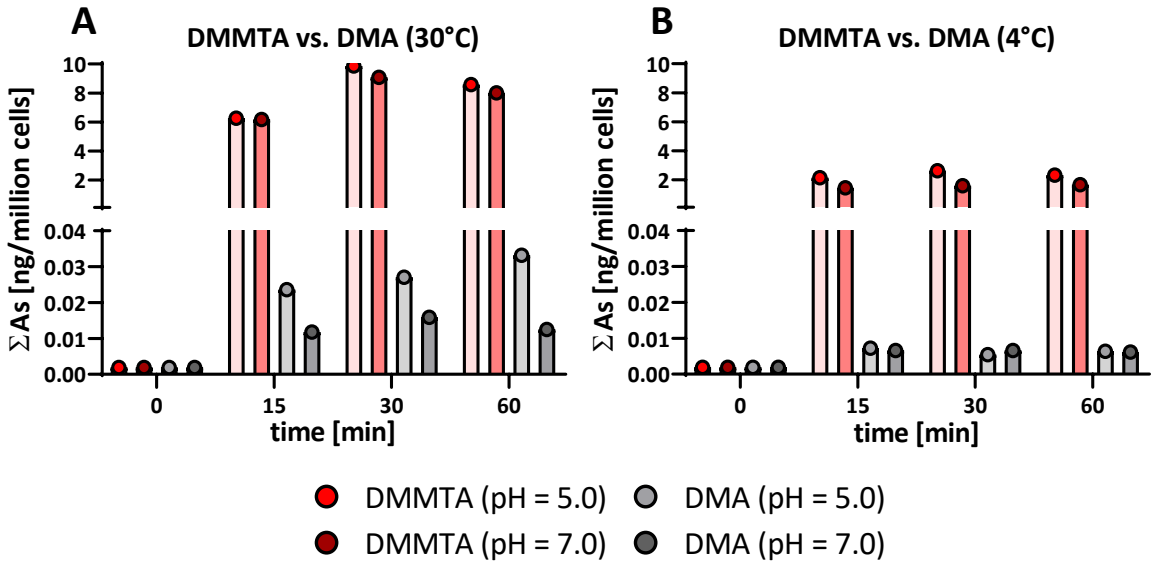

Fig. 22: DMMTA and DMA uptake in WT cells at pH 5.0 and 7.0. *S. cerevisiae* WT (Cen.PK2-1c) cells were exposed to DMMTA [10 µM] or DMA [10 µM] at 30°C (A) or 4°C (B). ∑As in the cells were measured via ICP-MS after 0, 15, 30, and 60 min. Data represent one biological replicates.

Unlike DMA, DMMTA uptake showed no clear difference between cells treated at pH 5 and pH 7 with 10 µM DMMTA (Fig. 22A). In contrast, arsenic levels in cells treated with 10 µM DMA at pH 5 were twice as high as those at pH 7. Notably, cells exposed to DMA at pH 5 took up 285 times less arsenic than those treated with the same concentration of DMMTA. Control experiments conducted at 4°C (Fig. 22B) confirmed that DMA uptake occurred at low rates , consistent with previous reports for other model organisms[83]. However, the striking differences between DMA and DMMTA uptake, along with the absence of a pH-dependent effect on DMMTA uptake, suggest that a pK_a value between 6.0 and 7.0 is unlikely.

Assuming that DMMTA toxicity correlates with its protonation state, toxicity assays were performed on *S. cerevisiae* WT treated with DMMTA at pH values ranging from 4 to 6 (Fig. 23). To ensure consistent growth across this pH range, 2xYNB + 0.1 CPB with 4% (w/v) glucose was used as the SD-medium for cultivation. As shown in Fig. 23A, no adverse growth effects were observed under control conditions within the tested pH range.

With increasing DMMTA concentrations, cells cultivated at pH 4.0 deviated from the growth curve progression of cells grown at higher pH values (Fig. 23B+C). In line with the initial experiments, the standard deviation of DMMTA treatments was much higher compared to those treated with As^{III}.

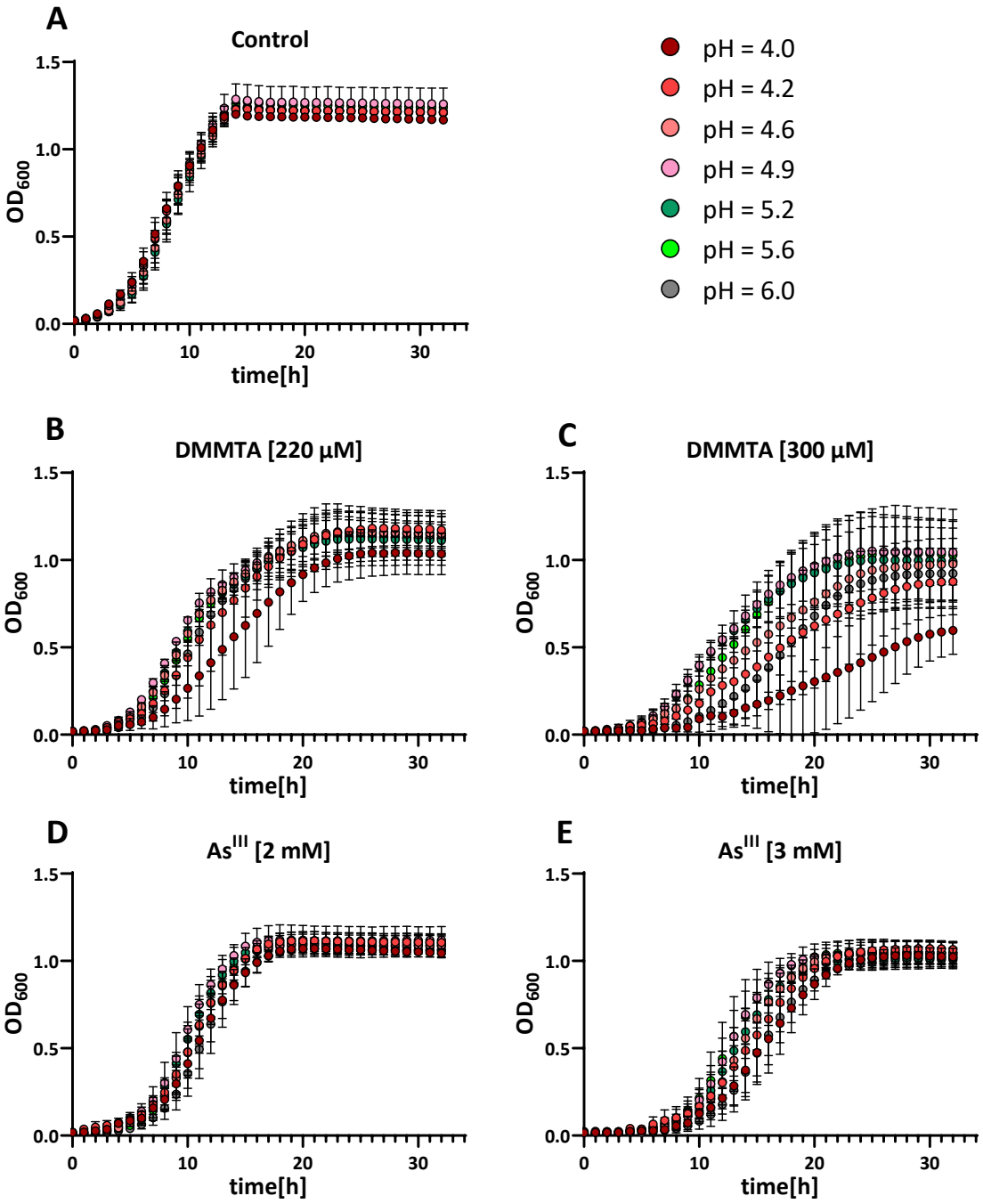

Fig. 23: Arsenic tolerance of *S. cerevisiae* WT cultivated within a pH range from 4.0 to 6.0. The growth curve progression of WT (CEN.PK2-1c) was measured every hour for 32 hours in 2xYNB 0.1 CPB buffered at pH 4.0 (dark red), 4.2 (red), 4.6 (orange), 4.9 (pink), 5.2 (dark green), 5.6 (green) and 6.0 (grey). Logarithmically growing cells were treated with no arsenic (A), 220 µM DMMTA (B), 300 µM DMMTA (C), 2 mM As^{III} (D) or 3 mM As^{III} (E). To evaluate growth differences between WT grown in medium buffered at different pH values, the sum of OD_{600} values for each condition were compared with each other. Statistical analysis was performed using the Kruskal Wallis Test ($p < 0.05$). No significant differences were found. Data represent three biological replicates ($n = 1$ per condition/genotype) and are shown as mean ± standard deviation.

In contrast, As^{III} toxicity (pK_{a1} = 9.23) remained unaffected across the tested pH range (Fig. 23 D+E). Due to the concentrations required to induce toxicity under elevated sugar conditions and limitations in the available As^{III} standard, fewer concentrations were tested compared to DMMTA. Nonetheless, cultures exposed to 3 mM As^{III} showed a similar growth reduction to those treated with the highest DMMTA concentration, without any noticeable divergence in the growth curve.

Although DMMTA remained stable for 20 h of incubation in unbuffered YNB at pH 5.0, both with and without cells (Fig. 24A), the possibility of DMMTA converting into other As-species in 2xYNB 0.1 CPB was tested, to confirm its stability. Therefore, samples of SD-medium containing either DMMTA alone or SD-medium with *S. cerevisiae* WT and DMMTA were speciated (Fig. 24B). At pH 4.0, the ratio of DMMTA to DMA (1.85) was significantly higher compared to pH 5.4 (0.11) in both the medium alone and the medium with cells, after 20 h of incubation at 32 °C. Compared to the stock solution, the percentage of DMMTA decreased from 86% to 63% at pH 4.0, and from 86% to 9.7% at pH 5.4. Meanwhile, the percentage of DMA increased from 2% to 35% at pH 4.0 and to 90% at pH 5.4. Unlike DMMTA in SD-medium buffered at pH 4.0, elevated DMA concentrations were present from the start at pH 5.4.

When calculating the proportion of ∑As remaining in the medium compared to the concentrations at time point 0 h, it was found that cells exposed at pH 4.0 resorbed more of the initially added ∑As (87.31%) than those exposed at pH 5.4 (72.43%). Despite comparable amounts of DMMTA remaining in the medium (pH 4.0: DMMTA ≈ 5.15 µmol; pH 5.4: DMMTA ≈ 6.4 µmol), the detected DMA concentrations differed significantly (pH 4.0: DMA ≈ 1.77 µmol; pH 5.4: DMA ≈ 6.29 µmol).

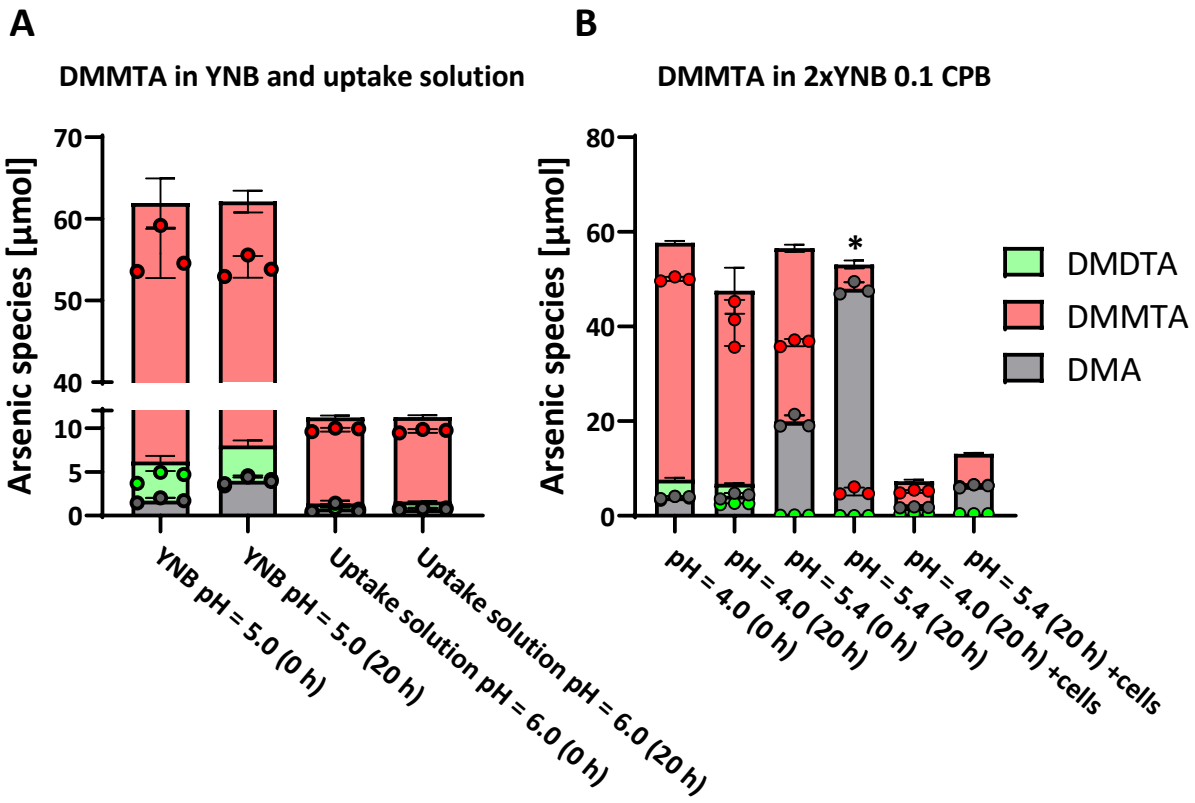

Fig. 24: Evaluation of DMMTA stability in unbuffered YNB, the uptake solution and 2xYNB 0.1CPB at pH 4.0 and pH 5.4. Distribution of arsenic species in 75 µM DMMTA (YNB, pH 5.0) and 10 µM DMMTA (uptake solution, pH 6.0) after 0 h and 20 h of incubation at 30°C (A). Distribution of arsenic species in 75 µM DMMTA in 2×YNB 0.1 CPB buffered at pH 4.0 or pH 5.4, with or without *S. cerevisiae* (Cen.PK2-1c) cells, after 0 h and 20 h of incubation at 30°C (B). Statistical analysis was performed using the Kruskal-Wallis test ($p < 0.05$) to assess significant differences in the distribution of arsenic species between 0-h and 20-h time points for each medium and pH condition. Significant differences are indicated by an asterisk (*). No significant differences were observed in (A). Data represent three biological replicates with $n = 1$ per replicate; +/- the standard deviation.

In contrast to DMMTA detected at pH 4.0 in both cell-containing and cell-free SD-medium, DMMTA at pH 5.4 was only found in SD-medium under biotic conditions, implying that it originated from the cells or that it was stabilized in their presence. Relative to the DMDTA proportion determined in the stock solution (≈24%), the detected DMDTA levels in cell-free medium at both pH values were about 4 to 5 times lower and further decreased over time - at pH 4.0 (from 6.46% to 0.23%) and at pH 5.4 (from 5.28% to n.d.) - likely contributing to the DMA detected. Medium samples derived from the cultivation of WT exposed to DMMTA showed a less pronounced loss of DMDTA for both pH values tested (pH 4.0: 14.71% vs. 96.46% and pH 5.4: 39.03% vs. 100%).

In contrast, standard YNB medium and the uptake solution (Fig. 24A) used throughout this study did not affect DMMTA's stability, as previously shown for other media[81,83].

Overall, the conversion of DMMTA/DMDTA to DMA occurred abiotically and was driven by the different pH levels in the medium.

3.2.4 Assessing *S. pombe* as a Model Organism for DMMTA Uptake and Toxicity Studies

Finally, uptake experiments with cells exposed to sublethal concentrations of DMMTA were conducted, to determine whether *S. pombe* is a more suitable model for investigating DMMTA uptake (Fig. 25). *S. pombe* cells grown in glucose-containing SD medium were transferred to an uptake solution with either glucose or sorbitol and exposed to 7.5 µM DMMTA or As^{III}. As^{III} uptake in WT cells was enhanced when glucose was used as the carbon source, while DMMTA was taken up by WT cells in both glucose and sorbitol. As observed previously, DMMTA uptake at 4°C was notably high, accounting for up to 20% of ∑As within 60 min. The elevated arsenic levels in WT cells exposed to As^{III} with glucose as the carbon source were mitigated by the ∑As detected at 4°C, which accounted for up to one-third of ∑As. As^{III} uptake was approximately 4 to 5 times lower than that of DMMTA and 90 times higher than in sorbitol-treated cells, suggesting that a significant amount of As^{III} was taken up via facilitated diffusion rather than active transport. Although the difference in DMMTA uptake compared to As^{III} was smaller between cells exposed to glucose- or fructose-containing medium, the addition of sorbitol reduced DMMTA uptake by approximately 40%. Even more strikingly, As^{III} uptake was almost completely abolished in the presence of sorbitol.

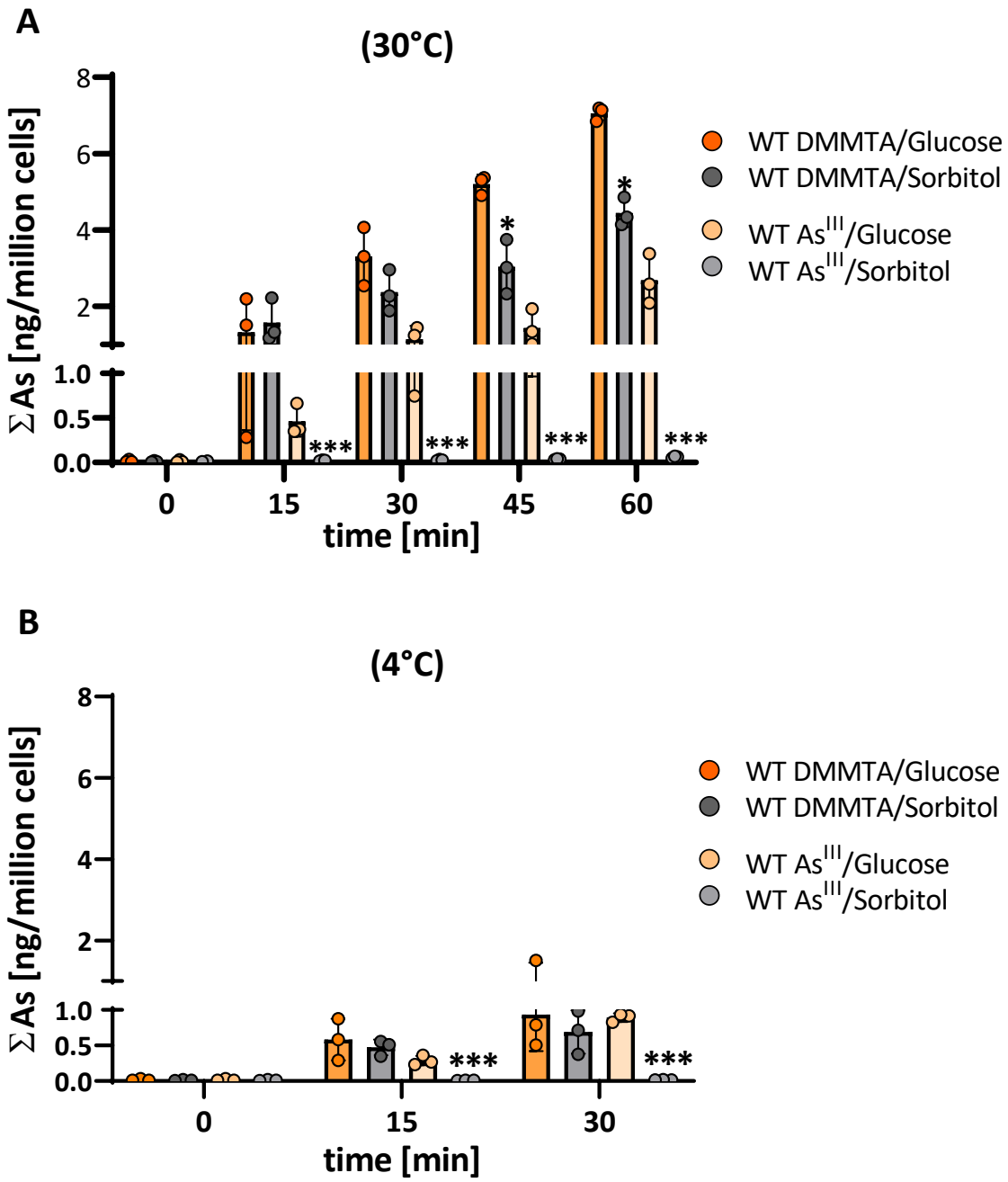

Fig. 25: *S. pombe* exposed to DMMTA or As^{III} in the presence of glucose or sorbitol. *S. pombe* WT (FY261) was exposed to DMMTA [7.5 µM] or As^{III} [7.5 µM] at 30°C (A) or 4°C (B) in the presence of glucose or sorbitol (2% w/v). The ∑As in cells was measured after 0, 15, 30, 45, and 60 min using ICP-MS. To evaluate differences in ∑As between WT cells exposed to DMMTA in the presence of glucose or sorbitol, and separately for As^{III}, values for each condition and time point were compared for statistical significance. Statistical analysis was performed using the Permutation Test, with significant differences in ∑As indicated by asterisks: $p < 0.05$ (*), $p < 0.01$ (**), $p < 0.001$ (***). Data represent three biological replicates ($n = 1$ per condition), with results shown as mean ± standard deviation.

3.3 The As^{III}-evolutionary project

Forward genetic screens have long been used to identify genes involved in specific biological processes. This method relies on mutagenesis followed by screening for phenotypic alterations under defined conditions. Ultimately, after multiple backcrosses and genetic mapping, the genes responsible for the observed phenotype can be identified. While forward screens are effective in identifying mutations that confer tolerance to toxic compounds, they are not well-suited for studying the evolution of traits such as arsenic tolerance. The primary limitation is that mutations arise randomly through mutagenesis rather than selective pressure from the stressor of interest. As a result, it is impossible to track the trajectory of genetic adaptations driven by environmental stress. Additionally, forward screens lack selective pressure to maintain competitiveness under control conditions and do not allow for an assessment of dose-dependent genetic changes. This is critical because the stability of genetic alterations can depend on exposure levels. For instance, Torres-Garcia et al. (2020)[235] demonstrated that *S. pombe* exposed to different doses of caffeine exhibited distinct adaptation mechanisms. High doses led to stable mutations, whereas low doses more frequently induced epigenetic changes that enhanced tolerance.

To investigate mechanisms underlying As^{III} tolerance, a similar approach was adopted using the *pcsΔ* mutant of *S. pombe* in the As^{III}-Evolutionary Project (As^{III}-EvoP) (see scheme Fig. 26). This strategy aimed to identify genes and/or epigenetic modifications associated with reduced As^{III} sensitivity in the absence of the PC-based detoxification pathway.

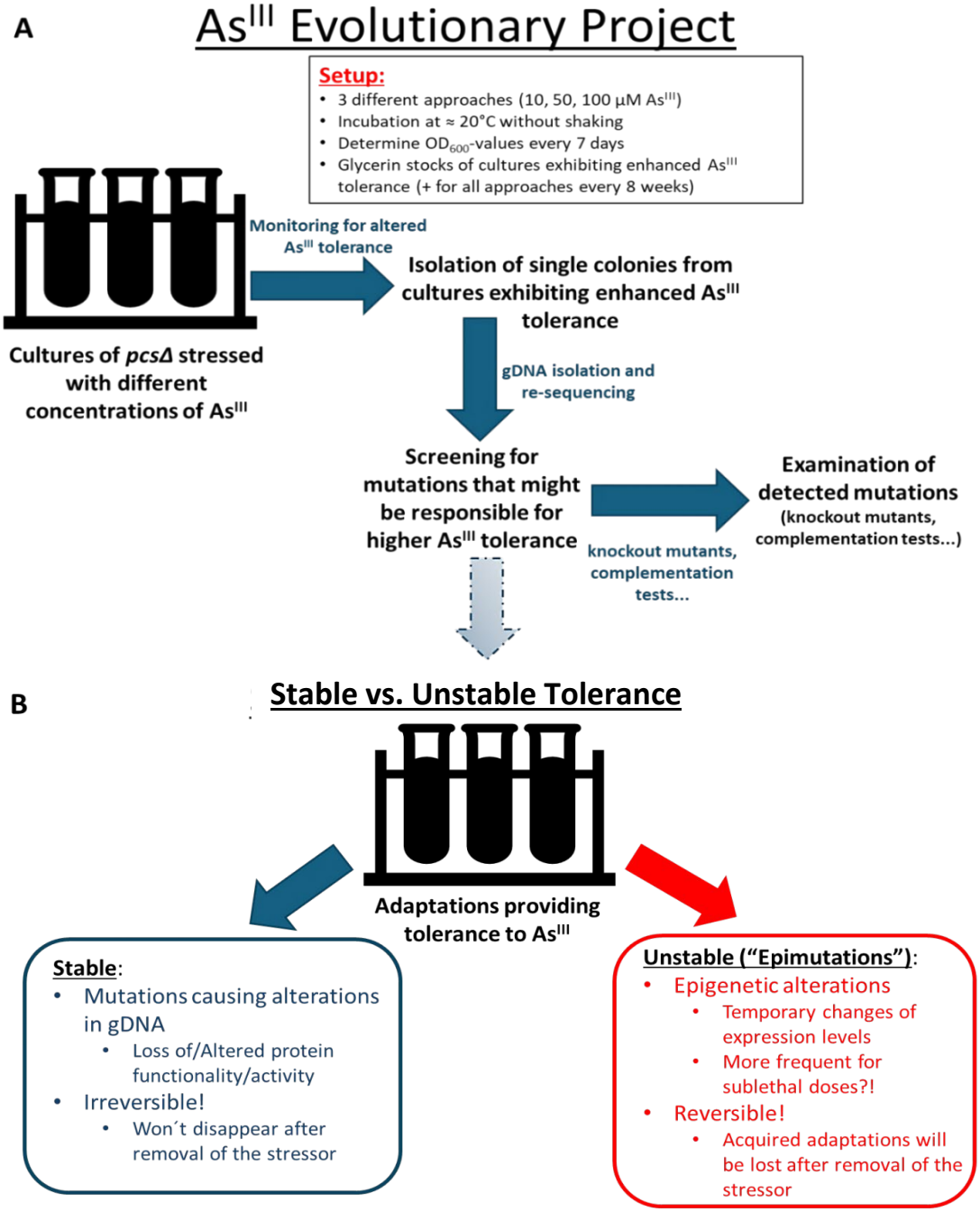

Fig. 26: Schematic Overview of the As[III] evolutionary project. The scheme illustrates the experimental setup of the As[III] evolutionary project conducted with the *S. pombe pcsΔ* mutant (A). Cultures were exposed to sublethal doses of As[III] and monitored for increased As[III] tolerance, indicated by higher OD_{600} values. Glycerol stocks were prepared from cultures exhibiting enhanced As[III] tolerance, and the As[III] concentration was incrementally increased to maintain selective pressure. Single colonies were isolated from glycerol stocks samples and tested for As[III] tolerance. Finally, gDNA from four candidates was extracted and subjected to gDNA re-sequencing to identify genetic alterations. Prior to re-sequencing, the stability of the acquired tolerance was assessed, as depicted below (B).

Anticipating As^{III} tolerant mutant emergence, *S. pombe* cultures were treated with sublethal As^{III} doses at 20°C and monitored growth for several months by measuring OD_{600} weekly. Using two sublethal As^{III} concentrations (10 µM, 50 µM) and one near-lethal concentration (100 µM) across six independent cultures each, multiple cases of increased As^{III} tolerance at lower doses were observed. Screening isolated colonies from these cultures for enhanced As^{III} tolerance, five promising candidates that exhibited higher tolerance against As^{III} without any adverse growth effects under control conditions were selected for further analysis (Fig. 27). The mutants were

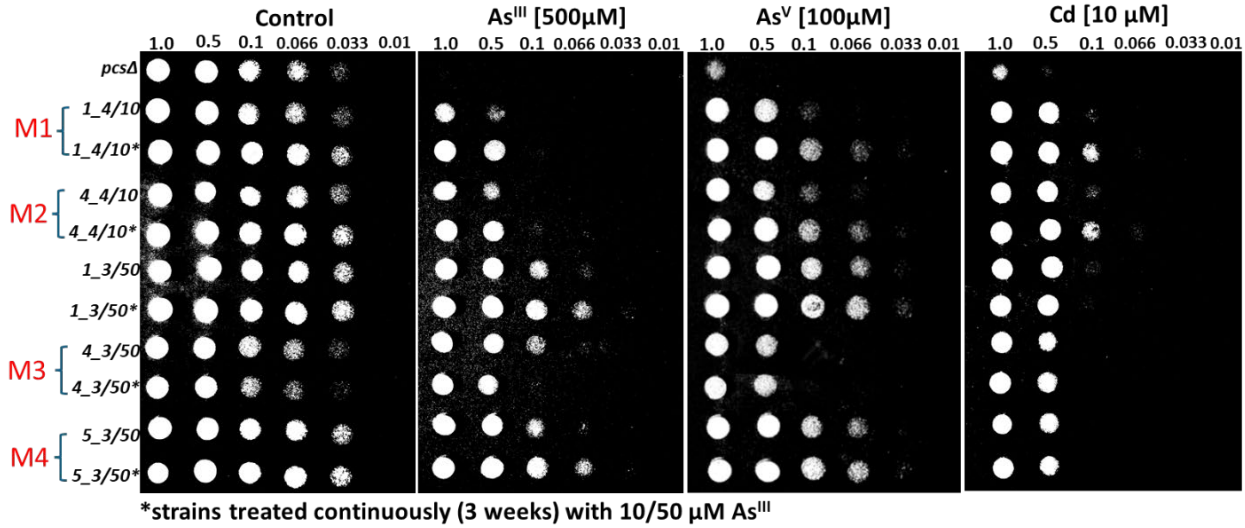

Fig. 27: Screening for Stable vs. Unstable As^{III} Tolerance. Serial dilution assay of the *S. pombe pcsΔ* mutant and mutants derived from the As^{III} evolutionary project. Cultures were either continuously exposed to sublethal doses of As^{III} for three weeks or cultivated without As^{III} under the same conditions at 20°C. Asterisks indicate mutant strains that remained under the same sublethal As^{III} concentrations from which they were originally isolated [10 or 50 µM]. The names of the mutants with which the experiments were continued are highlighted in red, placed before the nomenclature of the cultures from which they were derived. The numbers above each spot indicate the OD_{600} value of the corresponding dilution step. An additional assay testing epigenetic adaptation leading to enhanced arsenic tolerance can be found in the appendix.

designated M1 to M4 based on the order of the cultures from which they were derived. M1 and M2 originated from cultures exposed to 10 µM As^{III}, while M3 and M4 were derived from cultures exposed to 50 µM As^{III}.

Considering the possibility that enhanced tolerance could result from epigenetic alterations due to ongoing exposure to sublethal As^{III} doses, the stability of the acquired tolerance was evaluated.

After cultivating the isolated mutant strains for three weeks with or without a non-toxic As^{III} dose, a serial dilution assay to assess whether tolerance remained stable in the absence of the stressor was conducted. Despite slight variations, all strains remained more tolerant to As^{III}, suggesting that the acquired tolerance probably resulted from stable mutations, although the involvement of heritable epigenetic changes cannot be completely ruled out (Fig. 27).

Following gDNA resequencing, SNPs in coding sequences were identified using Geneious Prime with default settings by comparison to the *pcsΔ* reference genome. Distinct SNPs in four different coding sequences were identified in four out of five candidate strains (Tab. 10).

Tab. 10: Identification of SNPs in the coding sequences (CDS) of mutant strains M1–M4 derived from the As^{III} evolutionary project.

Strain	Systematic ID	Gene name	Chr.	Gene Product	SNPs	SNP Effect
M1 (1_4/10)	SPAC57A10.05c	***pof1***	I	**F-box/WD Repeat Protein Pof1**	**A-Insertion** (pos.: Between 1.374.882 and 1.374.883; residue 1)	**Frame shift**
M2 (4_4/10)	SPAC1A6.04c	***plb1***	I	**Phospholipase B Homolog Plb1**	**T-Insertion** (pos. Between 1.075.685 and 1.075.686; codon residue 312)	**Frame shift**
	SPAC664.09	***ggt1***	I	**γ-Glutamyl Transpeptidase Ggt1**	**G-Insertion** (pos.: Between1.720.980 and 1.720.981; codon residue 496)	**Frame shift**
M3 (4_3/50)	SPAC57A10.05c	***pof1***	I	**F-box/WD Repeat Protein Pof1**	**C-Deletion** (pos.: 1.374.787; residue 33)	**Frame shift**
M4 (5_3/50)	SPAC56E4.06c	***ggt2***	I	**γ-Glutamyl Transpeptidase Ggt2**	**T>G Transition** (pos.:1.256.871; residue 511)	**S > R**

A frameshift-causing mutation in the *pof1* gene, encoding an F-box/WD repeat protein, was found in both the M1 and M3 mutants. In M1, an A insertion between CDS base pairs 2 and 3 (codon 1/605) led to the loss of the start codon and a frameshift, whereas in M3, a C deletion at position 97 (codon 33) also caused a frameshift.

The M2 mutant had two SNPs, each causing a frameshift in respective CDS. The first, in *plb1* (Phospholipase 1), resulted from a T insertion between positions 933 and 934 (codon 312/613). The second, in *ggt1* (γ-glutamyl Transpeptidase 1), was a G insertion between positions 1484 and 1485 (codon 496/630).

Unlike the other mutants, M4 did not exhibit a frameshift-causing SNP. Instead, it carried a T-to-G transition at position 1530 of the CDS, leading to a serine-to-arginine substitution in the C-terminal catalytic domain of *ggt2* (γ-glutamyl Transpeptidase 2) (codon 511/611).

Interestingly, knockout mutations in two of the four identified candidate genes have been reported or assumed to cause lethality[236] (*pombase.org*). Temperature-sensitive *pof1* mutants are known[237], yet all attempts to fully knock out this gene have been unsuccessful. By contrast, despite *ggt1* being annotated as essential, the viability has been documented in the *pcsΔpdt1Δggt1Δ* triple mutant background (Dissertation: Fabian Hollmann).

All isolated mutant strains exhibited increased tolerance to As^{III} compared to the *pcsΔ* mutant (Fig. 28B+C). Additionally, tolerance to As^{V} (Fig. 27 + Fig. 29) and Cd (Fig. 28D+E) was also increased in all four mutant strains (Fig. 28B+C), while their sensitivity to DMMTA remained similar to WT and the *pcsΔ* strain (Fig. 29).

Notably, the M1 and M3 but also the M2 mutant outperformed the WT in liquid assays under high Cd levels, despite being derived from the *pcsΔ* mutant, which is highly Cd-sensitive and less As^{III}-tolerant.

Aside from their shared characteristic of increased tolerance to As^{III}, As^{V}, and Cd, the isolated mutant strains harbored SNPs in genes associated with GSH metabolism[237–240], except for *plb1*, which plays a role in the osmotic stress response[241].

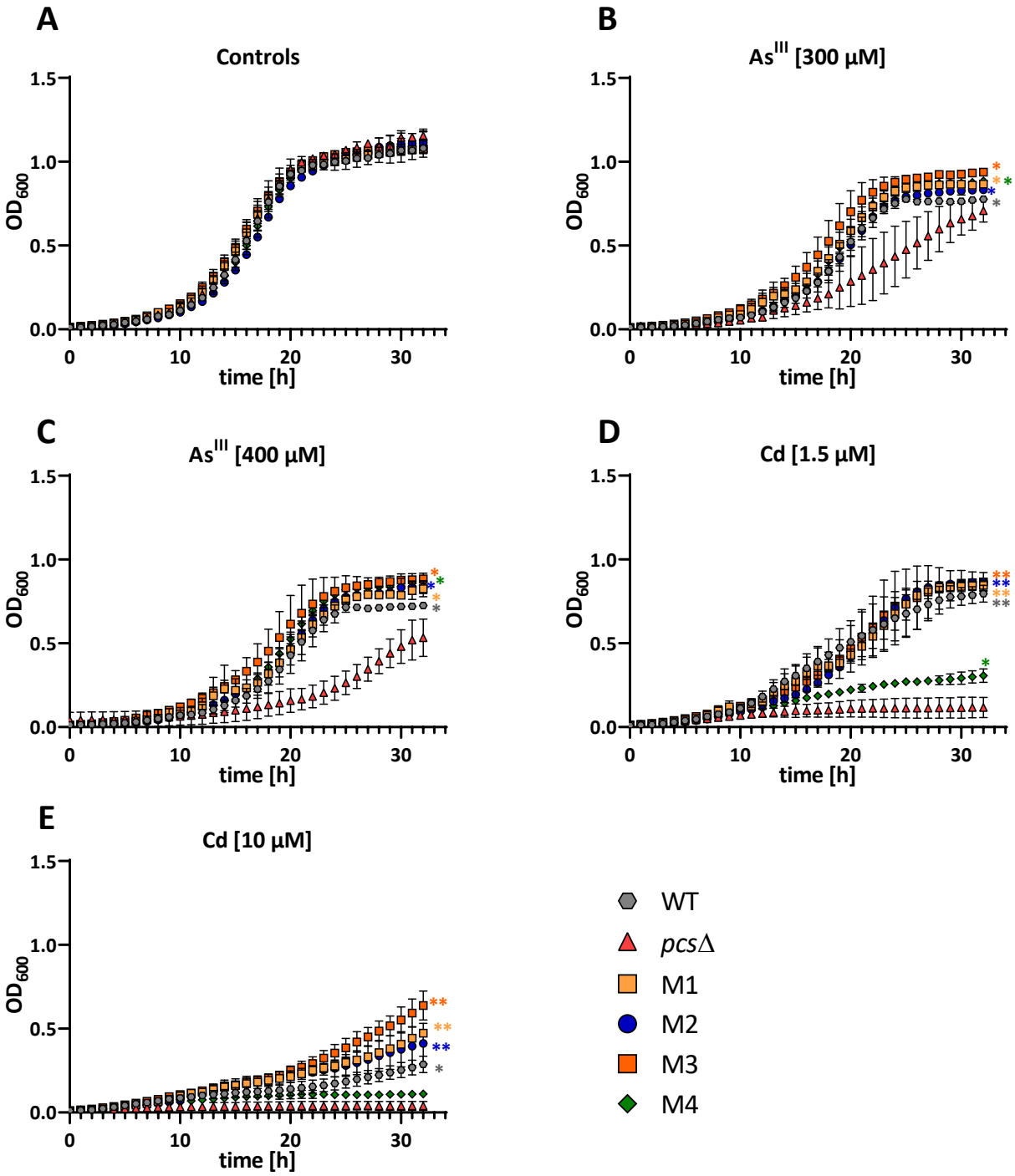
A
Controls
B
As[III] [300 µM]
C
As[III] [400 µM]
D
Cd [1.5 µM]
E
Cd [10 µM]
OD600
time [h]
WT
pcsΔ
M1
M2
M3
M4

Fig. 28: As^{III} tolerance of *S. pombe* WT, *pcsΔ* and mutant strain derived from the As^{III} evolutionary project (M1-M4). Growth curve progression was measured every hour for 32 hours of *S. pombe* WT (FY261) (grey hexagon), the knockout mutant *pcsΔ* (red triangle), and the As^{III} evolved mutants M1 (orange square), M2 (blue circle), M3 (dark orange square) and M4 (green hash) under various conditions. Logarithmically growing cells were treated with no arsenic (A), 300 µM As^{III} (B), 400 µM As^{III} (C), 1.5 µM Cd (D) or 10 µM Cd (E). Growth differences among *pcsΔ*, WT, and M1–M4 were evaluated by comparing the sum of OD_{600} values for each condition/strain relative to *pcsΔ* growth at the respective As^{III} or Cd concentration. Statistical analysis was performed using the Wilcoxon Rank-Sum Test, with significant differences in growth curve profiles indicated by asterisks in the respective treatment colors: $p < 0.05$ (*), $p < 0.01$ (**), $p < 0.001$ (***). Data represent three biological replicates ($n = 1$ per condition/genotype) and are shown as mean ± standard deviation. No significant differences were found between WT and the mutants M1-M4 in any treatment condition.

Next, the respective knockout strains were generated to evaluate whether the observed increase in As^{III} tolerance resulted from the identified mutations. Using the previously described CRISPR-Cas9 system SpEDIT[210], optimized for *S. pombe*, the double mutants *pcsΔggt1Δ#1*, *pcsΔggt1Δ#2*, *pcsΔggt2Δ#1*, *pcsΔggt2Δ#2*, and the triple mutant *pcsΔggt1Δplb1Δ#1* were generated. Additionally, the *ggt2* CDS was disrupted via homologous recombination in both the WT and M4 backgrounds to investigate the effect of a *ggt2* knockout in the presence of PCs and to confirm whether the serine-to-arginine transition in M4 truly causes *ggt2* loss of function. Sanger sequencing confirmed that the mutations in the isolated strains were frameshift-causing deletions or KanMX4 insertions, most likely leading to knockout of the respective genes (Tab. S1).

Attempts to generate a knockout mutant of *pof1* in both WT and *pcsΔ* backgrounds using SpEDIT and homologous recombination were unsuccessful, as were attempts to knock out *ggt1* in the WT background. These results supported the hypothesis that *pof1* might be essential regardless of the genetic background, whereas *ggt1* might only be essential in the WT background and may be dispensable in the *pcsΔ* background. Overexpression of *ggt1* and *pof1* in both WT and *pcsΔ* backgrounds reduced cell viability but did not cause lethality (Fig. S7). Additionally, attempts to knock out *ggt1* and *pof1* via homologous recombination failed due to the lack of selection for hygromycin and geneticin on selective medium[242,243] (discussed later).

By testing the generated knockout strains for their tolerance to As^{III}, Cd, and DMMTA, it was confirmed that the loss of *ggt1* and *ggt2* enhances As^{III} and Cd tolerance (Fig. 29). Furthermore, comparing *pcsΔggt1Δ#1* and *pcsΔggt1Δ#2* with the triple mutant *pcsΔggt1Δplb1Δ* suggested that

the SNP found in *ggt1* of M2 contributes the most - if not exclusively - to the gain of As^{III} and Cd tolerance.

Similarly, the M4 mutant strain and the respective double knockout strains exhibited reduced sensitivity to As^{III} and Cd, though the degree of tolerance varied. A comparison of the double mutants *pcsΔggt2Δ#1* and *pcsΔggt2Δ#2* with M4 revealed variations in the degree of acquired tolerance.

By contrast to their weaker As^{III} tolerance than M4, both mutants were as sensitive to DMMTA as the M4 mutant and M4*_ggt2ΔKanMX4* (Fig. 32C). Although the loss of *ggt2* activity conferred Cd and As^{III} tolerance in the *pcsΔ* background, it was accompanied by increased sensitivity to elevated DMMTA concentrations. However, knockout of *ggt1*, another γ-glutamyl transpeptidase-encoding gene, did not affect DMMTA tolerance. The increased DMMTA sensitivity in mutant strains lacking Ggt2 activity was clearly observed only at higher DMMTA concentrations in YE5S medium (Fig. 32C), while at lower concentrations in EMM medium, only a slight tendency was noticeable (Fig. 32A+B).

Overall, except for the double mutants *pcsΔggt2Δ#1*, *pcsΔggt2Δ#2* and M4, none of the other knockout strains or As^{III}-evolved mutants displayed altered DMMTA tolerance compared to the *pcsΔ* mutant or WT. While the SNP in *ggt1* appears to be the key factor behind the enhanced As^{III} and Cd tolerance in M2 (Fig. 29 and 30), the higher tolerance of M4 does not solely result from *ggt2* loss of function (Fig. 29 and 31). Given the weaker As^{III} and Cd tolerance of the *pcsΔggt2Δ#1* and *pcsΔ ggt2Δ#2* double mutants, the data contradicts the initial hypothesis that M4 tolerance resulted exclusively from a *ggt2* loss-of-function mutation. Nevertheless, the absence of phenotypic differences between M4 and the M4*_ggt2ΔKanMX4* knockout mutant suggests that the serine-to-arginine transition in M4 causes a loss of Ggt2 function, rather than merely altering it.

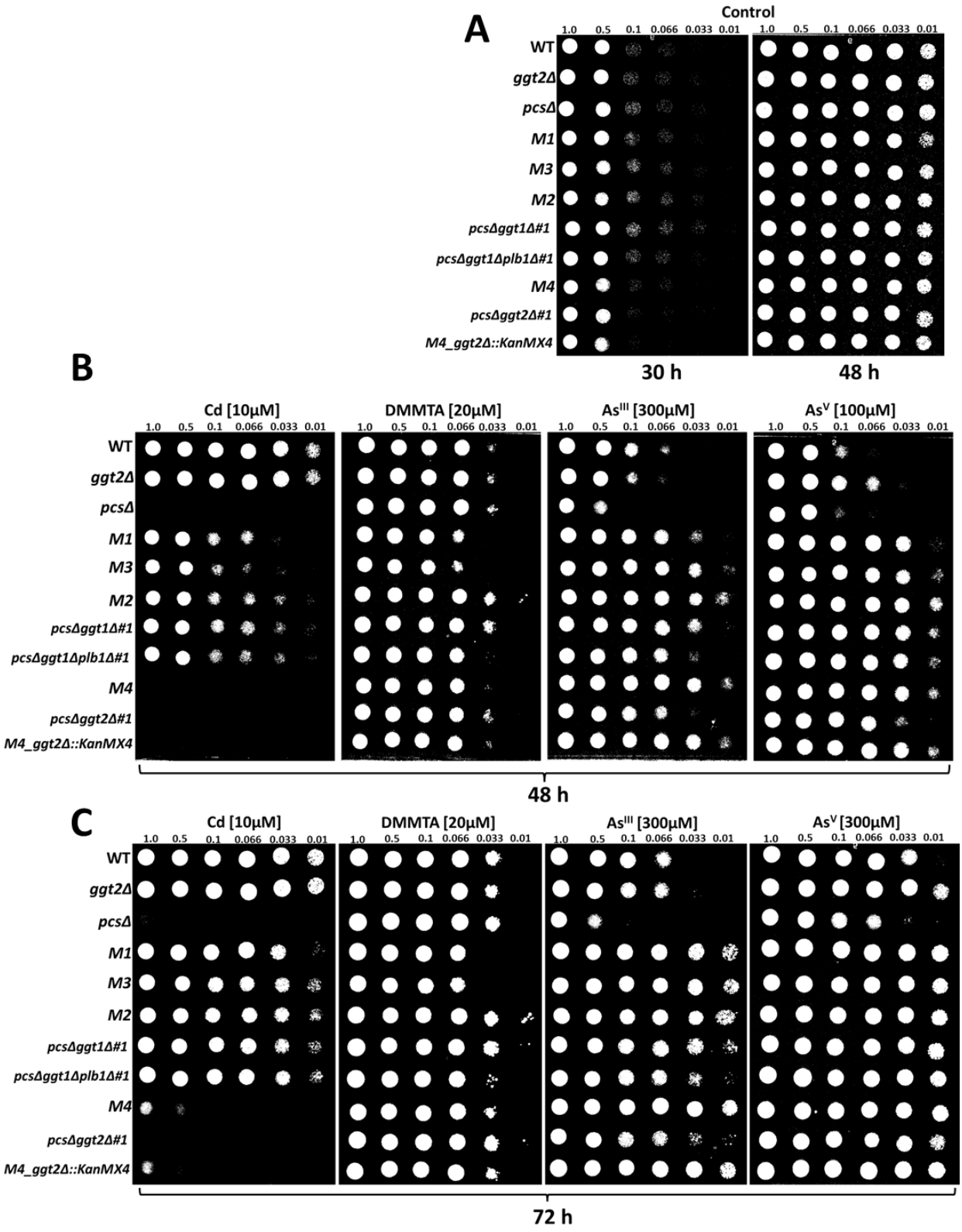
A
Control
1.0 0.5 0.1 0.066 0.033 0.01
WT
ggt2Δ
pcsΔ
M1
M3
M2
pcsΔggt1Δ#1
pcsΔggt1Δplb1Δ#1
M4
pcsΔggt2Δ#1
M4_ggt2Δ::KanMX4
30 h
48 h
B
Cd [10μM]
DMMTA [20μM]
AsIII [300μM]
AsV [100μM]
48 h
C
Cd [10μM]
DMMTA [20μM]
AsIII [300μM]
AsV [300μM]
72 h

Fig. 29: Comparison of M1–M4 with the corresponding knockout mutants, the WT and *pcsΔ* strain regarding their tolerance to Cd, DMMTA, As^{III}, and As^{V}. A serial dilution assay was performed using *S. pombe pcsΔ*, WT, the mutants derived from the As^{III} evolutionary project, and their respective knockout strains. Strains were spotted onto EMM plates containing Cd [10 µM], DMMTA [20 µM], As^{III} [300 µM], As^{V} [100 µM] (B+C) or without any stressor (A) and incubated at 30°C. Photos were taken after 30 h (A), 48 hours (A+B), and 72 hours (C). The numbers above each spot indicate the OD_{600} value of the corresponding dilution step. An additional representative replicate is provided in the appendix.

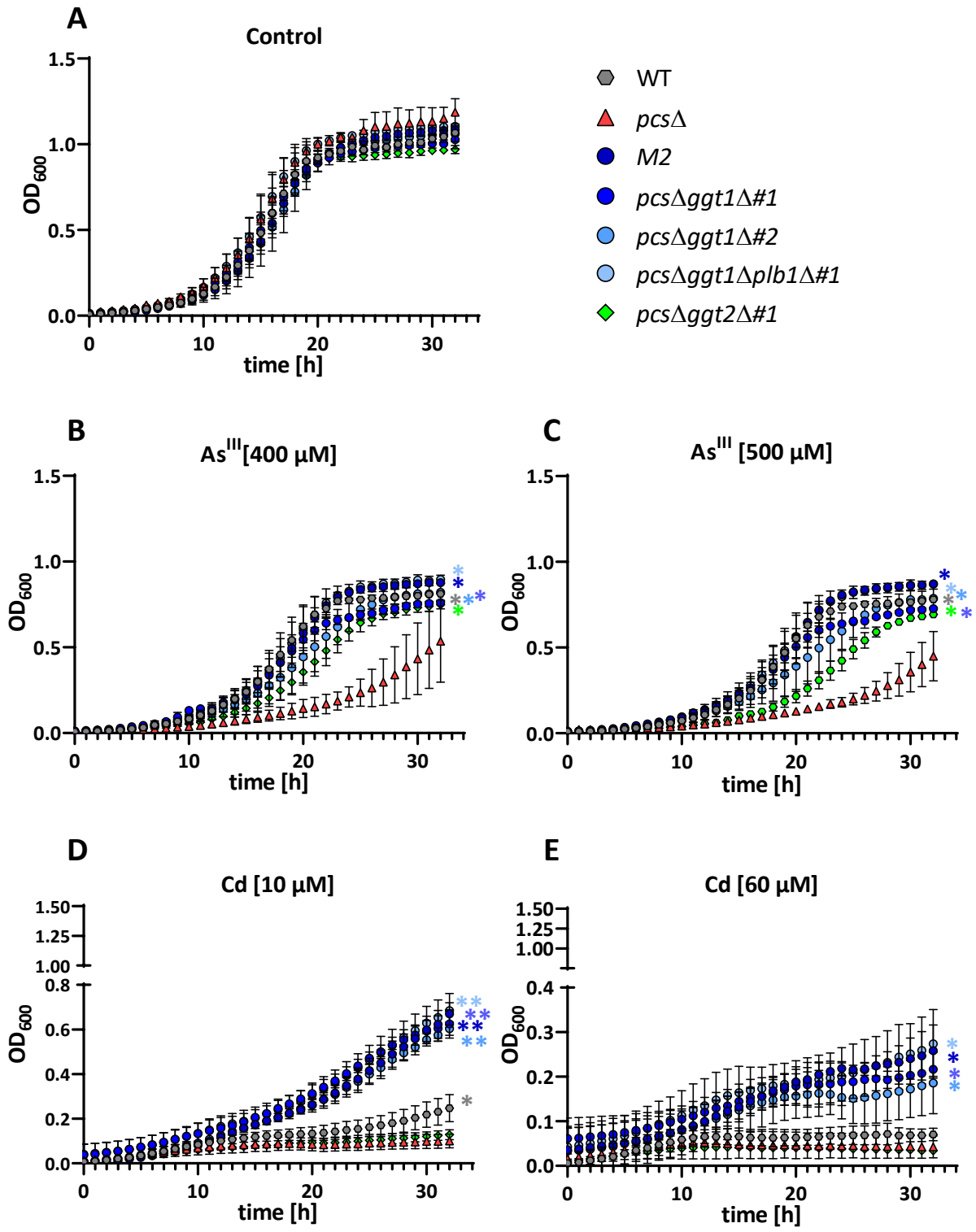
A
Control
OD600
time [h]
WT
pcsΔ
M2
pcsΔggt1Δ#1
pcsΔggt1Δ#2
pcsΔggt1Δplb1Δ#1
pcsΔggt2Δ#1
B
As[III][400 µM]
C
As[III] [500 µM]
D
Cd [10 µM]
E
Cd [60 µM]

Fig. 30: Comparison of As^{III} and Cd tolerance of the M2 mutant strain with its corresponding knockout mutants and WT and *pcsΔ*. Growth curve progression was measured every hour for 32 hours of *S. pombe* WT (FY261) (grey hexagon), the knockout mutant *pcsΔ* (red triangle), and the As^{III} evolved mutant M2 (dark blue circle), the knockout mutant *pcsΔgg1Δ#1* (blue circle), *pcsΔgg1Δ#2* (light blue circle), *pcsΔgg1Δplb1Δ#1* (pale blue circle) and *pcsΔgg2Δ#1* (pale green hash) under various conditions. Logarithmically growing cells were treated with no arsenic (A), 400 µM As^{III} (B), 500 µM As^{III} (C), 10 µM Cd (D) or 60 µM Cd (E). Growth differences among *pcsΔ*, WT, M2, and the corresponding knockout strains were evaluated by comparing the sum of OD_{600} values for each condition/strain relative to *pcsΔ* growth at the respective As^{III} or Cd concentration. Statistical analysis was performed using the Wilcoxon Rank-Sum Test, with significant differences in growth curve profiles indicated by asterisks in the respective treatment colors: $p < 0.05$ (*), $p < 0.01$ (**), $p < 0.001$ (***). Data represent three biological replicates ($n = 1$ per condition/genotype) and are shown as mean ± standard deviation.

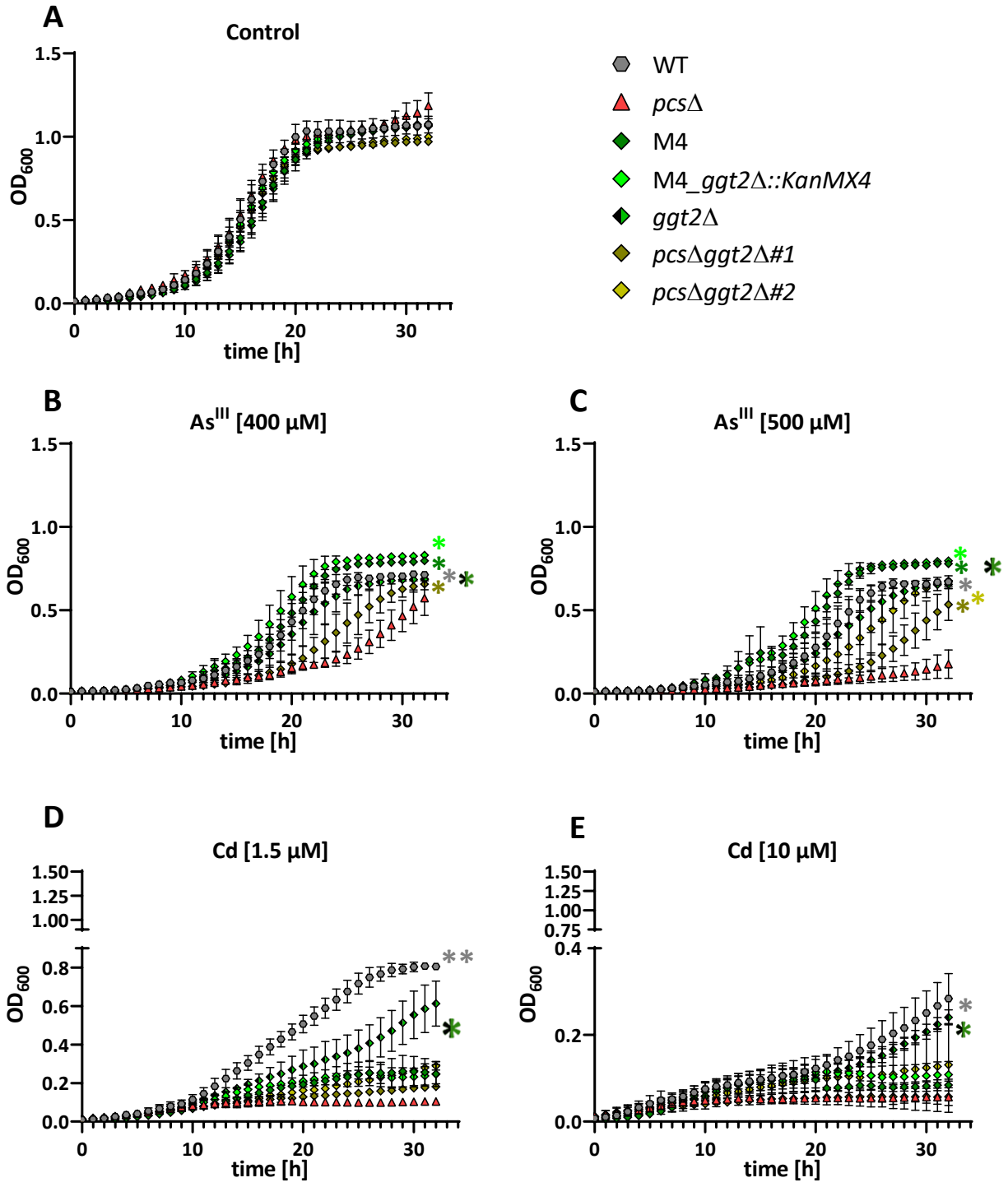
A
Control
B
As^III [400 µM]
C
As^III [500 µM]
D
Cd [1.5 µM]
E
Cd [10 µM]
OD600
time [h]
WT
pcsΔ
M4
M4_ggt2Δ::KanMX4
ggt2Δ
pcsΔggt2Δ#1
pcsΔggt2Δ#2

Fig. 31: Comparison of As^{III} and Cd tolerance of the M4 mutant strain with its corresponding knockout mutants and WT and *pcsΔ*. Growth curve progression was measured every hour for 32 hours of *S. pombe* WT (FY261) (grey hexagon), the knockout mutant *pcsΔ* (red triangle), and the As^{III} evolved mutant M4 (dark green hash), the knockout mutants M4_*gg2Δ::KanMX4* (pale green hash), *gg2Δ* (black/green hash) *pcsΔgg2Δ#1* (olive green hash), and *pcsΔgg2Δ#2* (light olive green hash), under various conditions. Logarithmically growing cells were treated with no arsenic (A), 400 µM As^{III} (B), 500 µM As^{III} (C), 1.5 µM Cd (D) or 10 µM Cd (E). Growth differences among *pcsΔ*, WT, M4, and the corresponding knockout strains were evaluated by comparing the sum of OD_{600} values for each condition/strain relative to *pcsΔ* growth at the respective As^{III} or Cd concentration. Statistical analysis was performed using the Wilcoxon Rank-Sum Test, with significant differences in growth curve profiles indicated by asterisks in the respective treatment colors: $p < 0.05$ (*), $p < 0.01$ (**), $p < 0.001$ (***). Data represent three biological replicates ($n = 1$ per condition/genotype) and are shown as mean ± standard deviation.

Based on the assumption that the polymorphisms found in M1-M4 should affect the GSH metabolism, the GSH content of M1-M4 and the respective double knockout strains was determined via HPLC analysis. Logarithmically grown cells were stressed with sublethal As^{III} concentrations and grown for 18 h (Fig. 33). Even under control conditions M1-M4 and the double mutants tested showed elevated GSH levels (Fig. 33A). Especially, the GSH concentrations of M1, M3 and M2 along with *pcsΔggt1Δ#1* were about four times higher than those measured in cells of *pcsΔ* and the WT. The GSH content in cells of the M4 mutant and the *pcsΔggt2Δ#1* double knockout was less enhanced (not significant) in comparison to *pcsΔ* and the WT. Nevertheless, GSH levels in *pcsΔggt1Δ#1* and *pcsΔggt2Δ#1* resembled those of the respective mutants M2 and M4. Additionally, GSH concentrations of M1 and M3, both harboring a SNP in the *pof1* encoding sequence, coincided with each other.

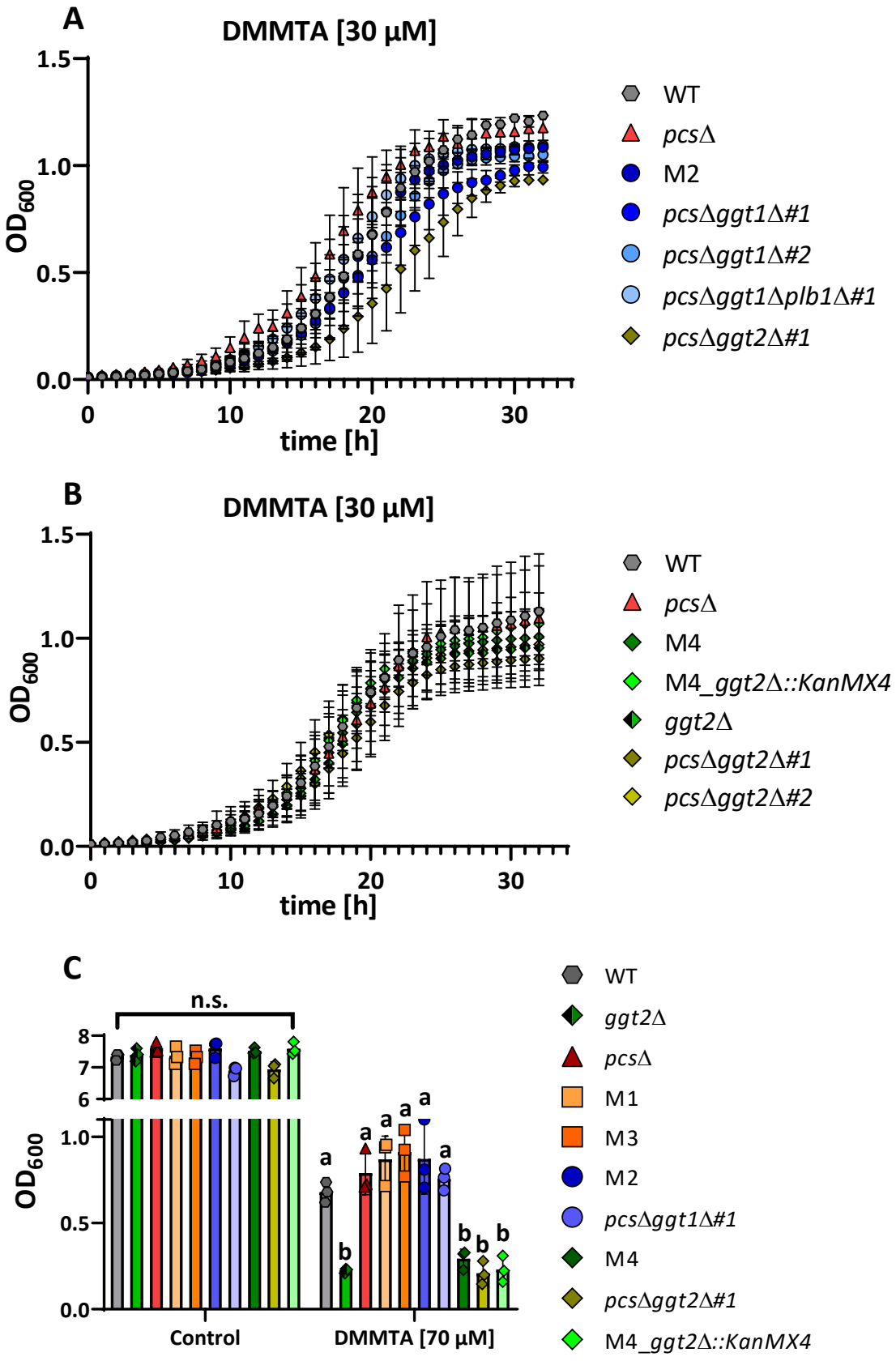
A
DMMTA [30 µM]
OD600
time [h]
WT
pcsΔ
M2
pcsΔggt1Δ#1
pcsΔggt1Δ#2
pcsΔggt1Δplb1Δ#1
pcsΔggt2Δ#1
B
DMMTA [30 µM]
OD600
time [h]
WT
pcsΔ
M4
M4_ggt2Δ::KanMX4
ggt2Δ
pcsΔggt2Δ#1
pcsΔggt2Δ#2
C
n.s.
OD600
Control
DMMTA [70 µM]
WT
ggt2Δ
pcsΔ
M1
M3
M2
pcsΔggt1Δ#1
M4
pcsΔggt2Δ#1
M4_ggt2Δ::KanMX4

Fig. 32: Comparison of DMMTA tolerance of the mutant strains derived from the As^{III} evolutionary project with the corresponding knockout mutants and WT and *pcsΔ*. (A) Growth curve progression of *S. pombe* WT (FY261), the knockout mutant *pcsΔ*, and the As^{III} evolved mutant M2, the knockout mutant *pcsΔgg1Δ#1*, *pcsΔgg1Δ#2*, *pcsΔgg1Δplb1Δ#1* and *pcsΔgg2Δ#1*, treated with 30 µM DMMTA. (B) Growth curve progression of *S. pombe* WT (FY261), the knockout mutant *pcsΔ*, and the As^{III} evolved mutant M4, the knockout mutants M4_*gg2Δ::KanMX4*, *gg2Δ*, *pcsΔgg2Δ#1*, and *pcsΔgg2Δ#2*, treated with 30 µM DMMTA. (A+B) Growth curve progression of logarithmically growing cells was monitored over 32 hours. The respective controls are shown in Fig. 30 and 31. Growth differences among *pcsΔ*, WT, the mutant strains M2 and M4, and their corresponding knockout strains were assessed by comparing the sum of OD_{600} values for each condition/strain relative to *pcsΔ* growth under 30 µM DMMTA. No significant differences were found. (C) OD_{600} values of the previously tested genotypes grown for 24 hours with or without 70 µM DMMTA. A three mL YE5S culture was inoculated with cells at an initial OD_{600} of 0.025 and incubated for 2.5 hours to ensure logarithmic growth before adding 70 µM DMMTA. Statistical analyses were performed using the Kruskal-Wallis Test ($p < 0.05$) to assess significant differences in the maximum growth of genotypes under each treatment separately, followed by a post hoc test for pairwise comparisons of OD_{600} values reached after 24 hours with or without 70 µM DMMTA ($p < 0.05$). Growth differences among genotypes are indicated by different letters. No significant differences were found among the genotypes grown under control conditions. (A-C) Data represent three biological replicates ($n = 1$ per condition/genotype) and are shown as mean ± standard deviation. The genotypes are indicated using the same color and symbol code as in Fig. 28, 30 and 31.

After 18 h of exposure to 10 µM As^{III}, neither M1, M3 nor M2 and *pcsΔggt1Δ#1* exhibited strong induction of GSH biosynthesis (Fig. 33A). The highest GSH induction was observed in cells of the *pcsΔ* strain (≈ 2x), slightly exceeding the GSH induction in cells of M4 and *pcsΔggt2Δ#1* (≈ 1.8 -2x). Contrary, As^{III} exposure led to a depletion of the GSH pool (≈ 0.25x) in WT cells due to PC2 and PC3 formation (Fig. 33B+C).

Related to the about 2x (control conditions) respectively 1.5x times (As^{III} treatment) higher GSH concentrations of M2 and *pcsΔggt1Δ#1* in comparison to M4 and *pcsΔggt2Δ#1*, their gamma glutamyl transpeptidase (γ-GT) activity was tested to evaluate whether the differences observed were related to their activity as transpeptidases.

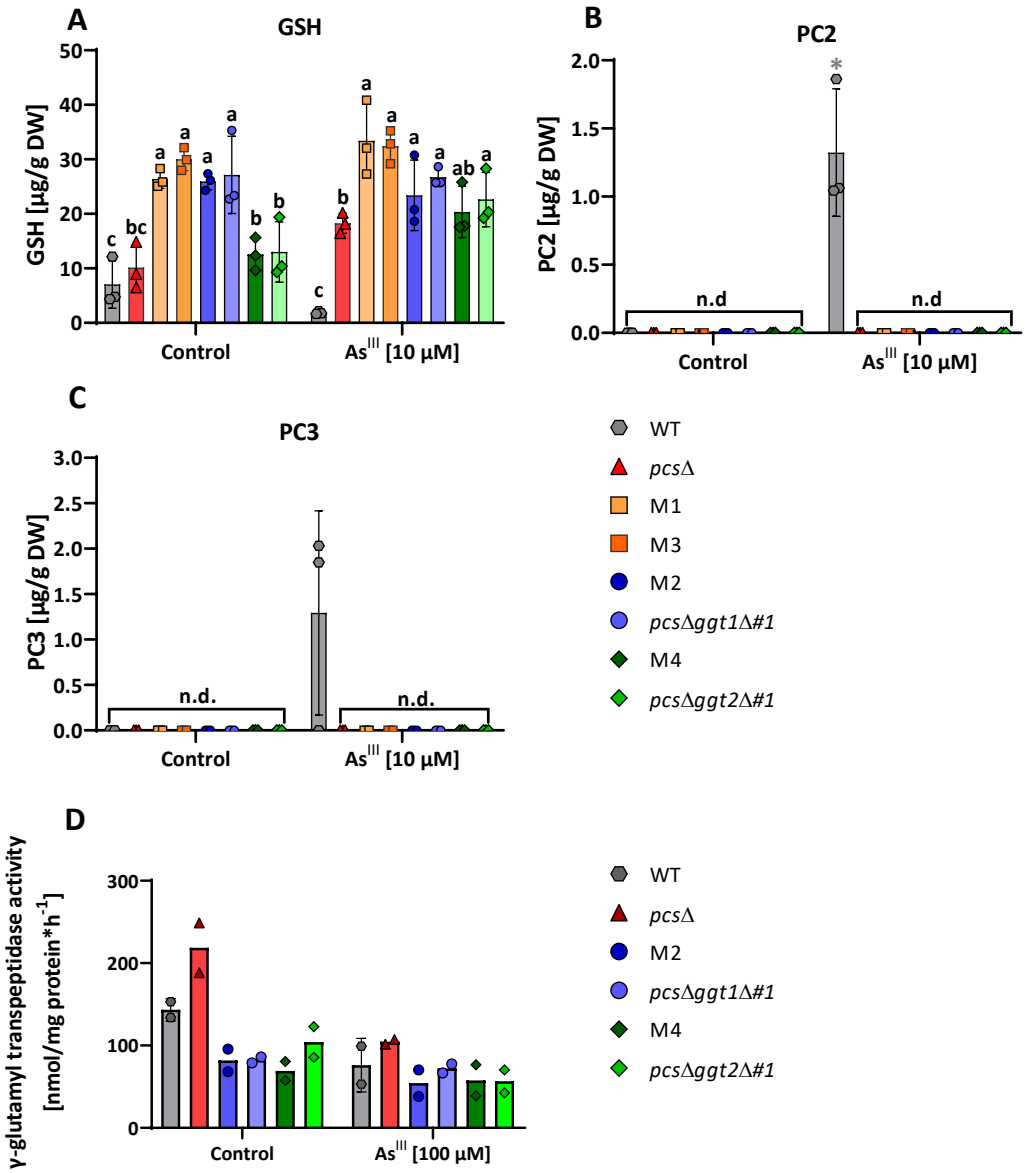

Fig. 33: Evaluation of GSH, PC contents and γ-GT activity in *S. pombe* cells from the As^{III} evolutionary project mutants M1-4 in comparison to WT, *pcsΔ* and the double mutants *pcsΔggtΔ1#1* and *pcsΔggtΔ2#1*. Thiol profiles of *S. pombe* WT (grey hexagon), *pcsΔ* (red triangle), M1 (light orange square), M3 (dark orange square), M2 (dark blue circle), *pcsΔggtΔ1#1* (blue circle), M4 (dark green hash) and *pcsΔggtΔ2#1* (green diamond) cells treated with or without 10 µM As^{III} (A-C). Concentrations of GSH (A), PC2 (B) and PC3 (C) are shown as bar blots with individual data points in µg/g dry weight (DW). Statistical analysis was performed using the Kruskal-Wallis Test ($p < 0.05$) to assess significant differences in the thiol profiles among genotypes for each treatment separately, followed by a post hoc test for pairwise comparisons of GSH contents ($p < 0.05$). Differences in GSH levels are indicated by different letters, whereas significant differences in PC2 and PC3 levels are marked with an asterisk (*). Data represent three biological replicates with $n = 1$ per replicate. Data points below the detection threshold are marked as n.d. (not detectable). (D) γ-GT activity in cells of WT (grey hexagon), *pcsΔ* (red triangle), M2 (dark blue circle), *pcsΔggtΔ1#1* (blue circle), M4 (dark green hash) and *pcsΔggtΔ2#1* (green diamond) grown under control condition or exposed to 100 µM As^{III}. Bar plots with individual data points represent the results from two biological replicates.

First, evaluating the γ-glutamyl-transpeptidase assay described by Adamis et al. (2009)[244,245], using the *S. cerevisiae* strain *ecm38* known for its deficient γ-GT activity (Fig. S10) for an initial test experiment, γ-GT activity was more than five times lower in comparison to the WT. Also, extracts of cultures treated with the sublethal dose of 200 µM As^{III} showed 4-5 times lower γ-GT activity than protein extracts derived from cells under control conditions. Applying the protocol for testing the M2 and M4 mutants together with the corresponding double knockout strains showed clearly lower γ-GT activity for all of them, in comparison to the *pcsΔ* and the WT (Fig. 33D). Moreover, under control conditions *pcsΔ* γ-GT activity was higher than that of the WT. Even though M2, M4 and the respective knockout strains showed lower γ-GT activity, the activity level measured was similar for all of them, thereby differing from the observation of higher GSH contents detected for M2 and *pcsΔggt1Δ#1* than for M4 and *pcsΔggt2Δ#1*. Additionally, even though γ-GT activity of WT and *pcsΔ* mutant protein extracts derived from As^{III} treated cultures was halved in comparison to the control, activity of the mutants and knockout strains seemed to be unaffected by the As^{III} treatment.

For complementation of the As^{III}-evolutionary project mutants and their corresponding knockout strains, both C-terminal GFP-tagged and tag-free versions of the identified candidate genes were cloned using the pSGP72 and pSGP72-GFP vector. In particular, the overexpression of *pof1* and *ggt1* was associated with adverse growth effects, indicating the necessity of tightly controlled expression levels for both genes (Fig. S7).

Complementation of M2 and the respective knockout strains (*pcsΔggt1Δ#1* and *pcsΔggt1Δ#2*) led to an almost complete loss of As^{III} and Cd tolerance compared to the vector controls (Fig. 34B). Unlike *pcsΔggt1Δ#1* and *pcsΔggt1Δ#2*, the M2 mutant retained slightly reduced susceptibility than the *pcsΔ* mutant. M2 complemented with *plb1* did not differ in its susceptibility to As^{III} and Cd compared to the M2 vector control, suggesting that Plb1 does not, or only weakly, contribute to the gain in As^{III} tolerance.

As expected, since M4 differs in its tolerance to As^{III} from the knockout strains (*pcsΔggt2Δ#1* and *pcsΔggt2Δ#2*), only partial complementation was achieved by the expression of *ggt2*, whereas in the double-knockout strains *pcsΔggt2Δ#1* and *pcsΔggt2Δ#2*, *ggt2* expression increased sensitivity to As^{III} and Cd to a level comparable to *pcsΔ*.

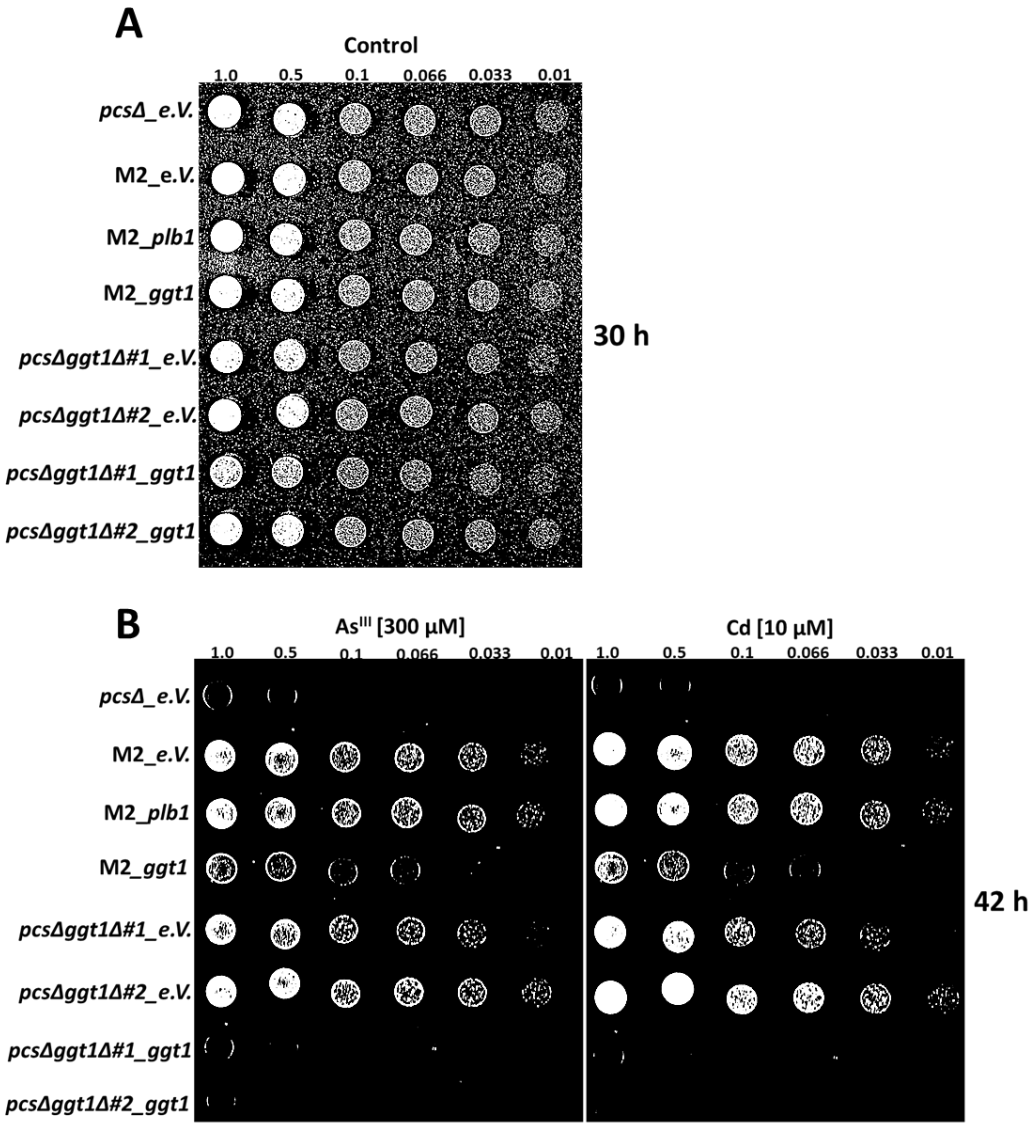

Fig. 34: Complementation of M2 and corresponding knockout mutants. A serial dilution assay was performed using *S. pombe pcsΔ*, the M2 mutant derived from the As^{III} evolutionary project, and their respective knockout strains. These strains harbored either the empty vector (pSGP72; e.V.) or constructs for the expression of the *ggt1* (pSGP72-*ggt1*) or *plb1* (pSGP72-*plb1*) in their respective mutant/knockout backgrounds, as indicated, to assess whether these constructs could complement the phenotype of enhanced As^{III} and Cd tolerance. Strains were spotted onto EMM -/- plates containing 25 nM thiamine with Cd [10 µM] or As^{III} [300 µM] (B) or without any stressor (A) and incubated at 30°C. Photos were taken after 30 h (A) or 48 hours (B). The numbers above each spot indicate the OD_{600} value of the corresponding dilution step. An additional representative replicate is provided in the appendix.

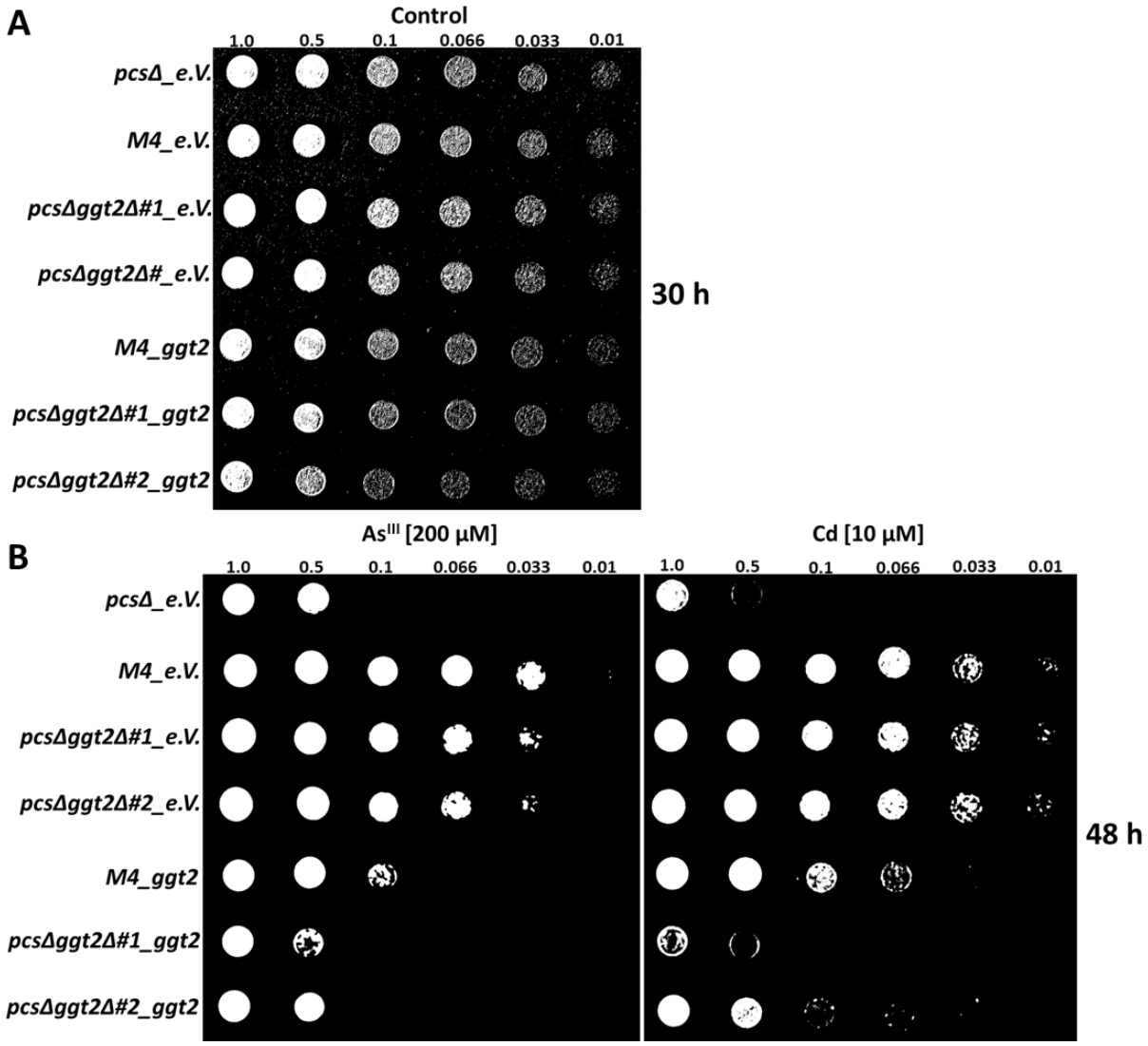

Fig. 35: Complementation of M4 and corresponding knockout mutants. A serial dilution assay was performed using *S. pombe pcsΔ*, the M4 mutant derived from the As^{III} evolutionary project, and their respective knockout strains. These strains harbored either the empty vector (pSGP72; e.V.) or a construct for the expression of *ggt2* (pSGP72-*ggt2*) in the respective mutant/knockout backgrounds, as indicated, to assess whether these constructs could complement the phenotype of enhanced As^{III} and Cd tolerance. Strains were spotted onto EMM -/- plates containing 15 nM thiamine with Cd [10 µM], As^{III} [300 µM] (B) or without any stressor (A) and incubated at 30°C. Photos were taken after 30 h (A) or 48 hours (B). The numbers above each spot indicate the OD_{600} value of the corresponding dilution step.

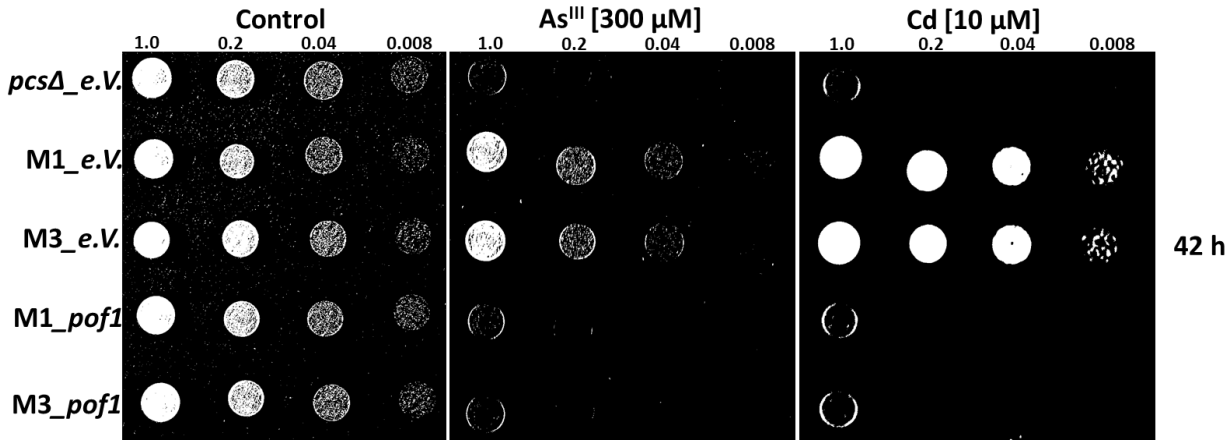

Fig. 36: Complementation of M1 and M3. A serial dilution assay was performed using *S. pombe pcsΔ*, the M1 and M3 mutant derived from the As^{III} evolutionary project. These strains harbored either the empty vector (pSGP72; e.V.) or a construct for the expression of *pof1* (pSGP72-*pof1*) in their respective mutant backgrounds, as indicated, to assess whether these constructs could complement the phenotype of enhanced As^{III} and Cd tolerance. Strains were spotted onto plates containing 17.5 nM thiamine with Cd [10 µM] or As^{III} [300 µM] (B) or without any stressor (A) and incubated at 30°C. Photos were taken after 30 h (A) or 48 hours (B). The numbers above each spot indicate the OD_{600} value of the corresponding dilution step. An additional representative replicate is provided in the appendix.

Given that Ggt1 and Ggt2 are hypothesized to differ in their intracellular localization, the C-terminal GFP-tagged complementation lines were tested by fluorescence microscopy to determine the localization of the respective γ-GTs. Ggt1, localized in the endoplasmic reticulum (ER) and Ggt2 in the vacuolar membrane, showed results consistent with the annotated information (pombase.org/uniprot.org) and previous literature[246], based on their respective localization sequence (Fig. 37).

Western blot analysis revealed a signal clearly below the expected full-size versions for both Ggt1-GFP (95.72 kDa) and Ggt2-GFP (94.82 kDa), with an observed signal at approximately 45-50 kDa (see Master thesis of Celine Fischer). A less pronounced but still detectable signal corresponding to the full-size Ggt1- and Ggt2-GFP was also observed. Considering the size of the GFP-tag and the annotated lengths of the small subunits of Ggt1 and Ggt2, the detected bands match the expected sizes for the GFP-tagged subunits of both proteins (Master Thesis of Celine Fischer).

These preliminary experiments imply a human γ-GT-like processing[247] of *S. pombe* Ggt1 and Ggt2, resulting in the cleavage of the initial pro-peptide after membrane integration.

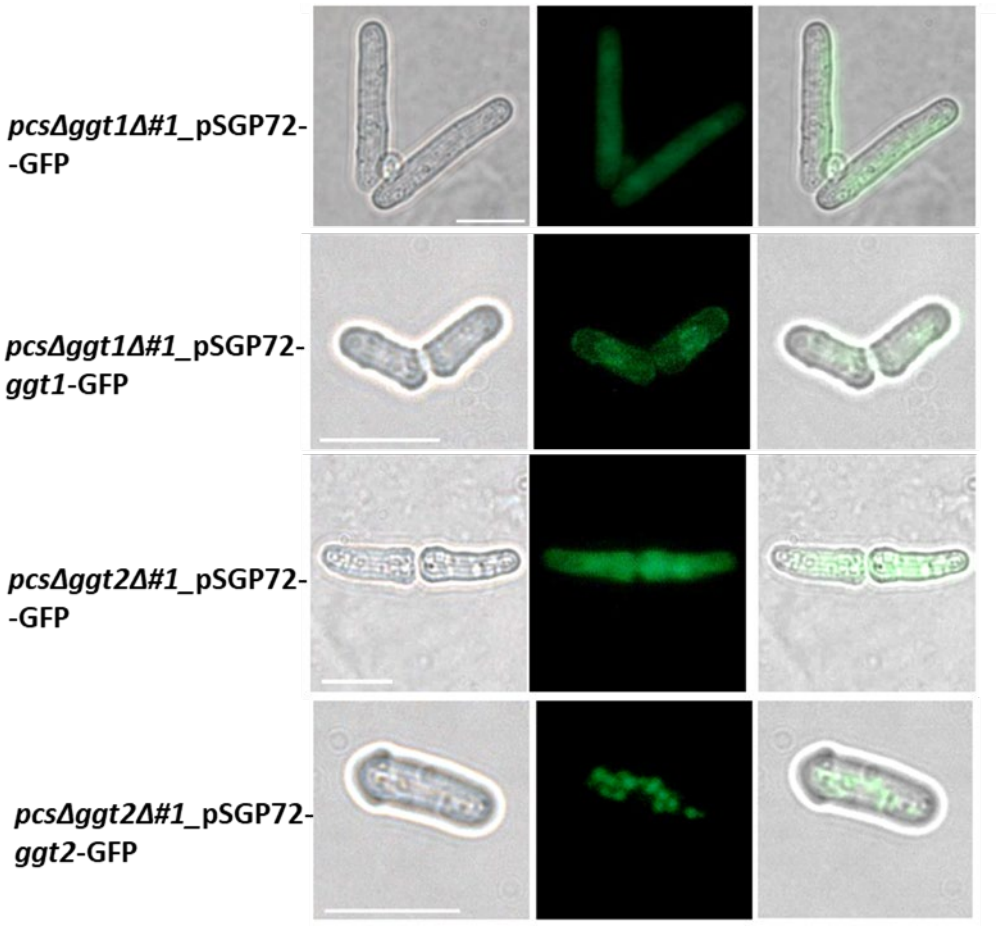

Fig. 37: Intracellular localization of GFP-tagged Ggt1 and Ggt2. Fluorescence microscopy images of the *S. pombe* double knockout strains *pcsΔggt1Δ#1* and *pcsΔggt2Δ#1*, heterologously expressing either *ggt1* (*pcsΔggt1Δ#1*) or *ggt2* (*pcsΔggt2Δ#1*), as indicated. Subcellular localization was compared to the corresponding strains carrying the empty vector (pSGP72-GFP). Cells were grown logarithmically for 6 hours in SD medium containing 15 nM thiamine (*pcsΔggt2Δ#1*-pSGP72-GFP and *pcsΔggt2Δ#1*-pSGP72-*ggt2*-GFP) or 20 nm thiamine (*pcsΔggt1Δ#1*-pSGP72-GFP and *pcsΔggt1Δ#1*-pSGP72-*ggt1*-GFP). White bars indicate 10 µm.

Finally, for a comparative analysis of *ggt1* and *ggt2*, both were examined for differences at the DNA and protein level. As shown in Fig. 38A+B, the primary differences between the *ggt1* and *ggt2* CDS are in the N-terminal region, where ggt1 probably harbors its ER localization sequence. Additionally, the SNP detected in the CDS of the M4 mutant, which causes a serine-to-arginine transition, affects a highly conserved residue in the catalytically active site of Ggt2. This residue is also conserved in Ggt1, apart from differences in other residues involved in active site formation.

A more detailed interpretation of this sequence and structural analysis in the context of the results reported above will be discussed further in the discussion section.

A

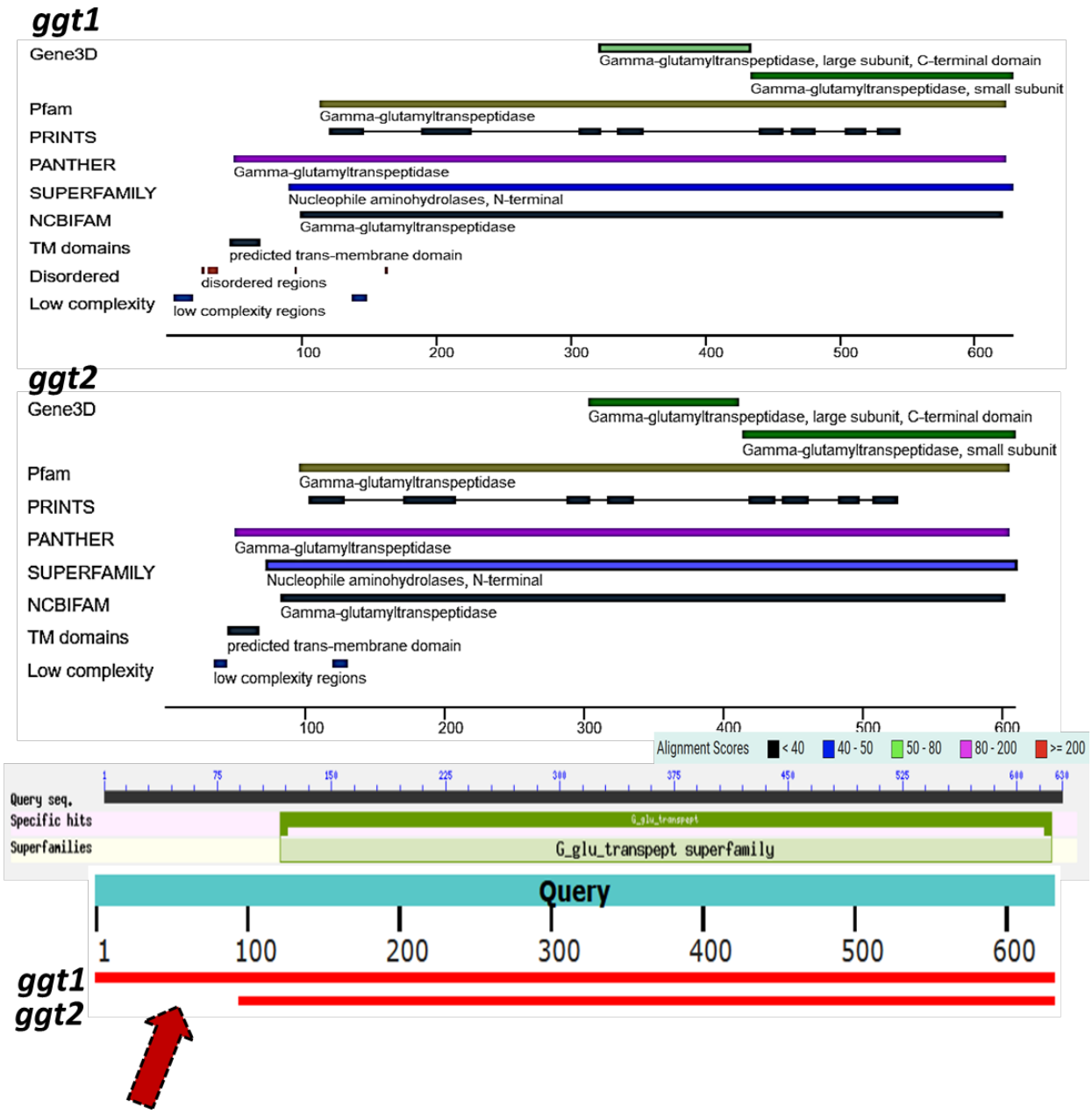
ggt1
Gene3D
Gamma-glutamyltranspeptidase, large subunit, C-terminal domain
Gamma-glutamyltranspeptidase, small subunit
Pfam
Gamma-glutamyltranspeptidase
PRINTS
PANTHER
Gamma-glutamyltranspeptidase
SUPERFAMILY
Nucleophile aminohydrolases, N-terminal
NCBIFAM
Gamma-glutamyltranspeptidase
TM domains
predicted trans-membrane domain
Disordered
disordered regions
Low complexity
low complexity regions
100
200
300
400
500
600
ggt2
Gene3D
Gamma-glutamyltranspeptidase, large subunit, C-terminal domain
Gamma-glutamyltranspeptidase, small subunit
Pfam
Gamma-glutamyltranspeptidase
PRINTS
PANTHER
Gamma-glutamyltranspeptidase
SUPERFAMILY
Nucleophile aminohydrolases, N-terminal
NCBIFAM
Gamma-glutamyltranspeptidase
TM domains
predicted trans-membrane domain
Low complexity
low complexity regions
100
200
300
400
500
600
Alignment Scores
< 40
40 - 50
50 - 80
80 - 200
>= 200
Query seq.
Specific hits
Superfamilies
G_glu_transpept superfamily
Query
1
100
200
300
400
500
600
ggt1
ggt2

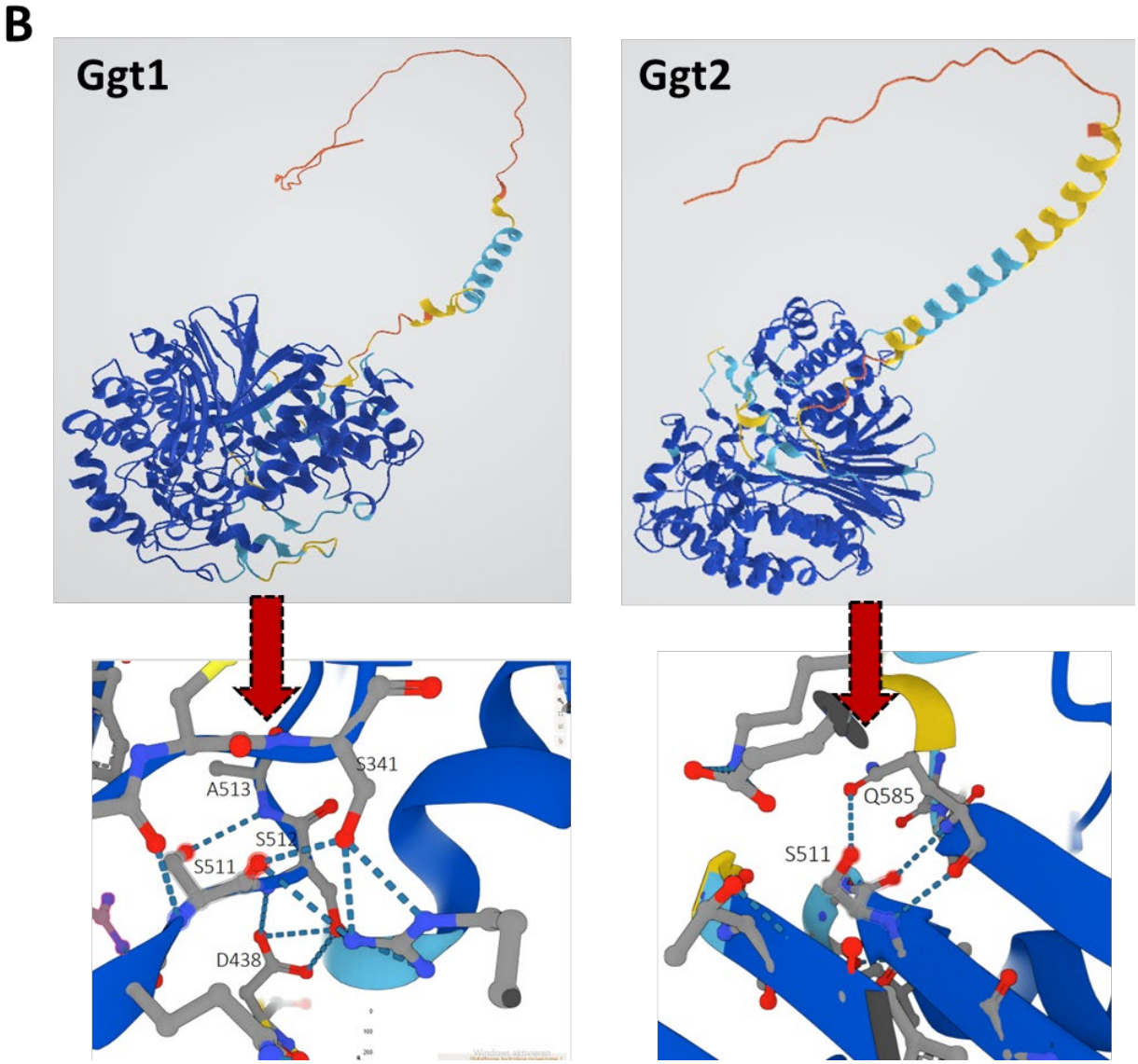

Fig. 38: Comparison of *ggt1* and *ggt2* in respect to their domains and 3-D structure. (A) Domain annotations of *S. pombe ggt1* and *ggt2* (pombase.org). The TM-BLAST analysis below highlights the high sequence redundancy between both enzymes, with the main differences in the N-terminus. (B) Predicted 3-D structure of Ggt1 and Ggt2 generated by alpha-Fold (version update: 2022-11-01). The active sites, featuring the highly conserved S511 residue, are depicted below.

4. Discussion

4.1 Uptake and Metabolization of Monothioarsenate (MTA)

4.1.1 P_i Transporter Mediated Uptake of MTA

For years, it has been assumed that MTA is taken up by transporters of the PHT family[6,60,83]; however, direct evidence for MTA hijacking P_i transporters has still been lacking until now. In the course of this work, a significant connection between MTA uptake and the abundance of P_i transporters could be demonstrated.

The loss of function in key P_i transporters, such as Pho84 in *S. cerevisiae* (*pho84*) and PHT1;1 in *A. thaliana* (*pht1;1*), significantly reduced arsenic accumulation upon MTA exposure, consistent with previous findings for As^V [52,59]. Using the double mutant *phr1-1 phl1*[202], it was demonstrated that MTA uptake and translocation can be similarly influenced by the P_i starvation response, like As^V [202,248]. The reduced arsenic accumulation in this mutant compared to WT indicates that an impaired P_i starvation response mitigates the increased uptake kinetics of MTA and As^V typically induced by the upregulation of P_i transporters under P_i-starved conditions[202,227].

While both the *pht1;1* mutant and the *phr1-1 phl1* mutant took up less MTA under P_i-starved conditions than the WT, arsenic accumulation in roots exposed to As^V was exclusively reduced in the double mutant. This likely resulted from the absence of upregulation in P_i transporters under P_i starved conditions[227,249,250]. Interestingly, while the ∑As in the shoots of the *pht1;1* mutant resembled that of *phr1-1 phl1*, both were significantly lower than in WT plants. These findings suggest that impaired translocation was a result of reduced uptake kinetics, accompanied by more efficient arsenic reduction and sequestration in the roots.

In both mutants, significantly reduced uptake compared to the WT was evident from the ∑As levels in the roots and shoots of MTA-exposed plants. In general, arsenic levels were more than 100 times lower in roots and 60 times lower in shoots compared to As^V treatments. Consequently, arsenic accumulation in the roots of plants exposed to MTA remained far below the levels of As^V exposed plants, indicates that differences in uptake kinetics between the phenotypes were not obscured by rapid influx, as observed in the As^V uptake experiments. Lower uptake rates for MTA

compared to As^V were previously also demonstrated in *O. sativa* by Kerl et al. (2018)[6], although no differences in the ∑As levels of shoots were observed in their study. Possible explanations might include differences in substrate discrimination between *A. thaliana* and *O. sativa* P_i transporters, similar to what has been observed in other species, such as *P. vittata*[182]. Another explanation could be that the rice plants were grown under P_i-sufficient conditions, in contrast to the uptake experiments conducted in this study with *A. thaliana* grown under P_i-depleted conditions.

Experiments with *S. cerevisiae* further highlighted significant differences in the uptake kinetics of MTA and As^V. These experiments demonstrated that MTA also hijacks P_i transporters in *S. cerevisiae* and provided additional evidence that As^V passes through P_i transporters more efficiently than MTA. Since both arsenic species share physicochemical properties with P_i, it is unsurprising that As^V - being closer in size and molecular weight to P_i - serves as a better substrate for P_i transporters than MTA[6]. When cells were exposed to As^{III}, the accumulation of ∑As was comparable between both genotypes (Fig. 4C), as expected, considering that this species is known to hijack other transporters, such as aquaglyceroporins[62,231] and hexose permeases[61]. Combined with the elimination of MTA and As^V toxicity under high P_i supply (Fig. 6), the absence of differences in As^{III} uptake between WT and *pho84* indicates that P_i transporters mediate uptake only of the pentavalent arsenic species, MTA and As^V.

Once taken up, MTA, like As^V, undergoes reduction to As^{III}, thereby inducing PC synthesis[60,123]. As seen in the As-speciation analysis both MTA and As^V were almost completely reduced to As^{III} within 24 hours. Consequently, the extent of PC formation following MTA and As^V exposure should reflect the rapid reduction process and highlight differences in arsenic accumulation among the tested genotypes. However, this was only partially observed in these results (Fig. 10A+B).

The analysis of thiol profiles in seedlings following MTA and As^V exposure showed that PC contents were significantly higher in both roots and shoots of As^V-exposed Col-0 plants. Roots of MTA-treated Col-0 seedlings tended to have higher PC levels than those of *pht1,1* and *phr1-1 phl1* mutants. These results were consistent with the ∑As measurements and As-speciation analysis as well as with previous reports showing that As^{III}, produced from the reduction of As^V and MTA,

induces PC formation[60]. In contrast, PC formation - especially in the shoots of MTA-exposed *pht1;1* seedlings and, to a lesser extent, *phr1-1 phl1* seedlings – exhibited a tendency to be higher than in Col-0. A plausible explanation is that both mutants exhibit reduced vigor under control conditions with limited P_i supply. This leads to lower shoot biomass, as reflected in the fresh weights observed in the growth assays (see Fig. 6 and 7). This may lead to apparently higher PC concentrations despite reduced As translocation.

Comparing both treatments (MTA and As^V, 24 hours), PC induction in seedlings was significantly higher when exposed to As^V, indicating faster uptake kinetics in comparison to MTA. Although MTA was found in much lower quantities than As^V in roots and shoots, the ratio of ∑PC formation to expected ∑As accumulation was significantly higher in plants exposed to MTA. Although PC synthesis is induced by As^{III} formation and thus depends on the amount of As^{III} equivalents produced from the reduction of MTA or As^V, the ratio of PC formation to uptake may be misleading. This is because the rapid uptake of As^V can quickly trigger PCS induction[251,252], potentially approaching its upper limit.

The relatively high PC formation following MTA exposure, despite low ∑As taken up and even lower ∑As translocated to the shoots, suggests that PC induction under these conditions may be triggered at least in part, or even primarily, by MTA itself or another metabolization by-product rather than by As^{III} derived from its reduction. Given the current lack of a comprehensive understanding of the reduction process (discussed further below), it is possible that the reduction of MTA to As^{III} involves distinct by-products compared to the reduction of As^V. Thus, PC formation might not only by the amount of As^{III} produced through reduction but eventually also by factors such as the rate of As^{III} formation and the level of ROS generated by MTA[253]. Therefore, further research is needed to clarify the metabolization of MTA, especially its reduction (discussed later).

Since both As^V and MTA can hijack P_i transporters due to their substrate specificity (shown here), it is plausible that P_i levels influence the rate of As^V and MTA reduction, given their structural similarity. This connection between P_i status and PC formation has been reported previously in *algae*[251]. Consequently, PC formation in shoots - where ∑As concentrations were several times lower than in roots - should be particularly sensitive to P_i limitation, thereby explaining the tendency for stronger PC induction in shoots of *pht1;1* and *phr1-1 phl1*.

Similarly, in other uptake experiments with *A. thaliana*[254] and *O. sativa*[6], the majority of As^{V} and MTA in the roots and shoots were almost entirely reduced to As^{III}. Notably, As^{V} was more readily reduced than MTA. Despite its slower uptake kinetics, MTA more frequently entered the shoots without reduction and root sequestration compared to As^{V}, indicating that PC formation was not solely determined by the reduction kinetics of MTA (Fig. 9). Although MTA being taken up less efficiently than As^{V}, its detection in small amounts in some samples of Col-0 and *pht1;1* suggests that MTA may escape reduction more readily. Since HAC1 activity seems largely confined to the outer root cell layers[255], MTA may more easily penetrate the inner layers, thereby partially avoiding reduction.This could result in enhanced translocation. Conversely, the exclusive presence of MTA in the shoots of As^{V}-exposed plants may result from thiolation processes, as previously observed for DMA[84].

In conclusion, the higher tolerance observed in the mutant and double mutant plants resulted from lower uptake kinetics and translocation rates for both MTA and As^{V}. This was indicated by higher chlorophyll concentrations, reduced anthocyanin accumulation, and greater fresh weights and root lengths compared to Col-0 plants exposed to MTA or As^{V}. However, while the overall level of tolerance was similar between *pht1;1* and *phr1-1 phl1*, the underlying mechanisms providing tolerance differed. These differences stemmed from distinct factors beyond their shared reduction in uptake kinetics. This striking similarity in MTA tolerance and uptake underscores that PHT1;1 plays a central role in MTA uptake, even in the presence of a highly redundant P_i transporter network in *A. thaliana*. Given that, unlike in *pht1;1*, the PSR-driven upregulation of PHT transporters is nearly abolished[202], the comparable tolerance levels in *phr1-1 phl1* and *pht1;1* suggest that PHT1;1 serves as the primary entry route for MTA, similar to its known role alongside PHT1;4 for As^{V} [51].

Although As^{V} was taken up approximately 100 times more in roots and 60 times more in shoots than As^{V}, only a fivefold higher concentration of MTA resulted in comparable toxicity in WT plants. This suggests that, once taken up, MTA has a higher cytotoxic potential than As^{V} in plants. Since both compounds are rapidly reduced to As^{III}, this observation suggests that factors beyond reduction kinetics contribute to the observed differences in toxicity. It remains to be determined whether additional intermediates formed during the reduction of MTA - or MTA itself - exhibit

greater cytotoxicity than As^{V}. It is conceivable that the reduction of MTA to As^{III} involves the release of a highly reactive sulfhydryl group, which may form disulfide bonds with proteins and thereby contributes to toxicity.

Notably, the fact that MTA - unlike As^{V} - was able to reach the shoot despite its overall lower uptake implies that reduction kinetics may still play a partial role. As will be discussed in the following section, a more detailed understanding of the reduction mechanisms of both species in plants is essential to elucidate the underlying processes driving their differential toxicity.

4.1.2 The Riddle of MTA Reduction: How Is It Reduced?

As^{V} reductases like AtHAC1[120], EcArsC[256] and ScAcr2[119] have been proven for their role in the detoxification process of As^{V}. Although these enzymes differ in their co-substrates and reduction mechanisms, the reaction product is consistently As^{III}. Astonishingly, when As^{V} was added to crude protein extracts from four different species - three encoding functional As^{V} reductases and one heterologously expressing one - no As^{III} formation was detectable. In contrast, MTA reduction to As^{III} was observed in protein extracts of all species tested. Notably, in *E. coli* and *S. pombe,* this reduction also occurred in denatured protein extracts, raising the question of whether MTA reduction is primarily enzymatic, as previously assumed[6].

Variability in MTA stability in denatured crude protein extracts has been reported before. A comparison of MTA reduction across different rice cultivars showed non-enzymatic reduction in extracts from the Yangdao cultivar[83]. The absence of As^{V} reduction in all crude protein extracts tested, combined with the non-enzymatic reduction of MTA in some of the cultivars, is not consistent with the assumed reaction mechanisms catalyzed by As^{V} reductases in the presence of these species. In light of the non-enzymatic MTA reduction reported by Kerl et al. (2019)[6] and in the course of this work, the differences may stem from variations in the concentrations and compositions of reducing agents among different species. Both As^{V} and MTA reduction have been shown to occur without the need for any reductase[60,257,258]. However, for unknown reasons MTA appears to be more readily reduced in denatured protein extracts than As^{V}. Differences in GSH levels among species cannot explain this phenomenon, suggesting the presence of other compounds capable of facilitating MTA reduction.

All previous studies on As^V reductases in plants have relied solely on measuring As^{III} levels in knockout strains lacking the presumed As^V reductase, without including enzymatic assays in plant extract.[121,255,259] Focusing on the two central issues derived from these findings, the lack of As^V reduction and the non-enzymatical reduction of MTA in crude protein extract, should be prioritized. The possibility of a general stabilizing effect of the buffer on As^V can be ruled out, as a non-enzymatic As^V reduction was observed when GSH was added (Fig. 12F). The lack of As^V reduction in crude protein has been previously reported[6]. While AtHAC1 As^V reductase activity has been demonstrated through an in vitro assay using purified protein with DTT as reducing agent, and by the significant reduced As^{III} formation and As^V tolerance in *AtHAC1* knockout mutants (*hac1-1; hac1-2*)[120,260], the exact reduction mechanism remains incompletely understood. Moreover, using buffer with As^V as the only negative control limits the evidential power of their experiment[120].

Other assays used to verify As^V reductase activity rely on an indirect approach, detecting NADPH oxidation via the preceding formation of GSSG by As^V reductase activity in presence of As^V and co-substrates GSH or Grx[261]. While this assay has been widely used[260–262], it provides only a partial solution to the issue. Ultimately, the lack of As^V reduction in crude protein extracts, as assessed through an indirect approach, is likely to remain unresolved.

The overall experimental data points to an involvement of As^V reductases and/or reducing agents in the detoxification of As^V and MTA. Similar to As^V, MTA detoxification appears to be a synergistic process involving reduction to As^{III}, followed by complexation with PCs and GSH (Fig. 12B-D) and subsequent vacuolar sequestration[60]. Although no differences in PC formation were observed between *S. pombe* WT heterologously expressing *AtHAC1* and the vector control, both MTA and As^V induced PC formation (Fig. 12B-D), implying intracellular reduction to As^{III}. The long-time exposure of 18 h probably resulted in an almost complete conversion of MTA and As^V to As^{III}, which may have obscured differences in the rate of PC formation.

Nevertheless, the initial hypothesis of a lack of As^V reductase capacity of *S. pombe* must be reconsidered in light of the reduction observed in WT vector control extract, along with the PC formation in both strains. These findings contradict the previous assumption about the absence of As^V reductase activity in *S. pombe*, or more specifically, MTA reductase activity. Although *S.*

pombe lacks true orthologs of *AtHAC1* and *EcArsB*, the tyrosine phosphatase SpCdc25 has been reported to exhibit As^V reduction capacity[263]. This has also been demonstrated for the two *Spcdc25* orthologs, *OsACR2.1* and *OsACR2.2*, in rice[264]. A sequence similarity search (SSS) using the EMBL-EBI PSI-BLAST algorithm revealed that the *S. pombe* dual-specificity phosphatase (*ibp1*), which also belongs to the *cdc25* family, is an ortholog of *S. cerevisiae ACR2* (25.0/43.9% identity/positives; e-value: 3.7e-04).

The instability of MTA in the crude protein extract of denatured samples prior to purification by PD10 columns suggests the predominance of a non-enzymatic pathway for MTA reduction in *S. pombe*. As described above, MTA reduction kinetics did not differ between Col-0 and *hac1* crude protein extracts and were also slightly reduced, albeit in lower quantities, in denatured protein extracts. Nonetheless, the underlying mechanisms of MTA reduction in *A. thaliana* protein extracts appear to differ from those in *S. pombe* and *E. coli* extracts, particularly given the much higher MTA stability observed in denatured plant protein extracts (Fig. 11B).

But how can the lack of differences between the MTA reduction kinetics of Col-0 and the *hac1* mutant protein extract be explained? The most plausible explanation is a high level of redundancy in As^V reductases in *A. thaliana*, similar to what is known for other plants such as *O. sativa*[121,259,260]. Using the EMBL-EBI PSI-BLAST algorithm for sequence similarity search (SSS), the *A. thaliana* dual-specificity phosphatase (*CDC25*) was predicted to be an ortholog of *S. cerevisiae acr2* (29.9/51.3% identity/positives; e-value: 5.7e-06).

Even though the function of the previously predicted As^V reductase AtACR2 has been shown to be completely redundant[265], it cannot be excluded that other enzymes may also exhibit As^V reduction capacity[266] and that MTA reduction could follow a similar pattern. By virtue of the less pronounced but still abundant background of non-enzymatic MTA reduction, desalting prior to MTA addition is recommended for future experiments using plant extracts.

Considering the strong deviation in MTA stability among the crude protein extracts of the model organisms tested, it is plausible that these differences are related to variations in concentration and/or presence of specific reducing agents capable of MTA reduction. Given that GSH is ubiquitously present in the millimolar range across all organisms used for this assay[132,145,146,157], it

is unlikely to be the key player in the observed non-enzymatic reduction. By contrast, the small, heat-stable oxidoreductases glutaredoxin (Grx) and thioredoxin (Trx) are potential candidates[267]. These redox proteins are found across all kingdoms, with various isoforms that have evolved to perform different tasks[261,268,269]. In the case of the Grx, two classes have been identified as unique to photosynthetically active organisms, while two others are generally associated with the kingdom of eukaryotes[270]. Regarding As^{V} reduction, both Grx and Trx can act as co-substrates for As^{V} reductases, depending on the reductase family[86].

The data presented here cannot exclude the potential role of AtHAC1 in the detoxification of MTA. The reduction of MTA by GSH or As^{V} reductases alone, appears to be unlikely regarding the non-enzymatic conversion observed. Previous experiments[6], along with those presented here, indicate the involvement of a heat-stable reductant in the conversion of MTA to As^{III}. Hence, until the issue of As^{V} stability in crude protein extract is resolved, it remains questionable whether the current understanding of As^{V} reduction and its proposed similarity to MTA, can be fully established. Therefore, further experiments are necessary to address this issue. A promising approach could be the purification of AtHAC1-GFP via pull-down. The purified protein could then be tested with various co-substrates to evaluate its MTA and As^{V} reduction capability, following the approach of Bermejo et al.(2014) [120] but incorporating the respective controls and co-substrates mentioned above.

4.2 Taking Different Paths: How DMMTA Uptake and Toxicity Differ from those of Other Arsenic Species

4.2.1 Identifying Transporter Candidates Involved in DMMTA Uptake

Testing various knockout strains associated with or hypothesized to be involved in the uptake of As^{V}, As^{III} and/or DMA did not result in the identification of any promising candidate for altered DMMTA uptake (see Fig. 1 and Fig. 13+14). Aside from the *hxt0* mutant, none of the other knockout mutants tested exhibited a tolerance to DMMTA that diverged from the WT. Neither the aquaglyceroporin Fps1, nor the P_i-transporter Pho84, the inositol transporter Itr1, nor the peptide transporter Ptr2 had any impact on DMMTA sensitivity. To fully exclude these transporters to mediate DMMTA uptake, further uptake experiments will be necessary. Nonetheless, given the lack of a phenotype in the toxicity assays and the fact that DMMTA is approximately ten times more toxic than As^{III}, it seems unlikely that any of these transporters are major contributors to DMMTA uptake.

Considering the strong effect of the *PHO84* knockout in the case of As^{V} [59] and MTA uptake (Fig. 4) and the significantly enhanced tolerance of the *fps1* mutant towards As^{III} (Fig. 13+14), as well as its major contribution to the overall uptake in sugar-containing medium[61,62,231], it is unlikely that these transporters play a similar role in DMMTA uptake.

Given the elucidated role of Itr1 in As^{III} translocation in *A. thaliana*[68], and the observation that its deletion in *S. cerevisiae* affected As^{III} but not DMMTA tolerance, these findings suggest that Itr1 does not contribute to DMMTA transport. The enhanced sensitivity to As^{III} observed in the *itr1* mutant may suggest a more prominent role for Itr2 in As^{III} uptake. Interestingly, the loss of Itr1 increased rather than decreased sensitivity, implying that Itr2 might compensate by taking up more As^{III}. This could reflect increased substrate competition between inositol and As^{III} for uptake via Itr2, particularly if Itr2 has a higher capacity for As^{III}.

Furthermore, although peptide transporters are known to mediate the uptake of methylated organic arsenicals[79], no evidence was found indicating their involvement in the uptake of the methylated thioarsenate DMMTA. Although DMA could not serve as an effective reference in the growth assays due to its lack of toxicity in *S. cerevisiae*, the combined uptake experiments with

DMA and DMMTA, together with the absence of a phenotype in toxicity assays of the *ptr2* mutant, indicate that this transporter is also not involved in the uptake of DMMTA. In general (as discussed below), DMMTA appears to differ from the methylated oAs in various respects.

Previous studies have shown that DMMTA differs from other thioAs, oAs, and iAs in uptake, translocation, and stress response characteristics observed in *A.thaliana*[81] and *O.sativa*[83]. These differences - including, among others, higher uptake kinetics compared to other methylated species and greater toxicity than inorganic arsenic - likely reflect factors beyond DMMTA's affinity for the tested transporters. In summary, it seems unlikely that DMMTA hijacks any of these transporters associated with the uptake of other arsenic species.

4.2.2 Despite Similar Uptake Kinetics: Why WT and *hxt0* Differ in DMMTA Tolerance

Among the mutant strains tested for an altered tolerance towards DMMTA, only the *hxt0* mutant differed from the WT. By reproducing the phenotype of strongly increased As^{III} tolerance and reduced uptake[61] (Fig. 15D+E, Fig. 16 and 17A), DMMTA uptake in *hxt0* resembled that of the WT. Since substantial amounts of DMMTA are detected when cells are exposed to it at 4°C, facilitated diffusion or cell surface adhesion may significantly contribute to the observed ∑As, partially obscuring differences in uptake.

At elevated DMMTA concentrations, the *hxt0* mutant's growth curves were slightly above those of the WT, with a less delayed entry into the logarithmic growth phase (Fig. 15B+C, Tab.9). At elevated DMMTA concentrations, the WT strain grown in glucose-containing medium exhibited superior growth compared to its growth in maltose-containing medium. However, when treated with As^{III}, elevated glucose concentrations reduced toxicity, whereas they increased DMMTA toxicity. This effect was also observed in assays with *S. pombe* (Fig. 19B+C). Although this effect appeared to be carbon source-related, these findings contradict the assumption of uptake-related effects regarding DMMTA, given the absence of a competitive interaction between glucose and DMMTA, such as known[61] and here shown for As^{III} (Fig. 15D+E; Fig. 19D+E). Hence, a similar role of hexose permeases, similar to that known for As^{III} can largely be ruled out[61].

Disaccharides like maltose are taken up through proton-coupled symporters encoded within the *MALX* cluster[271,272], and thus do not strongly compete with monosaccharides transported by

hexose permeases via facilitated diffusion[64]. However, the hypothesis that maltose transporters mediate DMMTA uptake appears doubtful. First, DMMTA toxicity was not affected by elevated maltose concentrations, which would be expected if DMMTA competes with maltose for uptake. Second, the comparison of uptake experiments conducted with WT cells cultivated and exposed in maltose-containing medium (Fig. 18A) and glucose-containing medium (Fig. 22), revealed a high correlation of ∑As detected, irrespective of the carbon source. Thus, the role for maltose transporters in DMMTA uptake seems to be improbable.

A less delayed entry into the logarithmic growth phase of *hxt0* stressed with DMMTA in the growth curve assays, along with its superior growth within the first 24 hours in the serial dilution assays, appears counterintuitive when considering WT's superior growth over the course of 72 hours, and the absence of differences in DMMTA uptake. Similarly, the higher efflux of both DMMTA and As^{III} observed in the efflux assays seems contradictory at first glance. But how can these observations be explained?

Like Fps1[231], hexose permeases are known for their bidirectional transport of As^{III} [61]. Additionally, in *S. cerevisiae*, the efflux transporter Acr3, enables the efficient efflux of As^{III} and contributes significantly to reducing its intracellular accumulation[101,196]. Since WT and *hxt0* exhibit the same efflux capacity, WT cells would likely have a higher reuptake of As^{III} - and possibly DMMTA - via hexose permeases, explaining the increased arsenic levels in the medium of *hxt0* exposed to As^{III}. Whether DMMTA efflux is also driven by As^{III} efflux is questionable. In toxicity assays, the HD9, HD100 and HD200 strain - characterized by their partially or nearly abolished bidirectional As^{III} flux[61] - showed no differences in DMMTA tolerance compared to WT and *hxt0*. Consequently, the data do not support a role for Acr3 in DMMTA detoxification, as is known for As^{III} [61,194,196].

While differences in uptake kinetics do not appear to explain the phenotypic differences between WT and *hxt0* cells upon DMMTA exposure, underlying metabolic differences may be responsible.

Conceivably, the interference of DMMTA with carbohydrate metabolism could partially explain the phenotypic differences observed in these experiments comparing WT and *hxt0* strains or when cells were cultivated on maltose instead of glucose. Following the hypothesis that DMMTA affects carbohydrate metabolism, the metabolic states of WT and *hxt0* inevitably differ.

Once taken up via transporters such as the Malx1 permease, maltose is hydrolyzed into two glucose molecules[273,274]. In WT cells, the bidirectional activity of Hxt transporters leads to a partial loss of glucose derived from maltose hydrolysis, resulting in slightly lower intracellular glucose concentrations, as reported previously[275]. If DMMTA interferes with glucose signaling, the slightly higher glucose levels in *hxt0* cells may confer an advantage by mitigating DMMTA's interference under low-glucose conditions. This could, in turn, explain the slightly faster entry into the logarithmic growth phase observed under DMMTA exposure.

Nonetheless, this does not explain why WT cells grown at high glucose concentrations were more sensitive to DMMTA than those grown at lower concentrations. A possible explanation could be the impact of glucose levels on the activation of the cyclic AMP-dependent protein kinase (PKA) pathway, which promotes rapid growth and downregulates stress responses[276].

When glucose is scarce, Msn2 and Msn4 accumulate in the nucleus and activate the expression of several genes associated with environmental stress responses[277,278]. As these factors positively regulate autophagy and the ROS response[279], their downregulation under high-glucose conditions could increase sensitivity to DMMTA. Unlike As^{III}, this effect would not be counteracted by reduced uptake through substrate competition if DMMTA is not taken up via hexose permeases.

Previous reports provide evidence that intermediate glucose concentrations (2% w/v) influence glucose signaling differently than lower (<1%) and elevated concentrations[280]. This demonstrates that, depending on glucose concentrations, *S. cerevisiae*'s metabolic state shifts from positively regulating glycolysis and mitochondrial respiration at lower concentrations, to having no effect on glucose utilization at intermediate concentrations, and finally to positively regulating glycolysis, fatty acid and amino acid metabolism, as well as glucose transport at elevated concentrations. These findings align with the results on the effects of glucose on DMMTA and As^{III} toxicity, indicating that the observed effects cannot be solely attributed to competitive interactions between the arsenic species and the varying concentrations of glucose applied but were likely due to differences in metabolic states.

Supposing that DMMTA affects glucose signaling, a broad range of potential targets within the signaling cascade must be considered. For As^{III}, interference with glucose signaling, targeting the

protein phosphatase-1 complex (PP1) mediated by its regulatory subunit Reg1 and its target Snf1 has recently been demonstrated[281]. Since both play opposing roles in glucose signaling, they represent potential candidates for DMMTA, assuming its toxicity follows similar mechanisms to those reported for As^{III}.

Without supporting data, further interpretations, especially in respect to the differences on the metabolomic level, could be misleading. Short-term uptake experiments with different sugars along with metabolomic and transcriptomic data of DMMTA exposed cells, would be appropriate approaches to clarify the mechanisms underlying sugar-dependent DMMTA toxicity.

Lastly, considering that the 16 rounds of deletions using the LoxP/Cre system led to side effects such as gene losses and chromosomal rearrangements[282], the possibility that the altered DMMTA response in *hxt0* is a result of such off-target effects cannot be ruled out.

Overall, the experiments with *hxt0* suggest that this strain differs from WT in its response to DMMTA exposure. While the involvement of hexose permeases in DMMTA uptake cannot be excluded, their contribution (if any) appears to be minor in the overall uptake process. Unlike As^{III}, it is possible that only one or a few of the 20 identified hexose permeases in *S. cerevisiae* mediate DMMTA uptake.

Remarkably, although fructose has a lower affinity for hexose permeases than glucose[283] and is less effective in competing with As^{III} uptake[61], *S. pombe* and *S. cerevisiae* exhibited greater tolerance to As^{III} and DMMTA when grown in fructose-containing medium. These findings further support the hypothesis that DMMTA interferes with glucose metabolism and/or signaling.

4.2.3 Fructose Reduces DMMTA's Toxicity

Besides the conspicuous phenotype of the *hxt0* mutant, experiments conducted with different sugars suggest that DMMTA uptake and/or toxicity occur in a carbon source dependent manner. All three model organisms tested exhibited fewer adverse effects towards DMMTA when fructose was used as the carbon source for cultivation. In *S. cerevisiae* presence of glucose inhibits the expression of the galactose transporter encoding *GAL2* gene, thereby enhancing the uptake via hexose permeases[284,285]. Therefore, assays comparing the tolerance of WT and the *gal2* mutant

to DMMTA in glucose- or fructose-containing SD-medium ensured that inhibition of *GAL2* expression did not contribute to the effects observed.

Aside from this, when both were treated with As^{III} instead of DMMTA, the effect was only observed at very high As^{III} concentrations, likely due to glucose influencing stress responsive genes, as mentioned above[277,278]. Glucose has a higher affinity than fructose for hexose permeases[286,287], but substrate competition with As^{III} in terms of uptake would only be sufficient to counteract the increased sensitivity caused by reduced stress responsiveness at lower As^{III} concentrations. In *S. cerevisiae*, despite the 20 hexose carriers differing significantly in respect to their substrate affinity and selectivity, all high-, medium- and low-affinity transporters evaluated in previous studies preferentially transport glucose over fructose[288]. For example, the low-affinity transporter Hxt3 (note: unlike in CEN.PK2-1c, *HXT3* encodes a low-affinity glucose permease in the MC966A strain used here) and the high-affinity transporter Hxt7 exhibit about two times higher K_m values for glucose than for fructose (Hxt3 K_m: 65 mM versus 125 mM and Hxt7 K_m: 2.1 versus 4.6 mM)[283]. Hence, the superior DMMTA tolerance of *S. cerevisiae* in the presence of fructose instead of glucose, due to fructose being the better substrate in the competition for uptake with DMMTA by hexose permeases, seems improbable.

Especially the growth assays using *S. pombe* as the model of choice, provided evidence for a reduction of DMMTA toxicity when fructose instead of glucose was used as a carbon source (Fig. 19). Unfortunately, unlike *S. cerevisiae*, evaluating how different sugars affect DMMTA toxicity in *S. pombe* is restricted to only two monosaccharides, as *S. pombe* has a limited ability to metabolize a variety of sugars[289,290]. Thus, comparisons of the effects of different sugars on DMMTA toxicity were limited to fructose and glucose.

However, the hexose permeases of *S. pombe* diverged evolutionarily early from those found in mammals, *S. cerevisiae*, and *A. thaliana*[286]. Given that *S. pombe* and *S. cerevisiae* separated approximately 500 million years ago[291], it is possible that the reduced DMMTA toxicity in the presence of fructose as a carbon source results from another reason than in *S. cerevisiae* due to evolutionary divergence in fructose affinity or metabolism between these species. Although high affinity fructose/H^+ symporters have been identified in the ascomycetes lineage and are presumed to have emerged after the separation of the *Taphrinomycotina* (which includes *S.*

pombe)[292], it is plausible that a precursor of this transporter family existed earlier. If so, such a high-affinity fructose symporter could also serve as a potential entry route for DMMTA in *S. pombe*, provided it is preferentially utilized over other hexose permeases.

Indeed, among the six hexose permeases in *S. pombe*, the Ght6 transporter has been shown to exhibit a higher affinity for fructose than glucose[286], significantly differing from other members of the MST family found in mammals or in *S. cerevisiae*.

Uptake experiments comparing DMMTA uptake in cells grown in fructose- versus glucose-containing media will be essential to clarify this question and provide an initial indication of whether the carbon source-dependent toxicity of DMMTA is linked to its uptake. Nevertheless, as fructose and glucose are typically transported by hexose transporters with a higher affinity for glucose, it is more likely that these effects arise from metabolic differences rather than from differences in uptake.

4.2.4 How Sorbitol Might Affect DMMTA Uptake

Regarding the DMMTA uptake experiments conducted in the presence of glucose or sorbitol as a carbon source, another transporter family comes into focus. However, the dramatically reduced As^{III} uptake in presence of sorbitol - though less pronounced in the case of DMMTA - remains puzzling (Fig. 25A+B). A hyperosmotic concentration of 1 M sorbitol, which triggers the HOG pathway through the induction of the osmotic stress response, known to activate the HOG pathway by inducing an osmotic stress response, has been reported to significantly reduce As^{III} uptake in *S. cerevisiae* by causing the closure of the Fps1 channel[293].

Although sorbitol almost completely abolished As^{III} uptake and clearly reduced DMMTA uptake in these experiments, the concentration used (111 mM) was far below the threshold for inducing hyperosmotic stress. Previous studies have shown that sorbitol concentrations above 0.1 M are sufficient to alter turgor pressure in *S. pombe*[294], a process that is normally tightly regulated by aquaporins across all kingdoms[295].

The only known aquaglyceroporin in *S. pombe* is the Yfl054-like SPAC977.17[296], whose function remains unknown. It is possible that this transporter is regulated by sorbitol in a manner similar to Fps1 in *S. cerevisiae*. For instance, the knockout of SPAC977.17 in *S. pombe* has been shown to

enhance passive ethanol diffusion, suggesting a functional similarity to Fps1[297,298]. Given the lack of evidence for non-osmotic stress-inducing sorbitol concentrations affecting As^{III} uptake, it is possible that sorbitol alone is sufficient to trigger the closure of SPAC977.17 or other aquaporins in *S. pombe*. Notably, the ~30% reduction in ∑As observed when *S. pombe* was exposed to DMMTA in sorbitol-containing medium is comparable in magnitude to the estimated 20% contribution of Fps1 to overall As^{III} uptake in *S. cerevisiae* in the absence of glucose[61].

These findings suggest that SPAC977.17 could be a promising candidate for identifying transporters hijacked by DMMTA.

4.2.5 Further Evidence of DMMTA's Interference with Carbohydrate Metabolism in *A. thaliana*?

An initial experiment done with *A. thaliana* WT plants treated with DMMTA for 24 hours with or without different mono- and disaccharides, showed a strong reduction in ∑As regardless of the sugar added (Fig. 21C). This effect was less pronounced in roots than in shoots and manifested in a higher shoot/root ratio in plants treated with DMMTA in the absence of a carbons source. Due to the low sugar concentrations applied (300 µM), the observed decline in shoot ∑As was unlikely caused by an altered osmolarity of the medium. DMMTA, known to be highly stable and readily translocated in plants[81,83], was clearly less mobile when sugar was present in the medium. This suggests that DMMTA translocation -and eventually its uptake- is mediated by hexose permeases. One possible explanation is a sugar-dependent reduction of uptake kinetics, consequently leading to a decline in DMMTA xylem and phloem loading. This might be then reflected in the reduced ∑As levels in shoots, similar to what has been observed for the *pht1;1* mutant exposed to As^{V} under P_i-depleted conditions.

Another possible explanation for up to four times lower shoot ∑As is that DMMTA phloem loading may be hindered by the enrichment of root cells with the respective sugars. Likewise, hexose permeases, inositol transporters are members of the major facilitator family. These transporters mediate the long-distance transport of mesophyll-derived inositol to reproductive tissues[299,300] and have been shown to contribute to As^{III} phloem loading and seed accumulation[68].

Duan et al. (2016) observed a decline of 45-64 % in arsenic seed accumulation by disrupting *AtINT2* or *AtINT4*, while root ∑As remained comparable. Albeit both, AtINT2 and AtINT4 have

been shown to be highly specific for myo-inositol transport[299,300], they lack the ability to efficiently transport mono- or disaccharide.

In contrast, AtPLT5, a member of another subfamily (AtSTPs) of the MST-like superfamily, has been demonstrated to transport a wide range of substrates, including pentoses, hexoses, polyols of different chain length, and myo-inositol[301,302]. Interestingly, the heterologous expression of *AtPLT5* in *X. laevis* oocytes and *S. cerevisiae* (EBY.VW4000) revealed an even higher transport capacity for glucose than for myo-inositol.

While *AtPLT5* may be involved in DMMTA translocation, its transport rates for glucose and fructose are quite similar[301]. Thus, it cannot explain sugar-dependent differences observed in the toxicity assays with seedlings grown on plates with DMMTA. Among the highly redundant group of hexose transporters of the AtSTP subfamily, only AtSTP6 exhibits similar affinity for fructose and glucose[303], but its expression is restricted to the late stages of pollen development in the upper tissue. The remaining candidates of the highly redundant members of AtSTPs preferentially transport pyranose-ring- rather than furanose-ring-forming substrates[304–306].

Therefore, it is questionable whether the slightly reduced DMMTA toxicity in presence of fructose instead of glucose was related to the uptake via members of the AtSTP subfamily (Fig. 21). Combined with the initial uptake experiment showing a reduction of ∑As for all sugars tested, the overall data situation does not support a causal connection between uptake and the sugar-dependent differences in DMMTA toxicity.

Alternative explanations, including the role of glucose as a signaling molecule that influences gene expression and metabolic processes[307], could be related to the observed effects on toxicity. The pronounced deviation in DMMTA toxicity observed in assays with glucose - and especially sucrose - may reflect a disruption caused by DMMTA, potentially linked to glucose- and sucrose-signaling modules that regulate the juvenile-to-adult phase transition[308].

This is supported by the high standard deviation in root length and fresh weight, which resulted from a strong discrepancy between seedlings that advanced to a later developmental stage and those that experienced severe DMMTA toxicity at an early stage. These findings suggest that

DMMTA-induced disruption of the juvenile-to-adult phase transition pathway may be a plausible explanation.

For example, developmental repression - largely regulated by the Hexokinase 1 (HXT1) in a glucose-dependent but primarily catalysis-independent manner - mediates the combined response with plant's hormones such as auxin and cytokinin, to pilot the nutrient-dependent plant development[309–311]. If DMMTA interferes with glucose signaling - such as known for As^{III} [312] - HXT1 could be a potential target.

Alternatively, further possible interferences of DMMTA with glucose signaling and/or glycolysis - upstream of its shared pathway with fructose - cannot be ruled out. Clearly, a deeper investigation is needed to understand how DMMTA toxicity is established in plants and other organisms.

4.2.6 DMMTA Toxicity, Uptake and Physicochemical Characteristics

4.2.6.1 DMMTA's Uniqueness Among the Arsenic-Species Known

The high toxicity of DMMTA (IC_{50} ≈ 20 µM) shown for human lung (A549), bladder (UROtsa/T24) and hepatocytic (HepG2) cells, particularly in comparison to the highly toxic iAs, As^{III} (IC_{50} ≈ 72-74 µM) and As^{V} (IC_{50} ≈ 1400/ 3914 µM)[46,47], underscores its relevance in discussions about food safety thresholds[7]. These experiments suggest that DMMTA toxicity may result from its rapid uptake, leading to high intracellular concentrations within a short period of time. Neither DMA nor As^{III} were taken up to such an extent. Distinct from the other As-species tested, DMMTA uptake was between 20-25 times (As^{III}) to 285 times (DMA) higher in *S. cerevisiae* (Fig. 17A and Fig. 22A+B). Above, elevated levels of arsenic treated at 4 °C with DMMTA were even higher than those of As^{III}-treated cells at 30 °C, implying the occurrence of cell surface adhesion and/or a partial uptake by facilitated diffusion.

Although ∑As in DMMTA-treated cells were 20-25 times higher compared to As^{III}-treated cells, DMMTA toxicity was only 8-10 times greater in *S. cerevisiae*. While the ∑As in the uptake experiments showed low deviation between replicates, the toxicity assays were characterized by strong fluctuations. These deviations in DMMTA toxicity likely arose from differences between the cultures used in the assays. Since all experiments were conducted with logarithmically

growing cells, only minor physiological and metabolic differences between cultures can be expected. The narrow concentration window in which DMMTA toxicity occurs, just before it becomes lethal, is a characteristic shared with other elements like Cu and Ni [313].

For copper toxicity in *S. cerevisiae*, it has been shown that the fatty acid composition of the plasma membrane (PM) significantly affects toxicity[314]. Several hypotheses regarding metal-induced membrane permeabilization have been proposed, and evidence supporting these hypotheses varies depending on the compound investigated.

One possible explanation for the large fluctuations in DMMTA toxicity is membrane permeabilization resulting from lipid peroxidation[315], which is induced by ROS formation. However, unlike other metal ions, in addition to lipid peroxidation, a second major factor associated with membrane permeability may contribute to the unique characteristics of DMMTA toxicity[81]. Small discrepancies in parameters such as temperature, the accumulation of saturated fatty acids in overnight cultures, and other factors can alter the plasma membrane's composition and consequently affect its permeability[316,317]. Changes in the unsaturated fatty acid index of the plasma membrane may either enhance or reduce DMMTA toxicity, similar to what has been observed with copper.

X-ray diffraction and fluorescence spectroscopy have demonstrated that As^{III} exposure damages the lipid bilayer[318], thereby compromising membrane integrity. As^{III}, being an amphiphilic and chaotropic substance with effects related to the Hofmeister series[319], can alter plasma membrane properties and consequently disrupt intracellular osmolarity.

Whether DMMTA exhibits similar physicochemical properties remains unknown. Based on the previously described phenotype of epidermal root cell swelling[81], damage to the lipid bilayer causing osmotic stress due to uncontrolled solute influx seems conceivable. Consequently, given that DMMTA is approximately 10 times more toxic in *S. cerevisiae* and over 20 times in *S. pombe* than As^{III}, even minor variations in plasma membrane composition may have a tremendous impact on its toxicity, especially in consideration of DMMTA being eventually associated with strong cell surface adhesion or taken up by facilitated diffusion.

If the high ∑As observed in the uptake experiments at 4°C were due to cell surface adhesion rather than diffusion (Fig. 17A+B and Fig. 22), this suggests that DMMTA toxicity may also depend on the strength of accumulation. The strength of adhesion – shaped by membrane or cell wall composition – could be critical, as it may influence the ratio between surface-bound and intracellular arsenic. Although the results of the uptake experiments were highly reproducible, the ratio of surface-bound to intracellular DMMTA cannot be determined.

Since this effect has not been reported in uptake experiments conducted with *A. thaliana*[81] or *O. sativa*[83], it is likely related to the specific cell wall composition of yeast. The plant cell wall, which mainly consists of cellulose, hemicellulose and pectin in non-woody plants[320], differs significantly from that of yeast. Unlike plants, the yeast cell wall is primarily composed of the polysaccharides β-1,3-glucans and β-1,6-glucans, with chitin providing structural support and mannoproteins contributing to cell wall integrity and environmental interactions[321]. Mannoproteins, in particular, may serve as potential targets for interaction with DMMTA due to their known roles in environmental interactions, their affinity for a diverse range of binding partners[322,323], and their lower inertness compared to chitin and β-glucans.

Nevertheless, further experiments are necessary to clarify whether the high ∑As observed at 4°C resulted from DMMTA cell surface adhesion or diffusion. Determining ∑As in combination with speciation of yeast spheroplasts, and samples of the washing solution used for the removal of the cell wall components during the spheroplast isolation procedure will help to resolve this issue.

Another possible explanation for the small window in which DMMTA toxicity occurs is the existence of a threshold that must be surpassed before toxicity manifests. If DMMTA is sequestered by a specific ligand, toxicity rapidly progressing to lethality could result from the depletion of an as-yet-unknown DMMTA scavenger. Additionally, when present in excess intracellularly, as indicated by the uptake experiments, DMMTA may also cause toxicity by unintentionally binding to enzymes as a substrate analog, potentially disrupting essential metabolic processes.

Likewise to what is known for metal-ion toxicity[313,324], the affinity of the metalloid DMMTA for certain proteins or metabolites - present at varying concentrations - may contribute to such

fluctuations. For instance, copper, which ranks highest in the Irving-Williams series[325,326], exhibits strong toxicity when unbound. Under normal physiological conditions, the amount of free copper ions is expected to be lower than one.

No reports have indicated complexation or binding of DMMTA to a specific ligand. Although an equilibrium between DMMTA, DMDTA and DMA, dependent on available GSH, was previously observed[84], GSH appears to influence DMMTA abundance solely through its role in thiolation and de-thiolation processes, rather than through scavenging of DMMTA. Complexation with GSH or another low molecular weight compound seems unlikely due to DMMTA's high mobility and translocation rate, which is comparable to that of DMA[83].

Furthermore, the absence of phenotypic differences upon DMMTA exposure in the As^{III}-evolutionary project mutants and double knockouts with elevated intracellular GSH levels strongly suggests that DMMTA toxicity is not a result of GSH pool depletion. Unlike As^{III}, which is detoxified through the formation of GS-As^{III} or PC-As^{III} complexes followed by sequestration into the vacuole[98,101], DMMTA does not appear to undergo such a process[81].

Considering the possibility of a multicausal background for the observed deviations in DMMTA toxicity, further evidence is needed to gain insights into the underlying mechanisms. Therefore, the most promising approach to unravel the reasons for the observations made here is to distinguish which effects were related to uptake and which pertained to toxicity, independent of uptake.

4.2.6.2 The Physicochemical Properties of DMMTA

Previous claims of similarity between the physicochemical properties of DMMTA and DMA appear unsupported[229]. In these series of uptake and toxicity assays, neither the arsenic uptake nor pK_a-dependent changes in toxicity observed or reported for DMA were detected with DMMTA. Based on these assays, the previously estimated pK_a value for DMMTA (between 6.0 and 7.0) seems implausible. Furthermore, the pK_a of 5.39, calculated using the Marvin Sketch Tool (Version 23.14), did not align with the experimental findings. Instead, the pK_a value of 4.37, proposed by Liamatsau et al. (2020)[230], corresponded more closely with the data, particularly given the change in DMMTA's toxicity observed at pH 4.0 (Fig. 23B+C).

At first glance, the increase in toxicity at low pH was not in agreement with expectations, given that the dissociated form of DMMTA might be more reactive, or more membrane permeable, as reported for various other substances[327–329]. However, speciation analysis of the medium following long-term exposure at pH 4.0 and 5.4 revealed a pH dependent conversion of DMMTA in the medium used (Fig. 24B).

The significant conversion of highly toxic DMMTA (IC_{50} ≈ 20 µM) to the far less toxic DMA (IC_{50} ≈ 6030 µM)[46], observed at pH 5.4 appears to be the primary reason for the reduced DMMTA toxicity at pH values above 4.0. Samples from media buffered at pH 4.0 showed a substantially higher DMMTA to DMA ratio (1.8) compared to those at pH 5.4 (0.11) after 20 h of incubation. The higher levels of less toxic DMA at pH 5.4 suggest that DMMTA undergoes pH-dependent disproportionation.

Interestingly, while the conversion of DMMTA to DMA occurred in the medium without cells - raising the question of whether protonation influences DMMTA's stability - this abiotic conversion contrasts with previous reports of biotic turnover. Specifically, two studies highlighted biotic conversion in plants via the intracellular GSH pool[84] and in the nutrient solution of 20-day-old rice seedlings[83]. Eventually, DMMTA's conversion into DMDTA and DMA might explain high standard deviations and narrow toxicity windows observed in the experiments with *S. cerevisiae*.

Once DMMTA was taken up by *S. cerevisiae* cells, growth arrest would occur until a portion of DMMTA (IC_{50} ≈ 20 µM, as determined in human lung (A549) and bladder (T24) cells) was converted to the less toxic DMDTA (IC_{50} ≈ 4300 µM) and DMA (IC_{50} ≈ 6030 µM) [46]. Was DMMTA present at lower concentrations, its rapid intracellular conversion to DMA might prevent severe toxicity. At higher concentrations, however, DMMTA could exert its toxic effects, as a larger portion would remain before reaching the DMMTA:DMDTA:DMA equilibrium[84]. Moreover, if this intracellular conversion was depended on GSH - or indirectly on the redox state of the cell (described by the GSH:GSSG ratio) - then fluctuations in GSH levels and/or its redox state under normal physiological conditions could significantly affect DMMTA toxicity by altering de-thiolation kinetics.

A more likely explanation is that if DMMTA was rapidly and abiotically converted at pH values above 4.0, small differences in the speed of de-thiolation could have significant effects on the ∑As taken up and, consequently, on toxicity. As demonstrated in the uptake experiments with DMMTA and DMA, even small differences in the DMMTA-to-DMA ratio among cells exposed in the individual replicates should have strong effects on the observed toxicity, in respect to the differences in uptake kinetics of both species.

If various factors affect the kinetics of DMMTA's de-thiolation, it is not surprising that fluctuations in toxicity between replicates occurred. Therefore, while the conversion of DMMTA to DMA observed here was primarily abiotically driven and pH-dependent, further experiments are needed to identify the medium components catalyzing this conversion.

Unlike DMMTA, a biotically derived or stabilized proportion of DMDTA was detected in medium at pH 4.0 and 5.4 after 20 h of incubation but was not detectable in medium of the same pH without cells. As mentioned earlier, the role of GSH in the formation of methylated thioAs from DMA may have contributed to this effect[84].

Additionally, a pH dependent turnover must have occurred, as indicated by the near-complete loss of this species in the medium in the absence of any biotic factor, observed at both pH 4.0 and pH 5.4. Based on the literature, the pK_a value of DMDTA is assumed to be around 2.25 [230], suggesting that DMDTA should be deprotonated under all tested conditions. Whether the conversion of DMDTA was prevented by intracellular thiolation of DMA, followed by the efflux of the resulting DMDTA into the medium, remains unclear.

Consequently, the pH of the medium tested affected the stability of DMMTA and DMDTA, leading to disproportionation into the less toxic DMA. The stability of DMMTA at the lower pH values tested suggests a pK_a value within the range of >4.02 to 4.24 (Fig. 23). In contrast, a pK_a value below 4.0 seems more plausible for DMDTA, given its instability under both conditions tested.

Moreover, to fully understand the physicochemical properties of DMMTA, comprehensive uptake experiments across the relevant pH range, combined with chromatographic analysis to differentiate between the protonated and deprotonated forms of DMMTA, will be critical.

In addition to the potential impact of the pH on the stability of DMMTA and DMDTA due to changes in their protonation states, the effect could also arise from alterations in the protonation states of compounds in the yeast nitrogen base. Thiamine (pK_a = 4.8)[330,331], p-aminobenzoic acid (pK_a = 4.85)[332], folic acid (pK_a = 4.69)[333], and biotin (pK_a = 4.5)[334] undergo changes in their protonation states within the range where DMMTA and DMDTA experience disproportionation. Nevertheless, due to their low concentrations in the medium -ranging from 0.409 µM (biotin) to 1.186 µM (thiamine)- the almost complete conversion of DMMTA to DMA would contradict the expected stoichiometric ratio.

Finally, given the rapid uptake leading to saturation and the high toxicity of DMMTA observed in *S. cerevisiae* cells, it can be assumed that its instability in 2×YNB 0.1CPB did not account for the lack of differences in DMMTA tolerance among the knockout mutants in the liquid assays. Moreover, the observed pH-dependent disproportionation - although medium-dependent - suggests a pK_a of DMMTA ≥ 4.0. However, for future experiments, the use of 2×YNB 0.1CPB should be avoided, whereas YNB and the uptake solution used here appear to be suitable with regard to DMMTA stability.

4.2.7 Distilling the Key Points: DMMTA Uptake and Toxicity

The data presented here clearly demonstrate that DMMTA uptake and toxicity differ significantly from those of other known arsenic species, not only in plants such as *A. thaliana*[7,83] but also in *S. pombe* and *S. cerevisiae*. However, the underlying mechanisms of DMMTA uptake and toxicity remain unresolved. Based on these experiments, important tools have been provided for further elucidation of these processes.

By demonstrating pH-dependent effects on DMMTA stability, which in turn influence toxicity, it can be suggested that DMMTA's pK_a lies between 4.0 and 4.2, with additional instability observed at pH 5.4. Although a sugar-dependent effect on DMMTA uptake seems unlikely, the data indicate that DMMTA toxicity is carbon source-dependent, with fructose significantly reducing toxicity.

The rapid uptake of DMMTA in *S. cerevisiae* hindered a more detailed investigation due to fast intracellular saturation. However, uptake experiments with *S. pombe* demonstrated that this model organism is a more suitable choice for studying DMMTA uptake and toxicity. Establishing

a protocol for yeast sample preparation for speciation analysis will enable *S. pombe* to be used effectively for further research on the uptake and detoxification of DMMTA and thioarsenicals in general.

4.3 The As^{III}-Evolutionary Project

4.3.1 Evolution of As^{III} Tolerance: Selective Pressure on Genes Within the GSH Cycle?

While further experiments are necessary to understand the underlying reasons for the enhanced tolerance observed in the mutants from the As^{III}-evolutionary project, a preliminary assessment can be made based on the current data.

Toxicity assays and complementation analyses using the double knockout strains *pcsΔggt1Δ#1* and *#2*, indicated that in the case of the M2 mutant, the acquisition of reduced susceptibility to As^{III} and Cd was likely primarily due to the loss of function of *ggt1* (Fig. 29, 30 and 34).

Although a knockout of *pof1* was unsuccessful - as expected, given that *pof1* has previously been described as an essential gene in *S. pombe* [237,335] - the complementation analyses of both M1 and M3 mutants suggest that the SNP identified in *pof1* likely contributes significantly to the increased tolerance to As^{III} and Cd observed in these strains (Fig. 36).

Only the experiments involving the *pcsΔggt2Δ#1* and *#2* double knockout strains and their respective complementation analyses indicated that the SNP found in *ggt2* was either not responsible or not solely responsible for the enhanced tolerance to As^{III} and Cd (Fig. 31 and 35). Surprisingly the loss of *ggt2* was accompanied by increased DMMTA sensitivity in the WT and the *pcsΔ* background (Fig. 32). Given these findings, alternative mechanisms - such as epigenetic adaptation - could be considered as potential contributors to the observed metal tolerance, but no supporting evidence was found (Fig. 27).

In *S. pombe*, epigenetic adaptations induced by sublethal doses of caffeine have been shown to contribute to enhanced tolerance. However, no similar effect was detected when comparing the tolerance of mutants continuously grown in the presence or absence of As^{III} (Fig. 27). Unlike, what has been reported for *S. pombe* exposed to sublethal doses of caffeine[235], the increased As^{III} tolerance in mutants from the As^{III} evolutionary project was primarily - if not exclusively - based on stable mutations rather than epigenetic adaptations. Contrary to the findings of Torres et al. (2020)[235], which reported a rapid loss of acquired epigenetic adaptations, prolonged cultivation of the isolated mutants over multiple generations without stress exposure did not diminish their acquired tolerance. Due to the co-mutagenic effects of As^{III} [336] and its known ability to impair DNA

damage repair[337,338], an increased frequency of DNA alterations can be expected, which may explain the absence of "epimutants" in this relatively small candidate pool with elevated As^{III} tolerance.

4.3.2 Expanding the Glutathione Reservoir: A Broad-Spectrum Defense Against Cellular Stress

4.3.2.1 GSH-Cycle Alterations Drive Dual Tolerance to As^{III} and Cd in PC-Deficient Mutants

Given that the polymorphisms found were all associated with genes involved in the GSH cycle, the evolutionary pressure from ongoing exposure to sublethal doses of As^{III}, seems to follow a specific trajectory. All mutants and knockout strains tested exhibited elevated GSH levels to varying extents (Fig. 33). As expected, since GSH is also involved in the detoxification of Cd and As^{V}, the mutants exhibited a gain in tolerance against both.

Considering that the isolated mutants were deficient in PC synthesis, As^{III} detoxification in *S. pombe* might be primarily restricted to GSH in absence of PCs. In this context, an enhanced detoxification capacity, achieved through alterations of the GSH-cycle, might explain the co-occurrence of Cd and As^{III} tolerance in the isolated mutant strains.

Apart from being distinctly regulated, the response pathways for As^{III}, Cd and ROS-induced stress result in the induction of GSH synthesis and recovery of GSH from its oxidized form, GSSG[142,339–341]. The consumption of GSH upon the induction of PC synthesis leads to a continuous flux of GSH into the PC pathway[340], preventing an increase in GSH levels or even causing depletion, as demonstrated here for *S. pombe* WT (Fig. 33 A-C).

GSH itself, aside from its role as a redox buffer and ROS scavenger, serves as an important source for sulfur and cysteine[144,157,244,342]. The synthesis of reduced sulfur is energetically costly, requiring four NADPH molecules[340,343]. An additional two NADPH are needed to reduce the corresponding carbon backbone. Under stress conditions, conserving energy may therefore act as a common evolutionary driver. Thus, expanding the GSH pool - either to ensure rapid access to reduced sulfur or to support the synthesis of LMWs - could represent an effective adaptive strategy.

Further evidence for a more specific, non-random evolutionary pressure on modulating GSH metabolism in the absence of PC synthesis comes from the Cd-evolutionary project conducted by F. Hollmann (2021, unpublished data). Also using the *S. pombe pcsΔ* mutant, one isolated mutant with a SNP in the CDS of *ggt1* showed enhanced Cd tolerance, surpassing WT levels. Although both Ggt1 and the NRAMP transporter Pdt1 were lost in the mutant, the knockout of *ggt1* in the double mutant background *pcsΔpdt1Δ* further improved Cd tolerance. This improvement was also associated with higher GSH levels, as was shown here (Fig. 33). Consistent with the data generated in this work, it was demonstrated that Cd susceptibility can be reduced below WT levels when *ggt1* activity is lost in *pcsΔ*, even in the absence of PC synthesis.

Breaking it down to the key commonalities of As^{III} and Cd tolerance, it becomes apparent that GSH plays a central role in ensuring sufficient detoxification in both organisms capable of PC synthesis and those without PCS.

Assuming that increased As^{III} tolerance correlates with enhanced Cd tolerance due to a shared evolutionary mechanism that directs selective pressure, this relationship might offer insights into the development of detoxification mechanisms more broadly.

4.3.2.2 Controlling the GSH pool: The Signaling Cascades Behind GSH Synthesis and γ-GT Regulation

The induction of GSH synthesis occurs in response to nitrogen starvation[240], ROS formation, and metal/metalloid toxicity[339]. Since various stimuli affect the GSH pool, the requirement for distinct response pathways becomes apparent. Aside from As^{III} causing the formation of ROS - which itself triggers GSH synthesis - the induction of GSH production in a ROS-independent manner has been demonstrated[339]. Given the demonstrated regulation of γ-GT activity under nitrogen starvation[240], the response to As^{III} and Cd exposure may be similar, yet the effects on tolerance levels contrast, as GSH functions both as an antioxidative molecule and as a chelator of Cd and As^{III} [339,344].

Similar to Cd, As^{III} toxicity stabilizes the transcription factor Zip1, leading to the transcriptional activation of genes necessary for GSH production[237,339,342,345].

An induction of GSH synthesis by As^{III} became apparent in the PC-deficient mutant *pcsΔ*, but was diminished for M1, M3, M4, and the double-knockout strain *pcsΔggt2Δ#1*. HPLC analysis of the GSH content (Fig. 33) of the M1 and M3 mutant compared to the M2 mutant and the respective knockout strain *pcsΔggt1Δ#1* revealed comparable amounts of GSH under control conditions (≈ 27-30 µg/g DW). In contrast to M2 and *pcsΔggt1Δ#1*, a slight increase in GSH concentration was observed in M1 and M3 following As^{III} exposure.

To recover cysteine stored in the form of GSH, the initial step of GSH degradation may be catalyzed by γ-GTs, which have been shown in human cells to hydrolyze GSH[346]. By transferring the γ-glutamyl moiety of GSH to other peptides, γ-GTs occupy a central role in controlling the GSH pool[238,240,245]. However direct evidence for the enzymatic cleavage of GSH by γ-GTs in *S. pombe* is still lacking (discussed later).

If Ggt1 significantly contributes to GSH turnover and is a potential target for the downregulation via Zip1 to prevent GSH breakdown into L-cysteinylglycine and L-glutamate, the capacity for a further increase in GSH concentrations may be limited. It remained unclear, whether the lack of GSH induction in the M2 mutant and the corresponding *pcsΔggt1Δ#1* knockout strain was due to insufficient stimuli in these highly As^{III}-tolerant strains or from the constitutive upregulation of other γ-GTs that may compensate the loss of *ggt1*. Since M1 and M3 carry SNPs in the E3 ligase Pof1, which drives Zip1[339,345]degradation, their moderate GSH increase after As^{III} exposure may reflect γ-GT regulation by transcription factors other than Zip1.

A promising candidate might be Pap1[339], which acts downstream of Zip1 and can also be directly activated via the ROS signaling cascade[347]. Pap1 is involved in the transcriptional regulation of glutathione synthase (*gsa1*)[344], supporting the hypothesis that it plays a role in GSH regulation. Further evidence for this comes from experiments showing that GSH synthesis and γ-GT activity were subsequently upregulated under nitrogen starvation in WT but not in the *pap1Δ* mutant[348]. Moreover, both *ggt1* and *ggt2* were shown to be regulated in a Pap1-dependent manner; however, *ggt1* appears to be additionally regulated in a Pap1-independent manner[239,348,349].

Despite the marginal increase in GSH concentrations upon As^{III} exposure, M1 and M3 reached GSH levels slightly above those of M2 under control conditions. However, whether this increase

results from the downregulation of remaining Ggt1 activity - potentially linked to Pap1 regulation remains speculative[339].

While all mutants and their corresponding knockout strains already had higher intracellular GSH concentrations under control conditions than the *pcsΔ* mutant, the degree of GSH induction upon As^{III} exposure varied among them (Fig. 33A). GSH induction upon As^{III} treatment, observed in M4 and *pcsΔggt2Δ#1*, did not occur in M2 and *pcsΔggt1Δ#1*. The doubling of GSH concentrations in response to As^{III} exposure, observed in *pcsΔ*, M4 and *pcsΔggt2Δ#1* compared to control conditions, might be caused by the downregulation of *ggt1*. If *ggt1* is downregulated upon As^{III} exposure, then the absence of such an effect in M2 and *pcsΔggt1Δ#1* would be expected. Assuming that a constitutive upregulation of *ggt2* in the mutant and double mutant stabilizes the GSH pool at a certain level, this may explain the minor increase in GSH concentrations still observed in M1 and M3. Thus, γ-GT activity in *S. pombe* may be regulated by a feedback loop between both γ-GTs, akin to the regulation of expression levels observed in human γ-GTs[350].

Further investigation is needed to determine whether higher As^{III} concentrations would also induce GSH in M2. Overall, additional evidence is required to confirm whether the GSH increase upon As^{III} exposure is linked to changes in γ-GT activity, as suggested by initial assay results (Fig. 33D).

4.3.2.3 Beyond GSH: Hypotheses on the Role of Ggt1 in Cd Tolerance

Even though the As^{III} tolerance of all isolated mutants was clearly higher compared to *pcsΔ*, none of the mutants reached tolerance levels of the WT. Surprisingly, when exposed to very high Cd concentrations, the M2 mutant and the corresponding double mutants *pcsΔggt1Δ#1* and *#2* exhibited Cd tolerance exceeding WT levels (Fig. 30). Consequently, while PCs appear more effective than elevated GSH concentrations for the detoxification of As^{III}, the lack of PC synthesis can be overcompensated by the loss of *ggt1*, when detoxifying Cd. Reasoning that the reduction in Cd susceptibility below WT levels of M2 is primarily a consequence of enhanced GSH concentrations, which overlooks why comparable GSH levels in the mutants M1 and M3 were not sufficient to do so. Subsequently, the reasons underlying the acquired tolerance must be multifactorial and cannot exclusively be explained by higher GSH contents.

Human γ-GTs are primarily active in the extracellular space, where they play a key role in GSH turnover[247,346]. Thus, their enzymatic products are first expected outside the cell. Although our observations and current literature support the localization of Ggt1 to the ER, its enzymatic activity may still contribute to the formation of LMWs excreted into the medium, potentially enhancing the uptake capacity of Cd. Alternatively, it is also plausible that certain LMWs hinder vacuolar sequestration by retaining Cd in the cytosol, thereby impairing its detoxification. Consequently, the reduced Cd susceptibility observed in the mutant may result from a combined effect. The loss of Ggt1 contribution to Cd availability, and an elevated intracellular GSH content.

Initial insights into these questions may be gained through targeted uptake experiments combined with thiol profiling under Cd exposure. Including As^{III} as a reference in both experimental setups could provide valuable comparative data, helping to clarify differences in detoxification mechanisms for these two toxic elements in the mutant background.

4.3.3 Ggt1 and Ggt2: Similarities and Differences

Several similarities, including structural, functional, and regulatory homologies, have been reported for the γ-GTs Ggt1 and Ggt2. Apart from experimental data on the respective double knockout strains and mutant strains (Fig. 29, 30, 31, 33, 34 and 35), their roles within the GSH cycle and the mechanisms by which their loss of function confers tolerance to As^{III} and Cd remain incompletely understood.

An initial clue for the origin of differences of both γ-GTs, apart from their sequence homology, comes from comparing their localization. By fluorescence microscopy of the C-terminal GFP-tagged complementation lines, the predicted localization of Ggt1 in the ER and the vacuolar localization of Ggt2 was confirmed (Fig. 37). At first glance, the overall distribution of protein domains and properties appears quite similar (Fig. 38A), with a C-terminus divided into a large and a small subunit and a high degree of conservation between both (Ggt1/Ggt2 identity ≈ 50.19%; p-value = 2e-175). Notably, the most obvious difference in domain distribution along the protein sequence is the extended N-terminus of Ggt1 compared to Ggt2. This aligns with the highest divergence being in the N-terminal region, which corresponds to the distinct localizations of both γ-GTs as predicted (pombase.org) and observed.

Likewise to mammalian γ-GT enzymes[247], and based on the initial WB analysis (Master Thesis of Celine Fischer), the small subunit of Ggt1 and Ggt2 may be separated by cleavage after their integration into the respective membrane. Cleavage before entry into the membrane can be nearly excluded, considering that most ER and vacuolar localization sequences are found at the N-terminus[351–353]. Therefore, the N-termini of Ggt1 and Ggt2 are likely only a portion of the pro-peptide until it is cleaved off upon membrane integration, as reported previously.

Harboring the catalytic active site, the small subunit is the main region of interest when searching for further differences beyond localization. A comparison of the 3D structures of both enzymes (Fig. 38B)[224,225] and the results of a TM-alignment (Fig. 38A) indicate that, aside from the N-terminus, both enzymes exhibit a high degree of conservation in their 3D structures. Interestingly, the polymorphism found in the CDS of Ggt2 in the M4 mutant, resulting in a serine (S) to arginine (R) transition, directly affects the center of the predicted active site of Ggt2. According to the prediction via AlphaFold[225], the interaction between S511 and Q585 was likely disrupted by the substitution of S with R. The gene disruption of *ggt2* in M4*_ggt2Δ::KanMX4* did not affect the mutant's tolerance to As^{III} and Cd, nor did it alter the enhanced sensitivity to elevated concentrations of DMMTA observed in the M4 mutant (Fig. 29 + 31). This further supports the assumption that the S to R transition likely caused a loss of Ggt2 function.

The differential susceptibility levels of M4 and the double knockout mutants *pcsΔggt2Δ#1* and *#2* suggest that the loss of Ggt2 function alone cannot fully explain the reduced As^{III} sensitivity observed in M4. However, knockout of *ggt2* still enhanced tolerance to As^{III} and Cd, albeit less than the *ggt1* knockout.

Differences in As^{III} and Cd susceptibility align with variations between mutants and their double knockouts, as M2 and *pcsΔggt1Δ#1* showed roughly double the GSH levels. Loss of *ggt1* in the *pcsΔ* background led to greater Cd tolerance than in WT, while *ggt2* loss increased As^{III} and Cd tolerance in *pcsΔ*, though not to WT levels. In WT cells, *ggt2* loss slightly reduced As^{III} and Cd tolerance (Fig. 31), while As^{V} tolerance increased (Fig. 29).

Initial assays showed no clear differences in γ-GT activity between Ggt1- and Ggt2- deficient knockout strains and the M2 and M4 mutants, but all had lower γ-GT activity than the *pcsΔ* mutant and WT.

Seung-Hyung and Chang-Jin (2008) previously demonstrated that γ-GT activity drives sequential adaptations. Within nine hours of nitrogen starvation, they observed a fourfold increase in γ-GT activity. Given that the regulation of GSH synthesis and γ-GT activity upon nitrogen starvation occurs sequentially[348], γ-GT activity should also be measured at different time points for As^{III} exposed cells to avoid overlooking potential changes. Using protein extracts from long-term As^{III} exposed cells (18 h) to determine γ-GT activity (Fig. 33D) may be too late to detect differences among the tested strains. In these experiments, both *S. pombe* WT and *pcsΔ*, as well as *S. cerevisiae* WT, showed a strong reduction in γ-GT activity upon As^{III} exposure, in contrast to reports of increased γ-GT activity upon Cd exposure[245].

4.3.4 Closely Related yet Distinct: A Comparison of *ggt1* and *ggt2* with Their Ortholog *ECM38* in *S. cerevisiae*

Both γ-GTs, are annotated as orthologs of *ECM38*[354] (Ecm38/Ggt1 with ≈ 35.55% identity and Ecm38/Ggt2 with ≈ 35.94% identity; 3e-90 and 8e-87, respectively). Among them, Ggt2 appears more functionally related to Ecm38, based on its localization to the vacuolar membrane (Fig. 37)[355]. Knockout of the *ggt1* and *ggt2* ortholog *ECM38* in *S. cerevisiae* is associated with enhanced Cd accumulation. [220,245]

Assuming functional similarity between Ecm38 and Ggt2 and given that Ecm38 is localized to the vacuolar membrane based on previous reports[356], knockout of *ggt2* should impair the breakdown of GSH-Cd complexes in the vacuole, leading to higher rather than lower Cd toxicity. For unknown reasons, although Cd tolerance in *ggt2Δ* appeared to be slightly reduced, the double knockouts *pcsΔggt2Δ#1* and *#2*, as well as M4, were slightly more tolerant than the corresponding *pcsΔ* strain.

Based on these preliminary results, both Ggt1 and Ggt2 may indirectly modulate PC synthesis, though in different ways, by contributing to the catabolism of GSH. This, in turn, indirectly impacts PC synthesis through alterations in GSH homeostasis, causing variations in the available amount

of PC educts. Regarding *ggt1*, further evidence is needed to determine whether its knockout causes lethality in the WT background (discussed later), thereby indicating that PCS and γ-GT activities are functionally interconnected in the GSH cycle[343,357].

Based on predicted structural features and fluorescence imaging (Fig. 37), Ggt1 and Ggt2 likely influence different subcellular GSH pools due to their distinct localizations. Further studies are needed to clarify their precise positioning and functional impact, which could also provide the first hint as to whether Ggt2 shares functional homology with Ecm38.

Hence, precise identification of Ggt1 and Ggt2 localization is essential to determine whether their active sites face the ER lumen, the vacuolar lumen, or the cytosol. A promising approach might be a proteinase protection assay using N- and C-terminally tagged versions of both proteins. Depending on the protease sensitivity of each tag, this assay can reveal the membrane topology and compartmental orientation of Ggt1 and Ggt2, indicating, for example, whether the termini face the cytosol or are protected within organellar lumens[358]. This would be an important step toward determining whether they affect the cytosolic GSH pool, the ER-associated pool (Ggt1), or the vacuolar pool (Ggt2).

In this context, it can be expected that a γ-GT with an active site exposed to the cytosol would have a stronger impact on overall GSH levels than one targeting the ER or vacuolar GSH pool. Due to the lack of detailed information on GSH distribution in fission yeast, this hypothesis assumes a similar GSH distribution to that observed in *S. cerevisiae*[359]. HPLC analysis (Fig. 33A) of intracellular GSH levels in the mutants and double knockouts supports this assumption. It may explain why M2 and the double mutant *pcsΔggt1Δ#1* exhibited higher GSH concentrations than M4 and *pcsΔggt2Δ#1*, although these genotypes showed similar effects on γ-GT activity (Fig. 33D).

As the primary source of reduced sulfur, the recovery of GSH stored in the vacuole - whether for maintaining the cell's redox state or detoxifying electrophilic xenobiotics - is crucial for preserving cellular homeostasis. In *S. cerevisiae*, the collaboration between the vacuolar membrane-associated γ-GT Ecm38 and aminopeptidase Lap4 is needed for breaking down GSH into its constituent amino acids, L-cysteine, L-glycine, and L-glutamate[220,245], which are then translocated into the cytoplasm.

Extending these findings to the function of Ggt2, it is proposed that during As^{III} or Cd exposure, GSH - lost through detoxification via GS-As or GS-Cd complex formation and subsequent vacuolar sequestration[201] - can be recovered by the cleavage of the γ-peptide bond, followed by further degradation by an aminopeptidase, such as Ape2/4[360].

However, a major unresolved issue with this assumption is that the loss of Ggt2 function should theoretically increase, rather than decrease tolerance to As^{III} and Cd. Proteomic data suggest that the previously described GSH recycling mechanism in *S. cerevisiae* likely serves a sulfur-sparing purpose[343], in particular important under stress condition. Comparison of proteomic data from both, *S. pombe* and *S. cerevisiae* exposed to Cd revealed that about 80% of the upregulated proteins in *S. pombe* differ markedly from those upregulated in *S. cerevisiae*[361], implying that the detoxification mechanisms strongly differ among both species.

Moreover, a closer examination of sulfur assimilation and the response to sulfur starvation reveals further differences between the two yeasts[357]. *S. pombe* lacks the ability to synthesize cysteine from methionine due to the absence of a trans-sulfuration pathway, which is present in *S. cerevisiae*. Therefore, under sulfur starvation conditions, *S. pombe* probably depends on recovering cysteine from the degradation of GSH. Overall, while Ecm38 and Ggt2 are closely related in terms of sequence homology and localization, their physiological roles may differ more strongly than previously assumed.

Also, previous reports have highlighted a significant divergence in Cd detoxification mechanisms between *S. pombe* and *S. cerevisiae*. In *S. cerevisiae*, exposure to 30 µM Cd triggers a substantial shift in sulfur allocation. The proportion of sulfur-containing peptides used for protein synthesis decreased from 79% to 19%, while sulfur directed toward the GSH pathway increased from 11% to 70%[343,362]. This shift likely helps to conserve energy under stress conditions.

In this context, it is noteworthy to highlight another significant difference between *S. pombe* and *S. cerevisiae*. Unlike in *S. cerevisiae*, *S. pombe* primarily relies on vacuolar sequestration via PCs for As^{III} and especially Cd detoxification[160,194]. In contrast, in *S. cerevisiae*, Cd and As^{III} are bound by GSH and then either sequestered in the vacuole or, in the case of As^{III}, additionally exported from the cell[196]. The efflux of As^{III}, mediated by the As^{III}-efflux pump Acr3, was shown to

counteract the PC pathway during As^{V} detoxification[194]. Heterologous expression of the *S. pombe Sppcs2* in *S. cerevisiae* WT strain enhanced tolerance to As^{III} and Cd but reduced tolerance to As^{V}, likely due to the depletion of GSH, which is consumed in both As^{V} reduction and PC synthesis. This aligns with the observation that the knockout of *ggt2* slightly enhanced As^{V}, rather than As^{III}, tolerance in the WT background, if enhanced GSH levels contribute to or support As^{V} reduction (Fig. 29). Heterologous expression of *ScACR3* in *S. pombe* WT strains enhanced tolerance to both As^{III} and As^{V}, indicating differences between *S. pombe* and *S. cerevisiae* in their capacities for GSH consumption and regeneration. Consequently, in the *pcsΔ* mutant, where PC synthesis is abolished, reducing GSH degradation may enhance GSH levels, contributing to increased tolerance.

The fact that *ggt2* knockout in the WT background did not enhance As^{III} and Cd tolerance - and even tended to increase sensitivity - suggests a dual function of *ggt2* in *S. pombe*. Since PCs are primarily formed from GSH, cysteine and glycine, Ggt2 may play a role in recovering their precursor molecules, similar to Ecm38 in *S. cerevisiae*[220], which facilitates the recovery of GSH educts from GSH-conjugates. Thus, the knockout of *ggt2* would be advantageous in *pcsΔ* mutants if Ggt2 primarily functions as a PC-conjugate-cleaving enzyme and is only partially involved in recovering GSH educts from GSH conjugates, as Ecm38 does in *S. cerevisiae.* Hence, the increased As^{III} and Cd tolerance from *ggt2* loss can be explained by higher GSH levels due to reduced GSH breakdown, followed by its subsequent allocation from the vacuole to the cytosol.

Regarding the assumed evolutionary divergence in γ-GT function between *S. pombe* and *S. cerevisiae*, it is noteworthy that γ-GT versatility is also observed across different *S. cerevisiae* strains. In the *S. cerevisiae* strain YPH499 - congenic to the widely used S288C strain - 11 SNPs in the CDS and 8 SNPs in the promoter region of *ECM38* resulted in the loss of γ-GT function[354]. Despite this loss, *ECM38* in YPH499 is not considered a pseudogene; rather, it is proposed that this former γ-GT may have acquired an alternative function. Overall, the roles of γ-GTs appear to vary significantly not only between species but also among congenic organisms, making direct comparisons challenging and preventing a unified interpretation of their functions.

Finally, although unlikely, it is possible that both *ggt1* and *ggt2*, annotated as γ-GTs, share common features with another class of functionally related enzymes, namely γ-glutamyl

cyclotransferases. In *A. thaliana*, γ-glutamyl cyclotransferases contribute to GSH catabolism and mediate tolerance to As^{III} and Cd. The γ-glutamyl cyclotransferase *AtGGCT2;1*, when heterologously expressed in *S. cerevisiae* H9 strain[363], increased sensitivity to As^{III} and Cd. Furthermore, the *ggct2;1* knockout mutant in *A. thaliana* exhibited reduced susceptibility to As^{III} and Cd than the WT, which aligns with the experimental data (Fig. 29, 30, 31 and 35). Although γ-glutamyl cyclotransferases are not functionally equivalent to γ-GTs, moderate sequence homology between the glutathione-specific γ-glutamyl cyclotransferase (*ggg1*) and γ-GT *ggt2* (with ≈ 21.1% query cover, 100% identity, and e-value: 0.48) suggests that they might share functional features related to As^{III} and Cd detoxification.

4.3.5 A Potential Role for Ggt2 in Mediating DMMTA Tolerance

Following this, the arguments mentioned above still cannot explain why loss of Ggt2 function leads to increased sensitivity to DMMTA, as DMMTA tolerance did not correlate with intracellular GSH concentrations in these experiments (Fig. 32 and 33). While the impact of varying GSH concentrations on DMMTA thiolation and de-thiolation has been demonstrated in *A. thaliana*[84], the observations cannot be solely attributed to GSH concentration-dependent thiolation processes. Given that the increased sensitivity occurred only at very high DMMTA concentrations, it is possible that the observed toxicity was not caused by DMMTA itself but rather by the accumulation of its less toxic derivative, DMDTA, which accounts for up to 20% of the total arsenic in the DMMTA stocks. Nevertheless, even if it can be determined whether DMMTA or DMDTA causes the phenotype of enhanced sensitivity, the question of how the loss of *ggt2* reduces tolerance to these compounds would still remain.

The in planta thiolation of DMA and DMMTA, as well as the de-thiolation of DMDTA, is believed to depend on intracellular GSH levels. Nevertheless, apart from the decreased GSH:GSSG ratio in *cad2-1* and *pad2-1*, the total amounts of both GSH and GSSG remain below WT levels[364]. If thiolation depends on GSH, the observed effects were likely due to the reduced overall GSH content, rather than an altered reduced-to-oxidized glutathione ratio, as thiolation processes can be affected by the presence of reduced sulfur[44,365].

One of the main puzzles in the findings regarding the enhanced DMMTA sensitivity in the *ggt2* knockout mutants was the absence of altered DMMTA tolerance in the double knockout mutant *pcsΔggt1Δ#1* and M2. This suggests that, in general, γ-GT activity does not influence sensitivity. Moreover, the higher GSH levels in M1, M2, M3, and the double knockout *pcsΔggt1Δ#1* compared to M4 and *pcsΔggt2Δ#1* indicate that this increased sensitivity is not, or not directly, related to elevated GSH concentrations.

One possible explanation for the heightened DMMTA sensitivity upon *ggt2* loss, unlike *ggt1*, could be, that the observed effect was indirectly the result of the Ggt2 loss. Since both Ggt1 and Ggt2 are differentially regulated[239,240,349], their influence on the abundance or activity of other enzymes, particularly those involved in the GSH cycle, may be the true cause of the observed effect. Additionally, differences in the impact on the cellular redox state, which affects the distribution of LMWs, could promote the de-thiolation of DMDTA to DMMTA, thereby increasing cytotoxicity.

An even more speculative possibility is that Ggt2 itself may contribute to the de-thiolation of DMMTA and/or DMDTA, thereby reducing toxicity. However, the possibility of enzymatically driven de-/thiolation processes cannot be excluded[84]. This hypothesis could be addressed by adding DMMTA to crude protein extracts from the *ggt2* knockout and WT strains and monitoring thiolation or dethiolation over time. Based on current models for γ-GT regulation in *A. thaliana*[366,367], and insights from other species[357], it can be assumed that the GSH-deficient mutants used in this study[84] - *pad2-1* and *cad2-1* - exhibit reduced γ-GT activity in vivo. This reduction is likely due to limited GSH availability rather than impaired γ-GT function, under the presumption that γ-GT activity depends on GSH availability[368].

Until further experiments (discussed later) clarify the underlying mechanisms, the role of Ggt2 in providing tolerance to DMMTA and/or DMDTA remains uncertain.

4.3.6 Essential or Not Essential? Are *pof1* and *ggt1* essential genes?

Three of the five SNPs found in the mutant strains derived from the As^{III} evolutionary project lineage were located in genes annotated as essential (*pombase.org*). These mutations, which

either cause frameshifts or eliminate the start codon, make the likelihood of functional protein translation nearly zero. This raises the question of whether these genes are truly essential.

For *pof1*, several ts-mutants have been identified, which contributed to the investigation of SCF^{Pof1}-mediated Zip1 ubiquitylation and degradation, as previously discussed[237]. Another target of Pof1, as well as its paralog Pof3, is Wee1, which is a negative regulator of the G2/M transition[335]. Likewise, Zip1, Wee1 is ubiquitylated by the SCF^{Pof} complex for proteasomal degradation. However, studies have demonstrated that Wee1 degradation relies more on Pof3 than Pof1, suggesting differences in their substrate specificity and target proteins. Given that the *S. pombe* genome encodes 18 different F-box proteins[369,370], further redundancy in substrate recognition is likely.

Nonetheless, experiments with ts-mutants show that loss of Pof1 activity typically results in small cell size and growth arrest (Harrison et al., 2005)[237], which was not observed in M1 and M3. Since both Wee1 and Zip1 regulate cell cycle progression and growth arrest, the WT-like growth of M1 and M3 (Fig. 28 + 29) contradicts expectations for the loss of Pof1 activity and differs from previously characterized ts-mutant phenotypes. As the investigation focused on SNPs within coding sequences, the presence of mutations in non-coding regulatory regions - such as cis-elements controlling other F-box proteins - cannot be excluded. Such mutations could potentially compensate for Pof1 loss by upregulating paralogs with overlapping substrate specificity, allowing normal growth in M1 and M3.

Furthermore, one SNP leads to the loss of the start codon, while another introduces a frameshift in the N-terminal region. This raises the possibility that a shorter Pof1 variant might be expressed from an alternative start codon downstream of the detected SNPs. If such a truncated protein had reduced substrate specificity, higher Zip1 levels could increase GSH production without being sufficient to trigger growth arrest. Since Wee1-mediated G2/M inhibition is dose-dependent[335], both Wee1 and Zip1 could have dosage-dependent downstream effects. However, given that the next potential start codon would result in the loss of 47 N-terminal residues, it is unlikely that a functional Pof1 protein could still fold properly. However, initial complementation analyses indicate that the mutations identified in the CDS of *pof1* are the underlying cause of heightened As^{III} and Cd tolerance in M1 and M3 (Fig. 36).

Unlike *pof1*, double knockout mutants of *ggt1* in the *pcsΔ* background were successfully generated. Although being unsuccessful in generating a *ggt1* knockout in the WT, the viability of cells lacking Ggt1 activity remains WT-like under standard conditions (Fig. 29 and 31). Again, the divergence between *ggt1* and *ggt2* in *S. pombe* metabolism becomes evident, as the knockout of *ggt2* in the WT background was successful. Thus, while *ggt1* appears essential for WT cells, it might be dispensable in the *pcsΔ* background.

Ggt1 and Pcs are involved in GSH homeostasis and GS-conjugate breakdown, and they differentially influence the levels of specific LMWs that affect the cellular redox state[143,146,162]. While one enzyme requires cysteine for the formation of PCs[160], the other is involved in the initial step of cysteine recovery through GSH breakdown[238,239]. Studies on *A. thaliana* mutants deficient in PC synthesis revealed that AtPCS1 additional plays also a key role in GS-conjugate catabolism by removing the carboxyterminal glycine residue[371–373].

Despite both enzymes being involved in GS-conjugate breakdown, their products differ as PCS-mediated GS-conjugate degradation results in the formation of γ-EC, whereas γ-GTs are suspected of generating cysteinyl-glycine adducts in plants. It is further hypothesized that the subsequent dipeptide hydrolysis of γ-EC and cysteinyl-glycine leads to the formation of cysteinyl-conjugates in *A. thaliana*.

Thus, an imbalance in these LMWs may lead to cytotoxicity. Contrary, vacuolar-localized Ggt2, may have a lesser impact on maintaining the cell's redox state. This may explain why Ecm38 in *S. cerevisiae* is not essential[245,354]; as its loss likely affects only vacuolar GSH levels, similar to Ggt2.

As demonstrated by F. Hollmann (2021, unpublished data) and in this work (Fig. S7), there is only a narrow window of *ggt1* expression that allows normal growth without adverse effects on vitality. The correlation between γ-GT activity and cell vitality has also been demonstrated in plants, as treatments with the γ-GT inhibitor acivicin significantly reduced biomass, complicating efforts to distinguish the contributions of the PCS and γ-GT pathways in GS-conjugate breakdown[373].

Nevertheless, until further evidence confirms *ggt1* as essential in WT cells, investigating the potential interplay between *S. pombe* Ggt1 and Pcs remains a secondary priority.

4.4 Concluding Remarks and Outlook

Further experiments are needed to uncover the mechanisms behind the increased As^{III}, As^{V}, and Cd tolerance in mutant strains from the As^{III} evolutionary project.

The identification of two genes, which are either annotated as or proven to be essential, has hindered the elucidation of the mechanisms underlying the heightened tolerance levels. Therefore, determining whether *ggt1* and *pof1* are essential should be a primary focus for the continuation of this project.

Since knockout attempts using CRISPR-Cas9 and homologous recombination in *pof1*- and *ggt1*-overexpressing strains were unsuccessful, an alternative approach may be more promising. In previous knockout attempts using selection markers such as geneticin 418, hygromycin, and nourseothricin, it was not possible to select potential candidates on SD medium. For future trials aiming to generate *pof1* and *ggt1* knockouts, the selection marker zeocin should be prioritized, as it allows selection in minimal defined media[243], unlike the markers used here. Therefore, the parallel inducible episomal expression of the target genes in the overexpression strains (Fig. S7) should facilitate the disruption of genomic *ggt1* and *pof1* via homologous recombination, even if they are essential in the WT or *pcsΔ* background. A successful knockout in the overexpression lines would then enable further investigations into the necessity of *ggt1* and *pof1*. If these genes are truly essential, inhibition of episomal expression by applying 20 µM thiamine should result in lethality of the respective knockout strains.

Toxicity assays conducted with the double knockout strains *pcsΔggt1Δ#1,* and *pcsΔggt1Δ#2* (Fig. 29 + 30), together with complementation analysis (Fig. 34) demonstrated that the SNP found in the CDS of *ggt1* primarily contributes to the acquired tolerance to As^{III} and Cd. However, *ggt1* expression in the M2 mutant did not fully restore the enhanced tolerance phenotype. Although *plb1* expression did not alter As^{III} and Cd tolerance in M2, a potential synergistic effect of *ggt1* and *plb1* loss cannot be ruled out. Therefore, co-expressing both genes should be tested to determine whether this results in *pcsΔ*-like As^{III} and Cd sensitivity. As As^{III} and Cd are both known to induce lipid peroxidation[318,374], it is plausible that alterations in membrane composition - expected by changes of the lipid bilayer composition from the loss of *plb1*[241] - may influence cellular susceptibility. Given the likely low contribution of *plb1* to the overall tolerance of M2,

achieving complete complementation might require higher expression levels than those suitable for *ggt1* expression. Nevertheless, the overall reduced sensitivity of M2 appears to be primarily associated with *ggt1*.

By contrast, *ggt2* expression in M4 only partially restored As^{III} and Cd susceptibility, suggesting the presence of an additional SNP in non-coding genomic regions. This was further supported by the observation that the double mutants *pcsΔggt2Δ#1* and *pcsΔggt2Δ#2* were less As^{III} tolerant than M4. To evaluate the underlying reasons for M4's tolerance (even though for M1 and M3), a promising approach would be to backcross it with *pcsΔ* to identify the remaining SNP(s) associated with elevated tolerance levels[375]. This should be followed by an analysis of the progeny pool, comparing tolerant vs. sensitive individuals to map the responsible mutations.

Further questions, such as the fate of the N-terminal portion of *ggt1* and *ggt2*, can be addressed by WB analysis using N-terminally tagged *ggt1* and *ggt2*. This would provide additional evidence to answer the question whether these enzymes are processed similarly to human γ-GTs[247].

The observed DMMTA sensitivity in *ggt2* mutants - only at high concentrations - may be due to DMDTA contamination, as DMMTA stocks contain ~24% DMDTA (Fig. S8). To clarify this, toxicity assays with pure DMDTA should precede further studies on uptake and sulfur metabolism. If *ggt2* is truly linked to DMMTA sensitivity, it may indicate a role in DMMTA metabolism. Otherwise, *ggt2* might still be involved in DMDTA processing, possibly via de-thiolation to DMMTA.

Lastly, since the increase in As^{III} tolerance correlated with varying degrees of elevated GSH levels across all mutants, a comprehensive metabolomic and transcriptomic analysis would be a promising approach to further elucidate the mechanisms underlying As^{III} and Cd tolerance. Especially, transcriptomic analysis via RNA-seq in the M1 and M3 mutants could provide new insights into SCF^{Pof1}-controlled pathways, including those regulated by the transcription factors Zip1 and Wee1. Furthermore, metabolomic analysis may reveal changes in other LMWs and uncover previously unknown functions of Pcs and γ-GTs in maintaining the cell's redox state.

5. References

5.1 List of References

1. Lera-Ramírez, M. *et al.* Revised fission yeast gene and allele nomenclature guidelines for machine readability. *GENETICS* **225**, iyad143 (2023).

2. Sherman, F. Getting started with yeast. in *Methods in Enzymology* vol. 350 3–41 (Elsevier, 2002).

3. Price, C. A. & Reardon, E. M. Mendel, a database of nomenclature for sequenced plant genes. *Nucleic Acids Res.* **29**, 118–119 (2001).

4. Demerec, M., Adelberg, E. A., Clark, A. J. & Hartman, P. E. A proposal for a uniform nomenclature in bacterial genetics. *Genetics* **54**, 61–76 (1966).

5. Bruford, E. A. *et al.* Guidelines for human gene nomenclature. *Nat. Genet.* **52**, 754–758 (2020).

6. Kerl, C. F., Rafferty, C., Clemens, S. & Planer-Friedrich, B. Monothioarsenate Uptake, Transformation, and Translocation in Rice Plants. *Environ. Sci. Technol.* **52**, 9154–9161 (2018).

7. Planer-Friedrich, B., Kerl, C. F., Colina Blanco, A. E. & Clemens, S. Dimethylated Thioarsenates: A Potentially Dangerous Blind Spot in Current Worldwide Regulatory Limits for Arsenic in Rice. *J. Agric. Food Chem.* **70**, 9610–9618 (2022).

8. Colina Blanco, A. E., Kerl, C. F. & Planer-Friedrich, B. Detection of Thioarsenates in Rice Grains and Rice Products. *J. Agric. Food Chem.* **69**, 2287–2294 (2021).

9. Dai, J. *et al.* Widespread Occurrence of the Highly Toxic Dimethylated Monothioarsenate (DMMTA) in Rice Globally. *Environ. Sci. Technol.* **56**, 3575–3586 (2022).

10. Huang, C. F. *et al.* Arsenic and diabetes: Current perspectives. *Kaohsiung J. Med. Sci.* **27**, 402–410 (2011).

11. El-Ghiaty, M. A. & El-Kadi, A. O. S. The Duality of Arsenic Metabolism: Impact on Human Health. *Annu. Rev. Pharmacol. Toxicol.* **63**, 341–358 (2023).

12. Pal, S. & Firdous, S. M. Unraveling the role of heavy metals xenobiotics in cancer: a critical review. *Discov. Oncol.* **15**, 615 (2024).

13. *A Review of Human Carcinogens*. (International agency for research on cancer, Lyon, 2012).

14. Zhu, Q. *et al.* Toxic and essential metals: metabolic interactions with the gut microbiota and health implications. *Front. Nutr.* **11**, 1448388 (2024).

15. Bradford, S. *Lucrezia Borgia: Life, Love and Death in Renaissance Italy*. (Penguin, London, 2005).

16. Arab YarMohammadi, A., Arbabi Bidgoli, S. & Ziarati, P. Increased urinary arsenic concentration in newly diagnosed type 2 diabetes mellitus: a gender-independent, smoking-dependent exposure biomarker in older adults in Tehran. *Environ. Sci. Pollut. Res.* **28**, 27769–27777 (2021).

17. Hossain, E. *et al.* Elevated levels of plasma Big endothelin-1 and its relation to hypertension and skin lesions in individuals exposed to arsenic. *Toxicol. Appl. Pharmacol.* **259**, 187–194 (2012).

18. Huda, N. *et al.* Elevated levels of plasma uric acid and its relation to hypertension in arsenic-endemic human individuals in Bangladesh. *Toxicol. Appl. Pharmacol.* **281**, 11–18 (2014).

19. Valappil, A. V. & Mammen, A. Subacute Arsenic Neuropathy: Clinical and Electrophysiological Observations. *J. Neurosci. Rural Pract.* **10**, 529–532 (2019).

20. Mochizuki, H. *et al.* Peripheral neuropathy induced by drinking water contaminated with low-dose arsenic in Myanmar. *Environ. Health Prev. Med.* **24**, 23 (2019).

21. Quansah, R. *et al.* Association of arsenic with adverse pregnancy outcomes/infant mortality: a systematic review and meta-analysis. *Environ. Health Perspect.* **123**, 412–421 (2015).

22. Navasumrit, P. *et al.* Exposure to arsenic in utero is associated with various types of DNA damage and micronuclei in newborns: a birth cohort study. *Environ. Health* **18**, 51 (2019).

23. Signes-Pastor, A. J., Carey, M. & Meharg, A. A. Inorganic arsenic in rice-based products for infants and young children. *Food Chem.* **191**, 128–134 (2016).

24. Shaji, E. *et al.* Arsenic contamination of groundwater: A global synopsis with focus on the Indian Peninsula. *Geosci. Front.* **12**, 101079 (2021).

25. Drahota, P. & Filippi, M. Secondary arsenic minerals in the environment: A review. *Environ. Int.* **35**, 1243–1255 (2009).

26. Chung, J.-Y., Yu, S.-D. & Hong, Y.-S. Environmental source of arsenic exposure. *J. Prev. Med. Public Health Yebang Uihakhoe Chi* **47**, 253–257 (2014).

27. Mania, M. *et al.* Total and inorganic arsenic in fish, seafood and seaweeds--exposure assessment. *Rocz. Panstw. Zakl. Hig.* **66**, 203–210 (2015).

28. Berg, M. *et al.* Magnitude of arsenic pollution in the Mekong and Red River Deltas — Cambodia and Vietnam. *Sci. Total Environ.* **372**, 413–425 (2007).

29. Buschmann, J., Berg, M., Stengel, C. & Sampson, M. L. Arsenic and Manganese Contamination of Drinking Water Resources in Cambodia: Coincidence of Risk Areas with Low Relief Topography. *Environ. Sci. Technol.* **41**, 2146–2152 (2007).

30. Rodríguez-Lado, L. *et al.* Groundwater Arsenic Contamination Throughout China. *Science* **341**, 866–868 (2013).

31. Bhattacharya, P., Chatterjee, D. & Jacks, G. Occurrence of Arsenic-contaminatedGroundwater in Alluvial Aquifers from Delta Plains, Eastern India: Options for Safe Drinking Water Supply. *Int. J. Water Resour. Dev.* **13**, 79–92 (1997).

32. Nickson, R. T., McArthur, J. M., Shrestha, B., Kyaw-Myint, T. O. & Lowry, D. Arsenic and other drinking water quality issues, Muzaffargarh District, Pakistan. *Appl. Geochem.* **20**, 55–68 (2005).

33. Aziz, S. N., Aziz, K. M. S. & Boyle, K. J. Arsenic in Drinking Water in Bangladesh: Factors Affecting Child Health. *Front. Public Health* **2**, (2014).

34. Williams, P. N. *et al.* Greatly Enhanced Arsenic Shoot Assimilation in Rice Leads to Elevated Grain Levels Compared to Wheat and Barley. *Environ. Sci. Technol.* **41**, 6854–6859 (2007).

35. Li, G., Sun, G.-X., Williams, P. N., Nunes, L. & Zhu, Y.-G. Inorganic arsenic in Chinese food and its cancer risk. *Environ. Int.* **37**, 1219–1225 (2011).

36. Flora, S. J. S. *Handbook of Arsenic Toxicology*. (Academic Press, an imprint of Elsevier Science, London, 2015).

37. Humans, I. W. G. on the E. of C. R. to. *Arsenic, Metals, Fibres and Dusts*. (International Agency for Research on Cancer, Place of publication not identified, 2012).

38. Chiang, H. S., Guo, H. R., Hong, C. L., Lin, S. M. & Lee, E. F. The Incidence of Bladder Cancer in the Black Foot Disease Endemic Area in Taiwan. *Br. J. Urol.* **71**, 274–278 (1993).

39. Hopenhayn-Rich, C. Lung and kidney cancer mortality associated with arsenic in drinking water in Cordoba, Argentina. *Int. J. Epidemiol.* **27**, 561–569 (1998).

40. Chiu, H. Lung cancer mortality reduction after installation of tap-water supply system in an arseniasis-endemic area in Southwestern Taiwan. *Lung Cancer* **46**, 265–270 (2004).

41. Heck, J. E., Park, A. S., Qiu, J., Cockburn, M. & Ritz, B. Risk of leukemia in relation to exposure to ambient air toxics in pregnancy and early childhood. *Int. J. Hyg. Environ. Health* **217**, 662–668 (2014).

42. EFSA Panel on Contaminants in the Food Chain (CONTAM) *et al.* Update of the risk assessment of inorganic arsenic in food. *EFSA J.* **22**, (2024).

43. Planer-Friedrich, B., London, J., McCleskey, R. B., Nordstrom, D. K. & Wallschläger, D. Thioarsenates in Geothermal Waters of Yellowstone National Park: Determination, Preservation, and Geochemical Importance. *Environ. Sci. Technol.* **41**, 5245–5251 (2007).

44. Stauder, S., Raue, B. & Sacher, F. Thioarsenates in Sulfidic Waters. *Environ. Sci. Technol.* **39**, 5933–5939 (2005).

45. Naranmandura, H. *et al.* Evidence for toxicity differences between inorganic arsenite and thioarsenicals in human bladder cancer cells. *Toxicol. Appl. Pharmacol.* **238**, 133–140 (2009).

46. Moe, B. *et al.* Comparative cytotoxicity of fourteen trivalent and pentavalent arsenic species determined using real-time cell sensing. *J. Environ. Sci.* **49**, 113–124 (2016).

47. Hinrichsen, S., Lohmayer, R., Zdrenka, R., Dopp, E. & Planer-Friedrich, B. Effect of sulfide on the cytotoxicity of arsenite and arsenate in human hepatocytes (HepG2) and human urothelial cells (UROtsa). *Environ. Sci. Pollut. Res.* **21**, 10151–10162 (2014).

48. Maciaszczyk-Dziubinska, E., Wawrzycka, D. & Wysocki, R. Arsenic and Antimony Transporters in Eukaryotes. *Int. J. Mol. Sci.* **13**, 3527–3548 (2012).

49. Zhao, F.-J., Tang, Z., Song, J.-J., Huang, X.-Y. & Wang, P. Toxic metals and metalloids: Uptake, transport, detoxification, phytoremediation, and crop improvement for safer food. *Mol. Plant* **15**, 27–44 (2022).

50. Tawfik, D. S. & Viola, R. E. Arsenate Replacing Phosphate: Alternative Life Chemistries and Ion Promiscuity. *Biochemistry* **50**, 1128–1134 (2011).

51. Shin, H., Shin, H., Dewbre, G. R. & Harrison, M. J. Phosphate transport in *Arabidopsis* : Pht1;1 and Pht1;4 play a major role in phosphate acquisition from both low- and high-phosphate environments. *Plant J.* **39**, 629–642 (2004).

52. Catarecha, P. *et al.* A Mutant of the *Arabidopsis* Phosphate Transporter PHT1;1 Displays Enhanced Arsenic Accumulation. *Plant Cell* **19**, 1123–1133 (2007).

53. Wu, Z., Ren, H., McGrath, S. P., Wu, P. & Zhao, F.-J. Investigating the Contribution of the Phosphate Transport Pathway to Arsenic Accumulation in Rice. *Plant Physiol.* **157**, 498–508 (2011).

54. Wang, P., Zhang, W., Mao, C., Xu, G. & Zhao, F.-J. The role of OsPT8 in arsenate uptake and varietal difference in arsenate tolerance in rice. *J. Exp. Bot.* **67**, 6051–6059 (2016).

55. Cao, Y. *et al.* Knocking Out *OsPT4* Gene Decreases Arsenate Uptake by Rice Plants and Inorganic Arsenic Accumulation in Rice Grains. *Environ. Sci. Technol.* **51**, 12131–12138 (2017).

56. DiTusa, S. F. *et al.* A member of the Phosphate transporter 1 (Pht1) family from the arsenic-hyperaccumulating fern *Pteris vittata* is a high-affinity arsenate transporter. *New Phytol.* **209**, 762–772 (2016).

57. Willsky, G. R., Bennett, R. L. & Malamy, M. H. Inorganic Phosphate Transport in *Escherichia coli* : Involvement of Two Genes Which Play a Role in Alkaline Phosphatase Regulation. *J. Bacteriol.* **113**, 529–539 (1973).

58. Willsky, G. R. & Malamy, M. H. Effect of arsenate on inorganic phosphate transport in Escherichia coli. *J. Bacteriol.* **144**, 366–374 (1980).

59. Shen, M. W. Y., Shah, D., Chen, W. & Da Silva, N. Enhanced arsenate uptake in Saccharomyces cerevisiae overexpressing the Pho84 phosphate transporter. *Biotechnol. Prog.* **28**, 654–661 (2012).

60. Planer-Friedrich, B. *et al.* Thioarsenate Toxicity and Tolerance in the Model System *Arabidopsis thaliana*. *Environ. Sci. Technol.* **51**, 7187–7196 (2017).

61. Liu, Z., Boles, E. & Rosen, B. P. Arsenic Trioxide Uptake by Hexose Permeases in Saccharomyces cerevisiae. *J. Biol. Chem.* **279**, 17312–17318 (2004).

62. Wysocki, R. *et al.* The glycerol channel Fps1p mediates the uptake of arsenite and antimonite in *Saccharomyces cerevisiae*. *Mol. Microbiol.* **40**, 1391–1401 (2001).

63. Boles, E. & Hollenberg, C. P. The molecular genetics of hexose transport in yeasts. *FEMS Microbiol. Rev.* **21**, 85–111 (1997).

64. Wieczorke, R. *et al.* Concurrent knock-out of at least 20 transporter genes is required to block uptake of hexoses in *Saccharomyces cerevisiae*. *FEBS Lett.* **464**, 123–128 (1999).

65. Jochem, M. *et al.* Targeted Degradation of Glucose Transporters Protects against Arsenic Toxicity. *Mol. Cell. Biol.* **39**, e00559-18 (2019).

66. Liu, Z. *et al.* Mammalian glucose permease GLUT1 facilitates transport of arsenic trioxide and methylarsonous acid. *Biochem. Biophys. Res. Commun.* **351**, 424–430 (2006).

67. Ali, R. *et al.* Altered Regulation of the Glucose Transporter GLUT3 in PRDX1 Null Cells Caused Hypersensitivity to Arsenite. *Cells* **12**, 2682 (2023).

68. Duan, G.-L. *et al.* Inositol transporters AtINT2 and AtINT4 regulate arsenic accumulation in Arabidopsis seeds. *Nat. Plants* **2**, 15202 (2016).

69. Zhao, F.-J., McGrath, S. P. & Meharg, A. A. Arsenic as a Food Chain Contaminant: Mechanisms of Plant Uptake and Metabolism and Mitigation Strategies. *Annu. Rev. Plant Biol.* **61**, 535–559 (2010).

70. Liu, Z., Carbrey, J. M., Agre, P. & Rosen, B. P. Arsenic trioxide uptake by human and rat aquaglyceroporins. *Biochem. Biophys. Res. Commun.* **316**, 1178–1185 (2004).

71. Meng, Y.-L., Liu, Z. & Rosen, B. P. As(III) and Sb(III) Uptake by GlpF and Efflux by ArsB in Escherichia coli. *J. Biol. Chem.* **279**, 18334–18341 (2004).

72. Mitani, N., Yamaji, N. & Ma, J. F. Characterization of substrate specificity of a rice silicon transporter, Lsi1. *Pflüg. Arch. - Eur. J. Physiol.* **456**, 679–686 (2008).

73. Ma, J. F. *et al.* Transporters of arsenite in rice and their role in arsenic accumulation in rice grain. *Proc. Natl. Acad. Sci.* **105**, 9931–9935 (2008).

74. Ma, J. F. *et al.* An efflux transporter of silicon in rice. *Nature* **448**, 209–212 (2007).

75. Lomax, C. *et al.* Methylated arsenic species in plants originate from soil microorganisms. *New Phytol.* **193**, 665–672 (2012).

76. Arao, T., Kawasaki, A., Baba, K., Mori, S. & Matsumoto, S. Effects of Water Management on Cadmium and Arsenic Accumulation and Dimethylarsinic Acid Concentrations in Japanese Rice. *Environ. Sci. Technol.* **43**, 9361–9367 (2009).

77. Li, R.-Y. *et al.* The Rice Aquaporin Lsi1 Mediates Uptake of Methylated Arsenic Species. *Plant Physiol.* **150**, 2071–2080 (2009).

78. McDermott, J. R., Jiang, X., Beene, L. C., Rosen, B. P. & Liu, Z. Pentavalent methylated arsenicals are substrates of human AQP9. *BioMetals* **23**, 119–127 (2010).

79. Tang, Z., Chen, Y., Chen, F., Ji, Y. & Zhao, F.-J. OsPTR7 (OsNPF8.1), a Putative Peptide Transporter in Rice, is Involved in Dimethylarsenate Accumulation in Rice Grain. *Plant Cell Physiol.* **58**, 904–913 (2017).

80. Tang, Z., Kang, Y., Wang, P. & Zhao, F.-J. Phytotoxicity and detoxification mechanism differ among inorganic and methylated arsenic species in Arabidopsis thaliana. *Plant Soil* **401**, 243–257 (2016).

81. Pischke, E. *et al.* Dimethylmonothioarsenate Is Highly Toxic for Plants and Readily Translocated to Shoots. *Environ. Sci. Technol.* **56**, 10072–10083 (2022).

82. Wang, Y.-J., Dong, C.-Y., Tang, Z. & Zhao, F.-J. Translocation, enzymatic reduction and toxicity of dimethylarsenate in rice. *Plant Physiol. Biochem.* **207**, 108393 (2024).

83. Kerl, C. F. *et al.* Methylated Thioarsenates and Monothioarsenate Differ in Uptake, Transformation, and Contribution to Total Arsenic Translocation in Rice Plants. *Environ. Sci. Technol.* **53**, 5787–5796 (2019).

84. Colina Blanco, A. E. *et al. In Planta* Arsenic Thiolation in Rice and *Arabidopsis thaliana*. *Environ. Sci. Technol.* **57**, 21846–21854 (2023).

85. Cullen, W. R. *et al.* Methylated and thiolated arsenic species for environmental and health research — A review on synthesis and characterization. *J. Environ. Sci.* **49**, 7–27 (2016).

86. Mukhopadhyay, R. & Rosen, B. P. Arsenate Reductases in Prokaryotes and Eukaryotes. *Environ. Health Perspect.* **110**, 745–748 (2002).

87. Silver, S. & Phung, L. T. Genes and Enzymes Involved in Bacterial Oxidation and Reduction of Inorganic Arsenic. *Appl. Environ. Microbiol.* **71**, 599–608 (2005).

88. Williams, R. J. . P. & Fraústo Da Silva, J. J. R. Evolution was Chemically Constrained. *J. Theor. Biol.* **220**, 323–343 (2003).

89. Anbar, A. D. Elements and Evolution. *Science* **322**, 1481–1483 (2008).

90. Zhu, Y.-G., Yoshinaga, M., Zhao, F.-J. & Rosen, B. P. Earth Abides Arsenic Biotransformations. *Annu. Rev. Earth Planet. Sci.* **42**, 443–467 (2014).

91. Holland, H. D. The oxygenation of the atmosphere and oceans. *Philos. Trans. R. Soc. B Biol. Sci.* **361**, 903–915 (2006).

92. Chen, S.-C. *et al.* The Great Oxidation Event expanded the genetic repertoire of arsenic metabolism and cycling. *Proc. Natl. Acad. Sci.* **117**, 10414–10421 (2020).

93. Chen, G. *et al.* Reconstructing Earth's atmospheric oxygenation history using machine learning. *Nat. Commun.* **13**, 5862 (2022).

94. Allen, J. F., Thake, B. & Martin, W. F. Nitrogenase Inhibition Limited Oxygenation of Earth's Proterozoic Atmosphere. *Trends Plant Sci.* **24**, 1022–1031 (2019).

95. Ben Fekih, I. *et al.* Distribution of Arsenic Resistance Genes in Prokaryotes. *Front. Microbiol.* **9**, 2473 (2018).

96. Palmgren, M. *et al.* AS3MT-mediated tolerance to arsenic evolved by multiple independent horizontal gene transfers from bacteria to eukaryotes. *PLOS ONE* **12**, e0175422 (2017).

97. Inskeep, W. P. *et al.* Detection, diversity and expression of aerobic bacterial arsenite oxidase genes. *Environ. Microbiol.* **9**, 934–943 (2007).

98. Clemens, S. Evolution and function of phytochelatin synthases. *J. Plant Physiol.* **163**, 319–332 (2006).

99. Li, M. *et al.* Evolution and functional differentiation of recently diverged phytochelatin synthase genes from Arundo donax L. *J. Exp. Bot.* **70**, 5391–5405 (2019).

100. Sheehan, D., Meade, G., Foley, V. M. & Dowd, C. A. Structure, function and evolution of glutathione transferases: implications for classification of non-mammalian members of an ancient enzyme superfamily. *Biochem. J.* **360**, 1–16 (2001).

101. Ghosh, M., Shen, J. & Rosen, B. P. Pathways of As(III) detoxification in *Saccharomyces cerevisiae*. *Proc. Natl. Acad. Sci.* **96**, 5001–5006 (1999).

102. Mukhopadhyay, R., Rosen, B. P., Phung, L. T. & Silver, S. Microbial arsenic: from geocycles to genes and enzymes. *FEMS Microbiol. Rev.* **26**, 311–325 (2002).

103. Saltikov, C. W. & Newman, D. K. Genetic identification of a respiratory arsenate reductase. *Proc. Natl. Acad. Sci.* **100**, 10983–10988 (2003).

104. Zhang, P. *et al.* Arsenite oxidation and (thio)arsenates formation in arsenite- and sulfide-containing solution under air atmosphere. *Appl. Geochem.* **142**, 105344 (2022).

105. Rehman, K. *et al.* Trivalent methylated arsenic metabolites induce apoptosis in human myeloid leukemic HL-60 cells through generation of reactive oxygen species. *Metallomics* **6**, 1502–1512 (2014).

106. Chen, S.-C. *et al.* Recurrent horizontal transfer of arsenite methyltransferase genes facilitated adaptation of life to arsenic. *Sci. Rep.* **7**, 7741 (2017).

107. Carey, A. *et al.* Phloem transport of arsenic species from flag leaf to grain during grain filling. *New Phytol.* **192**, 87–98 (2011).

108. Li, J., Pawitwar, S. S. & Rosen, B. P. The organoarsenical biocycle and the primordial antibiotic methylarsenite. *Metallomics* **8**, 1047–1055 (2016).

109. Yoshinaga, M., Cai, Y. & Rosen, B. P. Demethylation of methylarsonic acid by a microbial community. *Environ. Microbiol.* **13**, 1205–1215 (2011).

110. Gao, A.-X. *et al.* Soil redox status governs within-field spatial variation in microbial arsenic methylation and rice straighthead disease. *ISME J.* **18**, wrae057 (2024).

111. Xu, X. Y., McGrath, S. P. & Zhao, F. J. Rapid reduction of arsenate in the medium mediated by plant roots. *New Phytol.* **176**, 590–599 (2007).

112. Zhao, F. *et al.* The role of the rice aquaporin Lsi1 in arsenite efflux from roots. *New Phytol.* **186**, 392–399 (2010).

113. Duan, G., Kamiya, T., Ishikawa, S., Arao, T. & Fujiwara, T. Expressing ScACR3 in Rice Enhanced Arsenite Efflux and Reduced Arsenic Accumulation in Rice Grains. *Plant Cell Physiol.* **53**, 154–163 (2012).

114. Wysocki, R. & Tamás, M. J. How *Saccharomyces cerevisiae* copes with toxic metals and metalloids. *FEMS Microbiol. Rev.* **34**, 925–951 (2010).

115. Chen, J. & Rosen, B. P. The Arsenic Methylation Cycle: How Microbial Communities Adapted Methylarsenicals for Use as Weapons in the Continuing War for Dominance. *Front. Environ. Sci.* **8**, 43 (2020).

116. Chen, J., Bhattacharjee, H. & Rosen, B. P. ArsH is an organoarsenical oxidase that confers resistance to trivalent forms of the herbicide monosodium methylarsenate and the poultry growth promoter roxarsone. *Mol. Microbiol.* **96**, 1042–1052 (2015).

117. Rensing, C. & Rosen, B. P. Heavy Metals Cycle (Arsenic, Mercury, Selenium, others). in *Encyclopedia of Microbiology* 205–219 (Elsevier, 2009). doi:10.1016/B978-012373944-5.00053-5.

118. Messens, J. *et al.* All intermediates of the arsenate reductase mechanism, including an intramolecular dynamic disulfide cascade. *Proc. Natl. Acad. Sci.* **99**, 8506–8511 (2002).

119. Mukhopadhyay, R. & Rosen, B. P. *Saccharomyces cerevisiae ACR2* gene encodes an arsenate reductase. *FEMS Microbiol. Lett.* **168**, 127–136 (1998).

120. Sánchez-Bermejo, E. *et al.* Natural variation in arsenate tolerance identifies an arsenate reductase in Arabidopsis thaliana. *Nat. Commun.* **5**, 4617 (2014).

121. Xu, J. *et al.* OsHAC4 is critical for arsenate tolerance and regulates arsenic accumulation in rice. *New Phytol.* **215**, 1090–1101 (2017).

122. Yang, H.-C., Fu, H.-L., Lin, Y.-F. & Rosen, B. P. Pathways of Arsenic Uptake and Efflux. in *Current Topics in Membranes* vol. 69 325–358 (Elsevier, 2012).

123. Liu, W.-J. *et al.* Complexation of arsenite with phytochelatins reduces arsenite efflux and translocation from roots to shoots in Arabidopsis. *Plant Physiol.* **152**, 2211–2221 (2010).

124. Farooq, M. A. *et al.* Arsenic toxicity in plants: Cellular and molecular mechanisms of its transport and metabolism. *Environ. Exp. Bot.* **132**, 42–52 (2016).

125. Muller, D., Lièvremont, D., Simeonova, D. D., Hubert, J.-C. & Lett, M.-C. Arsenite Oxidase *aox* Genes from a Metal-Resistant β-Proteobacterium. *J. Bacteriol.* **185**, 135–141 (2003).

126. Santini, J. M., Sly, L. I., Schnagl, R. D. & Macy, J. M. A New Chemolithoautotrophic Arsenite-Oxidizing Bacterium Isolated from a Gold Mine: Phylogenetic, Physiological, and Preliminary Biochemical Studies. *Appl. Environ. Microbiol.* **66**, 92–97 (2000).

127. Vanden Hoven, R. N. & Santini, J. M. Arsenite oxidation by the heterotroph Hydrogenophaga sp. str. NT-14: the arsenite oxidase and its physiological electron acceptor. *Biochim. Biophys. Acta BBA - Bioenerg.* **1656**, 148–155 (2004).

128. Schmöger, M. E. V., Oven, M. & Grill, E. Detoxification of Arsenic by Phytochelatins in Plants. *Plant Physiol.* **122**, 793–802 (2000).

129. Cobbett, C. & Goldsbrough, P. P HYTOCHELATINS AND M ETALLOTHIONEINS : Roles in Heavy Metal Detoxification and Homeostasis. *Annu. Rev. Plant Biol.* **53**, 159–182 (2002).

130. Qi, Z., Wang, Q., Wang, H. & Tan, M. Metallothionein Attenuated Arsenic-Induced Cytotoxicity: The Underlying Mechanism Reflected by Metabolomics and Lipidomics. *J. Agric. Food Chem.* **69**, 5372–5380 (2021).

131. Adeoye, O., Olawumi, J., Opeyemi, A. & Christiania, O. Review on the role of glutathione on oxidative stress and infertility. *JBRA Assist. Reprod.* (2017) doi:10.5935/1518-0557.20180003.

132. Dorion, S., Ouellet, J. C. & Rivoal, J. Glutathione Metabolism in Plants under Stress: Beyond Reactive Oxygen Species Detoxification. *Metabolites* **11**, 641 (2021).

133. Gipp, J. J., Chang, C. & Timothy Mulcahy, R. Cloning and nucleotide sequence of a full-length cDNA for human liver γ-glutamylcysteine synthetase. *Biochem. Biophys. Res. Commun.* **185**, 29–35 (1992).

134. Diaz Vivancos, P., Wolff, T., Markovic, J., Pallardó, F. V. & Foyer, C. H. A nuclear glutathione cycle within the cell cycle. *Biochem. J.* **431**, 169–178 (2010).

135. Fahey, R. C. Glutathione analogs in prokaryotes. *Biochim. Biophys. Acta BBA - Gen. Subj.* **1830**, 3182–3198 (2013).

136. Zimdars, S., Schrage, L., Sommer, S., Schieber, A. & Weber, F. Influence of Glutathione on Yeast Fermentation Efficiency under Copper Stress. *J. Agric. Food Chem.* **67**, 10913–10920 (2019).

137. Noctor, G. Interactions between biosynthesis, compartmentation and transport in the control of glutathione homeostasis and signalling. *J. Exp. Bot.* **53**, 1283–1304 (2002).

138. Michelet, L., Zaffagnini, M. & Lemaire, D. Thioredoxins and Related Proteins. in *The Chlamydomonas Sourcebook* 401–443 (Elsevier, 2009). doi:10.1016/B978-0-12-370873-1.00019-8.

139. Mir, R. A. & Khah, M. A. Recent progress in enzymatic antioxidant defense system in plants against different environmental stresses. in *Improving Stress Resilience in Plants* 203–224 (Elsevier, 2024). doi:10.1016/B978-0-443-18927-2.00014-5.

140. Mhamdi, A. *et al.* Arabidopsis GLUTATHIONE REDUCTASE1 Plays a Crucial Role in Leaf Responses to Intracellular Hydrogen Peroxide and in Ensuring Appropriate Gene Expression through Both Salicylic Acid and Jasmonic Acid Signaling Pathways. *Plant Physiol.* **153**, 1144–1160 (2010).

141. Wu, G., Lupton, J. R., Turner, N. D., Fang, Y.-Z. & Yang, S. Glutathione Metabolism and Its Implications for Health. *J. Nutr.* **134**, 489–492 (2004).

142. Meister, A. Glutathione metabolism and its selective modification. *J. Biol. Chem.* **263**, 17205–17208 (1988).

143. Bachhawat, A. K. & Yadav, S. The glutathione cycle: Glutathione metabolism beyond the γ-glutamyl cycle. *IUBMB Life* **70**, 585–592 (2018).

144. Meister, A. & Anderson, M. E. GLUTATHIONE. *Annu. Rev. Biochem.* **52**, 711–760 (1983).

145. Penninckx, M. An overview on glutathione in versus non-conventional yeasts. *FEMS Yeast Res.* **2**, 295–305 (2002).

146. Lu, S. C. Glutathione synthesis. *Biochim. Biophys. Acta BBA - Gen. Subj.* **1830**, 3143–3153 (2013).

147. Ribas, V., GarcÃ-a-Ruiz, C. & FernÃ¡ndez-Checa, J. C. Glutathione and mitochondria. *Front. Pharmacol.* **5**, (2014).

148. Zechmann, B. Subcellular Roles of Glutathione in Mediating Plant Defense during Biotic Stress. *Plants* **9**, 1067 (2020).

149. Wachter, A., Wolf, S., Steininger, H., Bogs, J. & Rausch, T. Differential targeting of GSH1 and GSH2 is achieved by multiple transcription initiation: implications for the compartmentation of glutathione biosynthesis in the *Brassicaceae*. *Plant J.* **41**, 15–30 (2005).

150. Pasternak, M. *et al.* Restricting glutathione biosynthesis to the cytosol is sufficient for normal plant development. *Plant J.* **53**, 999–1012 (2008).

151. Cairns, N. G., Pasternak, M., Wachter, A., Cobbett, C. S. & Meyer, A. J. Maturation of Arabidopsis Seeds Is Dependent on Glutathione Biosynthesis within the Embryo. *Plant Physiol.* **141**, 446–455 (2006).

152. Winkler, A. *et al.* Glutathione is essential for early embryogenesis – Analysis of a glutathione synthetase knockout mouse. *Biochem. Biophys. Res. Commun.* **412**, 121–126 (2011).

153. Lei, X. G. *et al.* Paradoxical Roles of Antioxidant Enzymes: Basic Mechanisms and Health Implications. *Physiol. Rev.* **96**, 307–364 (2016).

154. Bagiyan, G. A., Koroleva, I. K., Soroka, N. V. & Ufimtsev, A. V. Oxidation of thiol compounds by molecular oxygen in aqueous solutions. *Russ. Chem. Bull.* **52**, 1135–1141 (2003).

155. Held, K. D. & Biaglow, J. E. Mechanisms for the oxygen radical-mediated toxicity of various thiol-containing compounds in cultured mammalian cells. *Radiat. Res.* **139**, 15–23 (1994).

156. Summers, A. O. Damage control: regulating defenses against toxic metals and metalloids. *Curr. Opin. Microbiol.* **12**, 138–144 (2009).

157. Baba, S. P. & Bhatnagar, A. ROLE OF THIOLS IN OXIDATIVE STRESS. *Curr. Opin. Toxicol.* **7**, 133–139 (2018).

158. Jozefczak, M., Remans, T., Vangronsveld, J. & Cuypers, A. Glutathione is a key player in metal-induced oxidative stress defenses. *Int. J. Mol. Sci.* **13**, 3145–3175 (2012).

159. Clemens, S., Schroeder, J. I. & Degenkolb, T. *Caenorhabditis elegans* expresses a functional phytochelatin synthase. *Eur. J. Biochem.* **268**, 3640–3643 (2001).

160. Clemens, S., Kim, E. J., Neumann, D. & Schroeder, J. I. Tolerance to toxic metals by a gene family of phytochelatin synthases from plants and yeast. *EMBO J.* **18**, 3325–3333 (1999).

161. Ahner, B. A. & Morel, F. M. M. Phytochelatin production in marine algae. 2. Induction by various metals. *Limnol. Oceanogr.* **40**, 658–665 (1995).

162. Grill, E., Löffler, S., Winnacker, E. L. & Zenk, M. H. Phytochelatins, the heavy-metal-binding peptides of plants, are synthesized from glutathione by a specific gamma-glutamylcysteine dipeptidyl transpeptidase (phytochelatin synthase). *Proc. Natl. Acad. Sci. U. S. A.* **86**, 6838–6842 (1989).

163. Cobbett, C. S. Phytochelatins and Their Roles in Heavy Metal Detoxification. *Plant Physiol.* **123**, 825–832 (2000).

164. Vatamaniuk, O. K., Mari, S., Lu, Y.-P. & Rea, P. A. Mechanism of Heavy Metal Ion Activation of Phytochelatin (PC) Synthase. *J. Biol. Chem.* **275**, 31451–31459 (2000).

165. Oven, M., Page, J. E., Zenk, M. H. & Kutchan, T. M. Molecular Characterization of the Homo-phytochelatin Synthase of Soybean Glycine max. *J. Biol. Chem.* **277**, 4747–4754 (2002).

166. Maitani, T., Kubota, H., Sato, K. & Yamada, T. The Composition of Metals Bound to Class III Metallothionein (Phytochelatin and Its Desglycyl Peptide) Induced by Various Metals in Root Cultures of Rubia tinctorum. *Plant Physiol.* **110**, 1145–1150 (1996).

167. Howden, R., Goldsbrough, P. B., Andersen, C. R. & Cobbett, C. S. Cadmium-Sensitive, cad1 Mutants of Arabidopsis thaliana Are Phytochelatin Deficient. *Plant Physiol.* **107**, 1059–1066 (1995).

168. Loeffler, S., Hochberger, A., Grill, E., Winnacker, E.-L. & Zenk, M. H. Termination of the phytochelatin synthase reaction through sequestration of heavy metals by the reaction product. *FEBS Lett.* **258**, 42–46 (1989).

169. Chen, J., Zhou, J. & Goldsbrough, P. B. Characterization of phytochelatin synthase from tomato. *Physiol. Plant.* **101**, 165–172 (1997).

170. Uraguchi, S. *et al.* Phytochelatin Synthase has Contrasting Effects on Cadmium and Arsenic Accumulation in Rice Grains. *Plant Cell Physiol.* **58**, 1730–1742 (2017).

171. Hayashi, S. *et al.* Phytochelatin synthase Os PCS 1 plays a crucial role in reducing arsenic levels in rice grains. *Plant J.* **91**, 840–848 (2017).

172. Olsson, S. *et al.* Horizontal Gene Transfer of Phytochelatin Synthases from Bacteria to Extremophilic Green Algae. *Microb. Ecol.* **73**, 50–60 (2017).

173. Keeling, P. J. & Palmer, J. D. Horizontal gene transfer in eukaryotic evolution. *Nat. Rev. Genet.* **9**, 605–618 (2008).

174. Richards, T. A. *et al.* Phylogenomic Analysis Demonstrates a Pattern of Rare and Ancient Horizontal Gene Transfer between Plants and Fungi. *Plant Cell* **21**, 1897–1911 (2009).

175. Fru, E. C. *et al.* The rise of oxygen-driven arsenic cycling at ca. 2.48 Ga. *Geology* **47**, 243–246 (2019).

176. Carapito, C. *et al.* Identification of genes and proteins involved in the pleiotropic response to arsenic stress in Caenibacter arsenoxydans, a metalloresistant beta-proteobacterium with an unsequenced genome. *Biochimie* **88**, 595–606 (2006).

177. Zhang, S.-Y. *et al.* High arsenic levels increase activity rather than diversity or abundance of arsenic metabolism genes in paddy soils. Preprint at https://doi.org/10.1101/2021.05.03.442544 (2021).

178. Hrimpeng, K. *et al.* Challenging *Xanthomonas campestris* with low levels of arsenic mediates cross-protection against oxidant killing. *FEMS Microbiol. Lett.* **262**, 121–127 (2006).

179. Kaur, A., Rana, R., Saroha, T. & Patil, P. B. Discerning the role of a functional arsenic-resistance cassette in the evolution and adaptation of a rice pathogen. *Microb. Genomics* **7**, (2021).

180. Ribeiro, G. M. & Lahr, D. J. G. A comparative study indicates vertical inheritance and horizontal gene transfer of arsenic resistance-related genes in eukaryotes. *Mol. Phylogenet. Evol.* **173**, 107479 (2022).

181. Zhao, F. J., Ma, J. F., Meharg, A. A. & McGrath, S. P. Arsenic uptake and metabolism in plants. *New Phytol.* **181**, 777–794 (2009).

182. Danh, L. T., Truong, P., Mammucari, R. & Foster, N. A Critical Review of the Arsenic Uptake Mechanisms and Phytoremediation Potential of *Pteris vittata*. *Int. J. Phytoremediation* **16**, 429–453 (2014).

183. Dolphen, R. & Thiravetyan, P. Reducing arsenic in rice grains by leonardite and arsenic–resistant endophytic bacteria. *Chemosphere* **223**, 448–454 (2019).

184. Srivastava, M., Ma, L. Q., Singh, N. & Singh, S. Antioxidant responses of hyper-accumulator and sensitive fern species to arsenic. *J. Exp. Bot.* **56**, 1335–1342 (2005).

185. Singh, N. & Ma, L. Q. Arsenic speciation, and arsenic and phosphate distribution in arsenic hyperaccumulator Pteris vittata L. and non-hyperaccumulator Pteris ensiformis L. *Environ. Pollut.* **141**, 238–246 (2006).

186. Singh, N., Ma, L. Q., Srivastava, M. & Rathinasabapathi, B. Metabolic adaptations to arsenic-induced oxidative stress in Pteris vittata L and Pteris ensiformis L. *Plant Sci.* **170**, 274–282 (2006).

187. Su, Y. H., McGrath, S. P., Zhu, Y. G. & Zhao, F. J. Highly efficient xylem transport of arsenite in the arsenic hyperaccumulator Pteris vittata. *New Phytol.* **180**, 434–441 (2008).

188. Sakai, Y. *et al.* Influence of arsenic stress on synthesis and localization of low-molecular-weight thiols in Pteris vittata. *Environ. Pollut.* **158**, 3663–3669 (2010).

189. Dutton, J. & Fisher, N. S. Bioaccumulation of As, Cd, Cr, Hg(II), and MeHg in killifish (Fundulus heteroclitus) from amphipod and worm prey. *Sci. Total Environ.* **409**, 3438–3447 (2011).

190. Jung, D. *et al.* A Novel Aquaporin 3 in Killifish (Fundulus heteroclitus) Is Not An Arsenic Channel. *Toxicol. Sci.* **127**, 101–109 (2012).

191. Jung, D. *et al.* A novel variant of aquaporin 3 is expressed in killifish (Fundulus heteroclitus) intestine. *Comp. Biochem. Physiol. Part C Toxicol. Pharmacol.* **171**, 1–7 (2015).

192. Altenhoff, A. M. *et al.* OMA orthology in 2024: improved prokaryote coverage, ancestral and extant GO enrichment, a revamped synteny viewer and more in the OMA Ecosystem. *Nucleic Acids Res.* **52**, D513–D521 (2024).

193. Bardou, P., Mariette, J., Escudié, F., Djemiel, C. & Klopp, C. jvenn: an interactive Venn diagram viewer. *BMC Bioinformatics* **15**, 293 (2014).

194. Wysocki, R. *et al.* Metalloid tolerance based on phytochelatins is not functionally equivalent to the arsenite transporter Acr3p. *Biochem. Biophys. Res. Commun.* **304**, 293–300 (2003).

195. Lee, S. *et al.* Overexpression of Arabidopsis Phytochelatin Synthase Paradoxically Leads to Hypersensitivity to Cadmium Stress. *Plant Physiol.* **131**, 656–663 (2003).

196. Wysocki, R., Bobrowicz, P. & Ułaszewski, S. The Saccharomyces cerevisiae ACR3 Gene Encodes a Putative Membrane Protein Involved in Arsenite Transport. *J. Biol. Chem.* **272**, 30061–30066 (1997).

197. Tang, Z. *et al.* Arsenic Methylation in Arabidopsis thaliana Expressing an Algal Arsenite Methyltransferase Gene Increases Arsenic Phytotoxicity. *J. Agric. Food Chem.* **64**, 2674–2681 (2016).

198. Zhou, X. *et al.* A genome-wide screen in Saccharomyces cerevisiae reveals pathways affected by arsenic toxicity. *Genomics* **94**, 294–307 (2009).

199. Wysocki, R. & Tamás, M. J. Saccharomyces cerevisiae as a Model Organism for Elucidating Arsenic Tolerance Mechanisms. in *Cellular Effects of Heavy Metals* (ed. Banfalvi, G.) 87–112 (Springer Netherlands, Dordrecht, 2011). doi:10.1007/978-94-007-0428-2_4.

200. Sipiczki, M. Where does fission yeast sit on the tree of life? *Genome Biol.* **1**, reviews1011.1 (2000).

201. Clemens, S. & Simm, C. *Schizosaccharomyces pombe* as a model for metal homeostasis in plant cells: the phytochelatin-dependent pathway is the main cadmium detoxification mechanism. *New Phytol.* **159**, 323–330 (2003).

202. Bustos, R. *et al.* A Central Regulatory System Largely Controls Transcriptional Activation and Repression Responses to Phosphate Starvation in Arabidopsis. *PLoS Genet.* **6**, e1001102 (2010).

203. Grant, S. G., Jessee, J., Bloom, F. R. & Hanahan, D. Differential plasmid rescue from transgenic mouse DNAs into Escherichia coli methylation-restriction mutants. *Proc. Natl. Acad. Sci. U. S. A.* **87**, 4645–4649 (1990).

204. Carlin, A., Shi, W., Dey, S. & Rosen, B. P. The ars operon of Escherichia coli confers arsenical and antimonial resistance. *J. Bacteriol.* **177**, 981–986 (1995).

205. Brachmann, C. B. *et al.* Designer deletion strains derived from Saccharomyces cerevisiae S288C: a useful set of strains and plasmids for PCR-mediated gene disruption and other applications. *Yeast Chichester Engl.* **14**, 115–132 (1998).

206. Winzeler, E. A. *et al.* Functional Characterization of the *S. cerevisiae* Genome by Gene Deletion and Parallel Analysis. *Science* **285**, 901–906 (1999).

207. Giaever, G. *et al.* Functional profiling of the Saccharomyces cerevisiae genome. *Nature* **418**, 387–391 (2002).

208. Entian, K.-D. & Kötter, P. 25 Yeast Genetic Strain and Plasmid Collections. in *Methods in Microbiology* vol. 36 629–666 (Elsevier, 2007).

209. Liu, Z. *et al.* Arsenite transport by mammalian aquaglyceroporins AQP7 and AQP9. *Proc. Natl. Acad. Sci.* **99**, 6053–6058 (2002).

210. Torres-Garcia, S. *et al.* SpEDIT: A fast and efficient CRISPR/Cas9 method for fission yeast. *Wellcome Open Res.* **5**, 274 (2020).

211. Spirek, M. *et al. S. pombe* genome deletion project: An update. *Cell Cycle* **9**, 2399–2402 (2010).

212. Prins, R. C. & Billerbeck, S. A buffered media system for yeast batch culture growth. *BMC Microbiol.* **21**, 127 (2021).

213. Estelle, M. A. & Somerville, C. Auxin-resistant mutants of Arabidopsis thaliana with an altered morphology. *Mol. Gen. Genet. MGG* **206**, 200–206 (1987).

214. Clemens, S., Antosiewicz, D. M., Ward, J. M., Schachtman, D. P. & Schroeder, J. I. The plant cDNA *LCT1* mediates the uptake of calcium and cadmium in yeast. *Proc. Natl. Acad. Sci.* **95**, 12043–12048 (1998).

215. Ticconi, C. A., Delatorre, C. A. & Abel, S. Attenuation of Phosphate Starvation Responses by Phosphite in Arabidopsis. *Plant Physiol.* **127**, 963–972 (2001).

216. *Experimental Phycology: A Laboratory Manual*. (Cambridge University Press, Cambridge ; New York, 1988).

217. Li, H., He, K., Zhang, Z. & Hu, Y. Molecular mechanism of phosphorous signaling inducing anthocyanin accumulation in Arabidopsis. *Plant Physiol. Biochem.* **196**, 121–129 (2023).

218. Orr-Weaver, T. L., Szostak, J. W. & Rothstein, R. J. Yeast transformation: a model system for the study of recombination. *Proc. Natl. Acad. Sci.* **78**, 6354–6358 (1981).

219. Jansen, G., Wu, C., Schade, B., Thomas, D. Y. & Whiteway, M. Drag&Drop cloning in yeast. *Gene* **344**, 43–51 (2005).

220. Adamis, P. D. B. *et al.* Lap4, a vacuolar aminopeptidase I, is involved in cadmium-glutathione metabolism. *Biometals Int. J. Role Met. Ions Biol. Biochem. Med.* **22**, 243–249 (2009).

221. Smith, P. K. *et al.* Measurement of protein using bicinchoninic acid. *Anal. Biochem.* **150**, 76–85 (1985).

222. Wallschläger, D. & London, J. Determination of Methylated Arsenic-Sulfur Compounds in Groundwater. *Environ. Sci. Technol.* **42**, 228–234 (2008).

223. Fischer, S., Kühnlenz, T., Thieme, M., Schmidt, H. & Clemens, S. Analysis of Plant Pb Tolerance at Realistic Submicromolar Concentrations Demonstrates the Role of Phytochelatin Synthesis for Pb Detoxification. *Environ. Sci. Technol.* **48**, 7552–7559 (2014).

224. Jumper, J. *et al.* Highly accurate protein structure prediction with AlphaFold. *Nature* **596**, 583–589 (2021).

225. Varadi, M. *et al.* AlphaFold Protein Structure Database in 2024: providing structure coverage for over 214 million protein sequences. *Nucleic Acids Res.* **52**, D368–D375 (2024).

226. Ayadi, A. *et al.* Reducing the genetic redundancy of Arabidopsis PHOSPHATE TRANSPORTER1 transporters to study phosphate uptake and signaling. *Plant Physiol.* **167**, 1511–1526 (2015).

227. Bari, R., Datt Pant, B., Stitt, M. & Scheible, W.-R. PHO2, MicroRNA399, and PHR1 Define a Phosphate-Signaling Pathway in Plants. *Plant Physiol.* **141**, 988–999 (2006).

228. Wang, Z., Zheng, Z. & Liu, D. Comparative functional analyses of PHR1, PHL1, and PHL4 transcription factors in regulating Arabidopsis responses to phosphate starvation. *Front. Plant Sci.* **15**, 1379562 (2024).

229. Raml, R., Goessler, W. & Francesconi, K. A. Improved chromatographic separation of thio-arsenic compounds by reversed-phase high performance liquid chromatography-inductively coupled plasma mass spectrometry. *J. Chromatogr. A* **1128**, 164–170 (2006).

230. Liamtsau, V., Fan, C., Liu, G., McGoron, A. J. & Cai, Y. Speciation of thioarsenicals through application of coffee ring effect on gold nanofilm and surface-enhanced Raman spectroscopy. *Anal. Chim. Acta* **1106**, 88–95 (2020).

231. Maciaszczyk-Dziubinska, E., Migdal, I., Migocka, M., Bocer, T. & Wysocki, R. The yeast aquaglyceroporin Fps1p is a bidirectional arsenite channel. *FEBS Lett.* **584**, 726–732 (2010).

232. Ouyang, J. *et al.* Identification and analysis of eight peptide transporter homologs in rice. *Plant Sci.* **179**, 374–382 (2010).

233. Léran, S. *et al.* A unified nomenclature of NITRATE TRANSPORTER 1/PEPTIDE TRANSPORTER family members in plants. *Trends Plant Sci.* **19**, 5–9 (2014).

234. Cao, Y. *et al.* Phosphate Transporter PvPht1;2 Enhances Phosphorus Accumulation and Plant Growth without Impacting Arsenic Uptake in Plants. *Environ. Sci. Technol.* **52**, 3975–3981 (2018).

235. Torres-Garcia, S. *et al.* Epigenetic gene silencing by heterochromatin primes fungal resistance. *Nature* **585**, 453–458 (2020).

236. Kim, D.-U. *et al.* Analysis of a genome-wide set of gene deletions in the fission yeast Schizosaccharomyces pombe. *Nat. Biotechnol.* **28**, 617–623 (2010).

237. Harrison, C. *et al.* SCFPof1-ubiquitin and its target Zip1 transcription factor mediate cadmium response in fission yeast. *EMBO J.* **24**, 599–610 (2005).

238. Park, H.-J. *et al.* Characterization and regulation of the gamma-glutamyl transpeptidase gene from the fission yeast Schizosaccharomyces pombe. *Can. J. Microbiol.* **50**, 61–66 (2004).

239. Park, H.-J. *et al.* Characterization of a second gene encoding gamma-glutamyl transpeptidase from Schizosaccharomyces pombe. *Can. J. Microbiol.* **51**, 269–275 (2005).

240. Song, S.-H. & Lim, C.-J. Nitrogen depletion causes up-regulation of glutathione content and gamma-glutamyltranspeptidase in Schizosaccharomyces pombe. *J. Microbiol. Seoul Korea* **46**, 70–74 (2008).

241. Yang, P., Du, H., Hoffman, C. S. & Marcus, S. The phospholipase B homolog Plb1 is a mediator of osmotic stress response and of nutrient-dependent repression of sexual differentiation in the fission yeast Schizosaccharomyces pombe. *Mol. Genet. Genomics MGG* **269**, 116–125 (2003).

242. Hentges, P., Van Driessche, B., Tafforeau, L., Vandenhaute, J. & Carr, A. M. Three novel antibiotic marker cassettes for gene disruption and marker switching inSchizosaccharomyces pombe. *Yeast* **22**, 1013–1019 (2005).

243. Benko, Z. & Zhao, R. Y. Zeocin for Selection of BleMX6 Resistance in Fission Yeast. *BioTechniques* **51**, 57–60 (2011).

244. Kumar, C., Sharma, R. & Bachhawat, A. K. Utilization of glutathione as an exogenous sulfur source is independent of Î³-glutamyl transpeptidase in the yeast Saccharomyces cerevisiae: evidence for an alternative gluathione degradation pathway. *FEMS Microbiol. Lett.* **219**, 187–194 (2003).

245. Adamis, P. D. B., Mannarino, S. C. & Eleutherio, E. C. A. Glutathione and gamma-glutamyl transferases are involved in the formation of cadmium–glutathione complex. *FEBS Lett.* **583**, 1489–1492 (2009).

246. Matsuyama, A. *et al.* ORFeome cloning and global analysis of protein localization in the fission yeast Schizosaccharomyces pombe. *Nat. Biotechnol.* **24**, 841–847 (2006).

247. West, M. B. *et al.* Autocatalytic cleavage of human gamma-glutamyl transpeptidase is highly dependent on N-glycosylation at asparagine 95. *J. Biol. Chem.* **286**, 28876–28888 (2011).

248. Ródenas, R., Martínez, V., Nieves-Cordones, M. & Rubio, F. High External K+ Concentrations Impair Pi Nutrition, Induce the Phosphate Starvation Response, and Reduce Arsenic Toxicity in Arabidopsis Plants. *Int. J. Mol. Sci.* **20**, 2237 (2019).

249. Misson, J., Thibaud, M.-C., Bechtold, N., Raghothama, K. & Nussaume, L. Transcriptional regulation and functional properties of Arabidopsis Pht1;4, a high affinity transporter contributing greatly to phosphate uptake in phosphate deprived plants. *Plant Mol. Biol.* **55**, 727–741 (2004).

250. Ye, Q., Wang, H., Su, T., Wu, W.-H. & Chen, Y.-F. The Ubiquitin E3 Ligase PRU1 Regulates WRKY6 Degradation to Modulate Phosphate Homeostasis in Response to Low-Pi Stress in Arabidopsis. *Plant Cell* **30**, 1062–1076 (2018).

251. Wang, Y., Zhang, C., Zheng, Y. & Ge, Y. Phytochelatin synthesis in Dunaliella salina induced by arsenite and arsenate under various phosphate regimes. *Ecotoxicol. Environ. Saf.* **136**, 150–160 (2017).

252. Song, W.-Y. *et al.* Arsenic tolerance in *Arabidopsis* is mediated by two ABCC-type phytochelatin transporters. *Proc. Natl. Acad. Sci.* **107**, 21187–21192 (2010).

253. Rea, P. A., Vatamaniuk, O. K. & Rigden, D. J. Weeds, Worms, and More. Papain's Long-Lost Cousin, Phytochelatin Synthase. *Plant Physiol.* **136**, 2463–2474 (2004).

254. Fischer, S. *et al.* Targeted expression of the arsenate reductase HAC1 identifies cell type specificity of arsenic metabolism and transport in plant roots. *J. Exp. Bot.* **72**, 415–425 (2021).

255. Fischer, S. *et al.* Targeted expression of the arsenate reductase HAC1 identifies cell type specificity of arsenic metabolism and transport in plant roots. *J. Exp. Bot.* **72**, 415–425 (2021).

256. Kaur, S., Kamli, M. R. & Ali, A. Diversity of Arsenate Reductase Genes (arsC Genes) from Arsenic-Resistant Environmental Isolates of E. coli. *Curr. Microbiol.* **59**, 288–294 (2009).

257. Scott, N., Hatlelid, K. M., MacKenzie, N. E. & Carter, D. E. Reactions of arsenic(III) and arsenic(V) species with glutathione. *Chem. Res. Toxicol.* **6**, 102–106 (1993).

258. Gailer, J. & Lindner, W. On-column formation of arsenic–glutathione species detected by size-exclusion chromatography in conjunction with arsenic-specific detectors. *J. Chromatogr. B. Biomed. Sci. App.* **716**, 83–93 (1998).

259. Shi, S. *et al.* OsHAC1;1 and OsHAC1;2 Function as Arsenate Reductases and Regulate Arsenic Accumulation. *Plant Physiol.* **172**, 1708–1719 (2016).

260. Chao, D.-Y. *et al.* Genome-wide Association Mapping Identifies a New Arsenate Reductase Enzyme Critical for Limiting Arsenic Accumulation in Plants. *PLoS Biol.* **12**, e1002009 (2014).

261. Shi, J., Vlamis-Gardikas, A., Åslund, F., Holmgren, A. & Rosen, B. P. Reactivity of Glutaredoxins 1, 2, and 3 fromEscherichia coli Shows That Glutaredoxin 2 Is the Primary Hydrogen Donor to ArsC-catalyzed Arsenate Reduction. *J. Biol. Chem.* **274**, 36039–36042 (1999).

262. Mukhopadhyay, R., Shi, J. & Rosen, B. P. Purification and Characterization of Acr2p, the Saccharomyces cerevisiae Arsenate Reductase. *J. Biol. Chem.* **275**, 21149–21157 (2000).

263. Salgado, A. *et al.* Response to arsenate treatment in Schizosaccharomyces pombe and the role of its arsenate reductase activity. *PloS One* **7**, e43208 (2012).

264. Duan, G. *et al.* A CDC25 homologue from rice functions as an arsenate reductase. *New Phytol.* **174**, 311–321 (2007).

265. Liu, W. *et al.* Knocking Out ACR2 Does Not Affect Arsenic Redox Status in Arabidopsis thaliana: Implications for As Detoxification and Accumulation in Plants. *PLoS ONE* **7**, e42408 (2012).

266. Salt, D. E. Would the real arsenate reductase please stand up? *New Phytol.* **215**, 926–928 (2017).

267. Luikenhuis, S., Perrone, G., Dawes, I. W. & Grant, C. M. The yeast Saccharomyces cerevisiae contains two glutaredoxin genes that are required for protection against reactive oxygen species. *Mol. Biol. Cell* **9**, 1081–1091 (1998).

268. Couturier, J., Przybyla-Toscano, J., Roret, T., Didierjean, C. & Rouhier, N. The roles of glutaredoxins ligating Fe–S clusters: Sensing, transfer or repair functions? *Biochim. Biophys. Acta BBA - Mol. Cell Res.* **1853**, 1513–1527 (2015).

269. Holmgren, A. Thioredoxin and Glutaredoxin: General Aspects and Involvement in Redox Regulation. in *Regulation of Photosynthesis* (eds Aro, E.-M. & Andersson, B.) vol. 11 321–330 (Springer Netherlands, Dordrecht, 2001).

270. Couturier, J., Jacquot, J.-P. & Rouhier, N. Evolution and diversity of glutaredoxins in photosynthetic organisms. *Cell. Mol. Life Sci.* **66**, 2539–2557 (2009).

271. Serrano, R. Energy Requirements for Maltose Transport in Yeast. *Eur. J. Biochem.* **80**, 97–102 (1977).

272. Henderson, R. & Poolman, B. Proton-solute coupling mechanism of the maltose transporter from Saccharomyces cerevisiae. *Sci. Rep.* **7**, 14375 (2017).

273. Needleman, R. Control of maltase synthesis in yeast. *Mol. Microbiol.* **5**, 2079–2084 (1991).

274. De Kok, S. *et al.* Increasing free-energy (ATP) conservation in maltose-grown Saccharomyces cerevisiae by expression of a heterologous maltose phosphorylase. *Metab. Eng.* **13**, 518–526 (2011).

275. Jansen, M. L. A., De Winde, J. H. & Pronk, J. T. Hxt-Carrier-Mediated Glucose Efflux upon Exposure of *Saccharomyces cerevisiae* to Excess Maltose. *Appl. Environ. Microbiol.* **68**, 4259–4265 (2002).

276. Tamaki, H. Glucose-stimulated cAMP-protein kinase a pathway in yeast Saccharomyces cerevisiae. *J. Biosci. Bioeng.* **104**, 245–250 (2007).

277. Görner, W. *et al.* Nuclear localization of the C2H2 zinc finger protein Msn2p is regulated by stress and protein kinase A activity. *Genes Dev.* **12**, 586–597 (1998).

278. Rajvanshi, P. K., Arya, M. & Rajasekharan, R. The stress-regulatory transcription factors Msn2 and Msn4 regulate fatty acid oxidation in budding yeast. *J. Biol. Chem.* **292**, 18628–18643 (2017).

279. Vlahakis, A., Lopez Muniozguren, N. & Powers, T. Stress-response transcription factors Msn2 and Msn4 couple TORC2-Ypk1 signaling and mitochondrial respiration to ATG8 gene expression and autophagy. *Autophagy* **13**, 1804–1812 (2017).

280. Lin, X. The regulation of Saccharomyces cerevisiae Snf1 protein kinase on glucose utilization is in a glucose-dependent manner. *Curr. Genet.* **67**, 245–248 (2021).

281. Schnell, H. M. *et al.* Reg1 and Snf1 regulate stress-induced relocalization of protein phosphatase-1 to cytoplasmic granules. *FEBS J.* **288**, 4833–4848 (2021).

282. Solis-Escalante, D. *et al.* The genome sequence of the popular hexose-transport-deficient Saccharomyces cerevisiae strain EBY.VW4000 reveals LoxP/Cre-induced translocations and gene loss. *FEMS Yeast Res.* **15**, (2015).

283. Reifenberger, E., Boles, E. & Ciriacy, M. Kinetic characterization of individual hexose transporters of Saccharomyces cerevisiae and their relation to the triggering mechanisms of glucose repression. *Eur. J. Biochem.* **245**, 324–333 (1997).

284. Horak, J. & Wolf, D. H. Glucose-Induced Monoubiquitination of the *Saccharomyces cerevisiae* Galactose Transporter Is Sufficient To Signal Its Internalization. *J. Bacteriol.* **183**, 3083–3088 (2001).

285. Horak, J. & Wolf, D. H. The ubiquitin ligase SCFGrr1 is required for Gal2p degradation in the yeast Saccharomyces cerevisiae. *Biochem. Biophys. Res. Commun.* **335**, 1185–1190 (2005).

286. Heiland, S., Radovanovic, N., Höfer, M., Winderickx, J. & Lichtenberg, H. Multiple hexose transporters of Schizosaccharomyces pombe. *J. Bacteriol.* **182**, 2153–2162 (2000).

287. Emmerich, W. & Radler, F. The Anaerobic Metabolism of Glucose and Fructose by Saccharomyces bailii. *Microbiology* **129**, 3311–3318 (1983).

288. Guillaume, C., Delobel, P., Sablayrolles, J.-M. & Blondin, B. Molecular basis of fructose utilization by the wine yeast Saccharomyces cerevisiae: a mutated HXT3 allele enhances fructose fermentation. *Appl. Environ. Microbiol.* **73**, 2432–2439 (2007).

289. Tsai, C. S., Mitton, K. P. & Johnson, B. F. Acetate assimilation by the fission yeast, Schizosaccharomyces pombe. *Biochem. Cell Biol. Biochim. Biol. Cell.* **67**, 464–467 (1989).

290. De Jong-Gubbels, P., Van Dijken, J. P. & Pronk, J. T. Metabolic fluxes in chernostat cultures of Schizosaccharomyces pombe grown on mixtures of glucose and ethanol. *Microbiology* **142**, 1399–1407 (1996).

291. Rhind, N. *et al.* Comparative functional genomics of the fission yeasts. *Science* **332**, 930–936 (2011).

292. Leandro, M. J., Fonseca, C. & GonÃ§alves, P. Hexose and pentose transport in ascomycetous yeasts: an overview. *FEMS Yeast Res.* **9**, 511–525 (2009).

293. Lee, J. & Levin, D. E. Intracellular mechanism by which arsenite activates the yeast stress MAPK Hog1. *Mol. Biol. Cell* **29**, 1904–1915 (2018).

294. Basu, R., Munteanu, E. L. & Chang, F. Role of turgor pressure in endocytosis in fission yeast. *Mol. Biol. Cell* **25**, 679–687 (2014).

295. Finn, R. N. & Cerdà, J. Evolution and Functional Diversity of Aquaporins. *Biol. Bull.* **229**, 6–23 (2015).

296. Pettersson, N., Filipsson, C., Becit, E., Brive, L. & Hohmann, S. Aquaporins in yeasts and filamentous fungi. *Biol. Cell* **97**, 487–500 (2005).

297. Toh, T. *et al.* Implications of deletion and membrane ergosterol content for glycerol efflux from. *FEMS Yeast Res.* **1**, 205–211 (2001).

298. Oliveira, R., Lages, F., Silva-Graça, M. & Lucas, C. Fps1p channel is the mediator of the major part of glycerol passive diffusion in Saccharomyces cerevisiae: artefacts and re-definitions. *Biochim. Biophys. Acta* **1613**, 57–71 (2003).

299. Schneider, S. *et al.* Arabidopsis INOSITOL TRANSPORTER4 mediates high-affinity H+ symport of myoinositol across the plasma membrane. *Plant Physiol.* **141**, 565–577 (2006).

300. Schneider, S. *et al.* Arabidopsis INOSITOL TRANSPORTER2 Mediates H^+ Symport of Different Inositol Epimers and Derivatives across the Plasma Membrane. *Plant Physiol.* **145**, 1395–1407 (2007).

301. Klepek, Y.-S. *et al.* Arabidopsis POLYOL TRANSPORTER5, a new member of the monosaccharide transporter-like superfamily, mediates H+-Symport of numerous substrates, including myo-inositol, glycerol, and ribose. *Plant Cell* **17**, 204–218 (2005).

302. Reinders, A., Panshyshyn, J. A. & Ward, J. M. Analysis of transport activity of Arabidopsis sugar alcohol permease homolog AtPLT5. *J. Biol. Chem.* **280**, 1594–1602 (2005).

303. Scholz-Starke, J., Büttner, M. & Sauer, N. AtSTP6, a new pollen-specific H+-monosaccharide symporter from Arabidopsis. *Plant Physiol.* **131**, 70–77 (2003).

304. Büttner, M. & Sauer, N. Monosaccharide transporters in plants: structure, function and physiology. *Biochim. Biophys. Acta* **1465**, 263–274 (2000).

305. Williams, L. E., Lemoine, R. & Sauer, N. Sugar transporters in higher plants – a diversity of roles and complex regulation. *Trends Plant Sci.* **5**, 283–290 (2000).

306. Slewinski, T. L. Diverse Functional Roles of Monosaccharide Transporters and their Homologs in Vascular Plants: A Physiological Perspective. *Mol. Plant* **4**, 641–662 (2011).

307. Sakr, S. *et al.* The Sugar-Signaling Hub: Overview of Regulators and Interaction with the Hormonal and Metabolic Network. *Int. J. Mol. Sci.* **19**, 2506 (2018).

308. Meng, L.-S. *et al.* Glucose- and sucrose-signaling modules regulate the Arabidopsis juvenile-to-adult phase transition. *Cell Rep.* **36**, 109348 (2021).

309. Moore, B. *et al.* Role of the *Arabidopsis* Glucose Sensor HXK1 in Nutrient, Light, and Hormonal Signaling. *Science* **300**, 332–336 (2003).

310. Cho, Y.-H., Yoo, S.-D. & Sheen, J. Glucose signaling through nuclear hexokinase1 complex in Arabidopsis. *Plant Signal. Behav.* **2**, 123–124 (2007).

311. Cho, Y.-H. & Yoo, S.-D. Signaling Role of Fructose Mediated by FINS1/FBP in Arabidopsis thaliana. *PLoS Genet.* **7**, e1001263 (2011).

312. Zhang, H. *et al.* Systematic identification of arsenic-binding proteins reveals that hexokinase-2 is inhibited by arsenic. *Proc. Natl. Acad. Sci.* **112**, 15084–15089 (2015).

313. Soares, E. V., Hebbelinck, K. & Soares, H. M. Toxic effects caused by heavy metals in the yeast Saccharomyces cerevisiae: a comparative study. *Can. J. Microbiol.* **49**, 336–343 (2003).

314. Avery, S. V., Howlett, N. G. & Radice, S. Copper toxicity towards Saccharomyces cerevisiae: dependence on plasma membrane fatty acid composition. *Appl. Environ. Microbiol.* **62**, 3960–3966 (1996).

315. Stohs, S. Oxidative mechanisms in the toxicity of metal ions. *Free Radic. Biol. Med.* **18**, 321–336 (1995).

316. Murata, N. Low-temperature effects on cyanobacterial membranes. *J. Bioenerg. Biomembr.* **21**, 61–75 (1989).

317. Hazel, J. The role of alterations in membrane lipid composition in enabling physiological adaptation of organisms to their physical environment. *Prog. Lipid Res.* **29**, 167–227 (1990).

318. Suwalsky, M. *et al.* Arsenite interactions with phospholipid bilayers as molecular models for the human erythrocyte membrane. *Biophys. Chem.* **127**, 28–35 (2007).

319. Cacace, M. G., Landau, E. M. & Ramsden, J. J. The Hofmeister series: salt and solvent effects on interfacial phenomena. *Q. Rev. Biophys.* **30**, 241–277 (1997).

320. Cosgrove, D. J. Structure and growth of plant cell walls. *Nat. Rev. Mol. Cell Biol.* **25**, 340–358 (2024).

321. Levin, D. E. Cell wall integrity signaling in Saccharomyces cerevisiae. *Microbiol. Mol. Biol. Rev. MMBR* **69**, 262–291 (2005).

322. Chalier, P., Angot, B., Delteil, D., Doco, T. & Gunata, Z. Interactions between aroma compounds and whole mannoprotein isolated from Saccharomyces cerevisiae strains. *Food Chem.* **100**, 22–30 (2007).

323. Manjón, E., Recio-Torrado, A., Ramos-Pineda, A. M., García-Estévez, I. & Escribano-Bailón, M. T. Effect of different yeast mannoproteins on the interaction between wine flavanols and salivary proteins. *Food Res. Int.* **143**, 110279 (2021).

324. Foster, A. W., Osman, D. & Robinson, N. J. Metal Preferences and Metallation. *J. Biol. Chem.* **289**, 28095–28103 (2014).

325. Irving, H. & Williams, R. J. P. Order of Stability of Metal Complexes. *Nature* **162**, 746–747 (1948).

326. Sailer, J. *et al.* Deadly excess copper. *Redox Biol.* **75**, 103256 (2024).

327. Perron, N. R. & Brumaghim, J. L. A Review of the Antioxidant Mechanisms of Polyphenol Compounds Related to Iron Binding. *Cell Biochem. Biophys.* **53**, 75–100 (2009).

328. York, E., McNaughton, D. A., Duman, M.-N., Gale, P. A. & Rawling, T. Fatty Acid-Activated Proton Transport by Bisaryl Anion Transporters Depolarises Mitochondria and Reduces the Viability of MDA-MB-231 Breast Cancer Cells. *Biomolecules* **13**, 1202 (2023).

329. Chng, C.-P., Gupta, S. & Huang, C. Protonation State of a Bioactive Compound Regulates Its Release from Lamellar Gel-Phase Bilayers. *J. Phys. Chem. B* **128**, 7180–7187 (2024).

330. Pérez-Caballero, G., Pérez-Arévalo, J. F., Morales-Hipólito, E. A., Carbajal-Arenas, M. E. & Rojas-Hernández, A. Potentiometric study of acid-base properties of thiamine hydrochloride and thiamine mononitrate in aqueous medium. *J. Mex. Chem. Soc.* **55**, 126–131 (2011).

331. Cain, A. H., Sullivan, G. R. & Roberts, J. D. The protonation site of vitamin B1 as determined from natural-abundance nitrogen-15 nuclear magnetic resonance spectra. *J. Am. Chem. Soc.* **99**, 6423–6425 (1977).

332. Rubino, J. T. & Berryhill, W. S. Effects of Solvent Polarity on the Acid Dissociation Constants of Benzoic Acids. *J. Pharm. Sci.* **75**, 182–186 (1986).

333. Blaga, A. C., Dragoi, E. N., Tucaliuc, A., Kloetzer, L. & Cascaval, D. Folic Acid Ionic-Liquids-Based Separation: Extraction and Modelling. *Molecules* **28**, 3339 (2023).

334. Said, H. M. Cell and Molecular Aspects of Human Intestinal Biotin Absorption. *J. Nutr.* **139**, 158–162 (2009).

335. Qiu, C. *et al.* F-box proteins Pof3 and Pof1 regulate Wee1 degradation and mitotic entry in fission yeast. *J. Cell Sci.* **131**, jcs202895 (2018).

336. Rossman, T. G., Uddin, A. N., Burns, F. J. & Bosland, M. C. Arsenite cocarcinogenesis: an animal model derived from genetic toxicology studies. *Environ. Health Perspect.* **110 Suppl 5**, 749–752 (2002).

337. Muenyi, C. S., Ljungman, M. & States, J. C. Arsenic Disruption of DNA Damage Responses-Potential Role in Carcinogenesis and Chemotherapy. *Biomolecules* **5**, 2184–2193 (2015).

338. Tam, L. M., Price, N. E. & Wang, Y. Molecular Mechanisms of Arsenic-Induced Disruption of DNA Repair. *Chem. Res. Toxicol.* **33**, 709–726 (2020).

339. Rodríguez-Gabriel, M. A. & Russell, P. Distinct Signaling Pathways Respond to Arsenite and Reactive Oxygen Species in *Schizosaccharomyces pombe*. *Eukaryot. Cell* **4**, 1396–1402 (2005).

340. Mendoza-Cózatl, D., Loza-Tavera, H., Hernández-Navarro, A. & Moreno-Sánchez, R. Sulfur assimilation and glutathione metabolism under cadmium stress in yeast, protists and plants. *FEMS Microbiol. Rev.* **29**, 653–671 (2005).

341. Sanchez-Marinas, M. *et al.* Cmk2 kinase is essential for survival in arsenite by modulating translation together with RACK1 orthologue Cpc2 in Schizosaccharomyces pombe. *Free Radic. Biol. Med.* **129**, 116–126 (2018).

342. Joshi, N. C., Meyer, A. J., Bangash, S. A. K., Zheng, Z. & Leustek, T. Arabidopsis γ-glutamylcyclotransferase affects glutathione content and root system architecture during sulfur starvation. *New Phytol.* **221**, 1387–1397 (2019).

343. Fauchon, M. *et al.* Sulfur Sparing in the Yeast Proteome in Response to Sulfur Demand. *Mol. Cell* **9**, 713–723 (2002).

344. Kim, S.-J., Kim, H.-G., Kim, B.-C., Park, E.-H. & Lim, C.-J. Transcriptional regulation of glutathione synthetase in the fission yeast Schizosaccharomyces pombe. *Mol. Cells* **18**, 242–248 (2004).

345. Guo, L., Ghassemian, M., Komives, E. A. & Russell, P. Cadmium-induced proteome remodeling regulated by Spc1/Sty1 and Zip1 in fission yeast. *Toxicol. Sci. Off. J. Soc. Toxicol.* **129**, 200–212 (2012).

346. Mitrić, A. & Castellano, I. Targeting gamma-glutamyl transpeptidase: A pleiotropic enzyme involved in glutathione metabolism and in the control of redox homeostasis. *Free Radic. Biol. Med.* **208**, 672–683 (2023).

347. Labunskyy, V. M. & Gladyshev, V. N. Role of reactive oxygen species-mediated signaling in aging. *Antioxid. Redox Signal.* **19**, 1362–1372 (2013).

348. Song, S.-H. & Lim, C.-J. Nitrogen depletion causes up-regulation of glutathione content and γ-glutamyltranspeptidase in Schizosaccharomyces pombe. *J. Microbiol.* **46**, 70–74 (2008).

349. Kim, H.-G. *et al.* The Schizosaccharomyces pombe gene encoding gamma-glutamyl transpeptidase I is regulated by non-fermentable carbon sources and nitrogen starvation. *J. Microbiol. Seoul Korea* **43**, 44–48 (2005).

350. Takemura, K., Board, P. G. & Koga, F. A Systematic Review of Serum γ-Glutamyltransferase as a Prognostic Biomarker in Patients with Genitourinary Cancer. *Antioxidants* **10**, 549 (2021).

351. Blobel, G. Intracellular protein topogenesis. *Proc. Natl. Acad. Sci. U. S. A.* **77**, 1496–1500 (1980).

352. Mason, D. L. & Michaelis, S. Requirement of the N-terminal extension for vacuolar trafficking and transport activity of yeast Ycf1p, an ATP-binding cassette transporter. *Mol. Biol. Cell* **13**, 4443–4455 (2002).

353. Novarina, D., Guerra, P. & Milias-Argeitis, A. Vacuolar Localization via the N-terminal Domain of Sch9 is Required for TORC1-dependent Phosphorylation and Downstream Signal Transduction. *J. Mol. Biol.* **433**, 167326 (2021).

354. Kumar, C., Sharma, R. & Bachhawat, A. K. Investigations into the polymorphisms at the *ECM38* locus of two widely used *Saccharomyces cerevisiae* S288C strains, YPH499 and BY4742. *Yeast* **20**, 857–863 (2003).

355. Ubiyvovk, V., Blazhenko, O., Gigot, D., Penninckx, M. & Sibirny, A. Role of γ-glutamyltranspeptidase in detoxification of xenobiotics in the yeasts Hansenula polymorpha and Saccharomyces cerevisiae. *Cell Biol. Int.* **30**, 665–671 (2006).

356. Huh, W.-K. *et al.* Global analysis of protein localization in budding yeast. *Nature* **425**, 686–691 (2003).

357. Ohtsuka, H., Shimasaki, T. & Aiba, H. Response to sulfur in *Schizosaccharomyces pombe*. *FEMS Yeast Res.* **21**, foab041 (2021).

358. White, C., Nixon, A. & Bradbury, N. A. Determining Membrane Protein Topology Using Fluorescence Protease Protection (FPP). *J. Vis. Exp. JoVE* 52509 (2015) doi:10.3791/52509.

359. Zechmann, B. *et al.* Subcellular distribution of glutathione and its dynamic changes under oxidative stress in the yeast Saccharomyces cerevisiae. *FEMS Yeast Res.* **11**, 631–642 (2011).

360. Lee, S., Kim, J. S., Yun, C. H., Chae, H. Z. & Kim, K. Aspartyl aminopeptidase of Schizosaccharomyces pombe has a molecular chaperone function. *BMB Rep.* **42**, 812–816 (2009).

361. Bae, W. & Chen, X. Proteomic study for the cellular responses to Cd2+ in Schizosaccharomyces pombe through amino acid-coded mass tagging and liquid chromatography tandem mass spectrometry. *Mol. Cell. Proteomics MCP* **3**, 596–607 (2004).

362. Vido, K. *et al.* A Proteome Analysis of the Cadmium Response in Saccharomyces cerevisiae. *J. Biol. Chem.* **276**, 8469–8474 (2001).

363. Paulose, B. *et al.* A γ-glutamyl cyclotransferase protects Arabidopsis plants from heavy metal toxicity by recycling glutamate to maintain glutathione homeostasis. *Plant Cell* **25**, 4580–4595 (2013).

364. Fukushima, A. *et al.* Effects of Combined Low Glutathione with Mild Oxidative and Low Phosphorus Stress on the Metabolism of Arabidopsis thaliana. *Front. Plant Sci.* **8**, 1464 (2017).

365. Dai, J. *et al.* Dynamics of Dimethylated Monothioarsenate (DMMTA) in Paddy Soils and Its Accumulation in Rice Grains. *Environ. Sci. Technol.* **55**, 8665–8674 (2021).

366. Leustek, T., Martin, M. N., Bick, J.-A. & Davies, J. P. PATHWAYS AND REGULATION OF SULFUR METABOLISM REVEALED THROUGH MOLECULAR AND GENETIC STUDIES. *Annu. Rev. Plant Physiol. Plant Mol. Biol.* **51**, 141–165 (2000).

367. Ohkama-Ohtsu, N. *et al.* A *γ* -Glutamyl Transpeptidase-Independent Pathway of Glutathione Catabolism to Glutamate via 5-Oxoproline in Arabidopsis. *Plant Physiol.* **148**, 1603–1613 (2008).

368. Pompella, A., Visvikis, A., Paolicchi, A., Tata, V. D. & Casini, A. F. The changing faces of glutathione, a cellular protagonist. *Biochem. Pharmacol.* **66**, 1499–1503 (2003).

369. Lehmann, A. *et al.* Molecular interactions of fission yeast Skp1 and its role in the DNA damage checkpoint. *Genes Cells* **9**, 367–382 (2004).

370. Hermand, D. F-box proteins: more than baits for the SCF? *Cell Div.* **1**, 30 (2006).

371. Lamoureux, G. L., Rusness, D. G. & Tanaka, F. S. Chlorimuron ethyl metabolism in corn. *Pestic. Biochem. Physiol.* **41**, 66–81 (1991).

372. Beck, A., Lendzian, K., Oven, M., Christmann, A. & Grill, E. Phytochelatin synthase catalyzes key step in turnover of glutathione conjugates. *Phytochemistry* **62**, 423–431 (2003).

373. Blum, R. *et al.* Function of phytochelatin synthase in catabolism of glutathione-conjugates. *Plant J.* **49**, 740–749 (2007).

374. Rajakumar, S., Abhishek, A., Selvam, G. S. & Nachiappan, V. Effect of cadmium on essential metals and their impact on lipid metabolism in Saccharomyces cerevisiae. *Cell Stress Chaperones* **25**, 19–33 (2020).

375. Amberg, D. C., Burke, D. J. & Strathern, J. N. *Methods in Yeast Genetics: A Cold Spring Harbor Laboratory Course Manual*. (Cold Spring Harbor Laboratory press, Cold Spring Harbor (N.Y.), 2005).

5.1 Submitted Manuscripts

08/2025: Phosphate Transporters Mediate the Uptake of Monothioarsenate.

6. Appendix

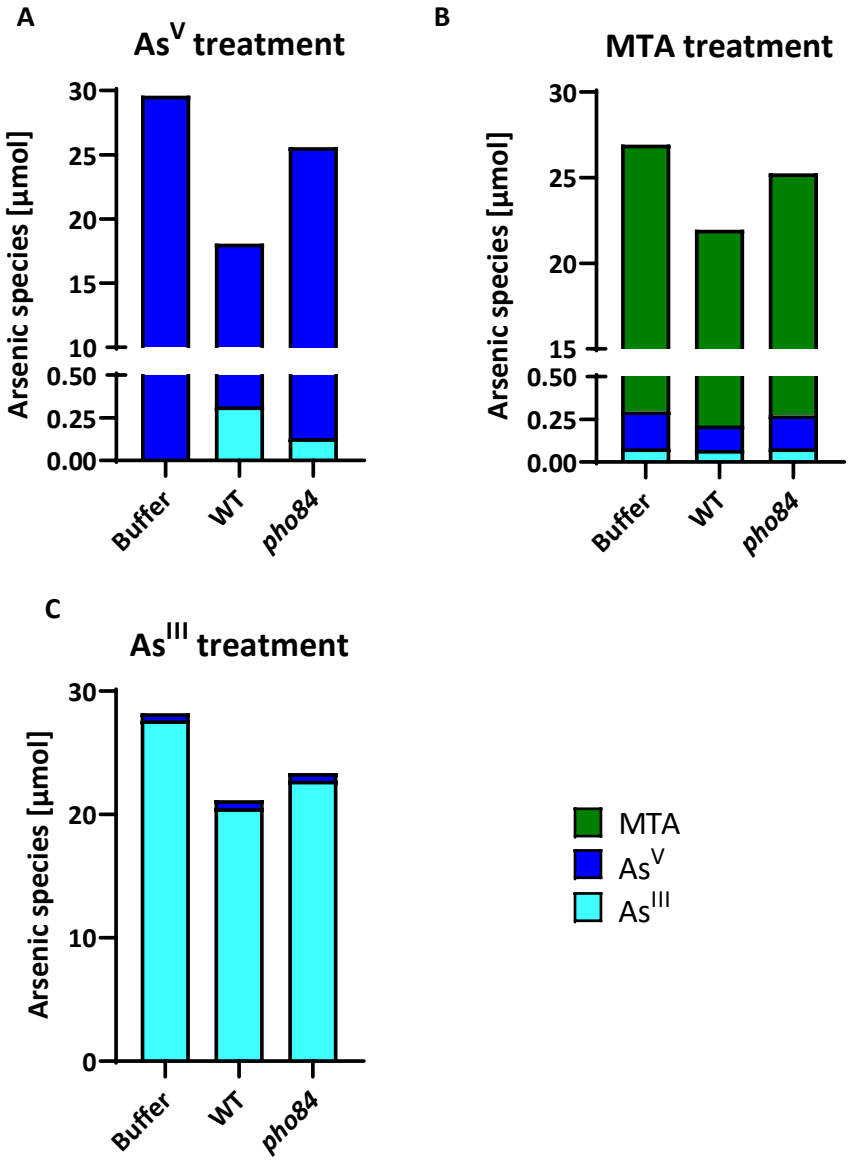

Fig. S1: Evaluation of medium samples from uptake experiments conducted with *S. cerevisiae* WT and *pho84*. Distribution of arsenic species in the uptake solution, as well as in medium from WT or *pho84* cells, after exposure to 50 µM As^{V} (A), MTA (B), or As^{III} (C) for 60 min at 30°C. The proportion in µmol of each species is represented by its respective color: MTA (green), As^{V} (dark blue), and As^{III} (pale blue). Medium samples were taken from one of the three replicates of the uptake experiments shown in Fig. 4. Data represent a single biological replicate (n = 1).

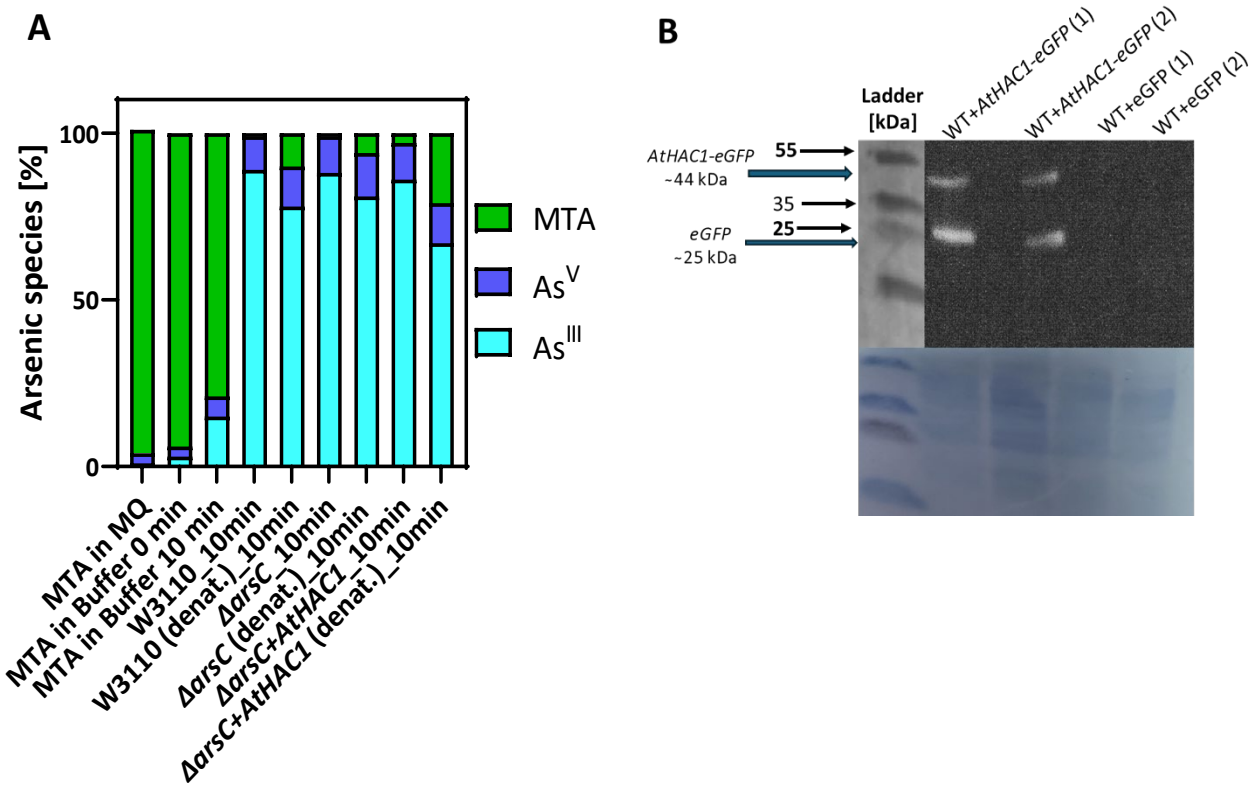

Fig. S2: Evaluation of the heterologous expression of AtHAC1 in *S. pombe* and *E. coli.* (A) Percentage distribution of arsenic species after the addition of 6.66 µM MTA, incubated for 10 min at 37°C. MTA was added to deionized water (MQ), buffer, or *E. coli* protein extract of W3110, *ΔarsC*, or *ΔarsC+AtHAC1*. As a control, MTA was added to boiled (denatured) protein extract. Data represent a single biological replicate (n = 1). (B) Representative WB analysis of pre-culture aliquots from *S. pombe* overexpressing AtHAC1-GFP, used for the As^V-reductase assays. The detection (top) and the respective Amido Black loading control (bottom) show protein extracts from two independent pre-culture aliquots of WT+*AtHAC1-eGFP* (samples 1 and 2) and WT (samples 1 and 2) as a negative control. Cultures were harvested to generate crude extracts for the As^V-reductase assays shown here.

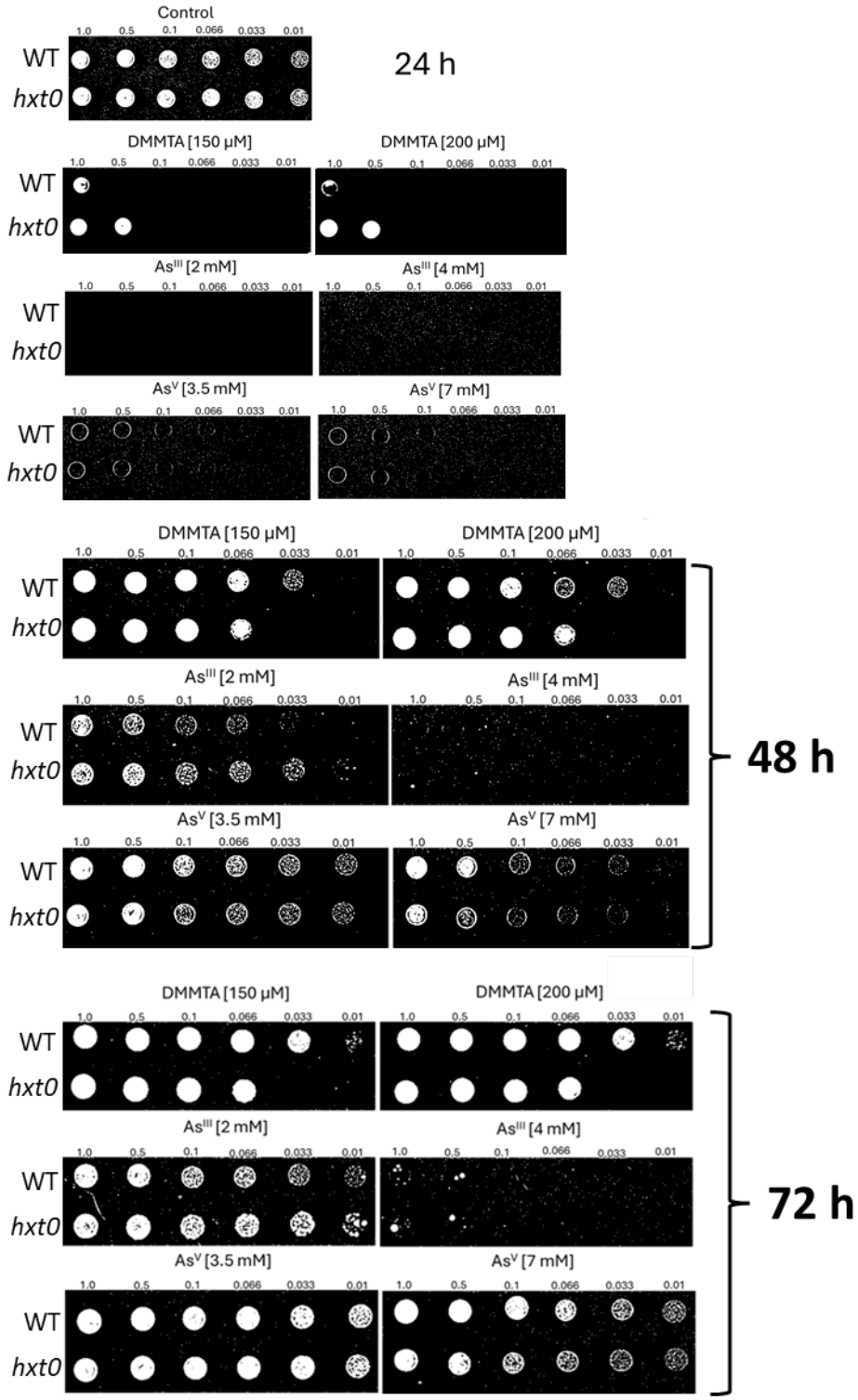

Fig. S3: Tolerance of the *hxt0* mutant to different arsenic species. The figure shows an additional replicate of the serial dilution assay shown in Fig. 16.

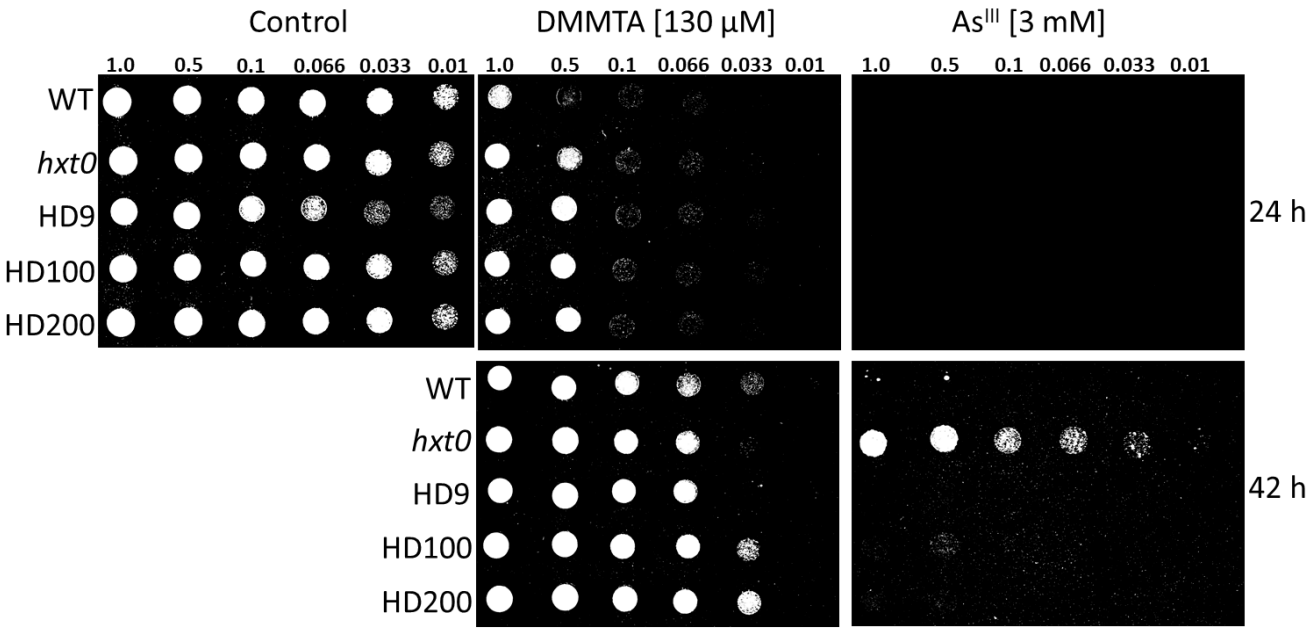

Fig. S4: The impact of the serial loss of bidirectional As^{III} transport capacity on DMMTA tolerance. The figure shows an additional replicate of the serial dilution assay shown in Fig. 18.

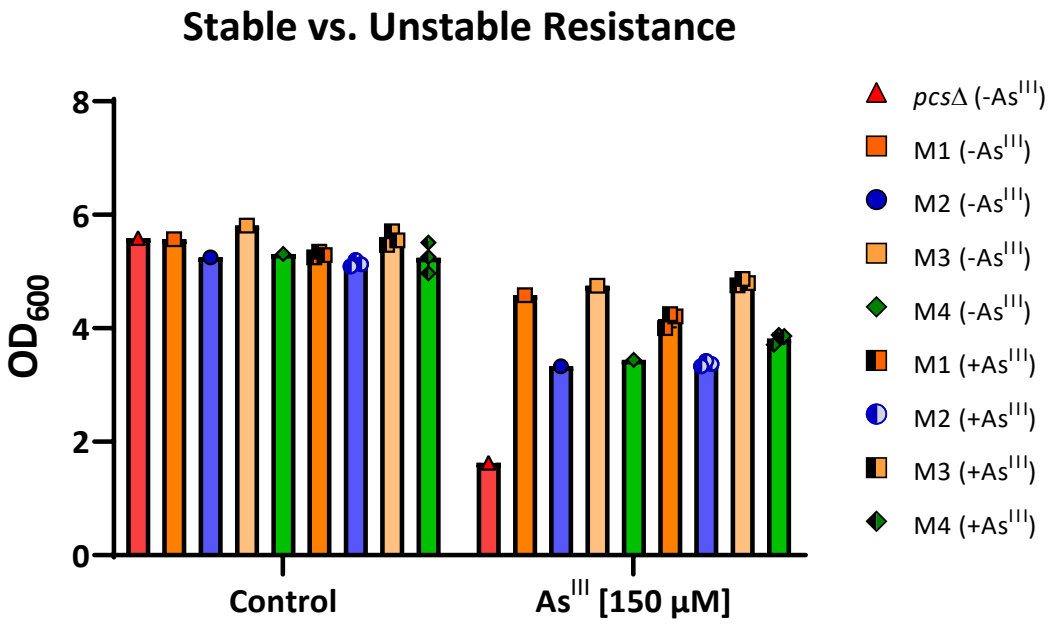

Fig. S5: Screening for Stable vs. Unstable As^{III} Tolerance. Cultures were either continuously exposed to sublethal doses of 10 µM As^{III} (+As^{III}) for three weeks or cultivated without As^{III} (-As^{III}) under the same conditions at 20°C. The assay was initiated by inoculating cultures at an OD_{600} of 0.05 using cells grown overnight at 30°C/220 rpm. Data represent one biological replicate for cells grown under control conditions and three biological replicates for cells grown in As^{III}-containing medium, shown as mean ± standard deviation (n = 1 per replicate for each genotype).

Tab. S1: Overview of mutant strains generated for the As^{III} evolutionary project.

Background	Product	Used Editing Tool	Target Gene Function	Mutation	Effect
pcsΔ	*pcsΔggt2Δ#1*	*CRISPR-Cas9*	*ggt1* γ-Glutamyl Transpeptidase Ggt1	**GT-Deletion** (4 and 5 bp upstream of the PAM sequence)	**Frame shift**
pcsΔ	*pcsΔggt1Δ#2*	*CRISPR-Cas9*	*ggt1* γ-Glutamyl Transpeptidase Ggt1	**T-Insertion** (3 bp upstream of the PAM sequence)	**Frame shift**
pcsΔggt1Δ#2	*pcsΔggt1Δplb1Δ#1*	*CRISPR-Cas9*	*plb1* Phospholipase B Homolog	G-Deletion (3 bp upstream of the PAM sequence)	**Frame shift**
WT (FY261)	*ggt2Δ*	Homologous Recombination	*ggt2* γ-Glutamyl Transpeptidase Ggt2	*ggt2Δ::KanMX4*	**Gene disruption**
pcsΔ	*pcsΔggt2Δ#1*	*CRISPR-Cas9*	*ggt2* γ-Glutamyl Transpeptidase Ggt2	**Insertion of unknown sequence 5 bp upstream the PAM motif** (5´-AGCCAGTTTAATGACCCTATTATGATG TCACAATAGCCCAATGTA-3´)	**Frame shift**
pcsΔ	*pcsΔggt2Δ#1*	*CRISPR-Cas9*	*ggt2* γ-Glutamyl Transpeptidase Ggt2	**A-Insertion** (4 bp upstream of the PAM sequence)	**Frame shift**
pcsΔ	*M4_ggt2Δ*	Homologous Recombination	*ggt2* γ-Glutamyl Transpeptidase Ggt2	*ggt2Δ::KanMX4*	**Gene disruption**

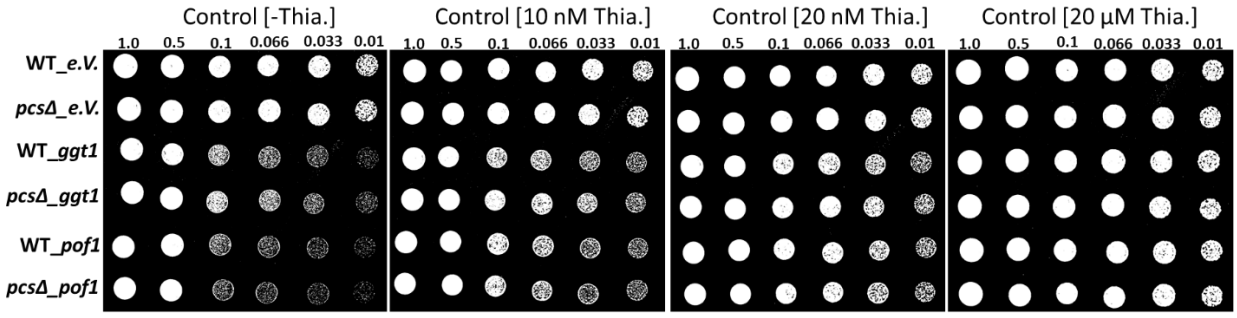

Fig. S7: Growth inhibition due to different expression levels of *ggt1* and *pof1* in *S. pombe* WT and *pcsΔ*. WT and *pcsΔ* strain carrying pSGP72 (e.V.), pSGP72-*ggt1* or pSGP72-*pof1* were plated on EMM -/- plates and incubated for 48 hours at 30°C with 0 (- Thia.), 10 nM, 20 nM or 20 µM thiamine. The numbers above each spot indicate the OD_{600} value of the corresponding dilution step.

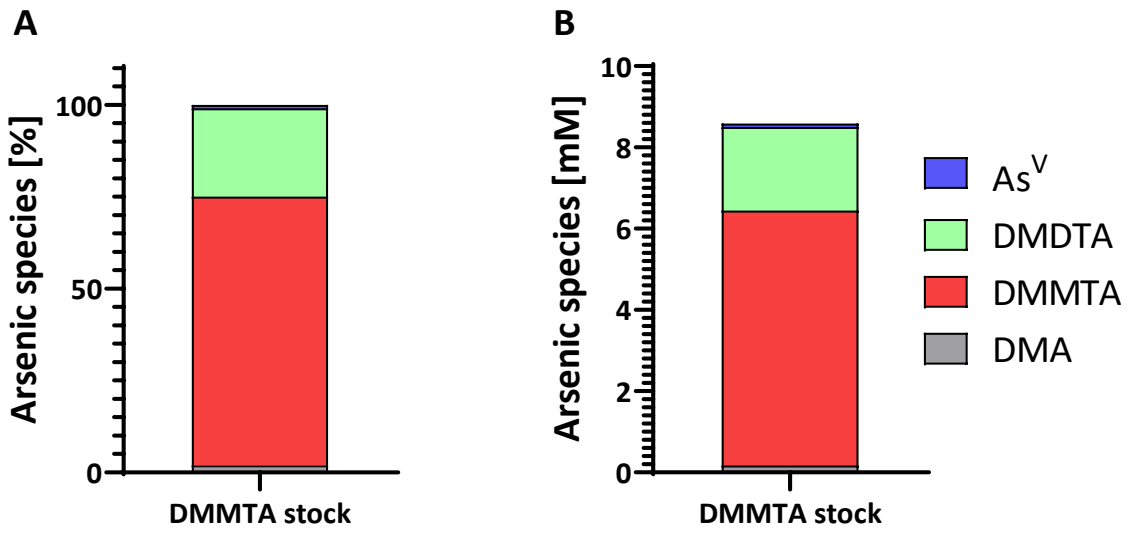

Fig. S8: Distribution of arsenic species in DMMTA stocks. The distribution of additional arsenic species in an 8.59 mM DMMTA stock is shown. The stacked bar blots present the percentage shares of each species (A), or their concentrations in mM (B). Data represent one replicate.

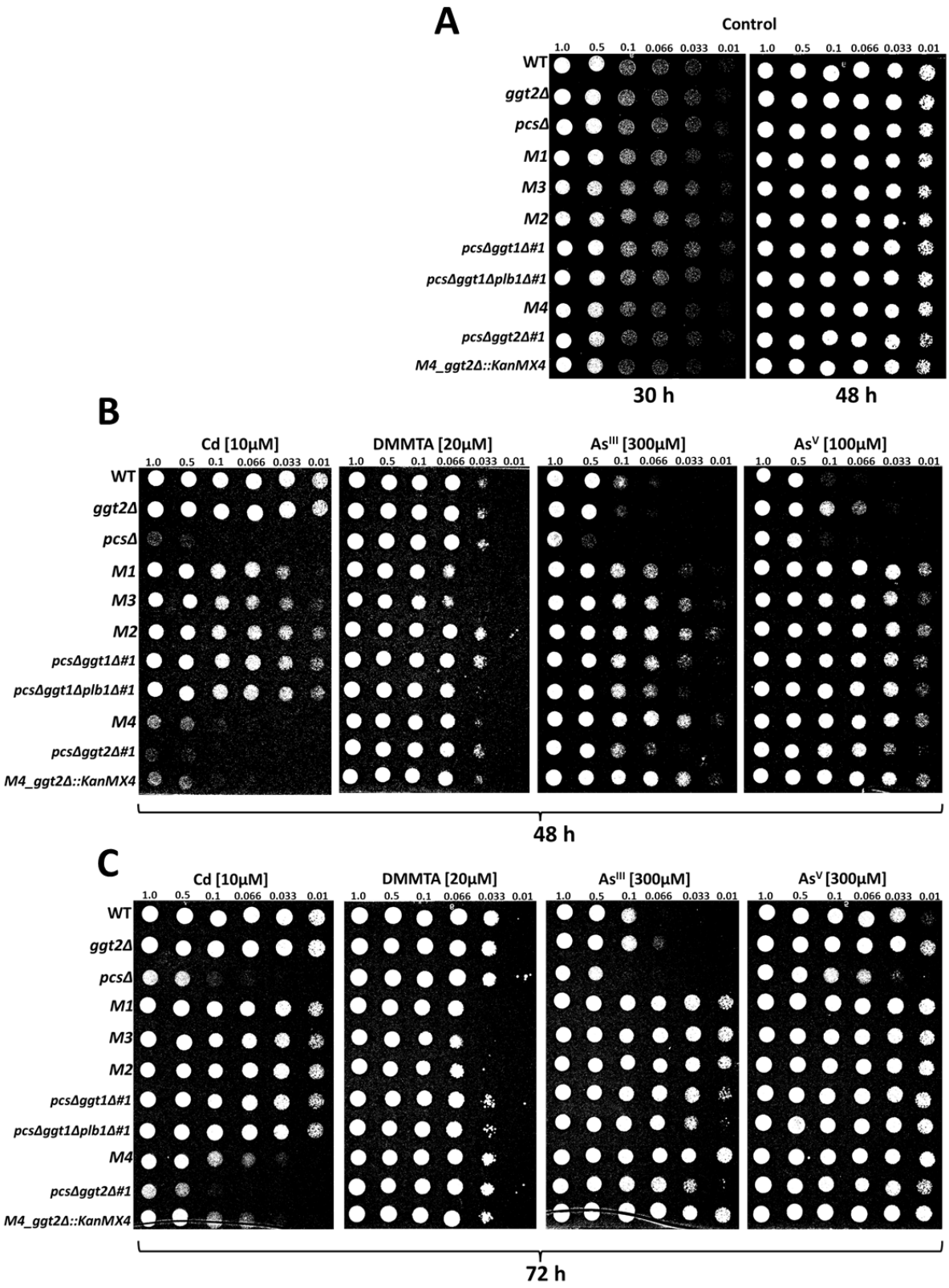

Fig. S9: Comparison of M1–M4 with the corresponding knockout mutants, the WT and *pcsΔ* strain regarding their tolerance to Cd, DMMTA, As^{III}, and As^{V}. The figure shows an additional replicate of the serial dilution assay shown in Fig. 29.

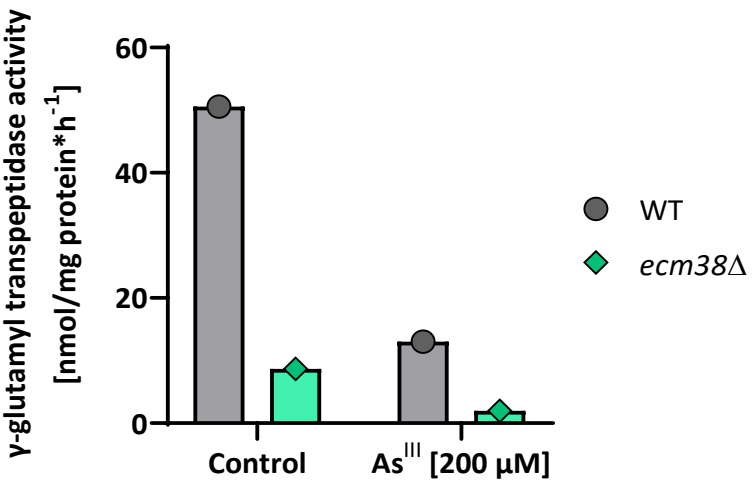

Fig. S10: γ-GT activity assay using *S. cerevisiae* WT (BY4741) and the γ-GT deficient *ecm38* mutant. Cells were grown under control conditions or exposed to As^{III} [200 µM] for 18 h. This initial test aimed to validate the assay protocol for measuring γ-GT activity in *S. cerevisiae* and *S. pombe* (as shown in Fig. 33D) by reproducing the results of P. Adamis et al. (2009)[238,239]. Data represent one biological replicate.

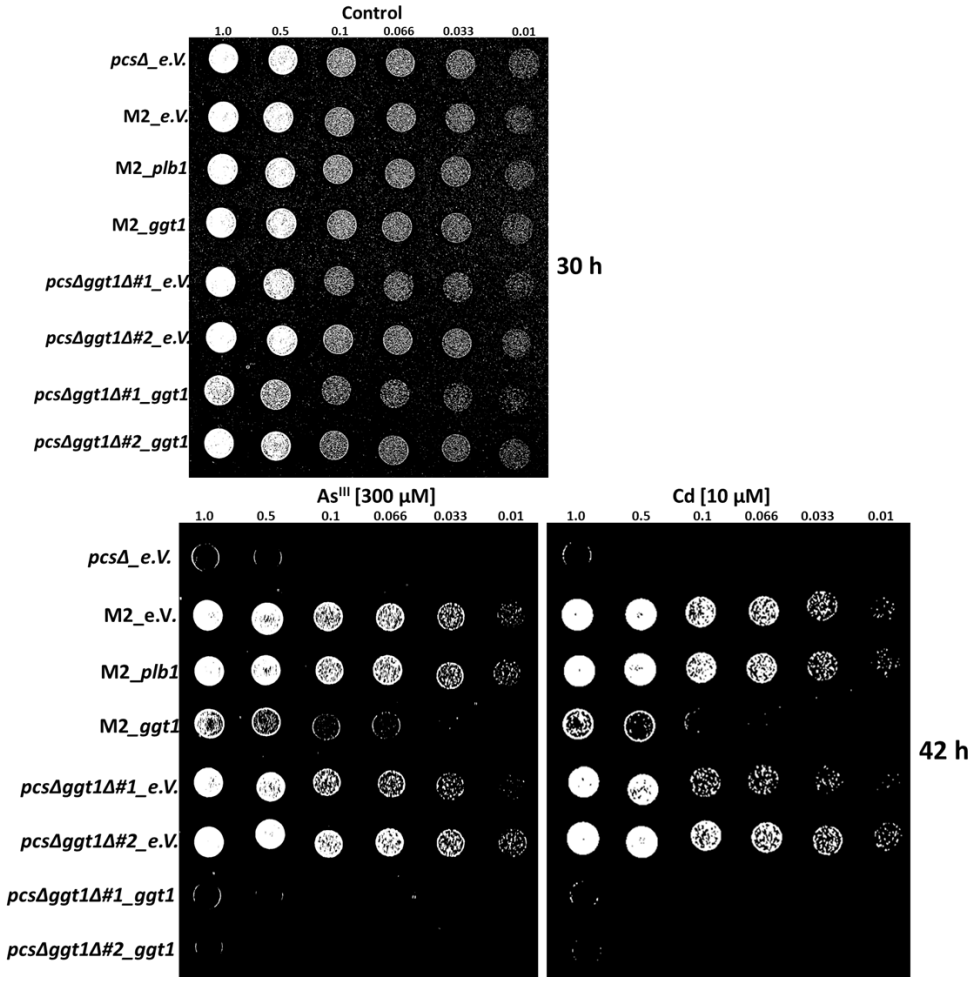

Fig. S11: Complementation of M2 and corresponding knockout mutants. The figure shows an additional replicate of the serial dilution assay shown in Fig. 34.

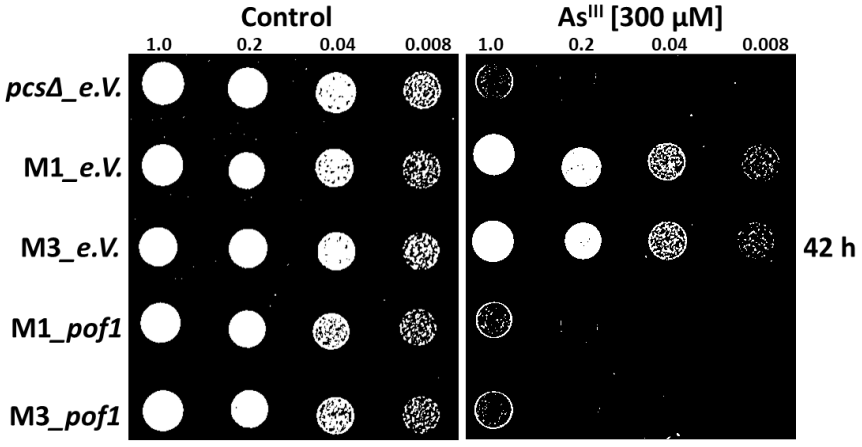

Fig. S12: Complementation of M1 and M3. The figure shows an additional replicate of the serial dilution assay shown in Fig. 36.

Acknowledgement

An erster Stelle möchte ich mich bei Prof. Stephan Clemens dafür bedanken, dass ich an einem spannenden Projekt in einem sowohl fachlich als auch menschlich herausragenden Umfeld arbeiten durfte. Seine fachliche und analytische Kompetenz, von der ich viel lernen konnte - und noch viel lernen könnte - sowie die Freiheit, die er mir bei der Bearbeitung verschiedener Projekte eingeräumt hat, waren von unschätzbarem Wert für meine persönliche Entwicklung.

Einen ebenso unschätzbaren Beitrag leisteten Prof. Britta Planer-Friedrich und ihr Team, insbesondere Sylvia Haffner. Ohne ihre Pionierarbeit, ihre fachliche Expertise und ihr umfassendes Know-how wäre diese Arbeit nicht möglich gewesen. Prof. Britta Planer-Friedrichs Wirken und Engagement reichen dabei weit über diese Arbeit hinaus und bleiben in dankbarer Erinnerung.

Darüber hinaus danke ich Dr. Michael Weber für seine Unterstützung – sowohl auf fachlicher als auch insbesondere auf persönlicher Ebene. Mein Dank gilt ebenfalls Prof. Angelika Mustroph, deren fachliche Begleitung für mich von großer Bedeutung war.

Weiterhin möchte ich Carmen Weber und Pia Schuster für ihre Unterstützung bei wichtigen Experimenten dieser Arbeit danken. Gemeinsam mit Kerstin Ackermann, Christiane Meinen und Waltraud Knauer waren sie mir auch auf persönlicher Ebene als aufmerksame Gesprächspartnerinnen wertvolle Wegbegleiterinnen.

Ein besonderer Dank geht an meine beiden Studenten Florian Lindbüchl für seinen äußerst wichtigen Beitrag zur Aufklärung der MTA-Aufnahme sowie Celine Fischer für ihre Mitarbeit bei der Untersuchung der Mutanten aus dem As^{III}-Evolutionsprojekt. Ich wünsche beiden viel Erfolg auf ihrem weiteren Weg. Auch meiner fleißigen Assistentin Lisa Neubauer möchte ich an dieser Stelle danken und wünsche ihr ebenfalls viel Glück auf ihrem weiteren Weg.

Der größte Dank gilt meinen Eltern Ulrike und Stefan Haider, die mit ihrer Unterstützung und dem Rückhalt, den sie mir gegeben haben, die wichtigste Grundlage für diesen Weg geboten haben. Insbesondere meiner Mutter gilt mein größter Dank, da sie immer für mich da war, unabhängig davon, wie es ihr selbst ging. Ebenso danke ich auch meinen Geschwistern Anna-Lena und Johannes, auf die ich mich jederzeit verlassen konnte und kann.

Eidesstattliche Versicherungen und Erklärungen

(§ 9 Satz 2 Nr. 3 PomO BayNAT)

Hiermit versichere ich eidesstattlich, dass ich die Arbeit selbstständig verfasst und keine anderen als die von mir angegebenen Quellen und Hilfsmittel benutz habe (vgl. Art. 97 Abs. 1 Satz 8 BayHIG).

(§ 9 Satz 2 Nr. 3 PomO BayNAT)

Hiermit erkläre ich, dass ich die Dissertation nicht bereits zur Erlangung eines akademischen Grades eingereicht habe und dass ich nicht bereits diese oder eine gleichartige Doktorprüfung endgültig nicht bestanden habe.

(§ 9 Satz 2 Nr. 4 PomO BayNAT)

Hiermit erkläre ich, dass ich Hilfe von gewerblichen Promotionsberatern bzw. –vermittlern oder ähnlichen Dienstleistern weder bisher in Anspruch genommen habe noch künftig in Anspruch nehmen werde.

(§ 9 Satz 2 Nr. 7 PomO BayNAT)

Hiermit erkläre ich mein Einverständnis, dass die elektronische Fassung meiner Dissertation unter Wahrung meiner Urheberrechte und des Datenschutzes einer gesonderten Überprüfung unterzogen werden kann.

(§ 9 Satz 2 Nr. 8 PomO BayNAT)

Hiermit erkläre ich mein Einverständnis, dass bei Verdacht wissenschaftlichen Fehlverhaltens Ermittlungen durch universitätsinterne Organe der wissenschaftlichen Selbstkontrolle stattfinden können.

(Ort und Datum) Unterschrift